mgr Anna Maria Mazurek

Analysis of isosymmetric phase transitions using molecular modelling methods

Dissertation for the degree of doctor of medical and health sciences
in the discipline of pharmaceutical sciences

Supervisor: dr hab. Łukasz Szeleszczuk
Assistant supervisor: dr Monika Franczak-Rogowska

Department of Organic and Physical Chemistry
Faculty of Pharmacy
Medical University of Warsaw

Defense of the doctoral dissertation to the Pharmaceutical Sciences Council of
Medical University of Warsaw

Warsaw, 2026

mgr Anna Maria Mazurek

Analiza izosymetrycznych przejść fazowych z wykorzystaniem metod modelowania molekularnego

Rozprawa na stopień doktora nauk medycznych i nauk o zdrowiu
w dyscyplinie nauki farmaceutyczne

Promotor: dr hab. Łukasz Szeleszczuk
Promotor pomocniczy: dr Monika Franczak-Rogowska

Zakład Chemii Organicznej i Fizycznej
Wydział Farmaceutyczny
Warszawski Uniwersytet Medyczny

Obrona rozprawy doktorskiej przed Radą Dyscypliny Nauk Farmaceutycznych
Warszawskiego Uniwersytetu Medycznego

Warszawa, 2026

Acknowledgements

This dissertation would not have been possible without the support, guidance, and encouragement of the people who accompanied me throughout this demanding scientific journey.

First and foremost, I would like to express my sincere gratitude to my supervisor, **dr hab. Łukasz Szeleszczuk**, for his continuous support, scientific guidance, and invaluable mentorship throughout the course of my doctoral studies. His knowledge, critical insight, and encouragement greatly influenced both the direction of this research and my development as a researcher. His trust, patience, and constant motivation allowed me to approach scientific challenges with confidence and determination.

I am also deeply grateful to my co-supervisor, **dr Monika Franczak-Rogowska**, for her support, valuable advice, and constructive discussions throughout every stage of this work. Her scientific perspective, attention to detail, and readiness to help were essential for the successful completion of this dissertation.

Finally, I would like to express my heartfelt gratitude to my family and close friends for their constant support, patience, understanding, and unwavering belief in me throughout this important stage of my life. Their encouragement gave me strength during the most challenging moments and made the completion of this work possible.

Table of contents

1. List of publications constituting the doctoral dissertation 7

2. Abstracts 8

3. List of Abbreviations 10

4. Introduction and justification of the research topic 11

4.1. Molecular crystals and polymorphism 11

4.2. Phase transitions in molecular crystals 12

4.3. Isosymmetric phase transitions in molecular crystals 14

4.4. Structural and thermodynamic aspects of isosymmetric phase transitions 15

4.5. Computational approaches to phase transitions: periodic DFT methods 17

4.6. Relevance of polymorphism and phase transitions in pharmaceutical sciences 18

5. Overview of publications 21

5.1. Publication No. 1 21

5.2. Publication No. 2 22

5.3. Publication No. 3 24

5.4. Publication No. 4 26

6. Aim of the thesis 28

7. Proposed methodological framework for identification and prediction of IPTs 29

8. Summary and Conclusions 31

9. References 33

10. Reprint of publications and co-authors' statements 37

10.1. Publication No.1 37

10.2. Publication No. 2 76

10.3. Publication No. 3 100

10.4. Publication No. 4 125

1. List of publications constituting the doctoral dissertation

Publication No. 1 (Review article)

Mazurek, A. M., Franczak-Rogowska, M., Szeleszczuk, Ł. (2025). Isosymmetric Phase Transitions in Crystals: From Subtle Rearrangements to Functional Properties. *Crystals*, *15*(9), 807.
https://doi.org/10.3390/cryst15090807
IF: 2.4; MNiSW=70

Publication No. 2 (Original article)

Mazurek, A. M., Franczak-Rogowska, M., Szeleszczuk, Ł. (2025). Predicting the Pressure-Induced Isosymmetric Phase Transition of Sulfamic Acid by Applying Periodic Density Functional Theory Calculations. *Applied Sciences*, *15*(8), 4185.
https://doi.org/10.3390/app15084185
IF=2.5; MNiSW=100

Publication No. 3 (Original article)

Mazurek, A. M., Franczak-Rogowska, M., & Szeleszczuk, Ł. (2026). Periodic DFT Investigation of Isosymmetric Alpha–Beta Phase Transition in Resorcinol Under Ambient and High Pressure. *Crystals*, *16*(3), 215.
https://doi.org/10.3390/cryst16030215
IF=2.4; MNiSW=70

Publication No. 4 (Original article)

Mazurek, A. M., Franczak-Rogowska, M., & Szeleszczuk, Ł. (2026). Entropy-Driven Isosymmetric Phase Transition in L-Serine under Pressure: A Periodic DFT Study. *Crystals*, *16*(4), 266.
https://doi.org/10.3390/cryst16040266
IF=2.4; MNiSW=70

2. Abstracts

Abstract

Isosymmetric phase transitions (IPTs) are solid-state transformations that are challenging to detect as the same space group is maintained throughout the transition despite significant changes in molecular configuration, hydrogen-bond topology, and thermodynamic stability. Understanding IPTs is crucial for solid-state chemistry and medicinal chemistry, given that small polymorphic changes might affect the physicochemical properties of molecular crystals.

The aim of this doctoral dissertation was to study IPTs in selected molecular crystals and determine the structural and thermodynamic factors that lead to their occurrence through molecular modelling methods. Sulfamic acid, resorcinol, and L-serine were selected as model systems exemplifying various types of IPT behaviour. Periodic density functional theory (DFT) calculations were utilized to investigate the selected systems, including structural optimisation, pressure-dependent lattice energy analysis, phonon calculations, and Raman spectrum simulation.

The findings indicated that IPTs should be considered as true first-order phase transitions rather than minor distortions within a single crystal structure. In all analysed systems, the transitions involved changes in thermodynamic stability, discontinuities in lattice parameters, and energetic barriers between closely related phases.

The accurate identification of IPTs requires a comprehensive approach, including molecular modelling methods. A methodological framework for predicting IPTs using periodic DFT methods was proposed based on the obtained results. This approach strengthens the understanding of subtle solid-state transformations and may facilitate future research on molecular crystals.

Keywords: isosymmetric phase transitions, molecular crystals, polymorphism, periodic DFT

Streszczenie

Izosymetryczne przejścia fazowe (IPTs) są przemianami w stanie stałym, które są trudne do wykrycia, ponieważ w trakcie przejścia zachowana zostaje ta sama grupa przestrzenna, mimo istotnych zmian w konfiguracji molekularnej, topologii wiązań wodorowych oraz stabilności termodynamicznej. Zrozumienie IPTs ma istotne znaczenie dla chemii ciała stałego oraz chemii farmaceutycznej, ponieważ nawet niewielkie zmiany polimorficzne mogą wpływać na właściwości fizykochemiczne kryształów molekularnych.

Celem niniejszej rozprawy doktorskiej było zbadanie izosymetrycznych przejść fazowych w wybranych kryształach molekularnych oraz określenie strukturalnych i termodynamicznych czynników odpowiedzialnych za ich występowanie z wykorzystaniem metod modelowania molekularnego. Jako układy modelowe wybrano kwas sulfaminowy, rezorcynę oraz L-serynę, reprezentujące różne typy zachowania IPTs. Do analizy badanych układów zastosowano periodyczne obliczenia w ramach teorii funkcjonału gęstości (DFT), obejmujące optymalizację struktury, analizę energii sieci krystalicznej w funkcji ciśnienia, obliczenia fononowe oraz symulację widm Ramana.

Uzyskane wyniki wykazały, że IPTs należy traktować jako rzeczywiste przejścia fazowe pierwszego rodzaju, a nie jako niewielkie deformacje w obrębie jednej struktury krystalicznej. We wszystkich analizowanych układach przemiany były związane ze zmianami stabilności termodynamicznej, nieciągłościami parametrów sieci oraz obecnością barier energetycznych pomiędzy blisko spokrewnionymi fazami.

Prawidłowa identyfikacja izosymetrycznych przejść fazowych wymaga kompleksowego podejścia, obejmującego również metody modelowania molekularnego. Na podstawie uzyskanych wyników zaproponowano ramy metodologiczne umożliwiające przewidywanie IPTs z wykorzystaniem periodycznych metod DFT. Podejście to pogłębia zrozumienie subtelnych przemian w stanie stałym i może wspierać dalsze badania nad kryształami molekularnymi.

Słowa kluczowe: izosymetryczne przejścia fazowe, kryształy molekularne, polimorfizm, periodyczne DFT

3. List of Abbreviations

aiMD	Ab Initio Molecular Dynamics
API	Active Pharmaceutical Ingredient
DFT	Density Functional Theory
DSC	Differential Scanning Calorimetry
EMA	European Medicines Agency
FDA	Food and Drug Administration
IPT	Isosymmetric Phase Transition
IR	Infrared Spectroscopy
MBD	Many-Body Dispersion
PXRD	Powder X-ray Diffraction
QHA	Quasi-Harmonic Approximation
SCXRD	Single-Crystal X-ray Diffraction
TS	Tkatchenko–Scheffler
XRD	X-ray Diffraction
ZPE	Zero-Point Energy

4. Introduction and justification of the research topic

4.1. Molecular crystals and polymorphism

Molecular crystals are a large class of solid-state materials wherein the crystal lattice is composed of distinct molecules connected by a network of non-covalent intermolecular interactions. The interactions, including hydrogen bonds, van der Waals forces, π–π stacking, and electrostatic interactions, determine the molecular arrangement within the crystal and ultimately define its structural and physicochemical properties. Molecular crystals, in contrast to covalently bonded materials, are characterised by relatively weak and strongly directed interactions, which contribute to their structural flexibility as well as susceptibility to external factors like temperature and pressure. **Figure 1** shows a representative example of polymorphism in molecular crystals, illustrating the crystal structures of L-serine polymorphs I and IV and the differences in hydroxyl-group orientation between them.

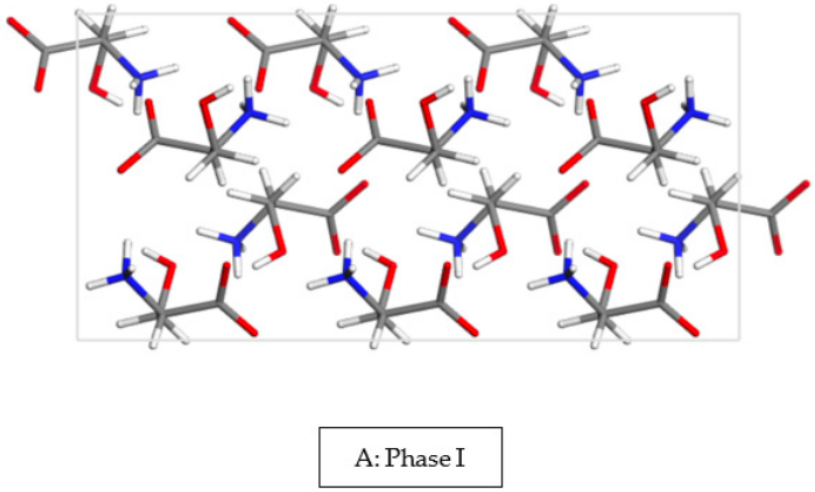

Figure 1. *Unit cells of L-serine (A) phase I and (B) phase IV. Gray: carbon, blue: nitrogen, red: oxygen, white: hydrogen.*

A key consequence of this structural diversity is polymorphism, defined as an ability of a compound to crystallise in more than one unique crystal structure while retaining the same chemical composition [1,2]. Polymorphic forms arise from distinct molecular configurations inside the crystal lattice and may differ in packing efficiency, intermolecular interaction patterns, and molecular conformation. Consequently, polymorphs of the same molecule may have significantly diverse physical properties, such as melting point, density, solubility, and mechanical behaviour [3,4].

Polymorphism is especially important in organic and pharmaceutical compounds, where minor alterations in crystal packing can lead to substantial differences in functional performance. A well-known example is the case of ritonavir, where the unforeseen formation of a more stable polymorphic form that was significantly less soluble, led to the need to change the formulation of the medicinal product [5]. This example demonstrates the crucial role of comprehensive polymorph screening and control in pharmaceuticals development and production, as the existence of unfavourable polymorphs could affect both the efficacy and stability of a drug.

From a thermodynamic perspective, polymorphic forms vary in their relative stability, determined by the correlation between enthalpic and entropic contributions to the Gibbs free energy. The most stable polymorph under particular conditions corresponds to the global minimum of free energy, but metastable forms may persist due to kinetic considerations, particularly nucleation barriers or slow transformation rates [6]. The transitions between polymorphic forms can be triggered by changes in external conditions, such as temperature or pressure, resulting in structural rearrangements within the crystal lattice. These solid-state transformations are crucial in determining the stability and performance of crystalline solids, particularly in pharmaceutical systems where solid-form control is essential for ensuring the quality, efficacy, and stability of drug substances.

Polymorphism presents the delicate balance between molecular conformation, intermolecular interactions, and thermodynamic stability in crystalline solids. Even minor structural alterations can result in the formation of distinct solid forms with substantially different physicochemical properties. A comprehensive understanding of polymorphism is crucial for predicting solid-state behaviour and managing the stability of molecular crystals.

4.2. Phase transitions in molecular crystals

Phase transitions in molecular crystals represent a fundamental phenomenon in solid-state chemistry, as they directly influence the structural stability and physicochemical properties of

crystalline solids. A phase transition occurs when a crystal shifts from one solid phase to another due to external factors such as temperature, pressure, mechanical stress, or irradiation. These transformations might involve alterations in molecular arrangement, unit-cell dimensions, intermolecular interactions, molecular conformation, or crystal symmetry, frequently leading to substantial modifications in macroscopic properties such as density, solubility, compressibility, and thermal behaviour [2]. Consequently, phase transitions are notably common and typically have a significant sensitivity to external factors.

The classical thermodynamic classification of phase transitions was established by Ehrenfest and further developed through Landau theory. This approach categorises phase transitions into first-order and second-order transitions. First-order transitions are defined by discontinuities in the first derivatives of Gibbs free energy, including entropy and volume, and are usually linked to latent heat, hysteresis, and phase coexistence. Examples include melting, sublimation, and multiple polymorphic transitions in molecular crystals. On the contrary, second-order transitions include discontinuities in the second derivatives of Gibbs free energy, including heat capacity or compressibility, and occur continuously without latent heat [7].

Phase transitions may also be classified from a crystallographic perspective based on their structural mechanisms. Displacive transitions include minor atomic or molecular displacements while typically maintaining the connectivity of the crystal structure, whereas reconstructive transitions involve a breakdown and restoration of intermolecular interactions and are linked to higher activation barriers. Order-disorder transitions result from alterations in molecular orientation or occupational disorder, whereas martensitic transformations include cooperative lattice distortions without diffusion [8].

The study of phase transitions in molecular crystals requires both experimental and computational methods. Single-crystal (SCXRD) and powder X-ray diffraction (PXRD) are basic techniques used for structural description, enabling accurate assessment of lattice changes in molecular packing, and symmetry relationships. Raman and infrared spectroscopy (IR) have very high sensitivity to hydrogen-bond rearrangements and structural alterations, often revealing subtle transformations that are not easily visible in diffraction data. Differential scanning calorimetry (DSC) yields thermodynamic evidence through enthalpic anomalies, whereas variable-pressure and variable-temperature studies enable direct observation of transition pathways. In recent years, periodic density functional theory (DFT) calculations have become widely recognised as a key tool for providing insight into experimental findings and predicting transition mechanisms, particularly in systems characterised by small energy differences between phases [9].

4.3. Isosymmetric phase transitions in molecular crystals

Isosymmetric phase transitions (IPTs) represent a relatively uncommon and especially intriguing class of solid-state transformations characterised by structural rearrangements occurring without changes in crystallographic symmetry. As compared to conventional polymorphic transitions, which typically involve a change in space group, IPTs maintain the same crystallographic space group throughout the transition. Despite this apparent preservation of symmetry, significant modifications might be observed in molecular conformation as well as intermolecular interactions, unit-cell parameters, molecular orientation, and hydrogen-bond topology, often resulting in noticeable changes in physical and functional properties. The exceptional combination of lack of space group change with structural alterations makes IPTs especially challenging to identify and analyse, particularly in molecular crystals where weak intermolecular interactions determine phase stability [9].

Due to the absence of symmetry reduction, identifying IPTs using traditional crystallographic criteria is often difficult. They do not display traditional signs such as superlattice reflections, or noticeable discontinuities in diffraction patterns. The transition is typically identified by small discontinuities in lattice parameters, anisotropic compressibility, abrupt changes in unit-cell volume, or changes in vibrational spectra [10]. In multiple cases, the preservation of space group symmetry may initially suggest absence of a meaningful phase transition, whereas comprehensive structural study exposes significant molecular rearrangements. Consequently, IPTs often involve the integrated interpretation of diffraction data, vibrational spectroscopy, and periodic DFT calculations.

Representative examples reported in the literature show that IPTs can originate from very distinct structural and thermodynamic mechanisms. Despite the lack of change of crystallographic symmetry, the underlying driving forces for these transformations may involve subtle conformational rearrangements, reorganization of hydrogen-bond networks, alterations in molecular packing efficiency, or the balance between enthalpic and entropic effects influencing phase stability. These systems demonstrate that the lack of symmetry breaking does not indicate structural equivalence, and that in-depth analysis is necessary to determine the true origin of the transition [11].

A noteworthy example is the pressure-induced IPT in biurea, where neutron diffraction and Raman spectroscopy showed a significant intramolecular reorientation accompanied by a sharp reduction in unit-cell volume. Computational study results indicated that the low-pressure

phase is stabilised by zero-point energy (ZPE) and entropy, while elevated pressure favours the high-pressure phase through a volume decrease [12,13].

Another representational example is α-glycylglycine, in which a high-pressure IPT was described through integrated experimental and theoretical studies. The transition was closely linked with alterations in hydrogen-bond geometry and molecular orientation, highlighting the significance of intermolecular interactions in determining phase stability in molecular crystals [14].

Resorcinol is a representative example among classical molecular crystals, as its α and β polymorphs crystallise in the same space group ($Pna2_1$) despite significant differences in molecular packing and hydroxyl-group orientation [15–18]. This indicates that lack of change in crystallographic symmetry does not necessarily imply structural equivalence, demanding a thorough study of intermolecular interactions to differentiate distinct isosymmetric phases. A comparable phenomenon has been reported in amino acid crystals like L-serine, where pressure-induced transitions are significantly influenced by vibrational entropy and minor alterations in the hydrogen-bond network [19–22]. In these systems, phase stability is determined by both lattice energy and dynamic and entropic factors, complicating the interpretation of isosymmetric transitions.

These examples demonstrate that IPTs may be determined by several thermodynamic factors, such as enthalpic stabilisation, vibrational entropy, conformational flexibility, and alterations in hydrogen-bond geometry. As a result, investigating the origin of isosymmetric phase transitions often demands an integrated use of diffraction techniques, vibrational spectroscopy, and periodic DFT calculations.

4.4. Structural and thermodynamic aspects of isosymmetric phase transitions

The interpretation of IPTs requires a comprehensive study of both thermodynamic stability and structural rearrangements, as the driving forces behind these transformations are typically subtle and cannot be defined solely from conventional crystallographic observations. In molecular crystals, even minor changes in molecular conformation, intermolecular contacts, or hydrogen-bond geometry can have a substantial impact on phase behaviour and result in the stabilisation of distinct phases in response to changing external conditions.

Structurally, IPTs are typically linked to cooperative although minor molecular displacements, including molecular rotations, reorientation of functional groups, or changes in donor–acceptor distances within hydrogen-bond networks. Despite seeming minor in atomic

coordinates, these distortions may profoundly affect macroscopic properties, such as compressibility, thermal expansion, dielectric response, and mechanical stability. The absence of symmetry change should not be regarded as a lack of structural importance, as IPTs may nonetheless lead to significant functional outcomes despite their subtle crystallographic signature [23].

From a thermodynamic perspective, the stability of competing phases is described by the Gibbs free energy:

$$G = H - TS$$

where the balance between enthalpy and entropy determines the favoured phase under specific external conditions. In numerous IPTs, the energy differences between competing structures are minimal, making precise prediction particularly difficult. Under pressure, a denser packing and reduced molar volume may favour one phase enthalpically, whereas under ambient conditions, another structure may remain thermodynamically favoured due to entropic stabilisation [24].

Significantly, not all pressure-induced IPTs are primarily determined by enthalpic effects. In many molecular systems, vibrational and configurational entropy play a crucial role in phase stability, especially in flexible hydrogen-bonded crystals where lattice vibrations and molecular liberations substantially affect the free energy landscape. Therefore, static lattice energy alone is usually insufficient to account for experimentally observed transitions, requiring the inclusion of vibrational contributions for accurate thermodynamic interpretation. This is one of the primary reasons why predicting polymorphism and phase stability in molecular crystals continues to be particularly challenging [24,25].

IPTs in molecular crystals are generally classified as first-order transitions due to their characteristic discontinuities in unit-cell volume, abrupt changes in lattice parameters, hysteresis, and the coexistence of phases within a narrow pressure or temperature range. The transition is typically linked to an inversion of thermodynamic stability between two closely similar structures differentiated by a finite energy barrier, rather than a continuous structural change [23].

For this reason, the integration of diffraction techniques, vibrational spectroscopy, calorimetric analysis, and computational modelling is necessary in order to get a reliable characterisation of IPTs.

4.5. Computational approaches to phase transitions: periodic DFT methods

Periodic DFT calculations have become one of the standard tools for investigating solid-state phase transitions as they enable the comparison of relative lattice energies, pressure-dependent stability, vibrational contributions, and potential transition pathways. It is only through the combination of theoretical modelling and experimental observations that it is possible to fully understand the true origin of the transformation and the mechanism of phase stability.

In contrast to molecular quantum-chemical calculations carried out on isolated molecules, periodic DFT incorporates the infinite repetition of the crystal lattice through periodic boundary conditions and facilitates the concurrent optimisation of atomic positions and unit-cell parameters [26]. This enables precise modelling of structural distortions, hydrogen-bond reconfigurations, and pressure-dependent shifts in crystal packing, along with quantitative comparisons of competing polymorphic forms. This approach is especially valuable when diffraction experiments reveal only subtle structural changes and when the energetic relationship between phases requires direct thermodynamic analysis.

A significant advantage of periodic DFT is its ability to directly compare the relative lattice energy of polymorphs and competing crystal phases. Due to the fact that several solid-state transformations are determined by energy differences of only a few $kJ \cdot mol^{-1}$, a precise characterisation of weak intermolecular forces is necessary. In molecular crystals, dispersion interactions significantly contribute to phase stability, and inadequate consideration of these interactions may result in inaccurate energy ordering of polymorphs. Consequently, dispersion-corrected approaches, like Grimme's methods, the Tkatchenko–Scheffler (TS) scheme, and many-body dispersion (MBD) models, are commonly utilised in crystal structure investigations, strengthening the accuracy of phase-stability predictions [27,28].

Periodic DFT is especially valuable for examining pressure-induced phase transitions, as external pressure may be directly introduced into structural optimisation, which enables the simulation of compression-dependent alterations in the crystal lattice. In addition to static energy calculations, vibrational analysis offers deeper understanding of the thermodynamic behaviour of crystalline phases. Phonon calculations enable the assessment of ZPE, vibrational entropy, and temperature-dependent Gibbs free energy under the quasi-harmonic approximation (QHA). These contributions are typically considered critical in molecular crystals due to the minimal enthalpic differences between competing phases. In some systems, entropy, rather than enthalpy, is identified as the main determinant of phase stability, which cannot be described

by only static lattice energy calculations. The incorporation of phonon contributions is crucial for the precise prediction of temperature-dependent phase transitions and for comprehending entropy-driven transformations [29].

Another important application of periodic DFT is the comparison and interpretation of experimental vibrational spectra obtained from Raman and IR spectroscopy with calculated spectra. The interpretation of experimentally observed band shifts, splitting, or intensity changes during phase transitions is significantly enhanced by the ability to assign individual vibrational modes to specific molecular motions and intermolecular interactions, which is facilitated by calculated spectra. This is especially useful in hydrogen-bonded crystals, as the vibrational region associated with O–H, N–H, and lattice modes is directly associated with changes in hydrogen-bond geometry. Therefore, spectroscopic analysis enabled by periodic DFT provides evidence of structural rearrangements, even when crystallographic changes are challenging to resolve unambiguously.

Periodic DFT, despite its extensive applicability, also has significant limitations. The results' precision is significantly influenced by the selection of the exchange–correlation functional, dispersion correction scheme, basis set, and pseudopotentials. The predicted phase stability may be significantly influenced by minor methodological differences, particularly when the energy of competing structures is only slightly different. Furthermore, structural disorder, solvent-mediated transformations, kinetic barriers, and anharmonic effects are frequently challenging to accurately describe using conventional DFT methods. This is the reason why computational results should be interpreted in combination with experimental observations, rather than being treated as independent proof of phase behaviour. Therefore, crystal structure prediction requires careful validation against experimental data in addition to theoretical precision [30].

4.6. Relevance of polymorphism and phase transitions in pharmaceutical sciences

Polymorphism continues to be one of the most significant solid-state phenomena in the field of pharmaceutical sciences, as distinct crystalline forms of the same active pharmaceutical ingredient (API) can exhibit significantly different physicochemical properties despite having identical chemical compositions. Parameters such as solubility, dissolution rate, melting point, mechanical behaviour, and chemical stability are directly influenced by variations in crystal structure. These parameters, in turn, affect bioavailability, manufacturability, storage conditions, and therapeutic performance. This is why the identification and regulation of solid

forms are essential during the development of pharmaceuticals and regulatory evaluation [31,32].

It is particularly evident that polymorphism is of practical importance during the development of formulations and industrial production. Even minor structural differences can result in significant variations in powder flowability, compressibility, tablet hardness, or moisture sensitivity. Therefore, comprehensive polymorph screening is essential in the initial phases of drug development to prevent unwanted solid-form transformations during production, storage, or transportation. Regulatory bodies like the Food and Drug Administration (FDA) and European Medicines Agency (EMA) mandate comprehensive characterisation of polymorphic forms, as uncontrolled phase transitions could compromise product quality, reproducibility, and patient safety [33–35].

A well-known example is ritonavir, an antiretroviral medication whose marketed formulation was withdrawn following the unexpected formation of a more stable yet substantially less soluble polymorph, referred to as Form II. This newly emerged form exhibited considerably reduced dissolution and bioavailability, making the batch unsuitable for therapeutic use [36,37]. The ritonavir case exemplifies that insufficient comprehension of polymorphism can result in significant scientific challenges as well as substantial clinical and economic consequences. It clearly established polymorph control as an essential element of pharmaceutical development.

In pharmaceutical manufacturing and storage, solid forms may undergo phase transitions due to temperature, humidity, pressure, or mechanical stress. These transformations involve polymorphic conversions, hydrate–anhydrate transitions, amorphization, and pressure-dependent structural rearrangements, all of which might compromise the stability and reproducibility of the final dosage form. Compression in tableting is crucial as localised pressure can induce structural changes not seen under normal conditions, affecting both manufacturability and the long-term efficacy of the product. Computational methods have therefore become of importance in pharmaceutical solid-state research as they enable the prediction and interpretation of phase stability prior to performing large-scale work. Periodic DFT calculations, crystal structure prediction, and lattice energy analysis facilitate the identification of the most stable polymorphs and the estimation of the probability of transitions induced by pressure or temperature. Integrating experimental and computational approaches mitigates the likelihood of unexpected polymorphs formation in late stages of drug development [38,39].

The significance of IPTs in pharmaceutical sciences is less frequently directly addressed than traditional polymorphism, yet it hold equal importance. Due to the lack of clearly visible crystallographic indicators, these transformations might pass undetected during standard solid-form screening. Nonetheless, minor alterations in molecular conformation and hydrogen-bond topology can still lead to significant variations in physicochemical properties. Consequently, the study of IPTs extends beyond pure crystallography and is directly relevant to pharmaceutical quality control, facilitating the development of safer, more stable, and more effective pharmaceutical formulations.

5. Overview of publications

5.1. Publication No. 1

Mazurek, A. M., Franczak-Rogowska, M., Szeleszczuk, Ł. (2025).

Isosymmetric Phase Transitions in Crystals: From Subtle Rearrangements to Functional Properties.

Crystals, *15*(9), 807. https://doi.org/10.3390/cryst15090807

This review article aimed to organise the current knowledge on IPTs in crystalline materials. The key objective was to explain their characteristics, structural and thermodynamic complexity, experimental identification, and the relevance of molecular modelling methods in their analysis.

Representative examples from the literature, including biurea, α-glycylglycine, chlorothiazide, and L-histidine [12,14,40,41], demonstrated that the absence of symmetry breaking does not imply structural equivalence. These transformations are typically governed by subtle cooperative rearrangements, including molecular rotations, functional group reorientation, and alterations of hydrogen bond networks. Despite their seemingly minor character, these alterations can significantly influence macroscopic properties and thermodynamic behaviour. The analysis indicated that the stability of competing phases relies on the balance between enthalpic and entropic contributions to Gibbs free energy, confirming the first-order transition behaviour.

A significant aspect of the review focused on periodic DFT calculations as a method for analysing IPTs in molecular crystals. Periodic DFT facilitates the comparison of relative lattice energies, the simulation of pressure-dependent structural alterations, phonon computations, and the analysis spectroscopic data. The primary conclusion is that accurate identification and prediction of subtle solid-state transformations require a comprehensive methodological approach integrating experimental observations with advanced computational techniques. This publication established the conceptual and methodological foundation for the subsequent original studies included in the dissertation.

5.2. Publication No. 2

Mazurek, A. M., Franczak-Rogowska, M., Szeleszczuk, Ł. (2025).

Predicting the Pressure-Induced Isosymmetric Phase Transition of Sulfamic Acid by Applying Periodic Density Functional Theory Calculations.

Applied Sciences, *15*(8), 4185. https://doi.org/10.3390/app15084185

Sulfamic acid is a model system for studying pressure-induced IPTs due to its previously documented high-pressure behaviour, described as a reversible transformation occurring around 10 GPa . Experimental Raman spectroscopy and synchrotron X-ray diffraction (XRD) indicated that this transition is linked to the reconfiguration of the hydrogen-bond network, a discontinuous contraction of the c-axis, and enhanced crystal packing [42]. These observations established sulfamic acid as an excellent system for assessing the effectiveness of periodic DFT methods in identifying and predicting pressure-induced IPTs.

Although compression of the lattice was reproduced correctly, during geometry optimization of both phases under increasing pressure, direct optimization did not result in the spontaneous transformation to the expected high-pressure phase. This revealed a presence of a finite energetic barrier between the two structures and indicated that the transition could not be explained solely by static lattice optimization alone, which is characteristic of first-order transition behaviour.

The comparison of theoretical and experimental Raman spectra strongly supported the computational model, especially regarding the NH_3^+ stretching and deformation modes, which are sensitive to hydrogen-bond rearrangement. The correlation between calculated and experimental spectra validated the accuracy of the high-pressure structure and indicated that the transition is linked to the reorganisation of intermolecular interactions rather than simple elastic compression. **Figure 2** shows that the pressure dependence of the NH_3^+-associated vibrational modes distinctly indicates these subtle structural alterations and provides direct spectroscopic evidence of cooperative molecular reconfiguration during the phase transition.

Ab initio molecular dynamics (aiMD) simulations demonstrated that the transition entails a cooperative rearrangement of hydrogen-bonded chains and a collective motion of NH_3^+ and SO_3^- groups, rather than merely a localised conformational alteration. This clarified why geometry optimisation alone was insufficient to replicate the transition and shows that dynamic effects are crucial for understanding pressure-induced IPTs.

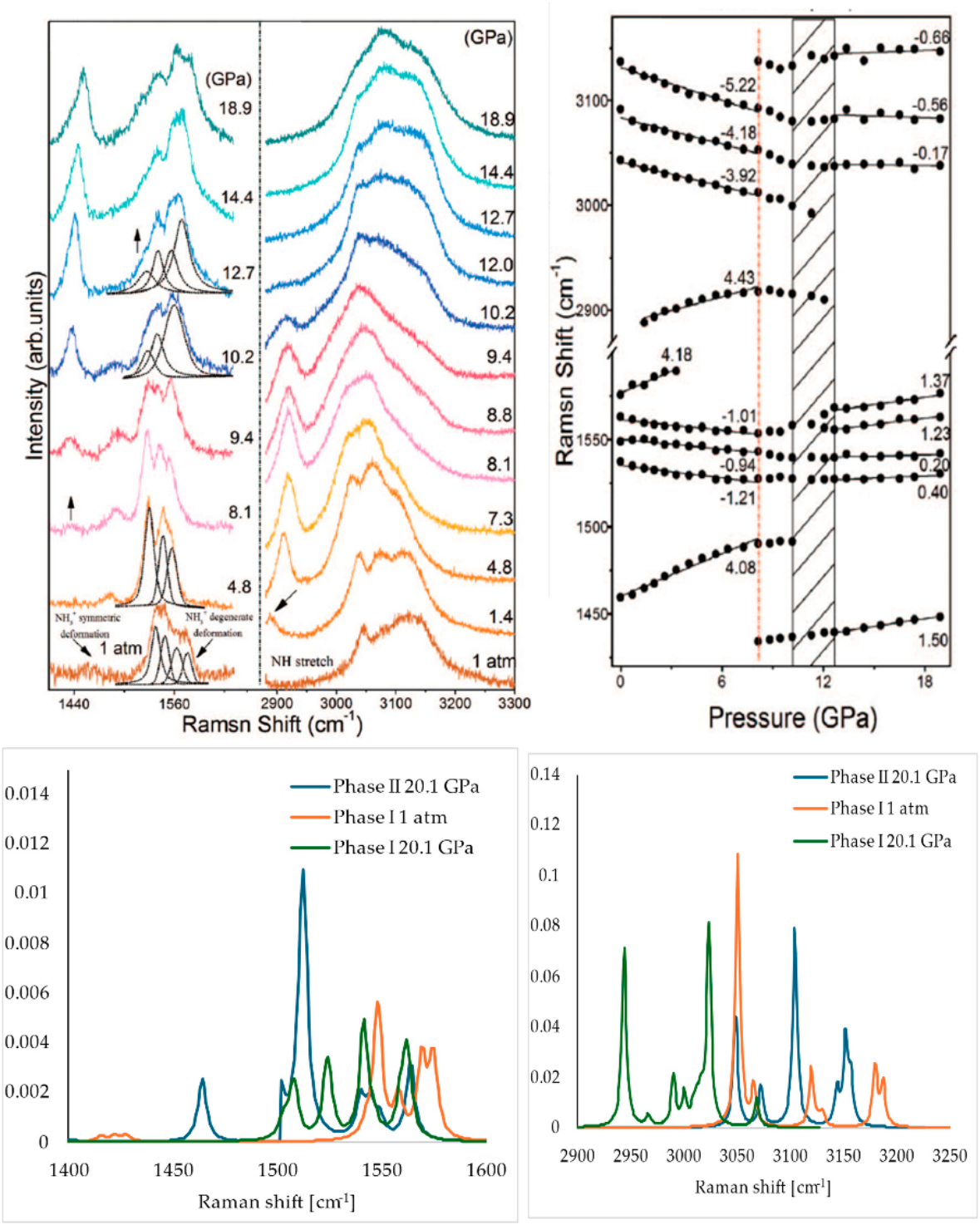

Figure 2. *Comparison of experimental (top) (recorded in the pressure range 1 atm–18.9 GPa) and theoretical (bottom) (calculated at 1 atm and 20.1 GPa) Raman spectra of SA. Reprinted from [42], with the permission of AIP Publishing.*

5.3. Publication No. 3

Mazurek, A. M., Franczak-Rogowska, M., & Szeleszczuk, Ł. (2026).

Periodic DFT Investigation of Isosymmetric Alpha–Beta Phase Transition in Resorcinol Under Ambient and High Pressure.

Crystals, *16*(3), 215. https://doi.org/10.3390/cryst16030215

Resorcinol is a classical example of isosymmetric polymorphism in molecular crystals, as its α and β polymorphs crystallise in the identical space group, $Pna2_1$, while exhibiting substantial differences in molecular configuration, hydroxyl-group orientation, and hydrogen-bond topology. Previous experimental investigations revealed that the α and β forms exhibit differences in stability and physical properties despite their crystallographic similarities, making this system particularly significant for understanding the structural and thermodynamic aspects of IPTs. [15,17]

Geometry optimisation of both polymorphs using periodic DFT calculations demonstrated strong agreement with crystallographic data and verified that the primary structural differences between the two forms originate from the orientation of hydroxyl groups and resulting hydrogen-bond network. **Figure 3** shows that the crystal structures of the α and β polymorphs illustrate how minor alterations in hydroxyl-group configuration and intermolecular interactions result in unique packing motifs.

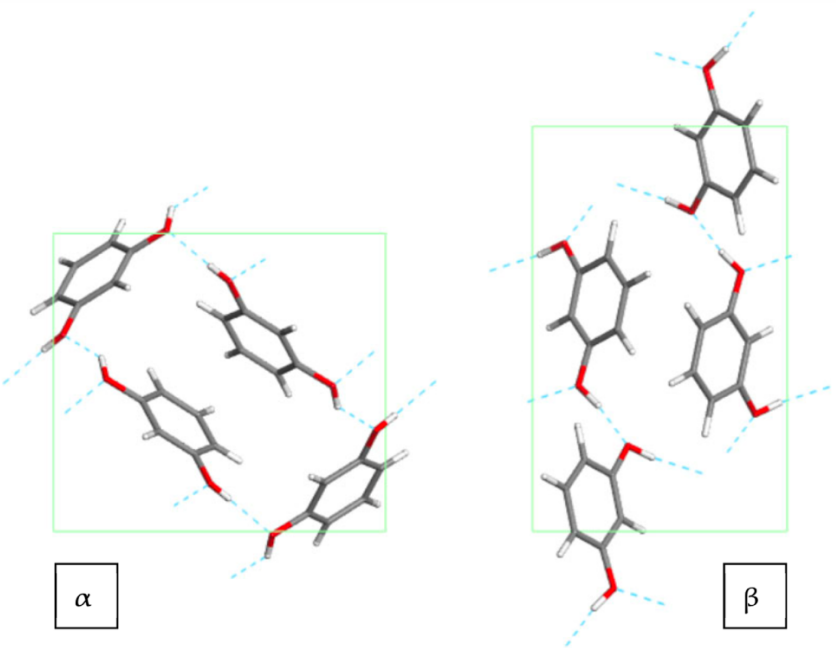

Figure 3. *Crystal structures of α and β polymorphs of resorcinol*

The main focus was the analysis of relative lattice energies and their dependence on pressure. At ambient conditions, the α form was determined to be thermodynamically favoured, whereas increasing pressure progressively lowered the energy difference between the two phases. This outcome confirmed the interpretation of the α–β relationship as an IPT.

Further analysis of intermolecular interactions revealed that pressure influences not only packing efficiency but also the balance between O–H···O hydrogen bonds and weaker intermolecular interactions. The reorganisation of these interactions under compression explains the pressure dependence of phase stability and shows that the transformation is determined by a subtle interplay between enthalpic and entropic factors.

5.4. Publication No. 4

Mazurek, A. M., Franczak-Rogowska, M., & Szeleszczuk, Ł. (2026).

Entropy-Driven Isosymmetric Phase Transition in L-Serine under Pressure: A Periodic DFT Study.

Crystals, *16*(4), 266. https://doi.org/10.3390/cryst16040266

Experimental studies showed L-serine undergoes multiple reversible polymorphic transitions under compression, including the IPT between Phase I and Phase IV. This transformation primarily involves the reorientation of hydroxyl groups and alteration of the hydrogen-bond network, exemplifying a subtle pressure-induced transition driven by local structural changes [43].

Geometry optimisation performed at ambient pressure and 8.8 GPa effectively replicated lattice compression and the pressure-induced stabilisation of Phase IV. Nonetheless, no spontaneous reorientation of the hydroxyl groups was detected during static optimisation, suggesting that the transition cannot be characterised solely within a static enthalpic framework. A series of modified crystal structures with different hydroxyl-group orientations was generated and analysed to further understand this behaviour. The calculations indicated a complex energy landscape at ambient conditions, which was notably simplified under compression, implying that pressure reduces the energetic cost linked to hydrogen-bond rearrangement.

A key finding of the study was derived from phonon calculations utilising the QHA. The calculations indicated that the experimentally observed Phase I structure is stabilised not by enthalpy, but by vibrational entropy, which increases with temperature. At ambient conditions, entropy balances the unfavourable lattice energy, leaving Phase I thermodynamically favoured; however, under pressure, the enthalpic stabilisation of Phase IV dominates. This demonstrated that the transformation is entropy-driven and cannot be described solely by static lattice energy.

Figure 4, which illustrates the pressure dependence of relative enthalpy, entropy contribution, and Gibbs free energy for both phases, is the essential figure of this study as it describes the mechanism of phase stabilisation and clarifies the favoured position of the experimentally observed structure under varying thermodynamic conditions. It provides the evidence that vibrational effects are crucial for understanding phase stability in L-serine.

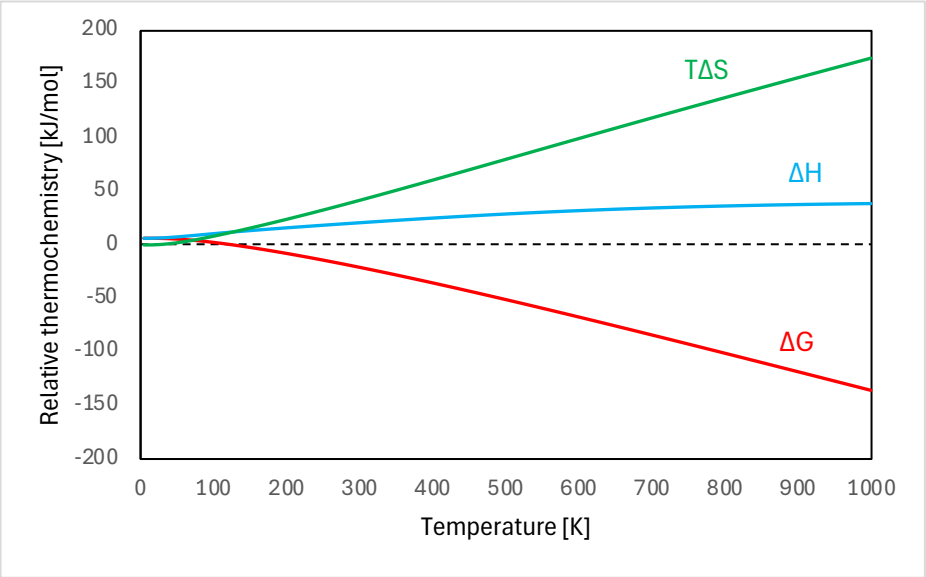

Figure 4. *Differences (Phase I–Phase IV) between the thermodynamic parameters: Gibbs free energy (ΔG), enthalpy (ΔH), and temperature times entropy (TΔS) of the structures modelled using PBE TS functional at 8.8 GPa, with respect to the temperature. The zero reference corresponds to the equal values of thermodynamic properties of Phase I and IV.*

6. Aim of the thesis

The first objective of this dissertation was to identify and characterise IPTs in selected molecular crystals. Through a literature analysis and review of the well described molecular systems demonstrating IPTs, representative compounds, namely sulfamic acid, resorcinol, and L-serine, were chosen for further investigation.

The second objective was to understand the molecular mechanisms underlying isosymmetric phase transitions, focusing specifically on the influence of hydrogen-bond rearrangement, molecular conformation, packing efficiency, and pressure-induced lattice compression. Given that IPTs are determined by small energetic differences between competing phases, particular emphasis was placed on the balance between enthalpic and entropic contributions to Gibbs free energy, as well as on identifying the factors that stabilise individual phases under diverse thermodynamic conditions.

Another objective was to verify the effectiveness of molecular modelling in identifying and interpreting IPTs. Periodic DFT calculations were employed to assess the reliability of computational methods in reproducing experimentally observed transitions, predicting transition pressure, and explaining the thermodynamic basis of phase stability. Particular focus was set on the importance of dispersion corrections, phonon calculations, vibrational entropy, and aiMD in systems where static lattice energy alone was insufficient for accurate interpretation.

The final objective was to develop a computational method that facilitates more accurate predictions of IPTs in molecular crystals. The proposed methodology was based on periodic DFT calculations to identify competing isosymmetric phases, assess their relative thermodynamic stability, and predict transition conditions. This work attempted to establish a methodological framework for examining subtle solid-state transformations and enhancing the prediction of polymorphic behaviour in molecular crystals through the integration of structural optimisation, lattice energy analysis, phonon calculations, and vibrational studies.

7. Proposed methodological framework for identification and prediction of IPTs

The obtained results enabled a development of a proposal of practical methodological framework for identification and prediction of IPTs in molecular crystals using periodic DFT calculations. The proposed approach begins with periodic DFT geometry optimisation of structurally related phases across a wide pressure spectrum, utilising suitable dispersion corrections. This stage facilitates precise replication of experimental crystal structures, examination of pressure-induced alterations in unit-cell parameters, and assessment of packing efficiency and hydrogen-bond geometry. Furthermore, relative lattice energies and enthalpy differentials among competing phases are computed as a function of pressure, facilitating the identification of thermodynamic stability inversion and the estimation of transition pressure. This step establishes the essential foundation for identifying IPTs. When the existence of competing isosymmetric phases is not evident from experimental data, the methodology may be extended by generating structural models with different functional-group orientations, allowing the identification of hidden metastable phases and a more reliable prediction of possible transition pathways.

The next stage of the framework involves vibrational analysis, which is particularly important in systems where geometry optimization alone does not fully explain the experimentally observed transformation. Phonon calculations provide detailed information about lattice dynamics, intermolecular vibrations, and hydrogen-bond rearrangements, allowing identification of subtle structural changes that may not be clearly observable in diffraction experiments. Furthermore, phonon calculations utilising the QHA facilitate the assessment of ZPE, vibrational entropy, and Gibbs free energy. This is crucial for systems where entropy plays a significant role in phase stability, as evidenced by L-serine, where the experimentally observed ambient-pressure phase was primarily stabilised by vibrational entropy rather than by static enthalpy.

The final stage includes aiMD simulations to account for scenarios where finite energetic barriers block direct structural transformation during static optimisation. This enables the examination of cooperative molecular dynamics and transition pathways that cannot be captured within static framework. The investigation of sulfamic acid revealed that pressure-induced IPT involves a collective reorganisation of hydrogen-bonded chains and concerted

motion of the molecular fragments, rather than just local distortion, hereby explaining why geometry optimisation alone was insufficient.

The integration of structural optimisation, pressure-dependent thermodynamic analysis, vibrational investigations, and dynamic simulations establishes an effective computational framework for identifying and potentially predicting IPTs. This framework could be utilised to conduct research on pharmaceutical systems, where the stability and manufacturability of APIs may be affected by unforeseen IPTs.

8. Summary and Conclusions

The dissertation investigated IPTs in molecular crystals. Such transitions represent one of the most challenging classes of solid-state phenomena, as maintaining of the same space group may suggest structural continuity despite significant molecular rearrangements. The findings of this study confirm that the lack of symmetry breaking does not necessarily correspond to structural equivalence, and that minor alterations in hydrogen-bond topology, molecular orientation, and packing efficiency can result in distinct thermodynamic phases with varying stability and functional characteristics.

The studies conducted on sulfamic acid, resorcinol, and L-serine indicated that IPTs should be considered as genuine first-order phase transitions instead of insignificant distortions within a crystal structure.

An analysis of sulfamic acid revealed that pressure-induced IPT arises from a thermodynamic stability inversion between two crystalline structures. The transformation observed experimentally at approximately 10 GPa was effectively described through pressure-dependent lattice energy calculations, supported by Raman spectroscopy and aiMD. While direct geometry optimisation did not spontaneously create the high-pressure phase, the integrated computational method indicated that the transition includes a cooperative reconfiguration of hydrogen-bonded chains and a collective movement of NH_3^+ and SO_3^- groups, rather than mere elastic compression. This indicated that static structural optimisation alone is insufficient for the reliable prediction of IPTs.

Resorcinol served as a significant model for isosymmetric polymorphism at ambient conditions. The α and β polymorphs crystallise in the same space group, $Pna2_1$, but present significant differences in the orientation of hydroxyl groups and the topology of hydrogen bonds. Periodic DFT calculations indicated that the fundamental structural variations originated from subtle reconfigurations of intermolecular interactions rather than significant molecular deformation. Elevated pressure progressively reduced the energetic preference of the α form, validating the interpretation of the α–β relationship as a model of isosymmetric polymorphism.

The investigation of L-serine provided the most significant thermodynamic conclusion of this dissertation. Calculations of static lattice energy indicated incorrect phase stability, while phonon calculations using the QHA revealed that the experimentally observed phase at ambient pressure is stabilised by vibrational entropy. Under compression, the enthalpic stabilisation of the denser high-pressure phase dominates. This demonstrated that the transformation is entropy-driven and that a comprehensive Gibbs free energy analysis is essential for accurate

interpretation of phase stability, rather than relying solely on enthalpy comparisons. The findings confirmed that vibrational contributions could be critical for IPTs in flexible hydrogen-bonded molecular crystals.

A consistent conclusion from all three studied systems is the dominant role of hydrogen-bond reorganisation in determining IPTs. The transformations were not caused by significant reconstructive alterations of the crystal lattice, but by subtle cooperative rearrangements concerning functional group reorientation, donor–acceptor distances, molecular rotations, and packing efficiency. These relatively minor local changes resulted in substantial macroscopic effects, involving discontinuities in compressibility, pressure response, and thermodynamic stability. This demonstrates that weak intermolecular interactions in molecular crystals can influence phase behaviour as significantly as the covalent structure itself, and that IPTs should be considered genuine first-order phase transitions rather than insignificant distortions within a single crystal structure.

This work demonstrated the significant predictive capability of periodic DFT calculations in an analysis of molecular-crystal phase transitions. Dispersion-corrected structural optimisation, pressure-dependent lattice energy calculations, vibrational analysis, Raman spectrum simulation, phonon calculations, and molecular dynamics provided a solid foundation for explaining experimentally observed transformations. The results confirmed that no single method is sufficient independently. Static lattice energies alone can lead to incorrect results, hence, accurate prediction of phase stability requires a combined investigation of structural, thermodynamic, vibrational, and dynamic factors.

A significant result was the proposal of a methodological framework for identifying and predicting isosymmetric phase transitions in molecular crystals. The proposed methodology incorporates pressure-dependent periodic DFT optimisation, phonon calculations, and aiMD.

In conclusion, this work demonstrates that IPTs constitute a significant and often underestimated class of polymorphic transformations. Their interpretation requires moving beyond crystallographic symmetry as the main determinant of phase identity and focusing on the balance between enthalpic and entropic contributions, hydrogen-bond cooperativity, and pressure-dependent free energy patterns. The findings for sulfamic acid, resorcinol, and L-serine indicate that periodic DFT methods, when combined with experimental data, serve as an effective instrument for understanding these transformations. Moreover, the dissertation confirms that vibrational entropy and intermolecular interactions are often the decisive factors controlling phase stability in molecular crystals, providing both fundamental insight into IPTs and practical guidance for future studies of this phenomena.

9. References

1. Cruz-Cabeza, A.J.; Reutzel-Edens, S.M.; Bernstein, J. Facts and Fictions about Polymorphism. *Chem. Soc. Rev.* **2015**, *44*, 8619–8635, doi:10.1039/C5CS00227C.

2. Bernstein, J. *Polymorphism in Molecular Crystals*; Oxford University Press, 2002; ISBN 978-0-19-923656-5.

3. Newman, A.W.; Byrn, S.R. Solid-State Analysis of the Active Pharmaceutical Ingredient in Drug Products. *Drug Discovery Today* **2003**, *8*, 898–905, doi:10.1016/S1359-6446(03)02832-0.

4. Jurczak, E.; Mazurek, A.H.; Szeleszczuk, Ł.; Pisklak, D.M.; Zielińska-Pisklak, M. Pharmaceutical Hydrates Analysis—Overview of Methods and Recent Advances. *Pharmaceutics* **2020**, *12*, 959, doi:10.3390/pharmaceutics12100959.

5. Bauer, J.; Spanton, S.; Henry, R.; Quick, J.; Dziki, W.; Porter, W.; Morris, J. Ritonavir: An Extraordinary Example of Conformational Polymorphism. *Pharm Res* **2001**, *18*, 859–866, doi:10.1023/A:1011052932607.

6. Yu, L. Inferring Thermodynamic Stability Relationship of Polymorphs from Melting Data. *Journal of Pharmaceutical Sciences* **1995**, *84*, 966–974, doi:10.1002/jps.2600840812.

7. Rietveld, I.B. Solid-Solid Phase Transitions between Crystalline Polymorphs of OrganicMaterials. *CPD* **2023**, *29*, 445–461, doi:10.2174/1381612829666221221114459.

8. Peng, J.; Zhang, S.; Refson, K.; Dove, M.T. Unique Features of the Structural Phase Transition in Acetylene Showing Simultaneous Characteristics of Reconstructive, Displacive and Order–Disorder. *Phys. Chem. Chem. Phys.* **2023**, *25*, 9909–9924, doi:10.1039/D3CP00400G.

9. Anwar, J.; Zahn, D. Polymorphic Phase Transitions: Macroscopic Theory and Molecular Simulation. *Advanced Drug Delivery Reviews* **2017**, *117*, 47–70, doi:10.1016/j.addr.2017.09.017.

10. Boldyreva, E.V. High-Pressure-Induced Structural Changes in Molecular Crystals Preserving the Space Group Symmetry: Anisotropic Distortion/Isosymmetric Polymorphism. *Crystal Engineering* **2003**, *6*, 235–254, doi:10.1016/j.cryseng.2003.11.005.

11. Napiórkowska, E.; Milcarz, K.; Szeleszczuk, Ł. Review of Applications of Density Functional Theory (DFT) Quantum Mechanical Calculations to Study the High-Pressure Polymorphs of Organic Crystalline Materials. *IJMS* **2023**, *24*, 14155, doi:10.3390/ijms241814155.

12. Bull, C.L.; Funnell, N.P.; Ridley, C.J.; Pulham, C.R.; Coster, P.L.; Tellam, J.P.; Marshall, W.G. Pressure-Induced Isosymmetric Phase Transition in Biurea. *CrystEngComm* **2019**, *21*, 5872–5881, doi:10.1039/C9CE01028A.

13. Yan, T.; Wang, K.; Tan, X.; Yang, K.; Liu, B.; Zou, B. Pressure-Induced Phase Transition in N–H···O Hydrogen-Bonded Molecular Crystal Biurea: Combined Raman Scattering and X-Ray Diffraction Study. *J. Phys. Chem. C* **2014**, *118*, 15162–15168, doi:10.1021/jp503803n.

14. Clarke, S.M.; Steele, B.A.; Kroonblawd, M.P.; Zhang, D.; Kuo, I.-F.W.; Stavrou, E. An Isosymmetric High-Pressure Phase Transition in α-Glycylglycine: A Combined Experimental and Theoretical Study. *J. Phys. Chem. B* **2020**, *124*, 1–10, doi:10.1021/acs.jpcb.9b07313.

15. Safari, F.; Olejniczak, A.; Katrusiak, A. Pressure-Dependent Crystallization Preference of Resorcinol Polymorphs. *Crystal Growth & Design* **2019**, *19*, 5629–5635, doi:10.1021/acs.cgd.9b00610.

16. Kichanov, S.E.; Kozlenko, D.P.; Bilski, P.; Wąsicki, J.; Nawrocik, W.; Medek, A.; Hancock, B.C.; Lukin, E.V.; Lathe, C.; Dubrovinsky, L.S.; et al. The Polymorphic Phase Transformations in Resorcinol at High Pressure. *Journal of Molecular Structure* **2011**, *1006*, 337–343, doi:10.1016/j.molstruc.2011.09.029.

17. Cook, C.; McKinley, J.L.; Beran, G.J.O. Modeling the α- and β-Resorcinol Phase Boundary via Combination of Density Functional Theory and Density Functional Tight-Binding. *The Journal of Chemical Physics* **2021**, *154*, 134109, doi:10.1063/5.0044385.

18. Ebisuzaki, Y.; Askari, L.H.; Bryan, A.M.; Nicol, M.F. Phase Transitions in Resorcinal. *The Journal of Chemical Physics* **1987**, *87*, 6659–6664, doi:10.1063/1.453401.

19. Boldyreva, E.V.; Sowa, H.; Seryotkin, Yu.V.; Drebushchak, T.N.; Ahsbahs, H.; Chernyshev, V.; Dmitriev, V. Pressure-Induced Phase Transitions in Crystalline l-Serine Studied by Single-Crystal and High-Resolution Powder X-Ray Diffraction. *Chemical Physics Letters* **2006**, *429*, 474–478, doi:10.1016/j.cplett.2006.08.092.

20. Fisch, M.; Lanza, A.; Boldyreva, E.; Macchi, P.; Casati, N. Kinetic Control of High-Pressure Solid-State Phase Transitions: A Case Study on l-Serine. *J. Phys. Chem. C* **2015**, *119*, 18611–18617, doi:10.1021/acs.jpcc.5b05838.

21. Moggach, S.A.; Marshall, W.G.; Parsons, S. High-Pressure Neutron Diffraction Study of L-Serine-I and L-Serine-II, and the Structure of L-Serine-III at 8.1 GPa. *Acta Crystallogr B Struct Sci* **2006**, *62*, 815–825, doi:10.1107/S010876810601799X.

22. Moggach, S.A.; Allan, D.R.; Morrison, C.A.; Parsons, S.; Sawyer, L. Effect of Pressure on the Crystal Structure of L-Serine-I and the Crystal Structure of L-Serine-II at 5.4 GPa. *Acta Crystallogr B Struct Sci* **2005**, *61*, 58–68, doi:10.1107/S0108768104031787.

23. Christy, A.G. Isosymmetric Structural Phase Transitions: Phenomenology and Examples. *Acta Crystallogr B Struct Sci* **1995**, *51*, 753–757, doi:10.1107/S0108768195001728.

24. Price, S.L. Why Don't We Find More Polymorphs? *Acta Crystallogr B Struct Sci Cryst Eng Mater* **2013**, *69*, 313–328, doi:10.1107/S2052519213018861.

25. Reilly, A.M.; Tkatchenko, A. Role of Dispersion Interactions in the Polymorphism and Entropic Stabilization of the Aspirin Crystal. *Phys. Rev. Lett.* **2014**, *113*, 055701, doi:10.1103/PhysRevLett.113.055701.

26. Mazurek, A.H.; Szeleszczuk, Ł.; Pisklak, D.M. Periodic DFT Calculations - Review of Applications in the Pharmaceutical Sciences. *Pharmaceutics* **2020**, *12*, 415, doi:10.3390/pharmaceutics12050415.

27. Tkatchenko, A.; Scheffler, M. Accurate Molecular Van Der Waals Interactions from Ground-State Electron Density and Free-Atom Reference Data. *Phys. Rev. Lett.* **2009**, *102*, 073005, doi:10.1103/PhysRevLett.102.073005.

28. Tkatchenko, A.; DiStasio, R.A.; Car, R.; Scheffler, M. Accurate and Efficient Method for Many-Body van Der Waals Interactions. *Phys. Rev. Lett.* **2012**, *108*, 236402, doi:10.1103/PhysRevLett.108.236402.

29. Baroni, S.; De Gironcoli, S.; Dal Corso, A.; Giannozzi, P. Phonons and Related Crystal Properties from Density-Functional Perturbation Theory. *Rev. Mod. Phys.* **2001**, *73*, 515–562, doi:10.1103/RevModPhys.73.515.

30. Oganov, A.R.; Glass, C.W. Crystal Structure Prediction Using Ab Initio Evolutionary Techniques: Principles and Applications. *The Journal of Chemical Physics* **2006**, *124*, 244704, doi:10.1063/1.2210932.

31. Lee, E.H. A Practical Guide to Pharmaceutical Polymorph Screening & Selection. *Asian Journal of Pharmaceutical Sciences* **2014**, *9*, 163–175, doi:10.1016/j.ajps.2014.05.002.

32. *Polymorphism: In the Pharmaceutical Industry*; Hilfiker, R., Ed.; 1st ed.; Wiley, 2006; ISBN 978-3-527-31146-0.

33. Committee for Medicinal Products for Human Use (CHMP) European Medicines Agency. *Guideline on the Chemistry of Active Substances*; EMA/CHMP/QWP/49484/2026; **2026**.

34. Food and Drug Administration *FDA Guidance for Industry: ANDAs: Pharmaceutical Solid Polymorphism: Chemistry, Manufacturing, and Controls Information*; FDA-2004-D-0182; **2007**.

35. Ticona Chambi, J.; Fandaruff, C.; Cuffini, S.L. Identification and Quantification Techniques of Polymorphic Forms - A Review. *Journal of Pharmaceutical and Biomedical Analysis* **2024**, *242*, 116038, doi:10.1016/j.jpba.2024.116038.

36. Chemburkar, S.R.; Bauer, J.; Deming, K.; Spiwek, H.; Patel, K.; Morris, J.; Henry, R.; Spanton, S.; Dziki, W.; Porter, W.; et al. Dealing with the Impact of Ritonavir Polymorphs on the Late Stages of Bulk Drug Process Development. *Org. Process Res. Dev.* **2000**, *4*, 413–417, doi:10.1021/op000023y.

37. Bauer, J.; Spanton, S.; Henry, R.; Quick, J.; Dziki, W.; Porter, W.; Morris, J. Ritonavir: An Extraordinary Example of Conformational Polymorphism. *Pharm Res* **2001**, *18*, 859–866, doi:10.1023/A:1011052932607.

38. Abramov, Y.A. Current Computational Approaches to Support Pharmaceutical Solid Form Selection. *Org. Process Res. Dev.* **2013**, *17*, 472–485, doi:10.1021/op300274s.

39. Price, S. The Computational Prediction of Pharmaceutical Crystal Structures and Polymorphism. *Advanced Drug Delivery Reviews* **2004**, *56*, 301–319, doi:10.1016/j.addr.2003.10.006.

40. Oswald, I.D.H.; Lennie, A.R.; Pulham, C.R.; Shankland, K. High-Pressure Structural Studies of the Pharmaceutical, Chlorothiazide. *CrystEngComm* **2010**, *12*, 2533, doi:10.1039/c001355b.

41. Novelli, G.; Maynard-Casely, H.E.; McIntyre, G.J.; Warren, M.R.; Parsons, S. Effect of High Pressure on the Crystal Structures of Polymorphs of L-Histidine. *Crystal Growth & Design* **2020**, *20*, 7788–7804, doi:10.1021/acs.cgd.0c01085.

42. Li, Q.; Li, S.; Wang, K.; Li, X.; Liu, J.; Liu, B.; Zou, G.; Zou, B. Pressure-Induced Isosymmetric Phase Transition in Sulfamic Acid: A Combined Raman and x-Ray Diffraction Study. *The Journal of Chemical Physics* **2013**, *138*, 214505, doi:10.1063/1.4807864.

43. Fisch, M.; Lanza, A.; Boldyreva, E.; Macchi, P.; Casati, N. Kinetic Control of High-Pressure Solid-State Phase Transitions: A Case Study on L-Serine. *J. Phys. Chem. C* **2015**, *119*, 18611–18617, doi:10.1021/acs.jpcc.5b05838.

10. Reprint of publications and co-authors' statements

10.1. Publication No.1

crystals

MDPI

Review

Isosymmetric Phase Transitions in Crystals: From Subtle Rearrangements to Functional Properties

Anna Maria Mazurek [1], Monika Franczak-Rogowska [2] and Łukasz Szeleszczuk [1,*]

[1] Department of Organic and Physical Chemistry, Medical University of Warsaw, 1 Banacha Str., 02-097 Warsaw, Poland; anna_m_mazurek@o2.pl
[2] Department of Drug Chemistry, Pharmaceutical and Biomedical Analysis, Medical University of Warsaw, 1 Banacha Str., 02-097 Warsaw, Poland; monika.franczak-rogowska@wum.edu.pl
* Correspondence: lukasz.szeleszczuk@wum.edu.pl; Tel.: +48-501-255-121

Abstract

Isosymmetric phase transitions (IPTs) represent a rare class of solid-state transformations in which substantial structural reorganization occurs without a change in crystallographic symmetry. These phenomena, though subtle, can have a profound impact on the physical and functional properties of materials, offering novel opportunities for property tuning without chemical modification. This review provides a comprehensive overview of the experimental and computational methods used to detect and characterize IPTs, including single-crystal and powder X-ray diffraction, Raman and FT-IR spectroscopy, differential scanning calorimetry, and advanced simulation techniques such as density functional theory, molecular dynamics, and crystal structure prediction. Special emphasis is placed on correlating local structural rearrangements—such as hydrogen-bond reconfiguration, polyhedral tilting, and molecular fragment reorientation—with macroscopic thermodynamic signatures. A broad selection of examples from the literature is discussed, covering molecular crystals, coordination compounds, organic functional materials, simple salts, and inorganic oxides, with detailed tables summarizing pressure- and temperature-induced IPTs. The review also analyses the primary factors that trigger IPTs, particularly temperature and pressure, and examines their role in governing structural stability and transformation pathways. By combining structural, spectroscopic, and thermodynamic perspectives, this work aims to consolidate the understanding of IPT mechanisms and to highlight their significance for the design of responsive crystalline materials.

Keywords: isosymmetric phase transition; solid-state transformation; high-pressure crystallography; temperature-induced transition; hydrogen bonding; X-ray diffraction; Raman spectroscopy; density functional theory; molecular dynamics; crystal structure prediction

check for updates

Academic Editor: Nikos Ch. Karayiannis

Received: 26 August 2025
Revised: 10 September 2025
Accepted: 11 September 2025
Published: 13 September 2025

Citation: Mazurek, A.M.; Franczak-Rogowska, M.; Szeleszczuk, Ł. Isosymmetric Phase Transitions in Crystals: From Subtle Rearrangements to Functional Properties. *Crystals* **2025**, *15*, 807. https://doi.org/10.3390/cryst15090807

Copyright: © 2025 by the authors. Licensee MDPI, Basel, Switzerland. This article is an open access article distributed under the terms and conditions of the Creative Commons Attribution (CC BY) license (https://creativecommons.org/licenses/by/4.0/).

1. Introduction

Solid state phase transitions affect the structural behavior of materials, influencing their physical, chemical, and functional properties. Of note within this category of phenomena are isosymmetric phase transitions (IPTs) that have attracted increasing attention recently. Unlike the other types of polymorphic transformations, IPTs involve reconfiguration of the crystal lattice without changing its overall symmetry. For example, in the pharmaceutical field, where polymorphism and solid-state transformations impact drug efficacy and manufacturability, understanding isosymmetric transitions is particularly

significant. Emerging studies suggest that IPTs could provide innovative pathways for tuning the solubility, mechanical properties, and bioavailability of medicinal compounds without the need for demanding chemical modifications.

The aim of this review is to present the current knowledge on the isosymmetric phase transition and methods employed for the analysis and understanding of this phenomenon. First part of this article briefly describes the physicochemical methods used to analyze the IPT. In the second part chosen examples are presented in more detailed way, supported by a table concluding the reported cases. Finally, the typical conditions at which the IPT occur and factors that trigger such transformations are analyzed.

This review is intended as a broad overview of isosymmetric phase transitions across various classes of materials. The primary focus is on the experimental and computational methods applied to their investigation, and on the external factors that trigger such transitions. The selected case studies serve to illustrate these approaches and phenomena rather than to provide exhaustive analyses of each individual system. Readers seeking complete crystallographic and thermodynamic datasets are referred to the original publications cited throughout the text.

2. Isosymmetric Phase Transition

An isosymmetric phase transition (IPT) is an uncommon and fascinating class of structural transitions in crystalline materials. In this review, we adopt a broad definition of IPTs as transformations that preserve the crystallographic space group, regardless of the magnitude of structural rearrangement. In this context, IPTs may involve very subtle changes—such as minor molecular rotations, conformational shifts, or small hydrogen-bond adjustments—as well as the extensive reorganization of molecular packing, as in the α/β-resorcinol system [1]. The latter demonstrates that space-group retention can accompany substantial changes in intermolecular arrangements, which remain mechanistically and thermodynamically distinct from symmetry-breaking phase transitions.

The key characteristic of an IPT is therefore not the scale of structural change, but the invariance of the space group. Structural similarity can vary greatly and should be assessed using molecule-by-molecule overlays, the analysis of the topology of interaction networks, and thermodynamic signatures. This broad definition allows the inclusion of both "strict" IPTs, where changes are minimal, and "extensive" IPTs, where reorganization is large but still occurs without symmetry reduction [2]. The traditional methods of symmetry analysis and group–subgroup relations fail to detect these transitions, where they constitute a subtle yet significant anomaly in solid-state physics and crystallography. Because no symmetry breaking occurs, classical Landau theory cannot fully describe their thermodynamic nature. In this review, we distinguish strict IPTs (space group and Wyckoff scheme unchanged) from pseudo-isosymmetric transitions, where minimal symmetry lowering (e.g., Z′ change under a pseudosymmetric relationship) accompanies a first-order rearrangement that preserves the topology of interactions and yields close structural overlays, and we focus solely on this first group.

The key characteristic of an IPT is a rearrangement of its internal degrees of freedom. These may emerge as rotations and tilts of coordination polyhedra, cooperative distortions of hydrogen-bonding frameworks, or reorientations of molecular fragments within the crystal structure. As an example, neutron diffraction and Raman spectroscopy studies of biurea demonstrated a pressure-induced IPT, marked by a rapid decrease in unit cell volume and reconfiguration of intermolecular interactions at around 0.6 GPa [3]. Similarly, in ammonium bicarbonate, in situ synchrotron X-ray diffraction revealed that biaxial compression of a "double-wine-rack" hydrogen-bond network may trigger an IPT with highly anisotropic elastic responses [4].

In addition to molecular systems, IPTs have been observed in inorganic structures, such as rare-earth orthoferrites ($RFeO_3$). The driving mechanism here is the competition between oxygen coordination shells surrounding the rare-earth cation and the softening of particular phonon modes. Experimental data showed changes in lattice parameters and octahedral distortions without any alteration in space group symmetry, hence offering definitive evidence of an IPT [5]. Covalent organic frameworks have demonstrated the ability to undergo IPT under pressure, demonstrating remarkable phenomena such as negative linear compressibility and breathing effects, which present promising opportunities for adjustable and adaptable functional materials [6].

Overall, IPTs are a unique and under explored class of phase transitions that present a challenge for conventional classification schemes. By maintaining macroscopic symmetry while allowing hidden microscopic reorganizations, they uncover new dimensions of structure–property interactions in materials. Their occurrence in several material classes, from basic molecule crystals to complex oxides and frameworks, underscores their universality and promise for technological applications, including responsive materials, sensors, and pressure-adaptive systems. Concurrently, their complex nature makes them challenging to detect experimentally and to predict computationally, emphasizing the necessity of ongoing methodological innovation in computational modeling, spectroscopy, and crystallography. It should be noted that the retention of the same space group is a necessary but not sufficient condition for classifying a transformation as strictly isosymmetric. Structural similarity must be assessed using molecule-by-molecule overlays, analysis of the topology of interaction networks, and thermodynamic signatures. For example, in the α/β-resorcinol system, both phases crystallize in the same space group ($Pna2_1$), yet their molecular packing differs substantially, making them structurally distinct despite apparent symmetry retention [1].

3. Methods Used to Analyze IPTs

The study of IPTs involves an experimental and theoretical challenge, as these transitions include significant structural reorganizations without a change in crystallographic symmetry. Therefore, conventional symmetry-based methods are insufficient, and exploration into combinations of complementary techniques that can capture both local and long-range effects is required. Diffraction techniques, particularly X-ray diffraction (XRD), are pivotal among experimental approaches, as they provide direct structural information and facilitate the confirmation of space-group invariance. Spectroscopic methods, such as Raman and Fourier-Transform Infrared (FT-IR), are similarly significant as they reveal vibrational abnormalities and local reorganizations. Thermal techniques like differential scanning calorimetry (DSC) provide thermodynamic evidence of first-order behavior, hence supporting the classification of these transitions.

Computational methods like molecular dynamics (MD) and density functional theory (DFT) are crucial for simulating IPT mechanisms and investigating the delicate energetic balance among competing phases. Crystal structure prediction (CSP) enhances these capabilities by mapping potential isosymmetric polymorphs and predicting changes under diverse thermodynamic conditions. Collectively, experimental and theoretical methodologies establish an effective framework that enables the accurate identification, characterization, and mechanistic comprehension of IPTs.

3.1. X-Ray Diffraction

XRD is a fundamental method utilized to examine crystalline structures and has long been recognized as the main method for analyzing structural phase transitions. Its role is particularly important in IPTs as these transitions are defined by subtle structural

reorganizations within the same crystallographic framework [7]. XRD techniques provide an accurate measurement of unit-cell dimensions, bond lengths, coordination environments, and atomic positions, making them essential for confirming that an observed transition is genuinely isosymmetric.

Differentiating between transformations that are truly isosymmetric and those that involve undetected or very subtle symmetry changes is one of the primary challenges in IPT research. This is particularly relevant for first-order transitions, where sudden discontinuities in structural parameters are to be expected [8]. Under variable temperature or pressure, XRD presents direct evidence of such discontinuities in lattice constants or unit-cell volumes, additionally at the same time confirming the lack of change in space group symmetry. By combining XRD with other techniques such as Raman spectroscopy or calorimetry, researchers may support their classification of a transition as an IPT [2]. Two main XRD-based methods are utilized in IPT studies: powder X-ray diffraction (PXRD), which is particularly effective for high-pressure and high-temperature analysis, and single-crystal X-ray diffraction (SCXRD), which is considered the standard for atomic-scale structural resolution.

3.1.1. Powder X-Ray Diffraction

PXRD enables the observation of changes in unit-cell dimensions and diffraction peak positions when external stimuli are applied. Despite the fact that PXRD does not offer the same level of atomic precision as single-crystal methods, it is highly effective in identifying discontinuous variations in lattice constants and unit-cell volumes. An excellent example of applying PXRD in IPT research is the analysis of orthopyroxene ($Mg_2Si_2O_6$), a silicate mineral significant in geology, where high-temperature synchrotron powder X-ray diffraction (HTXRD) showed a discontinuous change in unit-cell parameters at around 1230 K. The transition was classified as an IPT, driven by bond-switching mechanisms between Mg atoms and coordinated O atoms, and confirmed by MD simulations [9]. As another example, studies of sulfamic acid under pressure using synchrotron PXRD revealed sudden distortions in lattice parameters between 10.2 and 12.7 GPa, which is consistent with pressure-induced IPT involving hydrogen-bonding motif rearrangements [10].

PXRD is especially suitable for diamond anvil cell studies, capable of achieving pressures above tens of gigapascals. In such settings, PXRD facilitates the identification of compressibility anomalies, negative linear compressibility, and abrupt volume collapses, which are structural characteristics often linked to IPTs [5,11]. Therefore, whereas PXRD is incapable of directly detecting minor atomic displacements or molecular reorientations, its usefulness lies in recognizing macroscopic lattice anomalies and mapping phase boundaries.

3.1.2. Single Crystal X-Ray Diffraction

SCXRD is the most conclusive technique for identifying IPTs, as it provides knowledge of the arrangement of atoms within the unit cell. In contrast to PXRD, which offers averaged structural data, SCXRD can identify minor anisotropic displacements, molecular reorientations, hydrogen-bond rearrangements, or octahedral tilts. As a strictly isosymmetric, SCXRD-resolved example, L-histidine exhibits reversible pressure-induced IPTs wherein the space group is retained while discontinuous changes in unit-cell metrics and hydrogen-bond geometry occur; SCXRD, PXRD, and Raman jointly confirm the first-order nature without symmetry breaking [12]. This level of precision could not have been achieved only with powder techniques, highlighting the essential role of SCXRD in identifying IPT.

SCXRD is especially significant in high-pressure crystallography, since its capacity to identify anisotropic lattice distortions and coordination–shell rearrangements provide conclusive evidence for IPTs. In studies of rare-earth orthoferrites, SCXRD showed dis-

tortions in octahedral environments and abnormalities in lattice parameters indicative of an IPT mechanism driven by coordination–shell interactions [5]. By detecting minor yet abrupt changes, SCXRD offered the most accurate evidence that a structural transition occurred without symmetry breakdown. The primary limitations of SCXRD are its quality requirements for a sample, which needs to be well-formed single crystals and presenting technical difficulties under extreme pressures or temperatures.

In summary, SCXRD is the most important method for IPT study. Its unmatched atomic-level resolution enables researchers to definitively confirm that a structural transition, despite severe distortions and reconfigurations, maintains the overall crystallographic symmetry. When integrated with other methods, SCXRD establishes the conclusive structural basis for investigating IPTs.

3.2. Spectroscopic Methods

3.2.1. Raman Spectroscopy

Raman spectroscopy is a widely used spectroscopic technique employed in the investigation of IPTs, due to its exceptional sensitivity to lattice vibrations, phonon anomalies, and local bonding configurations. As IPTs maintain global crystallographic symmetry, conventional diffraction methods may not always disclose the full extent of structural reorganization. However, Raman spectroscopy can identify discontinuities in vibrational frequencies, mode splitting, and intensity alterations that indicate local atomic or molecular rearrangements, including molecular fragment reorientations, hydrogen-bond reorganizations, or polyhedral tilting.

A notable example is the pressure-induced IPT in sulfamic acid, where integrated Raman and synchrotron XRD analyses demonstrated a structural transition occurring between 10.2 and 12.7 GPa and Raman spectra exhibited abrupt alterations in NH_3^+ and SO_3^- vibrational modes, indicative of hydrogen bond reorganization [10]. Similarly, Raman spectroscopy detected phonon anomalies at 327 K and 347 K in $[(C_3H_7)_4N]_2Zn_2Cl_6$, which corresponded to two reversible IPTs involving the order–disorder processes of the organic cations. These anomalies were subsequently confirmed by calorimetry [13]. Raman spectroscopy used in analysis of fluorene up to 9 GPa revealed a reversible IPT involving molecular stacking rearrangement, with changes in intermolecular mode frequencies reflecting structural stiffening [14]. Raman spectroscopy is also valuable for its capability to detect IPTs across various temperature ranges. In $(NH_4)_3GeF_7$, variable-temperature Raman studies revealed symmetry-preserving structural reorganizations linked to ammonium ion ordering, exhibiting significant alterations in lattice vibrational modes, while GeF_6^{2-} groups remained mostly unaffected [15].

In summary, Raman spectroscopy is important for IPT research due to its ability to directly detect vibrational discontinuities and investigate local lattice dynamics. While it cannot independently verify symmetry invariance, Raman spectroscopy, when combined with XRD and calorimetry, offers essential spectroscopic evidence of the first-order nature of IPTs (Figure 1).

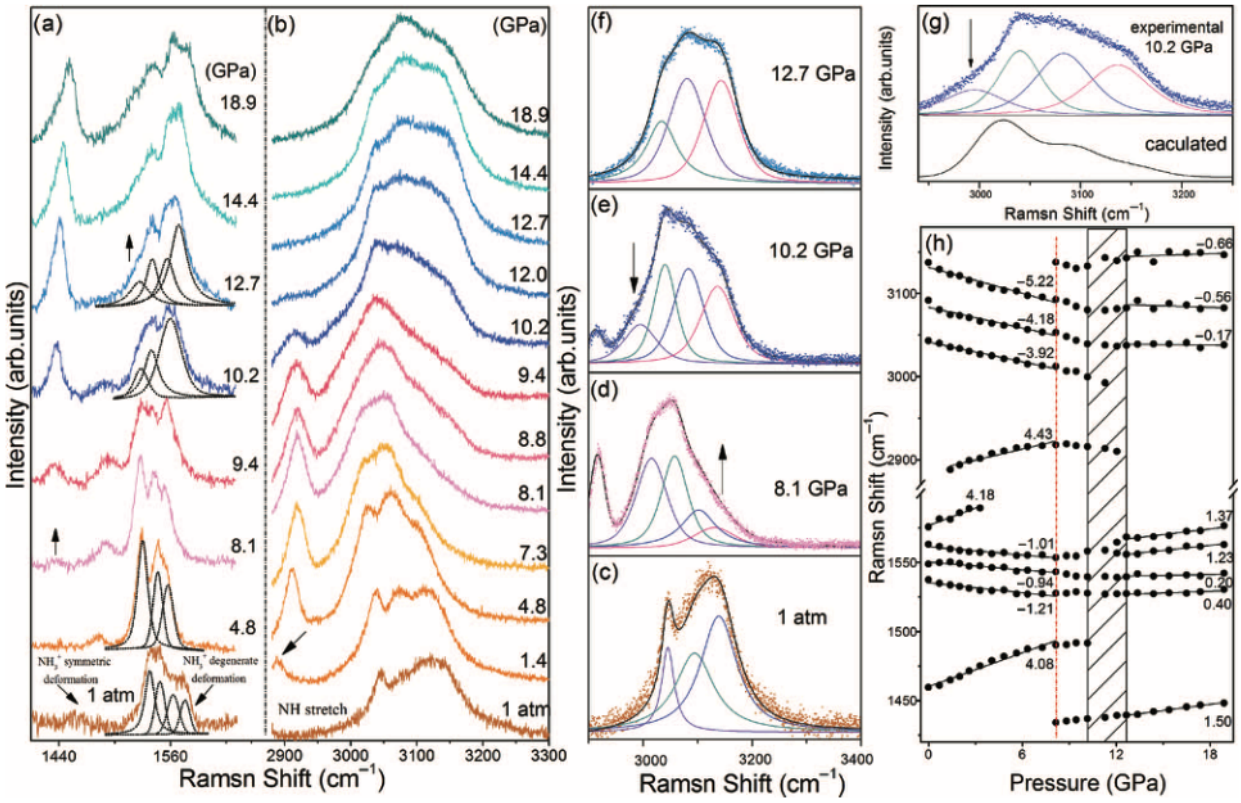

Figure 1. Representative high-pressure Raman spectra of NH_3^+-related modes in sulfamic acid: (**a**) deformation of NH_3^+, (**b**) N–H stretching, (**c**–**f**) decompositions of the N–H stretching region for clarity, (**g**) comparison of calculated and experimental N–H stretching modes, and (**h**) pressure dependence of peak positions for these NH_3^+ related modes. The vertical dotted line marks the beginning of changes in Raman spectra. The shadow represents the phase-transition region. Linear fits are conducted for clarity, and the neighboring numbers represent the slopes of the respective modes. The unit is cm^{-1}/GPa. Reprinted from [10] with the permission of AIP Publishing.

3.2.2. Fourier-Transform Infrared Spectroscopy

FT-IR spectroscopy [16], a commonly used vibrational technique, which provides comprehensive data on the local bonding environment in crystalline materials and facilitates the investigation of IPTs. In contrast to Raman spectroscopy, which is more sensitive to lattice and low-frequency modes, FT-IR primarily describes intramolecular vibrations, including the stretching and bending of polar functional groups. This method is sensitive to discontinuous shifts in absorption bands associated with O–H, N–H, or C=O stretching, which are IPT's fingerprints in hydrogen-bonded molecular crystals. For instance, the abrupt changes in the vibrational signature of hydrogen bonds can be used to directly trace order–disorder processes in ammonium-based salts or organic–inorganic hybrids, even in the absence of diffraction–detectable symmetry lowering.

The applicability of FT-IR to IPT research is demonstrated by several case studies. A conformational IPT was identified in oleic acid through the use of combined FT-IR and XRD investigations, which highlighted discontinuous changes in the arrangement of the olefinic chain. The transition was characterized by a splitting and intensity change in the C-H and C=C stretching bands, indicating molecular reorientation [17]. In another case, variable temperature FT-IR spectroscopy of $(NH_4)_3GeF_7$ revealed abrupt shifts in N–H stretching frequencies that were associated with ammonium ion reordering consistent with an IPT [15]. Although FT-IR alone cannot confirm that a transition is isosymmetric, its sensitivity to molecular vibrations makes it essential in multi-method studies.

3.3. Differential Scanning Calorimetry

DSC is a commonly used thermal analysis method that measures the heat flow resulting from structural changes as a function of temperature or time. In the analysis of IPTs, DSC is of importance since it offers thermodynamic confirmation of structural reconfigurations that transpire without alterations in crystallographic symmetry. Because many IPTs are first-order in nature, they are usually accompanied by sudden enthalpic changes, which appear as sharp endothermic or exothermic peaks in DSC traces, despite the lack of symmetry-breaking signs in diffraction data [18].

DSC has demonstrated significant value when utilized combined with diffraction and spectroscopic techniques. In the organic–inorganic hybrid crystal $[(C_3H_7)_4N]_2Zn_2Cl_6$, DSC identified significant calorimetric anomalies at 327 K and 347 K, indicating two reversible IPTs associated with the order–disorder dynamics of organic moieties. The transitions were concurrently identified by Raman spectroscopy, underscoring the efficacy of DSC as a supplementary method for investigating latent heat effects [13]. Similarly, calorimetric results from hydrogen-bonded molecular systems such as biurea supported pressure-induced IPTs, with sudden heat flow anomalies corresponding to intramolecular hydrogen bond reorganization [3].

In summary, DSC offers the thermodynamic validation of IPTs by identifying enthalpy changes associated with structural reorganizations that are undetectable through symmetry analysis. Although it cannot independently confirm the isosymmetric nature of a transition, when integrated with diffraction and spectroscopy methods, it provides conclusive evidence for the first-order nature of IPTs and continues to be an important tool in their analysis.

3.4. Computational Methods

3.4.1. Density Functional Theory

DFT has become known as a fundamental theoretical method in the analysis of IPTs, enabling the accurate assessment of the relative stability of competing structures with the same symmetry. Due to the absence of symmetry breaking, the experimental detection of IPTs is often difficult, and DFT offers essential assistance by modeling energetic landscapes, structural aberrations, and electronic contributions to stability.

DFT calculations in molecular crystals have recreated pressure-induced IPTs, such as the chlorothiazide transition, in which simulations demonstrated that entropic and pressure effects stabilize one polymorph over another [2]. As another example study on Na_3MnF_6 showed that orbital reorientation and pressure-induced Jahn–Teller distortions can stabilize alternate monoclinic forms, which explains the microscopic origin of the IPT [19].

In addition to static optimization, DFT, combined with phonon computations or ab initio molecular dynamics (aiMD) [20], has been utilized for strongly correlated systems like cerium and contributed to capturing the electronic balance that drives the α–γ transition [21]. These examples show that DFT not only confirms empirically observed IPTs but also offers a mechanistic understanding of their driving mechanisms, ranging from hydrogen-bond reorganizations to orbital reconstructions.

3.4.2. Molecular Dynamics Simulations

MD simulations have become recognized as a significant computational method for IPTs, enabling direct observation of atomic-scale dynamics in response to external stimuli like temperature and pressure. In contrast to static methods like geometry optimization, MD explicitly incorporates thermal vibrations, entropy, and transient bond rearrangements, proving it particularly effective at identifying the dynamic pathways of IPTs. This is especially significant as IPTs often entail subtle local reorganizations, such as bond

shifting or molecule reorientation, which cannot be effectively described by diffraction techniques alone.

An excellent example is the study of orthoenstatite ($Mg_2Si_2O_6$), where MD simulations replicated a first-order IPT at about 1230 K. The transition displayed abrupt changes in unit-cell parameters and Mg–O coordination shifts, which was consistent with synchrotron PXRD analysis [9]. Further studies confirmed similar high-temperature IPTs in orthopyroxenes by extended MD protocols, demonstrating the maintenance of structural stability across extensive compositional ranges [8]. In molecular systems, calcite ($CaCO_3$) has functioned as a model for MD analysis of order–disorder IPTS, where simulations demonstrated significant rotations and flipping of carbonate groups under temperature and pressure, resulting in discontinuous structural reorganizations [22].

MD may be combined with electronic structure calculations to enhance predictive precision. For instance, aiMD employed on chlorothiazide effectively replicated its pressure-induced IPT, demonstrating that real-time simulations can capture structural rearrangements not anticipated by static DFT alone [2]. These integrated methods show the versatility of MD as a method for both verifying experimental findings and revealing hidden structural pathways that may be thermodynamically accessible yet challenging to observe under laboratory conditions.

In summary, MD simulations offer essential insights into the mechanisms of IPTs by describing entropic contributions, transient atomic movements, and the dynamics of structural reorganization. Although they cannot substitute for diffraction or spectroscopy in confirming symmetry invariance, they are essential for developing a mechanistic comprehension of how IPTs occur at the atomic level.

3.4.3. Crystal Structure Prediction

CSP methods have gained recognition in the study of IPTs, as they facilitate the systematic identification of alternative structures that maintain the same space-group symmetry while differing in atomic arrangements or molecular conformations. In contrast to experimental methods, which are restricted to laboratory-accessible settings [23], CSP can reveal metastable or hidden polymorphs that could form under pressure, temperature, or entropic stabilization. This is especially significant in IPT research, where diffraction methods alone may fail to show the complete polymorphic landscape. CSP generally combines global search algorithms, including evolutionary or random sampling techniques, along with energetic ranking derived from force-field methods or quantum-mechanical calculations, so creating a strong predictive framework.

The applicability of CSP in IPT research is seen in numerous studies. A significant case is molecular oxygen at megabar pressures, where ab initio CSP revealed two energetically competing monoclinic phases with equal symmetry. The subtle change in stability among these polymorphs offers a microscopic explanation for the isosymmetric ε–ζ transition [24]. In intermetallic compounds like Zr_2Cu, CSP-guided DFT simulations predicted a pressure-induced IPT marked by a discontinuous alteration in axial ratio and volume collapse [25]. These examples demonstrate how CSP enables researchers to detect and explain IPTs across several material categories, including minerals, molecular solids, and metallic alloys.

Overall, CSP offers a predictive framework for the identification of potential IPTs and the comprehension of their underlying energetic competition. Although it is unable to independently confirm the occurrence of an IPT, CSP enables researchers to identify hidden polymorphic landscapes and predict structural reorganizations in an extensive range of crystalline systems when combined with experimental diffraction data and electronic-structure calculations. The addition of computational crystal engineering into IPT studies underscores its increasing significance in discovering new functional materials.

4. Factors Causing the Phenomenon of IPT

The phenomenon of IPTs is closely associated with the influence of external stimuli that disrupt the internal configuration of crystalline systems. Such stimuli generally function by shifting the balance of intermolecular interactions, adjusting coordination environments, or changing lattice dynamics, leading to structural rearrangements under the same space group conditions. Among the several potential triggers, temperature and pressure are the most fundamental and extensively studied. Both parameters directly impact the energetic stability of competing phases, temperature primarily through entropic contributions and dynamic disorder, and pressure by altering interatomic distances and the compressive forces applied on coordination shells. IPTs often appear as sudden, first-order transitions, resulting in discontinuous alterations in unit cell dimensions, polyhedral distortions, or molecular orientations. These discontinuities are often associated with abrupt changes in macroscopic physical properties, such as dielectric permittivity, compressibility, and elastic responsiveness, highlighting the importance of IPTs within the wider context of solid-state phase transitions [2]. Understanding the influence of temperature and pressure in triggering of IPTs offers significant insight into the microscopic mechanisms that determine structural stability, as well as a conceptual framework for predicting and manipulating these phenomena in functional materials.

4.1. Temperature

Temperature-induced IPTs are significantly affected by changes in vibrational amplitudes, entropy contributions, and the reorientation or ordering of molecular or ionic fragments. Often, the fundamental mechanism is associated with order–disorder phenomena, wherein specific structural components, such as anions or organic cations, reorganize or assume different orientations. Triethylbenzylammonium perchlorate is a well-documented example that exhibited a reversible IPT at approximately 196 K. The transition involved varying orientations of perchlorate anions and modifications in hydrogen-bonding interactions [26]. Similarly, cadmium–dabco coordination complexes underwent temperature-driven IPTs between 100 and 293 K, with torsional distortions of the organic moieties caused sudden changes in molecular conformation [27]. Furthermore, inorganic systems also exhibit temperature-induced IPTs; for instance, in orthopyroxene, HTXRD studies demonstrated a discontinuous alteration in cell parameters resulting from Mg–O coordination rearrangements [8]. These examples demonstrate that thermal energy can serve as a trigger for subtle reorientations and polyhedral adjustments that elude group-theoretical classification yet still induce sudden structural and physical transformations typical of IPTs.

4.2. Pressure

Pressure is another an important factor in the induction of IPTs, since it directly influences interatomic distances, polyhedra coordination, and hydrogen-bonding networks. Under compression, atoms are pushed into new configurations that often result in abrupt alterations in structural parameters. In molecular crystals, pressure-induced IPTs often arise from the reorientation of molecules or functional groups. For example, Biurea underwent a pressure-induced IPT at around 0.6 GPa, which was characterized by intramolecular reorientation and a sudden reduction in unit cell volume [3]. Hydrogen-bonded systems represent another significant class of pressure-sensitive IPTs. Ammonium bicarbonate, for instance, experienced an IPT under biaxial compression due to rearrangements within its "double-wine-rack" hydrogen-bonding structure, resulting in anisotropic compression and the establishment of new hydrogen bonds [4]. In inorganic oxides, pressure-induced IPTs are often associated with the tilting and distortion of octahedral units. This behavior was clearly shown by rare-earth orthoferrites ($RFeO_3$), which exhibited anomalies in

coordination–shell interactions and lattice parameters under pressure, revealing a hidden IPT [5]. These studies show that pressure-induced IPTs can significantly influence macroscopic mechanical properties, frequently resulting in uncommon events such as anisotropic elasticity or negative linear compressibility. Therefore, they have both fundamental crystallographic significance and potential for technological applications in adaptive and responsive materials.

5. Overview of Documented IPT Cases in Crystalline Materials

This literature review identified around 150 relevant articles on IPTs, based on a systematic search of the Scopus database performed on 3 April 2025. The chronological distribution of these studies indicates a distinct increase in interest over the last years, which is indicative of their escalating scientific significance and the progression of experimental and computational techniques facilitating their identification.

Tables 1 and 2 summarize selected studies on IPTs across various material classes. Significant emphasis has been placed on the experimental methodologies utilized to identify and characterize these transitions, with X-ray diffraction serving as a pivotal method. Although PXRD is extensively utilized, SCXRD is especially significant in IPT research. Its ability to precisely determine atomic positions, resolve anisotropic structural changes, and detect subtle distortions is essential for determining whether a given transition is truly isosymmetric. Consequently, SCXRD has been listed separately from other methods in the tables, as it offers a particularly significant role in the precise identification of IPTs.

Table 1. Summary of selected experimental studies on pressure-induced IPTs.

Name	Pressure Range	Transition Range	Space Group	System	SCXRD	Other Methods	Year	References
Resorcinol (1,3-Dihydroxybenzene)	ambient up to 14.5 GPa	0.5 GPa (α to β) and 5.6 GPa (to γ)	Pna21	Orthorhombic	N	Raman Spectroscopy, PL	2002	[1]
Sulfamic acid	ambient up to 20.1 GPa	10.2 GPa–12.7 GPa	Pbca	Orthorhombic	N	ADXRD, Raman Spectroscopy	2013	[10]
L-Histidine polymorphs	ambient up to 6.60 GPa (form I), ambient up to 6.85 GPa (form II)	4.5 GPa (form I), 3.1 GPa (form II)	P21 (form I) P212121 (form II)	Orthorhombic (form I), Monoclinic (form II)	Y	PXRD, Raman Spectroscopy	2020	[12]
N-isopropylpropionamide	ambient up to 10 GPa	4 GPa	P21/a	Monoclinic	Y	DTA	2015	[28]
Lead Fluoride	ambient up to 75 GPa	10–22 GPa	Pnma	Orthorhombic	N	ADXRD, DFT Calculations	2016	[29]
Lead Fluoride	ambient up to 28 GPa	10 GPa, 9.8–12.9 GPa	Pnam	Orthorhombic	N	ADXRD, Raman Spectroscopy	1998	[30]
Sodium Oxalate	ambient up to 8 GPa	3.8 GPa	P21/c	Monoclinic	N	HRXRD, Raman Spectroscopy	2003	[31]
Paracelsian	ambient up to 32 GPa	3–6 GPa	P21/c (I, II), Pna21 (III), Pn (IV)	Monoclinic (I, II, IV), Orthorhombic (III)	Y	DFT Calculations	2019	[32]
DL-Cysteine	ambient up to 7.90 GPa	0.1 GPa, 1.55 GPa and 6.20 GPa	P21/a	Monoclinic	N	HRXRD, Raman Spectroscopy	2010	[33]
Solid Ammonia	4 GPa–123 GPa	12 GPa	P212121 (for Phase IV and the phase above 12 GPa)	Orthorhombic	Y	Raman Spectroscopy, ND (for ND3)	2006	[34]
Rubrene (5,6,11,12-Tetraphenyl-tetracene)	ambient up to 7.2 GPa	7.1 GPa	P-1	Triclinic	Y	Hirshfeld Surface Analysis; PIXEL method for lattice and intermolecular interaction energy calculations	2014	[35]

Table 1. *Cont.*

Name	Pressure Range	Transition Range	Space Group	System	SCXRD	Other Methods	Year	References
Biurea	0.01 GPa–3.89 GPa	0.6 GPa–1.5 GPa	C2/c	Monoclinic	N	NPD, Raman Spectroscopy, DFT Calculations, Rietveld Refinement	2019	[3]
Potassium Titanyl Phosphate (KTP)	0.2 GPa–8.2 GPa	5.8 GPa	Pna21	Orthorhombic	Y	High-Raman Scattering	1996	[36]
Copper–Dicyanoaurate Complexes	ambient up to 3.6 GPa	1.2 GPa	P21/c	Monoclinic	Y	Raman Spectroscopy, IR Spectroscopy, UV-vis Absorption Spectroscopy	2022	[37]
Chlorothiazide	0 GPa–6.20 GPa	4.2 GPa	P21/c	Monoclinic	Y	DFT calculations, aiMD Simulations	2021	[2]
Hydroquinone–Formic Acid Clathrate	ambient up to 10.2 GPa	4.25 GPa	R-3	Trigonal	Y	Raman Spectroscopy, DSC, Energy Framework Calculations	2016	[38]
Ammonium Bicarbonate	ambient up to 3.4 GPa	2 GPa	Pccn	Orthorhombic	N	ADXRD, DFT calculations, Raman Spectroscopy	2023	[4]
α-Silver Sulfide	ambient up to 32 GPa	7.5 GPa and 15 GPa	P21/c	Monoclinic	N	DFT Calculations, XRD	2022	[39]
3D Covalent-Organic Framework (NPN-1)	0 GPa–5 GPa	0.14 GPa	P4b2	Tetragonal	N	DFT Calculations, aiMD	2023	[11]
Mixed-Valence Rare-Earth Fullerides	ambient up to 6 GPa	4 GPa	Pcab	Orthorhombic	N	SXRPD, PFY-XAS	2024	[40]
Cobalt Iodate	ambient up to 28 GPa	3.0 GPa and 9.0 GPa–11.0 GPa	P21	Monoclinic	N	Raman Spectroscopy, FT-IR Spectroscopy, DFT Calculations, HPXRD	2021	[41]
Barium Titanate	ambient up to 10 GPa	6 GPa	P4mm (tetragonal) and Pm-3m (cubic)	Tetragonal (at lower pressure) and Cubic (at higher pressure)	N	DFT Calculations	2022	[42]
Zinc Iodate	ambient up to 27.8 GPa	3.4 GPa and 8.9 GPa	P21	Monoclinic	N	HPXRD, Raman Spectroscopy, DFT Calculations	2021	[43]
Caesium Hydroxide	ambient up to 20 GPa	10 GPa	P212121	Orthorhombic	N	DFT Calculations, EDX	2016	[44]
α-Glycylglycine	ambient up to 14.5 GPa	6.7 GPa	P21/c	Monoclinic	N	PXRD, Raman Spectroscopy, DFT Calculations, CSP	2020	[45]
α-Silver Sulfide	ambient up to 32 GPa	7.5 GPa and 16 GPa	P21/c	Monoclinic	N	HPXRD, Raman Spectroscopy, DFT Calculations, Electrical Resistance Measurements	2020	[46]
L-Serine	ambient up to 14.5 GPa	5.3 GPa and 7.8 GPa	P212121	Orthorhombic	Y	HRXRD	2006	[47]
Sodium Manganese Fluoride	ambient up to 4.06 GPa	2.2 GPa ± 0.5 GPa	P21/n	Monoclinic	Y	Polarized Single-Crystal Optical Absorption Spectroscopy	1998	[48]
Blatter's Radical	ambient up to 6.07 GPa	5.34 GPa–5.54 GPa	$P2_1/n$	Monoclinic	Y	DFT calculations	2022	[49]

Table 2. Summary of selected experimental studies on temperature-induced IPTs.

Name	Pressure Range	Transition Range	Space Group	System	SCXRD	Other Methods	Year	References
Dabcodiium chlorochromate chloride	173–296 K	185 K	P21/m	Monoclinic	Y	DSC, Dielectric Measurements	2012	[50]
4-Ethylanilinium hydrogen (2R,3R)-tartrate	123–298 K	186 K	P1	Triclinic	Y	DSC, Dielectric Constant Measurements	2011	[51]
Ibuprofen lysine salt	30–110 °C (30–300 °C)	70–90 C	P21/n	Monoclinic	N	PXRD, DSC, TGA	2015	[52]
2-nitroanilinium bisulphate	100–300 K	232 K	P-1	Triclinic	Y	FT-IR Spectroscopy, DSC	2020	[53]
Dapsone	60–100 °C	78 °C ± 4 °C	P212121	Orthorhombic	Y	DSC, PXRD	2017	[54]
Triethylbenzylammonium Perchlorate	93–291 K	196 K ± 18 K	Pbca (93 K), Pbcm (291 K)	Orthorhombic	Y	DSC, Dielectric Measurements	2013	[26]
R-Cinacalcet Hydrochloride	room temperature up to 423 K (150 °C)	164.5 °C (437.65 K)	P212121 (form I, III), P1 (form II)	Orthorhombic (form I, III), Triclinic (form II)	Y	DSC, PXRD, FT-IR Spectroscopy, FT-Raman Spectroscopy	2008	[55]
Pyridinium-3-Carboxylic Acid Perchlorate	93 K–298 K	129 K	P21/c	Monoclinic	Y	DSC, Dielectric Measurements	2010	[56]
Lanthanum Gallate	room temperature up to 1100 °C	300–1100 °C	Pnma	Orthorhombic	N	PXRD, Raman Spectroscopy, TEM	2018	[57]
Yttrium manganite	room temperature up to 1403 K	920 K	P63cm	Hexagonal	N	NPD, DTA, Rietveld Analysis	2011	[58]
Yttrium Chromite	321 K–1200 K	900 K	Pmnb	Orthorhombic	N	NPD, DC Magnetization Measurements, Rietveld Refinement, Thermal Expansion Analysis	2020	[59]
Estradiol 17β Valerate (E2V)	room temperature down to 100 K	251.1 K (cooling) and 256.3 K (heating)	P21	Monoclinic	Y	FT-IR Spectroscopy, DSC, ssNMR Spectroscopy	2014	[60]
Potassium Lutetium Phosphate	100 K–293 K	230 K and 130 K	P-3 (at room temperature), P21/m (at 100 K and 200 K)	Hexagonal (at room temperature), Monoclinic (at 100 K and 200 K)	Y	NPD, DSC, Heat Capacity Measurements	2014	[61]
1,4-Diazoniabicyclo[2.2.2] octane-1-acetate-4-acetic Acid Chloride Trihydrate	135 K–298 K	210.7 K (heating) and 180.3 K (cooling) ± 30.4 K.	P21/n	Monoclinic	Y	DSC, Dielectric Measurements	2013	[62]
2-(3,5-Bis(trifluoromethyl) phenyl)-4,5-dihydro-1H-imidazole	100 K–298 K	150 K ± 15 K	P-1	Triclinic	Y	PXRD, DSC, TGA	2024	[63]
Layered Indium Selenide	room temperature up to 350 °C	220 °C (heating) and 190 °C (cooling)	R3m (for α-In2Se3) and P-3m1 (for β-In2Se3)	Rhombohedral	N	DSC, XRD, DFT Calculations, Raman Spectroscopy	2022	[64]
Hexathiocyanate Thulium(III) Anions	160 K–280 K	204.6 K (heating) and 188.7 K (cooling) ± 15.9 K	P-1	Triclinic	Y	DSC, Dielectric Measurements, PXRD	2021	[65]
Orthopyroxene	room temperature up to 1400 °C	1170 °C (both heating and cooling)	Pbca	Orthorhombic	N	SXRPD, Unit Cell Dimension Measurements	2008	[66]
Deuterated 3,5-Pyridinedicarboxylic Acid	15 K–300 K	150 K–200 K	$P2_1/n$	Monoclinic	Y	DFT Calculations, PXRD, NPD	2011	[67]
4,4′-(Benzo[b]benzo[4,5] thieno[2,3-d]thiophene-2,7-diyl)bis(butan-1-ol) (BTBT-C4OH)	100 K–300 K	200 K	P21/c	Monoclinic	Y	DSC, Thermal Expansion Measurements	2020	[68]
Estradiol 17β Valerate (E2V)	room temperature down to 100 K	251.1 K (cooling) and 256.3 K (heating)	P21	Monoclinic	N	FT-IR Spectroscopy, DFT Calculations	2021	[69]

Table 2. *Cont.*

Name	Pressure Range	Transition Range	Space Group	System	SCXRD	Other Methods	Year	References
Samarium Fulleride	4.2 K–295 K	32 K	Pcab	Orthorhombic	N	HRXRD, Magnetic Susceptibility Measurements	2003	[70]
$CaTiOSiO_4$—$CaTiOGeO_4$ Solid Solution	up to 1123 K	800 ± 25 K	P21/a (low temperature), A2/a (high temperature)	Monoclinic	Y	HTXRD, TEM, Spontaneous strain Analysis	2005	[71]
Lutetium Orthoborate	20–1450 °C	1020 °C	C2/c	Monoclinic	N	HTXRD, DSC, TGA, High-temperature Raman Spectroscopy	2020	[72]
Orthoenstatite	300 K–2000 K	1230 K	Pbca	Orthorhombic	N	aiMD Simulations	2004	[9]
Magnesium Aluminum Phosphate Oxide	room temperature up to 1170 °C	485 °C (758 K)	P21/c	Monoclinic	Y	HTXRD, DSC, Heat Capacity Measurements	2007	[73]

5.1. Low-Molecular-Weight Organic Compounds

5.1.1. Phenolic Compounds

Resorcinol

The high-pressure phase behavior of resorcinol (1,3-dihydroxybenzene), a hydrogen-bonded molecular solid, was investigated using Raman spectroscopy and photoluminescence up to 14.5 GPa. In addition to the extensively studied isosymmetric α→β transition at 0.5 GPa, a new disordered high-pressure phase (γ) was discovered at approximately 5.6 ± 0.2 GPa. The γ phase, characterized by weakened and broadened Raman signals, demonstrates reversibility with hysteresis during decompression. Significantly, fast pressurization that bypasses the α→β transition generates a unique, more ordered phase (δ) above 3 GPa, highlighting the impact of kinetic parameters and loading rate on phase development. This case also illustrates that the retention of the same space group is a necessary but not sufficient condition for a strict IPT; structural overlays and interaction topologies must be examined, as in α/β-resorcinol where $Pna2_1$ is preserved yet packing differs substantially [74,75].

The appearance of a broad photoluminescence band centered at 2.25 eV in both γ and δ phases indicated the formation of excimer-like states, suggesting a parallel stacking configuration of resorcinol molecules under high pressure. The disorder in the γ phase was attributed to pressure-induced polymorphism rather than amorphization, with the δ phase potentially signifying a crystalline polymorph among various energetically accessible configurations. These findings revealed the complex polymorphic setting of resorcinol under compression, influenced by hydrogen bonding, kinetic limitations, and transformation paths [1].

Hydroquinone–Formic Acid Clathrate

Eikeland et al. have examined the high-pressure characteristics of the hydroquinone–formic acid clathrate ($C_6H_4(OH)_2 \cdot 2HCOOH$), a host–guest system of hydroquinone ($C_6H_4(OH)_2$) frameworks that enclose disordered formic acid (HCOOH) molecules. The researchers employed SCXRD and Raman spectroscopy to investigate the evolution of the crystal structure up to 2 GPa using various pressure-transmitting media (PTMs).

A major finding was the identification of a reversible, pressure-induced IPT at around 1.3 GPa when subjected to compression in a non-penetrating PTM such as Daphne oil. The transition maintained the same space group ($P2_1/c$) but was marked by a sudden approximately 13% reduction in unit cell volume, signifying a first-order isosymmetric collapse. The structural change arises from a collapse of the hydrogen-bonded framework

due to densification, resulting in the expulsion of formic acid guest molecules from the one-dimensional channels formed by the hydroquinone hydrogen-bonded host framework.

In contrast, when a PTM such as a methanol–ethanol mixture was used—chemically distinct from the aqueous formic acid solvent of crystallization—the structural transition was suppressed. Fluid infiltration helps stabilize the open hydrogen-bonded framework and prevents collapse. This underlines the crucial influence of PTM selection on the pressure-induced structural response [38].

5.1.2. Amino Acids and Their Derivatives

L-Histidine

The pressure-induced structural transition of L-histidine ($C_6H_9N_3O_2$) was examined, focused on its polymorphs α and β. The authors employed HRXRD, complemented by SCXRD and Raman spectroscopy, to monitor the structural response of both polymorphs under escalating pressure up to 7.5 GPa. This comprehensive crystallographic analysis demonstrated that both forms experience reversible IPTs: α-L-histidine at approximately 2.6 GPa and β-L-histidine at around 2.3 GPa.

The transitions entailed important reorientations within the hydrogen-bonding network and rearrangements of molecular packing. The authors asserted that the response is mainly governed by cooperative molecular motions and the reallocation of intermolecular connections, rather than extensive reconstructions of the crystal lattice. The transitions were additionally defined by discontinuities in unit-cell volume and compressibility, substantiating their first-order characteristics.

The research illustrates that even basic amino acids can exhibit complex pressure responses, and that isosymmetric transitions may occur more frequently in biological molecules than previously believed and emphasizes the significance of integrating SCXRD, HRXRD, and vibrational spectroscopy to describe subtle transitions, underscoring the value of high-pressure crystallography in comprehending biomolecular solid-state changes [12].

DL-Cysteine

The complex relationship between temperature and pressure when inducing polymorphic transitions in DL-cysteine ($C_3H_7NO_2S$), an amino acid that has both hydrophilic and hydrophobic characteristics, was analyzed. The authors examined structural behavior at low temperatures (as low as 3 K) and pressures up to 2.6 GPa using a combination of PXRD, infrared spectroscopy (IR), and computational methods. They determined that both temperature and pressure stimuli can induce phase transitions, with particular emphasis on the transition from DL-cysteine-I to DL-cysteine-II.

An IPT was observed, showing that it was caused by internal rearrangements within the crystal rather than a symmetry-breaking. This transition pertains to the reconfiguration of hydrogen bonding interactions—specifically between the $–CH_2SH$ side groups and N–H···O hydrogen bonds—as the molecular packing modifies in response to external stimuli. Furthermore, the same polymorph (DL-cysteine-II) can be obtained through either cooling or compressing the primary DL-cysteine-I phase, underlining the similar structural reactions to thermal contraction and pressure-induced strain.

This study demonstrated that pressure may induce more significant strain changes than temperature, indicating that competing van der Waals and hydrogen bonding interactions determine the polymorphism landscape. These findings align with behaviors previously reported in other amino acids such as glycine and L-alanine (Figure 2) [33].

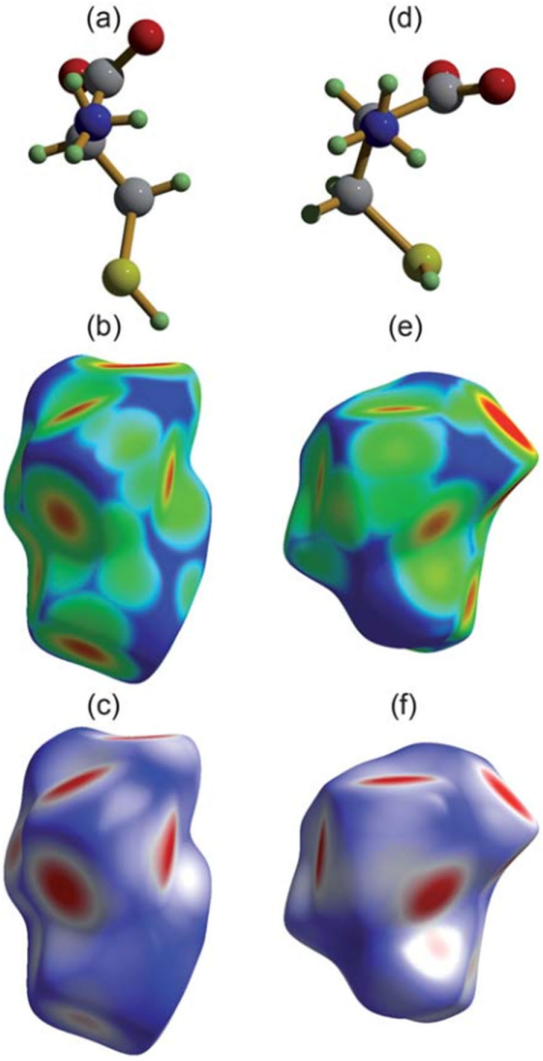

Figure 2. Molecular conformation and Hirshfeld surfaces of DL-cysteine-I at 225 K (**a**–**c**) and DL-cysteine-II at 200 K (**d**–**f**). Each molecule is shown with the Hirshfeld surface mapped with de (**b**,**e**); for these series mapped between 1.0 (red) and 2.0 A (blue)] and dnorm [(**c**,**f**); mapped between 0.71 (red) and 1.1 A (blue)], where de is the distance to the nearest atom center exterior to the surface and dnorm is the normalized contact distance, which takes the van der Waals radii of the atoms into account. Reprinted from [33] with permission from the Royal Society of Chemistry.

L-Serine

The high-pressure behavior of crystalline L-serine was examined using SCXRD and HRXRD within a diamond anvil cell. Two isosymetric pressure-induced phase transitions were observed: the first transition occurred at 5.3 GPa, resulting in polymorph II, and the second transition at 7.8 GPa, forming polymorph III. The first included only minor changes in unit-cell volume and showed significant modifications in molecule conformation and hydrogen-bond geometry. However, the second showed more significant structural reorganization and changes in packing density. PXRD data confirmed findings, enabling the precise identification of equation-of-state parameters and uncovering minor atomic displacements during the first transition. The integration of single-crystal and powder methods provided an extensive understanding of the compression mechanism, illustrating the gradual adaptation of hydrogen-bond networks under elevated pressure.

The behavior of L-serine is atypical as it has undergone two consecutive isosymmetric transitions, where a minor structural change is followed by a more significant reorganization, which is an unusual occurrence among amino acids under high pressure [47].

α-Glycylglycine

Clarke et al. have examined the high-pressure behavior of α-glycylglycine (α-digly) up to 14.5 GPa, utilizing synchrotron PXRD, Raman spectroscopy, and first-principles-based calculations, which demonstrated a notable change in lattice behavior beyond approximately 6.7 GPa. PXRD analysis revealed a modification in axial compressibility, particularly the strengthening of the c-axis alongside heightened compressibility in the a- and b-axes. This change does not entail a loss of monoclinic $P2_1/c$ symmetry, indicating an IPT. Complementary Raman spectra showed sudden frequency shifts, mode splitting, and changes in pressure coefficients between 6 and 7.5 GPa, especially in the N–H and C–H stretching regions, consistent with a reorganization of hydrogen-bond networks.

USPEX-based structure searches and DFT calculations have revealed multiple potential high-pressure polymorphs. An orthorhombic phase ($P2_12_12_1$) is anticipated to represent the lowest-enthalpy state above approximately 6.4 GPa; however, its simulated diffraction pattern did confirm the experimental results. The most feasible candidate, α′-digly, maintains the $P2_1/c$ symmetry characteristic of the low-pressure phase, yet exhibits subtle structural alterations: bending of the peptide backbone, rotation of the terminal amine group, and a reconfigured hydrogen-bonding arrangement that adds a new C–H···O interaction. These modifications aligned with the experimentally observed changes in axial compressibility. While calculations indicated that α′-digly is more stable only beyond approximately 11.4 GPa, the lsmall energy disparity from α-digly within the 6–9 GPa range, along with recognized computational constraints in modeling hydrogen bonds, confirmed that it is responsible for the observed transition.

The suggested driving force is the relief of strain in short N–H···O hydrogen bonds that approach critical bond-length thresholds under compression, a phenomenon observed in other amino acids as well. The α′-digly structure is chemically different from α-digly because of intramolecular charge redistribution, which potentially affect its reactivity [45].

5.1.3. Amides, Amidines, and Nitrogen-Containing Heterocyclic Compounds

N-Isopropylpropionamide

The P,T phase diagram of N-(isopropyl)propionamide (NiPPA) shows two solid-state transformations within the same molecular system: a low-pressure plastic crystalline (PC)–crystalline (C) transition and a high-pressure isosymmetric crystalline–crystalline transition above ~4 GPa. As determined by synchrotron X-ray diffraction, the latter was characterized by strong anisotropic compression, substantial molecular flattening, and isopropyl group reorientation, which resulted in a denser packing of the high-pressure β-form in comparison to the low-pressure α-form. Despite the existence of intermolecular hydrogen bonds in all solid phases, the PC–C boundary, measured at pressures as high as around 400 MPa, produced apparent ΔV and ΔH values that are similar to those of non-hydrogen-bonded analogs. The PC phase is metastable over the entire investigated P–T range, with extended coexistence regions resulting from kinetic effects. The phase diagram highlights the complex interactions between metastability, kinetics, and anisotropic structural responses by demonstrating the uncommon coexistence of a high-pressure isosymmetric transition and a pressure-dependent PC–C transition in the same molecular crystal (Figure 3) [28].

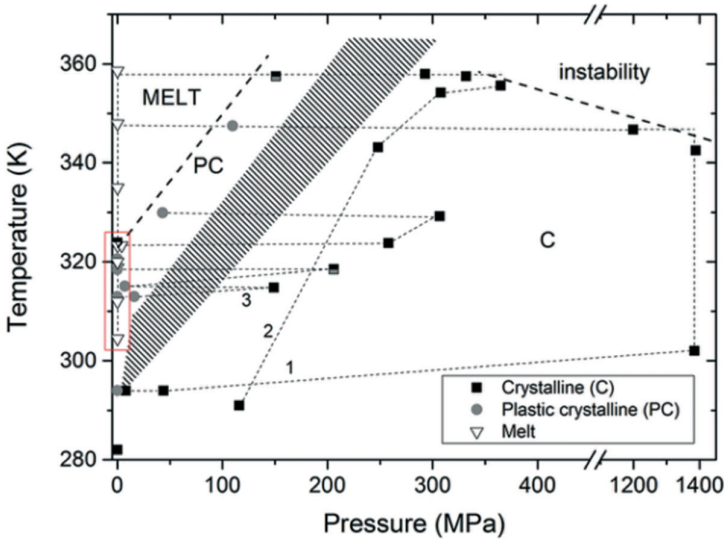

Figure 3. Diagram depicting the P–T trajectories (1, 2, and 3: dotted lines) employed to examine the phase transformation characteristics of NiPPA. The region marked in red illustrates the alteration of the compound subsequent to high-pressure and high-temperature treatment in run 2. It is important to note that the plastic crystalline phase remains metastable across all pressure and temperature levels. The shaded zone denotes the location where a metastable C–PC phase transition is anticipated to transpire. The dashed line in the upper right signifies a crystalline instability that leads to a fast reduction in pressure within the cell and the vanishing of the X-ray diffraction pattern. Reproduced from [28] with permission from the Royal Society of Chemistry.

Biurea

High-pressure neutron diffraction, Raman spectroscopy, and DFT calculations showed that biurea underwent a first-order IPT near 0.6 GPa, accompanied by a ~5% unit-cell volume collapse. The transition was driven by substantial intramolecular reorientation, specifically a change in the torsional angle between the two urea units, together with notable changes in hydrogen-bond geometries. In accordance with a "wine-rack" hinging mechanism, compression caused negative linear compressibility along one principal axis in both phases. Compared to Phase I, Phase II showed a higher density but unexpectedly higher compressibility. Hydrogen-bonding changes were anisotropic: some N-D···O interactions shortened continuously, while others lengthened at the transition, resulting in altered N-N bond characteristics and Raman mode intensity shifts. According to DFT results, Phase I was stabilized at ambient pressure by vibrational zero-point and entropic contributions, while Phase II was favored by static lattice energy. The pV term increased with increasing pressure, shifting stability toward Phase II. The study demonstrated the subtle yet significant impact of vibrational free-energy terms on phase stability under compression, emphasizing their role in stabilizing phases across isosymmetric transitions in molecular crystals [3].

1,4-Diazoniabicyclo[2.2.2]octane-1-acetate-4-acetic Acid Chloride Trihydrate

The 1:1:3 complex of 1,4-diazoniabicyclo[2.2.2]octane-1-acetate-4-acetic acid with chloride ions and water underwent a reversible first-order IPT between 210.7 K (heating) and 180.3 K (cooling), with a thermal hysteresis of 30.4 K. The transition, accompanied by dielectric anomalies, was confirmed by dielectric measurements and DSC. Both the high- and low-temperature structures adopted the monoclinic $P2_1/n$ space group; however, there were notable differences in cell parameters, especially a doubling of the a-axis and unit cell volume upon cooling. A reorganization of hydrogen-bonded anionic chains that were formed between water molecules and chloride ions was the driving force behind the tran-

sition. In the low-temperature phase, two different chain types with varying ring motifs, dihedral angles, and chloride–oxygen arrangements replaced the single chain type that was present in the high-temperature phase. Without significant changes in donor–acceptor distances, these rearrangements were caused by changes in the relative positions of water molecules and chloride ions. The water molecules' overall crystal symmetry and hydrogen-bond metrics were maintained when they were deuterated, but the thermodynamic and dielectric signatures changed, adding anomalies close to 243 K that were probably caused by isotope effects on proton dynamics. This study showed that IPTs in hydrogen-bonded molecular crystals could be caused by modifications in hydrogen-bond topology rather than symmetry breaking [62].

2-(3,5-Bis(trifluoromethyl)phenyl)-4,5-dihydro-1H-imidazole

The examined imidazole-based single-component molecular crystal, 2-(3,5-bis(trifluoromethyl)phenyl)-4,5-dihydro-1H-imidazole underwent an isosymmetric dynamic disorder-order reversible phase transition at around 150 K with a thermal hysteresis of ~15 K. Variable-temperature PXRD and SCXRD, supported by DSC, demonstrated the transition was driven by rotational disorder in the terminal $–CF_3$ groups, that became ordered upon cooling. The material showed distinct anisotropic thermal expansion, which was positive (PTE) along the a-axis, near-zero (ZTE) along the b-axis, and negative (NTE) along the c-axis, resulting in uniaxial NTE and biaxial PTE features in both high- and low-temperature phases. Structural analysis revealed that N–H···N hydrogen bonds formed scissor-like motifs, with the b-axis hinge explaining the ZTE and scissor-jack-like motion accounting for the axial PTE/NTE. The ordered low-temperature phase was found to be more stable than the disordered high-temperature phase, using the energy framework, lattice, and packing calculations. These results demonstrated that this organic system holds promise for environment-friendly thermoresponsive device applications [63].

5.1.4. Functional Organic Compounds for Electronic and Ionic Applications

Rubrene

A reversible isosymmetric single-crystal-to-single-crystal phase transition was observed in triclinic rubrene(5,6,11,12-Tetraphenyl-tetracene), using high-pressure SCXRD. Anisotropic shortening along the π–π stacking direction of the tetracene cores, along with progressive twisting of phenyl substituents and "scissoring" between phenyl pairs, caused the compression of form I up to 5.91 GPa to result in a ~23% reduction in molecular volume. PIXEL lattice energy calculations and Hirshfeld surface analysis showed that during compression, π–π interactions gradually decreased as C–H···π contacts increased. The structure changed into form II at 7.12 GPa, losing inversion symmetry and tripling the unit-cell volume. In comparison to the ambient-pressure form, this new conformation had a significant "double twist" of the tetracene backbone and substantial phenyl torsions, resulting in an intramolecular energy penalty of about 70 kJ mol^{-1}. The transition was primarily driven by packing efficiency and a reduction in the PV term, rather than conformational stabilization. When decompressed between 5.0 and 4.0 GPa, the transition was completely reversible without causing crystal deterioration. Structural analysis revealed that whereas compression of form I should enhance charge-transport properties, by decreasing π-π distances, form II may not demonstrate improved mobility due to decreased C···C contacts despite its higher density [35].

BTBT-C4OH

Dumitrescu et al. analyzed the temperature-dependent structural evolution of 4,4′-(benzo[b]benzo[4,5]thieno[2,3-d]thiophene-2,7-diyl)bis(butan-1-ol) (BTBT-C4OH) and

found a rare continuous crossover from positive to negative uniaxial thermal expansion along the monoclinic b-axis near 200 K.

SCXRD between 100 and 300 K showed that atomic displacement parameters (ADPs) for all non-hydrogen atoms displayed a distinct slope shift and negative discontinuity at the crossover. All translational tensor eigenvalues were discontinuous at the same temperature, according to rigid-body Translation–Liberation–Screw (TLS) analysis, whereas liberational eigenvalues merely changed in slope, which is consistent with a continuous type-0 first-order IPT.

BTBT-C4OH has a staggered herringbone packing and differs from BTBT-C6OH by having shorter side chains, lack of close S···S contacts, and weaker anharmonic molecular motion. These characteristics correspond to smaller negative expansion. The crossover was caused by steric compensation between herringbone arranged molecules, where contraction along b-axis was induced by increased liberational motion and herringbone angle with temperature. This mechanism, which is influenced by chain length, is similar to that in pentacene and BTBT-C6OH. Clear ADP and TLS anomalies and the lack of sudden changes in geometric parameters demonstrated the usefulness of displacement tensor analysis at identifying subtle isosymmetric transitions [68].

2-Nitroanilinium Bisulphate

The crystalline 2-nitroanilinium bisulphate underwent a reversible, first-order IPT at 232 K, which was characterized by abrupt changes in lattice characteristics and marked hysteresis. The transition was driven by a concerted double proton transfer within centrosymmetric $(HSO_4)_2$ dimers, which reconstructed the $R^2_2(8)$ hydrogen-bond ring motif into an alternative configuration without changing the overall donor/acceptor count. A topologically invariant component of the hydrogen-bond network was highlighted by graph-set analysis, which showed a consistent $R^6_6(20)$ pattern that was maintained throughout the transition. While π–π stacking between aromatic cations strengthened during cooling, structural rearrangements include shifts in ammonium hydrogen-bond acceptors and restructuring of ring patterns (e.g., $R^2_2(6)$ to $R^2_3(8)$, $R^4_6(16)$ to $R^4_4(12)$). The calorimetric signature of a first-order event was confirmed by DSC measurements, and the typical splitting of bisulphate bending modes was identified by IR spectroscopy, which was consistent with symmetry-preserving structural modifications. Two minima corresponding to different hydrogen-bond arrangements were observed using computational modeling of the relaxed potential energy surface for the $(HSO_4)_2$ dimer: non-centrosymmetric $[H_2SO_4/SO_4^{2-}]$ and centrosymmetric $[SO_4^{2-}/2H^+/SO_4^{2-}]$. The second one exhibited greater geometric distortion while possibly facilitating ion displacement [53].

4-Ethylanilinium Hydrogen (2R,3R)-Tartrate

The homochiral organic salt of ethylanilinium hydrogen (2R,3R)-tartrate underwent a reversible IPT at about 186 K. A configurational order–disorder mechanism was confirmed by calorimetric data, which showed a first-order transition with small thermal hysteresis (0.7 K) and an entropy change ($\Delta S = 0.89$ J K^{-1} mol^{-1}). Variable-temperature XRD revealed abrupt unit-cell changes and a near-doubling of cell volume. The transition involved extensive reorganization of hydrogen-bond networks and significant phenyl-ring reorientation (~22°), meanwhile dielectric measurements revealed no anomaly at accessible frequencies, implying low-frequency ferroelectric behavior. A reversible isosymmetric transition of this kind has never been observed in a homochiral organic salt before (Figure 4) [51].

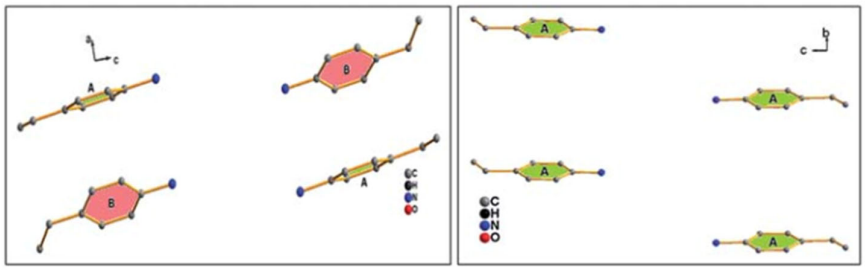

Figure 4. Packing diagrams of 4-ethylanilinium cation moieties in the homochiral organic salt of ethylanilinium hydrogen (2R,3R)-tartrate at 123(2) K (**left**) and 298(2) K (**right**) viewed along the b axis and a axis, respectively. The hydrogen tartrate anions and all hydrogen atoms were omitted for clarity. Reprinted from [51] with permission from the Royal Society of Chemistry.

Pyridinium-3-Carboxylic Acid Perchlorate

Ye at al. reported a reversible first-order isosymmetric transition in pyridinium-3-carboxylic acid perchlorate at around 129 K. Dielectric measurements and DSC confirmed the transition with a broad hysteresis of about 15 K. SCXRD showed that the unit-cell parameters, particularly the c axis and monoclinic angle, change suddenly, which is consistent with a discontinuous character.

The layered structure of the compound is formed by hydrogen-bonded pyridinium-3-carboxylic acid cation chains that are connected together by perchlorate anions. The most noticeable differences between phases were shortened distances between neighboring pyridinium ring planes and a significant displacement of hydrogen-bonded layers. The progressive ordering of the perchlorate anions upon cooling was considered a secondary effect. The reorientation of the pyridinium cations, which strengthened hydrogen bonding and stabilized the low-temperature phase, was found to be the main driving force (Figure 5) [56].

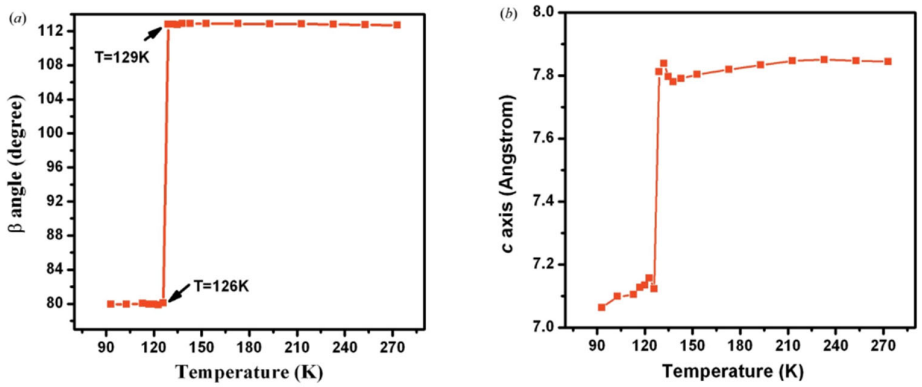

Figure 5. Temperature dependency of the c axis (**b**) and angle (**a**) in the 93–273 K range. Reprinted from [56] with the permission from IUCr journals.

5.1.5. Active Pharmaceutical Ingredients

Dapsone

The reversible IPT between dapsone (DDS) polymorphs II and III was observed using thermal analysis, variable-temperature XRD, and intermolecular energy calculations. This first-order solid–solid transition occurred at 78 ± 4 °C, with a low enthalpy of transformation (~2 kJ mol^{-1}) and minimal hysteresis, indicating fast kinetics and reversibility. The only differences between the two polymorphs were a relative shift in molecular layers and minor molecular conformations. According to structural analysis, despite being the high-temperature phase, form II adopted a denser packing arrangement than form III.

This is an exception from the density rule that is usually seen in enantiotropically related polymorphic pairings, which was further studied using pairwise intermolecular energy calculations. The results showed that the loss of a strong N–H···O hydrogen bond during the transition from III to II was compensated by increased dispersion contributions, stabilizing the more compact form II. The transition pathway included slight conformational changes and cooperative layer displacements, which was consistent with the transitions' single-crystal-to-single-crystal nature and the low activation barrier indicated by the calorimetric data [54].

Chlorothiazide

Chlorothiazide was found to undergo a pressure-induced IPT at 4.2 GPa. The authors utilized detailed periodic DFT calculations, along with phonon and thermodynamic analyses, to determine whether such a transition could be predicted computationally. The reverse transition (Form II → Form I under decompression) was reproduced using geometry optimization, however the forward pressure-driven process was not captured, which showed that there is a major energy barrier. Nevertheless, the energetic and Gibbs free energy comparisons consistently indicated that Form II was thermodynamically more stable at high pressures, which was consistent with experimental observations. The transition was also demonstrated to be entropy-driven, as evidenced by phonon-derived parameters. Significantly, the conversion of Form I into Form II under pressure was successfully replicated by aiMD simulations, overcoming the kinetic constraints of static optimization and showed the potential of aiMD as a predictive tool for IPTs (Figure 6) [2].

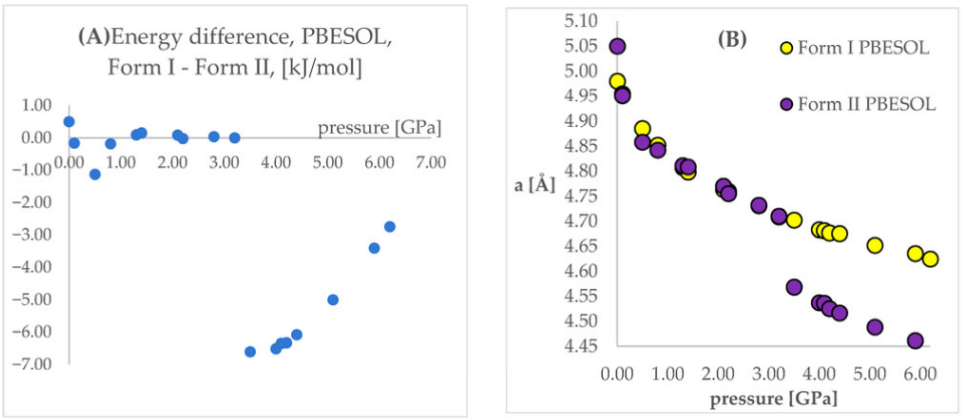

Figure 6. (**A**) Differences between the energies (Form I–Form II) of the chlorothiazide structures modeled using PBESOL functional, with respect to pressure. (**B**) The change in unit cell edge "a" length obtained from calculations using PBE TS functional, with respect to pressure. Yellow circles—using Form I as initial; violet circles—using Form II as initial. Reprinted from [2], licensed under CC BY 4.0.

Ibuprofen Lysine Salt

The solid-state behavior of ibuprofen lysine salt was studied using DSC and variable-temperature XRPD, which revealed a fully reversible polymorphic transition near 70 °C. Despite experimental difficulties related to powder data, two crystalline phases, identified as IBL-I (ambient temperature) and IBL-II (high temperature), were structurally described. Both polymorphs showed strong structural similarities in molecular conformation, hydrogen-bonding networks, and packing motifs. The transition was linked to anisotropic lattice strain, specifically an expansion along the b axis and a subtle contraction along the a axis. The extensive hydrogen-bonding structure was maintained throughout the phases, and the molecular rearrangements were confined to conformational shifts within lysine and minor torsional adjustments of the ibuprofen isopropyl group.

According to an analysis of structural strain tensors, the disengagement of interdigitated isopropyl groups, which resulted in a displacing but reversible rearrangement without bond cleavage, was the driving force behind the transition. The event's low enthalpy change (+2.3 kJ mol^{-1}) was in consistent with the structural disturbances' minor character [52].

R-Cinacalcet Hydrochloride

The polymorphic system of R-cinacalcet hydrochloride displayed a reversible solid–solid transition between form III° and the high-temperature form I, maintaining the orthorhombic space group ($P2_12_12_1$). The transition took place at 148.5 °C, exhibiting a significant hysteresis of approximately 30 K, as determined through DSC and variable-temperature PXRD. Although symmetry change was not observed, notable structural reorganization was reported. In form III°, molecular packing was characterized by distinct crankshaft-like chains formed by N–H···Cl^- hydrogen bonds. Meanwhile, form I showed dynamic orientational disorder of the phenyl moiety, along with minor changes in hydrogen-bond geometry and a rotation of the naphthyl group. The transition maintained the overall lattice structure while allowing for enhanced molecular mobility, representing an example of an IPT triggered by conformational dynamics. Significantly, the transformation was enantiotropic and fully reversible, with form III° remaining stable below the transition point and form I above it [55].

Estradiol 17β Valerate

Estradiol 17β valerate (E2V), an esterified derivative of the natural hormone estradiol, underwent a reversible IPT at 251 K. The structural change was triggered by a significant conformational reorientation of the valerate side chain, which was accompanied by an unusual contraction of the b axis. The first-order and discontinuous nature of the transition was confirmed by DSC, which also showed latent heat and thermal hysteresis that were consistent with an order–disorder mechanism involving the freezing of dynamic disorder in the high-temperature phase.

The discontinuity was verified by the solid-state ^{13}C NMR spectra, which showed noticeable spectrum broadening and chemical shift alterations below the transition. The valerate fragment's conformational reconfiguration was confirmed to be the primary structural driver by complementary vibrational spectroscopy, which revealed small but reversible intensity changes in selected infrared bands. The intermolecular hydrogen-bonding network was preserved throughout the transition, despite the noticeable conformational changes [60].

Pandey et al. reported a reversible low-temperature IPT in E2V, which occurred near 250 K and was triggered by subtle reorientations along the valerate side chain. Changes in this chain's torsional angles (ϕ1, ϕ2, ϕ3) caused conformational differences between the room- and low-temperature phases and altered hydrogen-bonding patterns. Vibrational spectroscopy and DFT calculations revealed a clear correlation between characteristic infrared bands at 1115, 1200, and 1415 cm^{-1} and the conformational changes in the valerate side chain, serving as transition fingerprints. Potential energy surface scans verified feasible conformers that corresponded to experimental torsional angles, supporting the order–disorder mechanism described by Buerger's classification. Furthermore, E2V maintained agonist activity toward estrogen receptor isoforms, as shown by molecular docking simulations, while the binding energies were modulated by conformational variation across phases [69].

5.1.6. Organic Radicals

Blatter's Radical

High-pressure crystallographic studies of Blatter's radical up to 6.07 GPa revealed a first-order IPT, followed by ongoing structural changes. Compression was highly anisotropic, with the highest strain occurring along the π-stacking direction. Between 3.42 and 5.34 GPa, gradual rotation of the N-phenyl substituent accommodated increasing intermolecular repulsion, serving as a cautionary second-order transition. This rotation underwent a discontinuous jump, indicating the first-order isosymmetric transition, upon further compression to 5.54 GPa. The transition was primarily driven by volume minimization rather than the relief of unfavorable contacts, whereas the triazinyl core's planarity was enhanced, as confirmed by DFT calculations connecting this conformational change to the alleviation of intramolecular H···H strain. The intermolecular coupling was strengthened as π-stacking contacts were shortened by 0.34 Å over the pressure range. Although radical dimerization was not observed, the transition suggested potential consequences for magnetic behavior, including a potential pressure-driven shift toward a diamagnetic ground state and enhanced antiferromagnetic interactions [49].

5.2. Inorganic Compounds and Metal Complexes

5.2.1. Simple Salts and Oxides

Sulfamic Acid

Raman spectroscopy and synchrotron XRD were used to investigate the structural response of sulfamic acid ($NH_3^+SO_3^-$) under high pressure. Results revealed a reversible IPT between 10.2 and 12.7 GPa. The transition was initiated by conformational distortions of the SO_3^- and NH_3^+ groups above 8 GPa and was characterized by a discontinuous contraction of the c-axis (~9%), resulting from the sliding of hydrogen-bonded chains along this direction, which rearranged the hydrogen-bonding network and strengthened electrostatic interactions between zwitterionic units. These rearrangements created a tighter packing pattern with decreased compressibility along c. The gradual character of the transition showed kinetic hindrance from short-range electrostatic repulsion, and decompression studies revealed full reversibility. The study established sulfamic acid as a model system for pressure-driven isosymmetric transformations in hydrogen-bonded molecular crystals by connecting anisotropic lattice distortions with molecular conformational changes [10].

Ammonium Bicarbonate

Ammonium bicarbonate (AB) underwent a pressure-induced IPT at approximately 2 GPa, driven by the interaction of its highly anisotropic elastic response and the structure of its hydrogen-bonding network. Synchrotron XRD and Raman spectroscopy demonstrated that compression along the bc-plane was countered by a "double-wine-rack" hydrogen-bonding motif, resulting in atypically rigid mechanical properties of the otherwise soft N–H···O and O–H···O bonds. The biaxial hard compression minimized major distortions in the bc-plane and facilitated quasi-uniaxial contraction along the a-axis, allowing for subtle structural rearrangements that led to the formation of new N–H···O hydrogen bonds between ammonium cations and bicarbonate anions. The lack of peak splitting in both Raman and XRD signatures supported the isosymmetric nature of the transition, indicating that only local hydrogen-bond reconfigurations occurred, rather than a global symmetry reduction [4].

Sodium Oxalate

A reversible first-order IPT in crystalline sodium oxalate ($Na_2C_2O_4$) was identified at 3.8 GPa, as revealed using high-pressure Raman spectroscopy in diamond anvil cells and

synchrotron PXRD methods. The transition involved abrupt changes in unit-cell parameters, specifically a significant reduction in the monoclinic angle β and a noticeable volume contraction from 176 $Å^3$ at 3.6 GPa to 167 $Å^3$ at 4.3 GPa. Raman spectra demonstrated significant frequency discontinuities in various vibrational modes, especially in the low-frequency range associated with the translational motions of Na^+ cations. The lack of a soft mode indicated that the transition did not occur through conventional phonon softening. Structural refinements showed that the oxalate anions underwent collective reorientations while largely maintaining their centroid packing. However, the sodium cations exhibited a change in coordination from sixfold (3O(1) + 3O(2)) to sevenfold (4O(1) + 3O(2)), with the most significant positional shifts observed for Na^+. The lattice-dynamics calculations of the elastic constants confirmed structural stability at pressures significantly exceeding the transition point, thereby ruling out elastic instabilities as the driving force (Figure 7) [31].

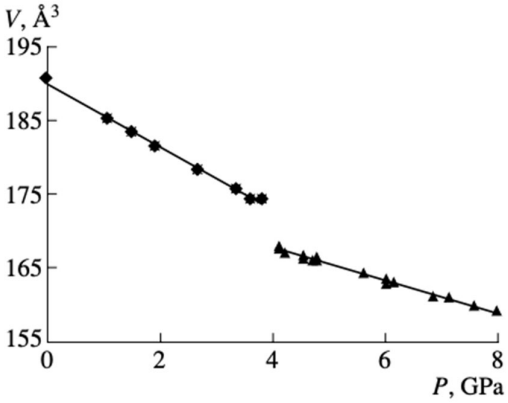

Figure 7. Cell volume of sodium oxalate vs. pressure. Reprinted from [31] with the permission from Pleiades Publishing.

Caesium Hydroxide

The compression behavior of Caesium Hydroxide (CsOH) and Rubidium Hydroxide (RbOH) was investigated computationally, and the results showed a richer sequence of high-pressure phases than had been previously identified. The structural assignment of the RbOH-VI phase has been revised, revealing a tetragonal topology similar to that of KOH-VI, defined by localized square-planar $(OH)_4$ units within a distorted CsCl-like cation framework. This transformation signifies a shift from layered structures to compact three-dimensional hydrogen-bonded networks, characterized by a significant increase in density and spectroscopic signatures indicative of weakened hydrogen bonding. Calculations showed that in CsOH, a pressure-induced IPT occurred around 10 GPa, resulting in the formation of a new phase, CsOH-VII. This phase exhibited a subtle reorganization of kinked one-dimensional OH chains and a reorientation of CsO_5 polyhedra into a three-dimensional network. The enthalpic driving force for this transition was relatively small, indicating sluggish kinetics and accounting for the lack of experimental confirmation, despite the possibility for detection through diffraction signatures. The dimensionalities of RbOH-VI and CsOH-VII, which ranged from localized clusters to extended one- and two-dimensional motifs, demonstrated the unexpected versatility of hydrogen-bond network formation in alkali hydroxides. This flexibility suggests that similar IPTs could occur in other hydrogen-bonded solids, affecting the structural diversity and physical properties of hydrous minerals in mantle conditions (Figure 8) [44].

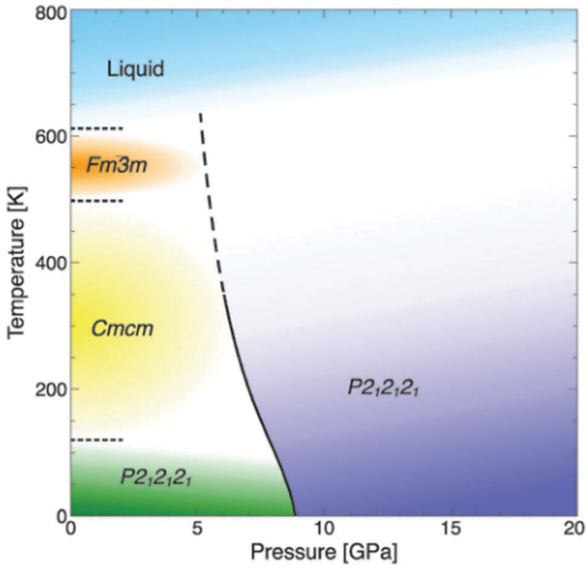

Figure 8. Phase diagram of CsOH, including the calculated transition line CsOH-IVc–VII (solid-dashed line), experimental data at P = 1 atm (dotted lines), and estimates for the high-temperature phases' stability fields (colored areas). Reprinted from [44] with the permission from the Royal Society of Chemistry.

Cobalt Iodate

Synchrotron XRD, Raman and IR spectroscopy, and DFT calculations revealed two symmetry-preserving phase transitions in cobalt iodate, $Co(IO_3)_2$, at ~3 GPa and 9–11 GPa. Both transitions included pressure-induced rearrangements fueled by the iodate ion's stereochemically active lone electron pair. Despite overall volume contraction, the lattice reaction was highly anisotropic, showing an unexpected expansion along the a and c axes, which was explained by the progressive elongation of specific I–O bonds, allowing for the formation of additional coordination environments at high pressure. The calculated vibrational properties and mode symmetries were consistent with the spectroscopic measurements, which showed clear anomalies in phonon frequencies and mode splitting across the transitions. Pressure-volume equations of state were established up to 27 GPa, resulting in bulk modulus values consistent with theoretical predictions. The role of iodine coordination increase in stabilizing isosymmetric high-pressure phases has been highlighted by the comparative analysis with related iodates like $Fe(IO_3)_3$ and $Zn(IO_3)_2$ [42,44,74,75].

Zinc Iodate

Zinc Iodate $(Zinc(IO_3))_2$, a metal iodate with stereoactive lone electron pairs on iodine, was analyzed using SCXRD, Raman spectroscopy, and DFT calculations and two reversible IPTs, which occurred in the approximate ranges of 2.5–3.4 GPa and 8–9 GPa were observed. The structural alterations were primarily caused by gradual distortions of the IO_6 polyhedra, including shortening of the long I-O bonds and elongation of the short ones, whilst ZnO_6 octahedra remained stiff. The transitions were accompanied by S-shaped compressions of unit-cell axes and anomalous, nonlinear changes in Zn–O distances, showing that the structural reaction was driven by local polyhedral adjustments. Raman spectra showed mode softening and reversible intensity changes in certain vibrations, indicating a gradual decrease in iodine lone electron pair stereoactivity and a minor reorganization of the coordination environment. The overall connectivity of the crystal structure remained preserved regardless of these significant bond rearrangements, showing that symmetry breaking did not occur the transitions [43].

Magnesium Aluminum Phosphate Oxide

The thermal behavior and polymorphism of $MgAlPO_4O$, a breakdown product of lazulite, were studied across a wide temperature range using DSC, thermogravimetric analysis, and in situ HTXRD. At 758 K, $MgAlPO_4O$ underwent a reversible IPT, during which minor rearrangements of the AlO_6 and PO_4 polyhedra were observed. The transition involved a discontinuous shift in lattice parameters, resulting in cooperative modifications in bond lengths and angles that improved structural packing efficiency. Thermochemical analysis showed a enthalpic anomaly associated with the transition, suggesting latent heat connected to the framework's reorganization [73].

Dabcodiium Chlorochromate Chloride

Dabcodiium chlorochromate chloride was shown to undergo a reversible structural phase transition at around 185 K, as confirmed by sharp DSC peaks with 4.9 K hysteresis and step-like dielectric anomalies. The isosymmetric nature of the transition was confirmed by variable-temperature crystallographic study, which showed that both high- and low-temperature structures remained monoclinic in $P2_1/m$. The a-axis tripled during the transition, while the b, c, and β parameters remained essentially unaltered. According to structural comparison, the transition was primarily driven by a ca. 60° reorientation of one-third of the chlorochromate anions by the rotation of the CrO_3 groups around the Cr–Cl bond with accompanying rotation of a subset of dabcodiium cations. However, the chloride counterions and hydrogen-bonding networks underwent minimal rearrangement, and the deuterated analog exhibited practically comparable thermal behavior, emphasizing the insignificant role of hydrogen bonding in the transition. The relatively weak dielectric response was explained by the discontinuous nature of the phenomenon, the structural similarity between high- and low-temperature phases, and the lack of notable dipole changes. In summary, these findings determined that the transition was a first-order, temperature-induced IPT dominated by anion reorientation rather than cation ordering (Figure 9) [50].

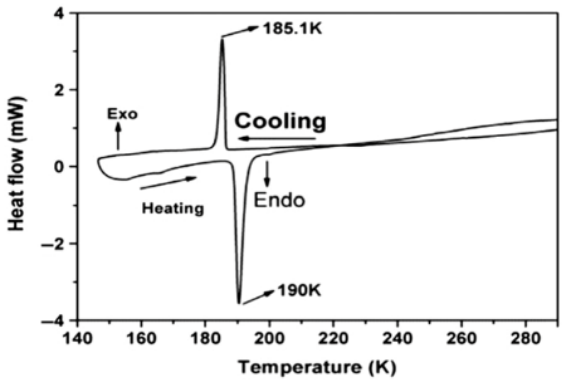

Figure 9. DSC curves displaying sharp peaks near 185 K, evidencing a reversible first-order phase transition. Reprinted from [50] from Elsevier.

5.2.2. Inorganic Fluorides

Lead Fluoride

Stan et al. observed that lead fluoride (PbF_2) compressed up to 75 GPa underwent a continuous isosymmetric transition from cotunnite- to Co_2Si-type phase between 10 and 22 GPa. XRD displayed unusual lattice behavior with significant anisotropy in axial compressibilities but no volume discontinuity. DFT calculations revealed a tenfold environment resembling the Co2Si-type phase, resulting from progressive bond rearrangements and the development of an additional Pb-F bond.

PbF_2 partially transformed to the 11-coordinated Ni2In-type phase upon heating above 1200 K, at and over 25.9 GPa; however, it returned to Co_2Si-type phase after the temperature was quenched, indicating a negative Clapeyron slope. Although only partial retention occurred at ambient conditions, near-complete transformation was achieved above 43 GPa at high temperatures. The values of the bulk modulus showed only minor differences in compressibility between the phases.

In contrast to alkaline earth difluorides, PbF_2 showed a unique high-pressure routing, with isosymmetric development dominating its structural response. This results align with predicted patterns for lanthanide and actinide dioxides at megabar pressures, emphasizing the importance of continuous transitions in AX_2 compounds [30,76–79].

High-pressure diffraction studies on orthorhombic PbF_2 revealed a first-order isosymmetric transition near 10 GPa. The cotunnite-type phase (Pnam, Z = 4, CN = 9) changed into a Co_2Si-related structure with the same symmetry but increased coordination (CN = 10). The transition resulted in a small volume collapse (~2%) and anisotropic lattice compression, primarily along the a-axis. Other cotunnite-type dihalides stabilize either monoclinic post-cotunnite or hexagonal Ni_2In phases. PbF_2, on the other hand, followed a different structural path, yielding a third high-pressure configuration in this family. The isosymmetric nature of the transition and its initiation in the minor modifications of the cation coordination environment were confirmed by both Raman data and theoretical calculations [30].

Sodium Manganese Fluoride

A pressure-induced, reversible IPT was observed in Na_3MnF_6 within the range of 1.7–2.2 GPa. Single-crystal diffraction data indicated that the transition was induced by a reorientation of the static Jahn–Teller distortion of Mn(III). At ambient pressure, the elongated axis of the MnF_6^{3-} octahedron was oriented approximately 20° from [001]. Above the transition, this axis rotates to about 70°, directing towards a distinct set of fluorine ligands. The distortion flip was confirmed by polarized optical absorption spectroscopy, revealing significant and fully reversible changes in the polarization of spin-allowed d–d transitions in Mn^{3+} depending on the transition pressure. Compressibility measurements indicated anisotropic lattice responses consistent with the packing of Na^+ and F^- layers, implying that the transition reflected a shift from distortions accommodated perpendicular to these layers to orientations within them. The hysteresis of approximately 0.5 GPa represents the first well-described instance of Jahn–Teller distortion reorientation in a Mn^{3+} compound subjected to pressure. The findings highlighted the significance of electronic configuration in stabilizing isosymmetric transformations, in contrast to the lack of a similar transition in isostructural Na_3ScF_6 [48].

5.2.3. Coordination Complexes and Ionic Compounds

Copper–Dicyanoaurate Complexes

A study of Cu-Au supramolecular compounds synthesized from chelating ligands and dicyanoaurate anions revealed architectures defined by aurophilic interactions and distinct responses to external stimuli. One of the five compounds obtained, ({Cu(L1)$_2$[(μ-CN)Au(CN)]}[Au(CN)$_2$]), has been investigated for pressure–temperature behavior. An isosymmetric distortive phase transition between 1.3 and 1.5 GPa was identified by high-pressure Raman spectroscopy combined with SCXRD. This transition was characterized by anomalous compression and reorganization of Au···Au contacts, along with distortions around the Cu(II) coordination environment. However, variable-temperature crystallography up to 343 K revealed only continuous lattice adjustments, emphasizing that pressure is the main factor responsible for initiating structural transformations in these systems. The findings show how subtle aurophilic interactions and Jahn–Teller effect driven distortions collaborate under compression to produce isosymmetric transitions [37].

Hexathiocyanate Thulium(III) Anions

The compound $[((nBu)_4N)_3][Tm(SCN)_6]$ underwent a reversible structural phase transition near 204 K, as confirmed by DSC and temperature-dependent dielectric measurements. The transition included by a significant thermal hysteresis (~15.9 K) and an entropy change that was consistent with an order–disorder mechanism. SCXRD confirmed that the transition was isosymmetric. According to structural analysis, the transition was caused by the disordering of the $[(nBu)_4N]^+$ cation's terminal carbon chain, while the $[Tm(SCN)_6]^{3-}$ anionic framework remained basically intact. The phase transition was accompanied by distinct dielectric anomalies, demonstrating the system's potential as a switchable dielectric material. The compound also showed solid-state photoluminescence, with a peak emission at 458 nm that was linked to the $^3D_2 \rightarrow {}^3F_4$ transition of Tm^{3+} (Figure 10) [65].

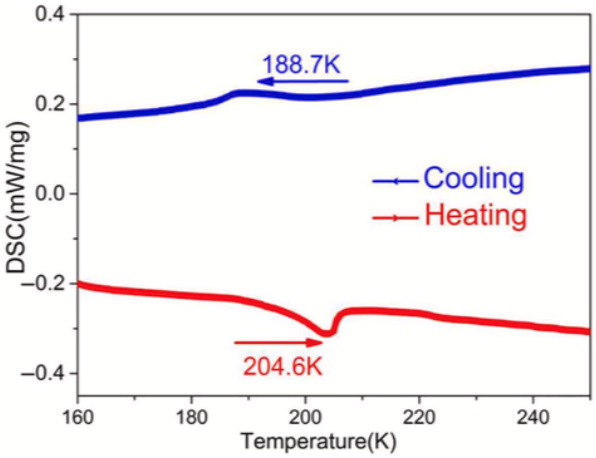

Figure 10. The heat anomalies of compound $[((nBu)_4N)_3][Tm(SCN)_6]$ in the cooling and heating cycle. Reprinted from [65] with permission from Elsevier.

Triethylbenzylammonium Perchlorate

Triethylbenzylammonium perchlorate underwent a reversible first-order IPT at approximately 196 K with a thermal hysteresis of 18 K, as shown by sharp endothermic and exothermic peaks in DSC measurements. In the same temperature range, the dielectric permittivity showed step-like changes, which further supported the discontinuous character of the transition. Variable-temperature SCXRD showed that the crystal structure changed from orthorhombic Pbcm at room temperature to Pbca at low temperature, and the unit cell volume doubled at the same time. The transition is described as isosymmetric by the authors; however, it must be noted that the two space groups are distinct and this classification is based on the preservation of the same orthorhombic point symmetry (D_2h) rather than strict space-group identity.

The main structural difference in the phases was the orientation and degree of order of the perchlorate anions, which were highly disordered at higher temperatures but became ordered during cooling. Modifications in the hydrogen-bonding network between cations and anions were also found, implying a cooperative role of weak hydrogen bond interactions in the formation of the low-temperature phase. Thermodynamic analysis revealed changes in entropy that were consistent with an order–disorder mechanism, suggesting that the change was caused by the reorientational dynamics of ClO_4^- anions [26].

5.3. Silicate Minerals and Orthopyroxenes

Paracelsian

High-pressure synchrotron SCXRD analysis of paracelsian ($BaAl_2Si_2O_8$) revealed a sequence of three pressure-induced polymorphic transitions up to 32 GPa. The first transition

that occurred between 3 and 6 GPa was found to be isosymmetric ($P2_1/c \rightarrow P2_1/c$). It was marked through the gradual formation of additional Al–O and Si–O bonds. This anomalous mechanism created three different intermediate states (IIa, IIb, and IIc), underscoring the role of fivefold coordination in the densification of tetrahedral frameworks [32].

Orthoenstatite

MD simulations of orthoenstatite ($Mg_2Si_2O_6$) showed a first-order IPT at ~1230 K, producing a distinct high-temperature orthorhombic polymorph with the same space group (Pbca) as the low-temperature form. The transition was characterized by discontinuous changes in unit-cell parameters and volume, which were associated with silicate chain stretching and switching of the M2-O3B bonds. These bonds are links between magnesium cations occupying the M2 crystallographic site in the orthoenstatite structure and the bridging oxygen atoms (O3B) of the silicate chains. Despite their identical symmetry, the two phases showed distinct structural differences, particularly in silicate chain geometry and Mg-O coordination. The simulated high-temperature structure was remarkably close to the results from in situ X-ray studies, indicating the possibility of its existence as a stable phase at high temperature [9].

Orthopyroxene

HTXRD studies on the Ca-bearing orthorhombic pyroxene composition $(Ca_{0.8}Mg_{1.8})Si_2O_6$ showed a reversible structural transition at approximately 1170 °C, with discontinuous changes volume and unit-cell parameters. The transition was determined to be first-order and isosymmetric. The high-temperature orthopyroxene was found to be thermodynamically distinct from the low-temperature orthoenstatite, despite preserving the same crystallographic symmetry [66].

6. Conclusions

The increasing amount of research on IPTs emphasizes the extraordinary structural versatility of crystalline solids in response to external factors like pressure and temperature [79]. The reviewed research papers indicate that IPTs, despite maintaining overall crystallographic symmetry, can lead to significant reorganizations of hydrogen-bond networks, conformational changes, and anisotropic lattice responses. The prevalent theme of these transitions is the delicate balance among local molecular flexibility, cooperative intermolecular interactions, and external constraints, resulting in discontinuous yet symmetry-preserving transformations.

The hydrogen bond reorganization is a primary structural driver in organic compounds. For example, L-histidine and L-serine undergo pressure-induced IPTs, which enable the crystal to accommodate compression without disrupting the space group symmetry due to cooperative changes in hydrogen-bond geometry. In L-serine, two consecutive isosymmetric transitions were observed at 5.3 and 7.8 GPa, demonstrating a rare instance of sequential symmetry-preserving polymorphism [28,48]. Additionally, DL-cysteine revealed that the same isosymmetric polymorph can be reached either by cooling or by compression [33]. This shows that pressure and temperature are both equally effective at reorganizing hydrogen-bonded frameworks.

Conformational flexibility represents another significant mechanism for inducing IPTs. In α-glycylglycine, the bending of the backbone and the rotation of terminal groups at pressures exceeding approximately 6.7 GPa resulted in a reorganized hydrogen-bond network, while maintaining monoclinic symmetry. Computational results indicated the existence of multiple nearly degenerate polymorphs, suggesting that isosymmetric transitions frequently occur in shallow energy landscapes that allow for several closely related structures [45]. A similar mechanism was observed in pharmaceutical systems, for example,

ibuprofen lysine salt and estradiol valerate displayed reversible IPTs driven by side-chain torsional alterations and minor reorganization of hydrogen bonding, which have significant implications for drug formulation and stability [53,60,69].

Dynamic disorder–order processes can be the driving force behind IPTs, in addition to hydrogen bonding. The imidazole derivative 2-(3,5-bis(trifluoromethyl)phenyl)-4,5-dihydro-1H-imidazole demonstrated low-temperature IPT linked to the freezing of CF_3 group rotations, resulting in significant anisotropic lattice behavior, including uniaxial negative thermal expansion [63]. In BTBT-C4OH, a temperature-driven isosymmetric crossover was observed as a transition from positive to negative uniaxial thermal expansion, indicating that IPTs can arise from subtle dynamical rearrangements of herringbone packing [68].

In several reviewed cases, IPTs demonstrated significant anisotropic lattice responses. Biurea underwent a first-order transition at approximately 0.6 GPa, which was characterized by anisotropic modifications of hydrogen bonds and negative linear compressibility in one crystallographic direction [3]. Similarly, $Co(IO_3)_2$ and $Zn(IO_3)_2$ exhibited IPTs, where iodine polyhedra distortions cause counterintuitive expansions along lattice axes [42,44]. This illustrates how stereoactive lone pairs enable unconventional elastic responses while maintaining symmetry.

The functional consequences are a significant aspect of IPTs. The emergence of disordered and ordered high-pressure polymorphs (γ and δ phases) in resorcinol is determined by the compression rate, with both phases displaying a broad photoluminescence band associated with excimer formation [1]. In rubrene, a high-pressure IPT involved reorganization of π–π and C–H$\cdots\pi$ contacts, directly influencing charge transport properties [35]. This is an example of how such transitions can modulate the performance of organic semiconductors. In ionic systems, hexathiocyanate thulium(III) salts exhibited IPTs that were associated with cation disordering and were accompanied by strong dielectric anomalies [65]. This suggests that they have the potential for switchable dielectric applications.

Another recurring theme is the role of kinetic effects. Resorcinol is an example of how rapid compression can bypass the $\alpha\rightarrow\beta$ transition, resulting in a distinct ordered phase (δ), whereas slow compression supports the stabilization of a disordered polymorph (γ) [1]. Similarly, the IPT's occurrence in clathrate systems like hydroquinone–formic acid is dependent upon the choice of the pressure-transmitting medium, emphasizing the transitions' sensitivity to external factors [38].

In inorganic compounds, IPTs typically arise from polyhedral distortions and alterations in coordination. PbF_2 underwent an isosymmetric transition from a cotunnite-type to a Co_2Si-type structure at approximately 10 GPa, accompanied by an increase in coordination from 9 to 10 [30]. Na_3MnF_6 experienced a distinctive IPT characterized by a shift in Jahn–Teller distortion axes, illustrating a rare instance in which electronic degeneracy directly drives a transition [48]. These examples highlight that IPTs in inorganic frameworks usually reflect the cooperative modifications of coordination environments, rather than changes in conformation or hydrogen-bond reorganizations.

All together, these examples show that IPTs, while preserving symmetry, constitute varied types of transformations characterized by unique structural factors: hydrogen bonding, conformational dynamics, polyhedral flexibility, dynamic disorder, or electronic effects. They usually generate significant anisotropy in lattice response, exhibit high sensitivity to kinetic conditions, and directly impact functional properties, including optical luminescence, dielectric behavior, electronic transport, and pharmaceutical performance. The evidence indicates that IPTs should not be viewed as uncommon crystallographic anomalies, but as a general structural adaptation strategy employed by various mate-

rials, ranging from simple salts to complex pharmaceuticals, in order to accommodate external stimuli.

Across the surveyed systems, the principal microscopic drivers of IPTs are hydrogen-bond reallocation, conformational torsions, and order–disorder freezing, while their first-order character is evidenced by enthalpy jumps and anisotropic compressibility. These features connect IPTs to shallow energy landscapes and make them attractive for responsive-material design.

Author Contributions: Conceptualization, Ł.S., M.F.-R. and A.M.M.; methodology, Ł.S.; software, Ł.S.; validation, Ł.S.; formal analysis, Ł.S. and A.M.M.; investigation, Ł.S. and A.M.M.; resources, Ł.S.; data curation, Ł.S. and A.M.M.; writing—original draft preparation, Ł.S. and A.M.M.; writing—review and editing, Ł.S., M.F.-R. and A.M.M.; visualization, Ł.S. and A.M.M.; supervision, Ł.S. and M.F.-R.; project administration, Ł.S.; funding acquisition, Ł.S. All authors have read and agreed to the published version of the manuscript.

Funding: This research received no external funding.

Institutional Review Board Statement: Not applicable.

Informed Consent Statement: Not applicable.

Data Availability Statement: No new data were created or analyzed in this study. Data sharing is not applicable to this article.

Conflicts of Interest: The authors declare no conflicts of interest.

Abbreviations

The following abbreviations are used in this manuscript:

ADXRD	Angle-Dispersive X-ray Diffraction
ADP	Atomic Displacement Parameter
aiMD	Ab Initio Molecular Dynamics
CN	Coordination Number
CSP	Crystal Structure Prediction
DFT	Density Functional Theory
DSC	Differential Scanning Calorimetry
DTA	Differential Thermal Analysis
EDX	Energy-Dispersive X-ray Spectroscopy
FT-IR	Fourier-Transform Infrared Spectroscopy
HRXRD	High-Resolution X-ray Diffraction
IPT	Isosymmetric Phase Transition
IR	Infrared Spectroscopy
MD	Molecular Dynamics
ND	Neutron Diffraction
ssNMR	Solid-State Nuclear Magnetic Resonance
NPD	Neutron Powder Diffraction
NTE	Negative Thermal Expansion
PC	Plastic Crystalline
PFY-XAS	Partial Fluorescence Yield–X-ray Absorption Spectroscopy
PTE	Positive Thermal Expansion
PL	Photoluminescence
PXRD	Powder X-ray Diffraction
SCXRD	Single-Crystal X-ray Diffraction

TEM	Transmission Electron Microscopy
TLS	Translation–Liberation–Screw
TGA	Thermogravimetric Analysis
UV-vis	Ultraviolet–Visible Absorption Spectroscopy
XRD	X-ray Diffraction
XRPD	X-ray Powder Diffraction
ZTE	Zero Thermal Expansion

References

1. Rao, R.; Sakuntala, T.; Godwal, B.K. Evidence for High-Pressure Polymorphism in Resorcinol. *Phys. Rev. B* **2002**, *65*, 054108. [CrossRef]
2. Szeleszczuk, Ł.; Mazurek, A.H.; Milcarz, K.; Napiórkowska, E.; Pisklak, D.M. Can We Predict the Isosymmetric Phase Transition? Application of DFT Calculations to Study the Pressure Induced Transformation of Chlorothiazide. *Int. J. Mol. Sci.* **2021**, *22*, 10100. [CrossRef]
3. Bull, C.L.; Funnell, N.P.; Ridley, C.J.; Pulham, C.R.; Coster, P.L.; Tellam, J.P.; Marshall, W.G. Pressure-Induced Isosymmetric Phase Transition in Biurea. *CrystEngComm* **2019**, *21*, 5872–5881. [CrossRef]
4. Qiao, Y.; Wang, L.; Yu, S.; Li, Z.; Li, Y. Biaxial Hard Compression, Anisotropic Elastic Property, and Pressure-Induced Isosymmetric Phase Transition in Ammonium Bicarbonate. *J. Phys. Chem. C* **2022**, *127*, 831–841. [CrossRef]
5. Kumar, H.; Tripathi, A.; Tripathi, S. Unambiguous Evidence of an Isosymmetric Phase Transition in Rare Earth Orthoferrites ($RFeO_3$) Driven by Interaction of R Cation with O Anions in First and Second Coordination Shells. *J. Phys. D Appl. Phys.* **2024**, *58*, 085303. [CrossRef]
6. Erkartal, M. Giant Negative Linear Compressibility, Isosymmetric Phase Transition, and Breathing Effect in a 3D Covalent Organic Framework. *J. Phys. Chem. C* **2023**, *128*, 588–596. [CrossRef]
7. Christy, A.G. Isosymmetric Structural Phase Transitions: Phenomenology and Examples. *Acta Crystallogr. B Struct. Sci.* **1995**, *51*, 753–757. [CrossRef]
8. Miyake, A.; Ohi, S. Isosymmetric Phase Transition in Orthopyroxene at High Temperature. *J. Crystallogr. Soc. Jpn.* **2011**, *53*, 36–41. [CrossRef]
9. Miyake, A.; Shimobayashi, N.; Kitamura, M. Isosymmetric Structural Phase Transition of Orthoenstatite: Molecular Dynamics Simulation. *Am. Mineral.* **2004**, *89*, 1667–1672. [CrossRef]
10. Li, Q.; Li, S.; Wang, K.; Li, X.; Liu, J.; Liu, B.; Zou, G.; Zou, B. Pressure-Induced Isosymmetric Phase Transition in Sulfamic Acid: A Combined Raman and x-Ray Diffraction Study. *J. Chem. Phys.* **2013**, *138*, 214505. [CrossRef]
11. Erkartal, M. Unveiling the Multifaceted Properties of a 3d Covalent-Organic Framework: Pressure-Induced Phase Transition, Negative Linear Compressibility and Auxeticity. *Comput. Mater. Sci.* **2023**, *227*, 112275. [CrossRef]
12. Novelli, G.; Maynard-Casely, H.E.; McIntyre, G.J.; Warren, M.R.; Parsons, S. Effect of High Pressure on the Crystal Structures of Polymorphs of L-Histidine. *Cryst. Growth Des.* **2020**, *20*, 7788–7804. [CrossRef]
13. Ben Gzaiel, M.; Oueslati, A.; Chaabane, I.; Bulou, A.; Hlel, F.; Gargouri, M. Using Raman Spectroscopy to Understand the Origin of the Phase Transitions Observed in [(C3H7)4N]2Zn2Cl6 Compound. *Spectrochim. Acta Part A Mol. Biomol. Spectrosc.* **2015**, *145*, 223–234. [CrossRef]
14. Terzidou, A.G.V.; Sorogas, N.; Pinakidou, F.; Paloura, E.C.; Arvanitidis, J. The Pressure-Induced Structural Phase Transition of Fluorene Studied by Raman Spectroscopy. *Vib. Spectrosc.* **2021**, *115*, 103272. [CrossRef]
15. Gerasimova, Y.; Laptash, N.; Krylov, A.; Vonog, V.; Vtyurin, A. Structural Phase Transition in $(NH_4)_3GeF_7$–Raman Spectroscopy Data. *Crystals* **2021**, *11*, 506. [CrossRef]
16. Husni, E.; Hamidi, D.; Pavvellin, D.; Hidayah, H.; Syafri, S. Metabolite Profiling, Antioxidant, and in Vitro Wound Healing Activities of Citrus Medica L. and Citrus x Microcarpa Bunge Peels and Leaves Essential Oils. *Prospect. Pharm. Sci.* **2024**, *22*, 122–130. [CrossRef]
17. Tandon, P.; Förster, G.; Neubert, R.; Wartewig, S. Phase Transitions in Oleic Acid as Studied by X-Ray Diffraction and FT-Raman Spectroscopy. *J. Mol. Struct.* **2000**, *524*, 201–215. [CrossRef]
18. Schick, C.; Lexa, D.; Leibowitz, L. Differential Scanning Calorimetry and Differential Thermal Analysis. In *Characterization of Materials*; Kaufmann, E.N., Ed.; Wiley: Hoboken, NJ, USA, 2012; pp. 1–13, ISBN 978-0-471-26882-6.
19. Charles, N.; Rondinelli, J.M. Microscopic Origin of Pressure-Induced Isosymmetric Transitions in Fluoromanganate Cryolites. *Phys. Rev. B* **2014**, *90*, 094114. [CrossRef]
20. Islamoğlu, F. Molecular Docking, Bioactivity, Adme, Toxicity Risks, and Quantum Mechanical Parameters of Some 1,2-Dihydroquinoline Derivatives Were Calculated Theoretically for Investigation of Its Use as a Pharmaceutical Active Ingredient in the Treatment of Multiple Sclerosis (MS). *Prospect. Pharm. Sci.* **2024**, *22*, 168–187. [CrossRef]

21. Casadei, M.; Ren, X.; Rinke, P.; Rubio, A.; Scheffler, M. Density-Functional Theory for f -Electron Systems: The $\alpha - \gamma$ Phase Transition in Cerium. *Phys. Rev. Lett.* **2012**, *109*, 146402. [CrossRef] [PubMed]
22. Kawano, J.; Miyake, A.; Shimobayashi, N.; Kitamura, M. Molecular Dynamics Simulation of the Rotational Order–Disorder Phase Transition in Calcite. *J. Phys. Condens. Matter* **2009**, *21*, 095406. [CrossRef]
23. Singireddy, A.R.; Pedireddi, S.R. Advances in Lopinavir Formulations: Strategies to Overcome Solubility, Bioavailability, and Stability Challenges. *Prospect. Pharm. Sci.* **2024**, *22*, 105–121. [CrossRef]
24. Ma, Y.; Oganov, A.R.; Glass, C.W. Structure of the Metallic ζ -Phase of Oxygen and Isosymmetric Nature of the $\varepsilon - \zeta$ Phase Transition: Ab Initio Simulations. *Phys. Rev. B* **2007**, *76*, 064101. [CrossRef]
25. Ning, J.; Zhang, X.; Zhang, S.; Sun, N.; Wang, L.; Ma, M.; Liu, R. Pressure-Induced Pseudoatom Bonding Collapse and Isosymmetric Phase Transition in Zr_2Cu: First-Principles Predictions. *J. Chem. Phys.* **2013**, *139*, 234504. [CrossRef]
26. Wu, D.-H.; Jin, L. Temperature-Induced Isosymmetric Reversible Structural Phase Transition in Triethylbenzylammonium Perchlorate. *Inorg. Chem. Commun.* **2013**, *29*, 151–156. [CrossRef]
27. Chen, L.-Z.; Huang, D.-D.; Pan, Q.-J.; Zhang, L. Temperature-Induced Isosymmetric Reversible Structural Phase Transition in $[Cl_2Cd(Dabco\text{-}CH_2Cl)]_2\cdot(\mu\text{-}Cl)_2$. *J. Mol. Struct.* **2014**, *1078*, 68–73. [CrossRef]
28. Quesada-Cabrera, R.; Filinchuk, Y.; McMillan, P.F.; Nies, E.; Dmitriev, V.; Meersman, F. Exploring the Pressure–Temperature Behaviour of Crystalline and Plastic Crystalline Phases of N-Isopropylpropionamide. *CrystEngComm* **2015**, *17*, 2562–2568. [CrossRef]
29. Stan, C.V.; Dutta, R.; White, C.E.; Prakapenka, V.; Duffy, T.S. High-Pressure Polymorphism of PbF_2 to 75 GPa. *Phys. Rev. B* **2016**, *94*, 024104. [CrossRef]
30. Haines, J.; Léger, J.M.; Schulte, O. High-Pressure Isosymmetric Phase Transition in Orthorhombic Lead Fluoride. *Phys. Rev. B* **1998**, *57*, 7551–7555. [CrossRef]
31. Goryainov, S.V.; Boldyreva, E.V.; Smirnov, M.B.; Ahsbahs, H.; Chernyshev, V.V.; Weber, H.-P. Isosymmetric Reversible Pressure-Induced Phase Transition in Sodium Oxalate at 3.8 GPa. *Dokl. Phys. Chem.* **2003**, *390*, 154–157. [CrossRef]
32. Gorelova, L.A.; Pakhomova, A.S.; Krivovichev, S.V.; Dubrovinsky, L.S.; Kasatkin, A.V. High Pressure Phase Transitions of Paracelsian $BaAl_2Si_2O_8$. *Sci. Rep.* **2019**, *9*, 12652. [CrossRef] [PubMed]
33. Minkov, V.S.; Tumanov, N.A.; Cabrera, R.Q.; Boldyreva, E.V. Low Temperature/High Pressure Polymorphism in Dl-Cysteine. *CrystEngComm* **2010**, *12*, 2551. [CrossRef]
34. Datchi, F.; Ninet, S.; Gauthier, M.; Saitta, A.M.; Canny, B.; Decremps, F. Solid Ammonia at High Pressure: A Single-Crystal x-Ray Diffraction Study to 123 GPa. *Phys. Rev. B* **2006**, *73*, 174111. [CrossRef]
35. Bergantin, S.; Moret, M.; Buth, G.; Fabbiani, F.P.A. Pressure-Induced Conformational Change in Organic Semiconductors: Triggering a Reversible Phase Transition in Rubrene. *J. Phys. Chem. C* **2014**, *118*, 13476–13483. [CrossRef]
36. Allan, D.R.; Nelmes, R.J. The Structural Pressure Dependence of Potassium Titanyl Phosphate (KTP) to 8 GPa. *J. Phys. Condens. Matter* **1996**, *8*, 2337–2363. [CrossRef]
37. Priola, E.; Curetti, N.; Marabello, D.; Andreo, J.; Giordana, A.; Andreo, L.; Benna, P.; Freire, P.T.C.; Benzi, P.; Operti, L.; et al. Crystal Engineering of Aurophilic Supramolecular Architectures and Coordination Polymers Based on Butterfly-like Copper–Dicyanoaurate Complexes: Vapochromism, P–T Behaviour and Multi-Metallic Cocrystal Formation. *CrystEngComm* **2022**, *24*, 2336–2348. [CrossRef]
38. Eikeland, E.; Thomsen, M.K.; Madsen, S.R.; Overgaard, J.; Spackman, M.A.; Iversen, B.B. Structural Collapse of the Hydroquinone–Formic Acid Clathrate: A Pressure-Medium-Dependent Phase Transition. *Chem. Eur. J.* **2016**, *22*, 4061–4069. [CrossRef]
39. Han, Z.; Gu, Y.; Zheng, X.; Liu, J.-X.; Zhang, G.-J.; Liang, Y. Ultrahigh Elasticity and Anomalous Softening of α-Ag_2S under Pressure. *Chem. Phys. Lett.* **2022**, *802*, 139801. [CrossRef]
40. Yoshikane, N.; Matsui, K.; Nakagawa, T.; Yamaoka, H.; Hiraoka, N.; Ishii, H.; Arvanitidis, J.; Prassides, K. Isosymmetric Lattice Collapse in Mixed-Valence Rare-Earth Fullerides at High Pressure—Coupling of Lattice and Electronic Degrees of Freedom. *J. Phys. Chem. C* **2023**, *127*, 10375–10383. [CrossRef]
41. Liang, A.; Popescu, C.; Manjon, F.J.; Turnbull, R.; Bandiello, E.; Rodriguez-Hernandez, P.; Muñoz, A.; Yousef, I.; Hebboul, Z.; Errandonea, D. Pressure-Driven Symmetry-Preserving Phase Transitions in $Co(IO_3)_2$. *J. Phys. Chem. C* **2021**, *125*, 17448–17461. [CrossRef]
42. Mellaerts, S.; Seo, J.W.; Afanas'ev, V.; Houssa, M.; Locquet, J.-P. Origin of Supertetragonality in $BaTiO_3$. *Phys. Rev. Mater.* **2022**, *6*, 064410. [CrossRef]
43. Liang, A.; Popescu, C.; Manjon, F.J.; Rodriguez-Hernandez, P.; Muñoz, A.; Hebboul, Z.; Errandonea, D. Structural and Vibrational Study of Zn(IO3)2 Combining High-Pressure Experiments and Density-Functional Theory. *Phys. Rev. B* **2021**, *103*, 054102. [CrossRef]
44. Hermann, A. High-Pressure Phase Transitions in Rubidium and Caesium Hydroxides. *Phys. Chem. Chem. Phys.* **2016**, *18*, 16527–16534. [CrossRef]

45. Clarke, S.M.; Steele, B.A.; Kroonblawd, M.P.; Zhang, D.; Kuo, I.-F.W.; Stavrou, E. An Isosymmetric High-Pressure Phase Transition in α-Glycylglycine: A Combined Experimental and Theoretical Study. *J. Phys. Chem. B* **2020**, *124*, 1–10. [CrossRef] [PubMed]
46. Liang, Y.; Ahmad, A.S.; Zhao, J.; Song, G.; Zhou, X.; Ji, J.; Zhang, W.; Han, Z.; Liu, J.; Stahl, K.; et al. Isosymmetric Phase Transitions, Ultrahigh Ductility, and Topological Nodal Lines in $\alpha - Ag_2S$. *Phys. Rev. B* **2020**, *102*, 140101. [CrossRef]
47. Boldyreva, E.V.; Sowa, H.; Seryotkin, Y.V.; Drebushchak, T.N.; Ahsbahs, H.; Chernyshev, V.; Dmitriev, V. Pressure-Induced Phase Transitions in Crystalline l-Serine Studied by Single-Crystal and High-Resolution Powder X-Ray Diffraction. *Chem. Phys. Lett.* **2006**, *429*, 474–478. [CrossRef]
48. Carlson, S.; Xu, Y.; Hålenius, U.; Norrestam, R. A Reversible, Isosymmetric, High-Pressure Phase Transition in Na_3MnF_6. *Inorg. Chem.* **1998**, *37*, 1486–1492. [CrossRef]
49. Broadhurst, E.T.; Wilson, C.J.G.; Zissimou, G.A.; Nudelman, F.; Constantinides, C.P.; Koutentis, P.A.; Parsons, S. A First-Order Phase Transition in Blatter's Radical at High Pressure. *Acta Crystallogr. B Struct. Sci. Cryst. Eng. Mater.* **2022**, *78*, 107–116. [CrossRef]
50. Ye, H.-Y.; Cai, H.-L.; Ge, J.-Z.; Xiong, R.-G. Isosymmetric Temperature-Triggered Structural Phase Transition of Dabcodiium Chlorochromate Chloride. *Inorg. Chem. Commun.* **2012**, *17*, 159–162. [CrossRef]
51. Wu, D.-H.; Ge, J.-Z.; Cai, H.-L.; Zhang, W.; Xiong, R.-G. Organic Salt of Hydrogen L-Tartaric Acid: A Novel Wide-Temperature-Range Ferroelectrics with a Reversible Phase Transition. *CrystEngComm* **2011**, *13*, 319–324. [CrossRef]
52. Vladiskovic, C.; Masciocchi, N. Reversibly Changing a Painkiller Structure: A Hot Topic for a Cold Case—Ibuprofen Lysine Salt. *J. Pharm. Biomed. Anal.* **2015**, *107*, 394–402. [CrossRef] [PubMed]
53. Rejnhardt, P.; Drozd, M.; Daszkiewicz, M. Phase Transition in 2-Nitroanilinium Bisulphate. Graph-Set Analysis, Spectroscopic and Theoretical Studies. *J. Mol. Struct.* **2020**, *1206*, 127772. [CrossRef]
54. Braun, D.E.; Krüger, H.; Kahlenberg, V.; Griesser, U.J. Molecular Level Understanding of the Reversible Phase Transformation between Forms III and II of Dapsone. *Cryst. Growth Des.* **2017**, *17*, 5054–5060. [CrossRef]
55. Braun, D.E.; Többens, D.M.; Kahlenberg, V.; Ludescher, J.; Griesser, U.J. Structural and Thermodynamic Features of Crystal Polymorphs of R-Cinacalcet Hydrochloride. *Cryst. Growth Des.* **2008**, *8*, 4109–4119. [CrossRef]
56. Ye, H.-Y.; Chen, L.-Z.; Xiong, R.-G. Reversible Phase Transition of Pyridinium-3-Carboxylic Acid Perchlorate. *Acta Crystallogr. B Struct. Sci.* **2010**, *66*, 387–395. [CrossRef]
57. Tang, Y.Q.; López-Cartes, C.; Avilés, M.A.; Córdoba, J.M. Isosymmetric Structural Phase Transition of the Orthorhombic Lanthanum Gallate Structure as a Function of Temperature Determined by Rietveld Analysis. *CrystEngComm* **2018**, *20*, 5562–5569. [CrossRef]
58. Gibbs, A.S.; Knight, K.S.; Lightfoot, P. High-Temperature Phase Transitions of Hexagonal $YMnO_3$. *Phys. Rev. B* **2011**, *83*, 094111. [CrossRef]
59. Zhu, Y.; Wu, S.; Tu, B.; Jin, S.; Huq, A.; Persson, J.; Gao, H.; Ouyang, D.; He, Z.; Yao, D.-X.; et al. High-Temperature Magnetism and Crystallography of a $YCrO_3$ Single Crystal. *Phys. Rev. B* **2020**, *101*, 014114, Erratum in *Phys. Rev. B* **2020**, *102*, 019901. [CrossRef]
60. Ellena, J.; De Paula, K.; De Melo, C.C.; Da Silva, C.C.P.; Bezerra, B.P.; Venâncio, T.; Ayala, A.P. Temperature-Driven Isosymmetric Reversible Phase Transition of the Hormone Estradiol 17β Valerate. *Cryst. Growth Des.* **2014**, *14*, 5700–5709. [CrossRef]
61. Farmer, J.M.; Boatner, L.A.; Chakoumakos, B.C.; Rawn, C.J.; Mandrus, D.; Jin, R.; Bryan, J.C. Polymorphism, Phase Transitions, and Thermal Expansion of $K_3Lu(PO_4)_2$. *J. Alloys Compd.* **2014**, *588*, 182–189. [CrossRef]
62. Zhang, Y.; Liao, W.-Q.; Ye, H.-Y.; Fu, D.-W.; Xiong, R.-G. Reversible Phase Transition of 1,4-Diazoniabicyclo [2.2.2]Octane-1-Acetate-4-Acetic Acid Chloride Trihydrate. *Cryst. Growth Des.* **2013**, *13*, 4025–4030. [CrossRef]
63. Vikas; Negi, L.; Munshi, P. Dynamic Order–Disorder Reversible Phase Transition and Anisotropic Thermal Expansions in a Single-Component Organic Molecular Crystal. *Cryst. Growth Des.* **2024**, *24*, 2533–2541. [CrossRef]
64. Li, T.; Wang, Y.; Li, W.; Mao, D.; Benmore, C.J.; Evangelista, I.; Xing, H.; Li, Q.; Wang, F.; Sivaraman, G.; et al. Structural Phase Transitions between Layered Indium Selenide for Integrated Photonic Memory. *Adv. Mater.* **2022**, *34*, 2108261. [CrossRef]
65. Dong, X.-X.; Song, N.; Huang, B.; Tan, Y.-H.; Tang, Y.-Z.; Wei, W.-J.; Li, Y.-K.; Shu, Q. Reversible Structural Phase Transition, Dielectric Switches and Photoluminescence Based on Hexathiocyanate Thulium(III) Anions. *Inorganica Chim. Acta* **2021**, *515*, 120051. [CrossRef]
66. Ohi, S.; Miyake, A.; Shimobayashi, N.; Yashima, M.; Kitamura, M. An Isosymmetric Phase Transition of Orthopyroxene Found by High-Temperature X-Ray Diffraction. *Am. Mineral.* **2008**, *93*, 1682–1685. [CrossRef]
67. Ford, S.J.; Delamore, O.J.; Evans, J.S.O.; McIntyre, G.J.; Johnson, M.R.; Radosavljević Evans, I. Giant Deuteron Migration During the Isosymmetric Phase Transition in Deuterated 3,5-Pyridinedicarboxylic Acid. *Chem. Eur. J.* **2011**, *17*, 14942–14951. [CrossRef] [PubMed]
68. Dumitrescu, D.G.; Roche, G.H.; Moreau, J.J.E.; Dautel, O.J.; Van Der Lee, A. A Positive to Negative Uniaxial Thermal Expansion Crossover in an Organic Benzothienobenzothiophene Structure. *Acta Crystallogr. B Struct. Sci. Cryst. Eng. Mater.* **2020**, *76*, 661–673. [CrossRef]

69. Pandey, J.; Prajapati, P.; Tandon, P.; Sinha, K.; Ayala, A.P.; Ellena, J. Vibrational and Conformational Analysis of Structural Phase Transition in Estradiol 17β Valerate with Temperature. *Spectrochim. Acta Part A Mol. Biomol. Spectrosc.* **2021**, *263*, 120219. [CrossRef]
70. Arvanitidis, J.; Papagelis, K.; Margadonna, S.; Prassides, K.; Fitch, A.N. Temperature-Induced Valence Transition and Associated Lattice Collapse in Samarium Fulleride. *Nature* **2003**, *425*, 599–602. [CrossRef]
71. Ellemann-Olesen, R. A High-Temperature Diffraction Study of the Solid Solution $CaTiOSiO_4$-$CaTiOGeO_4$. *Am. Mineral.* **2005**, *90*, 1325–1334. [CrossRef]
72. Biryukov, Y.P.; Bubnova, R.S.; Krzhizhanovskaya, M.G.; Filatov, S.K.; Povolotskiy, A.V.; Ugolkov, V.L. Thermal Behavior of Polymorphic Modifications of $LuBO_3$. *Solid State Sci.* **2020**, *99*, 106061. [CrossRef]
73. Schmid-Beurmann, P.; Brunet, F.; Kahlenberg, V.; Dachs, E. Polymorphism and Thermochemistry of $MgAlPO_4O$, a Product of Lazulite Breakdown at High Temperature. *Eur. J. Mineral.* **2007**, *19*, 159–172. [CrossRef]
74. Safari, F.; Katrusiak, A. High-Pressure Polymorphs Nucleated and Stabilized by Rational Doping under Ambient Conditions. *J. Phys. Chem. C* **2021**, *125*, 23501–23509. [CrossRef]
75. Safari, F.; Olejniczak, A.; Katrusiak, A. Pressure-Dependent Crystallization Preference of Resorcinol Polymorphs. *Cryst. Growth Des.* **2019**, *19*, 5629–5635. [CrossRef]
76. Liang, A.; Rahman, S.; Rodriguez-Hernandez, P.; Muñoz, A.; Manjón, F.J.; Nenert, G.; Errandonea, D. High-Pressure Raman Study of $Fe(IO_3)_3$: Soft-Mode Behavior Driven by Coordination Changes of Iodine Atoms. *J. Phys. Chem. C* **2020**, *124*, 21329–21337. [CrossRef]
77. Liang, A.; Rahman, S.; Saqib, H.; Rodriguez-Hernandez, P.; Muñoz, A.; Nénert, G.; Yousef, I.; Popescu, C.; Errandonea, D. First-Order Isostructural Phase Transition Induced by High Pressure in $Fe(IO_3)_3$. *J. Phys. Chem. C* **2020**, *124*, 8669–8679. [CrossRef]
78. Dorfman, S.M.; Jiang, F.; Mao, Z.; Kubo, A.; Meng, Y.; Prakapenka, V.B.; Duffy, T.S. Phase Transitions and Equations of State of Alkaline Earth Fluorides CaF_2, SrF_2, and BaF_2 to Mbar Pressures. *Phys. Rev. B* **2010**, *81*, 174121. [CrossRef]
79. Song, H.X.; Liu, L.; Geng, H.Y.; Wu, Q. First-Principle Study on Structural and Electronic Properties of CeO_2 and ThO_2 under High Pressures. *Phys. Rev. B* **2013**, *87*, 184103. [CrossRef]

Disclaimer/Publisher's Note: The statements, opinions and data contained in all publications are solely those of the individual author(s) and contributor(s) and not of MDPI and/or the editor(s). MDPI and/or the editor(s) disclaim responsibility for any injury to people or property resulting from any ideas, methods, instructions or products referred to in the content.

Publication co-author statement

As a co-author of the publication entitled:

"Isosymmetric Phase Transitions in Crystals: From Subtle Rearrangements to Functional Properties", *published in Crystals (2025, Volume 15, Issue 9, Article 807),* https://doi.org/10.3390/cryst15090807
Authors: Anna Maria Mazurek, Monika Franczak-Rogowska and Łukasz Szeleszczuk

I agree to include this publication into a collection of thematically related publications forming a doctoral dissertation prepared by mgr farm. Anna Maria Mazurek.

Additionally, I declare my contribution to the publication as follows: conceptualisation, Ł.S., M.F.-R. and A.M.M.; methodology, Ł.S.; software, Ł.S.; validation, Ł.S.; formal analysis, Ł.S. and A.M.M.; investigation, Ł.S. and A.M.M.; resources, Ł.S.; data curation, Ł.S. and A.M.M.; writing - original draft preparation, Ł.S. and A.M.M.; writing - review and editing, Ł.S., M.F.-R. and A.M.M.; visualisation, Ł.S. and A.M.M.; supervision, Ł.S. and M.F.-R.; project administration, Ł.S.; funding acquisition, Ł.S.

Oświadczenie współautora publikacji

Jako współautor publikacji pt.:

"Isosymmetric Phase Transitions in Crystals: From Subtle Rearrangements to Functional Properties", *opublikowanej w czasopiśmie Crystals (2025, tom 15, numer 9, artykuł 807),* https://doi.org/10.3390/cryst15090807
Autorzy: Anna Maria Mazurek, Monika Franczak-Rogowska and Łukasz Szeleszczuk

Wyrażam zgodę na włączenie tej publikacji do zbioru powiązanych tematycznie artykułów naukowych, stanowiących część pracy doktorskiej przygotowanej przez mgr farm. Annę Marię Mazurek.

Jednocześnie potwierdzam, że następujący zakres stanowi mój wkład w publikację: koncepcja, Ł.S., M.F.-R. oraz A.M.M.; metodologia, Ł.S.; oprogramowanie, Ł.S.; walidacja, Ł.S.; analiza formalna, Ł.S. oraz A.M.M.; badania, Ł.S. oraz A.M.M.; zasoby, Ł.S.; opracowanie danych, Ł.S. oraz A.M.M.; pisanie – przygotowanie pierwotnej wersji manuskryptu, Ł.S. oraz A.M.M.; pisanie - redakcja i korekta manuskryptu, Ł.S., M.F.-R. oraz A.M.M.; wizualizacja, Ł.S. oraz A.M.M.; nadzór, Ł.S. oraz M.F.-R.; zarządzanie projektem, Ł.S.; pozyskiwanie finansowania, Ł.S.

28.04.2026
Date / Data

Anna Mazurek
Legible signature / Czytelny podpis

Publication co-author statement

As a co-author of the publication entitled:

"Isosymmetric Phase Transitions in Crystals: From Subtle Rearrangements to Functional Properties", *published in Crystals (2025, Volume 15, Issue 9, Article 807),* https://doi.org/10.3390/cryst15090807
Authors: Anna Maria Mazurek, Monika Franczak-Rogowska and Łukasz Szeleszczuk

I agree to include this publication into a collection of thematically related publications forming a doctoral dissertation prepared by mgr farm. Anna Maria Mazurek.

Additionally, I declare my contribution to the publication as follows: conceptualisation, Ł.S., M.F.-R. and A.M.M.; methodology, Ł.S.; software, Ł.S.; validation, Ł.S.; formal analysis, Ł.S. and A.M.M.; investigation, Ł.S. and A.M.M.; resources, Ł.S.; data curation, Ł.S. and A.M.M.; writing - original draft preparation, Ł.S. and A.M.M.; writing - review and editing, Ł.S., M.F.-R. and A.M.M.; visualisation, Ł.S. and A.M.M.; supervision, Ł.S. and M.F.-R.; project administration, Ł.S.; funding acquisition, Ł.S.

Oświadczenie współautora publikacji

Jako współautor publikacji pt.:

"Isosymmetric Phase Transitions in Crystals: From Subtle Rearrangements to Functional Properties", *opublikowanej w czasopiśmie Crystals (2025, tom 15, numer 9, artykuł 807),* https://doi.org/10.3390/cryst15090807
Autorzy: Anna Maria Mazurek, Monika Franczak-Rogowska and Łukasz Szeleszczuk

Wyrażam zgodę na włączenie tej publikacji do zbioru powiązanych tematycznie artykułów naukowych, stanowiących część pracy doktorskiej przygotowanej przez mgr farm. Annę Marię Mazurek.

Jednocześnie potwierdzam, że następujący zakres stanowi mój wkład w publikację: koncepcja, Ł.S., M.F.-R. oraz A.M.M.; metodologia, Ł.S.; oprogramowanie, Ł.S.; walidacja, Ł.S.; analiza formalna, Ł.S. oraz A.M.M.; badania, Ł.S. oraz A.M.M.; zasoby, Ł.S.; opracowanie danych, Ł.S. oraz A.M.M.; pisanie – przygotowanie pierwotnej wersji manuskryptu, Ł.S. oraz A.M.M.; pisanie - redakcja i korekta manuskryptu, Ł.S., M.F.-R. oraz A.M.M.; wizualizacja, Ł.S. oraz A.M.M.; nadzór, Ł.S. oraz M.F.-R.; zarządzanie projektem, Ł.S.; pozyskiwanie finansowania, Ł.S.

28.04.2026
Date / Data

Szeleszczuk
Legible signature / Czytelny podpis

Publication co-author statement

As a co-author of the publication entitled:

"Isosymmetric Phase Transitions in Crystals: From Subtle Rearrangements to Functional Properties", *published in Crystals (2025, Volume 15, Issue 9, Article 807),* https://doi.org/10.3390/cryst15090807
Authors: Anna Maria Mazurek, Monika Franczak-Rogowska and Łukasz Szeleszczuk

I agree to include this publication into a collection of thematically related publications forming a doctoral dissertation prepared by mgr farm. Anna Maria Mazurek.

Additionally, I declare my contribution to the publication as follows: conceptualisation, Ł.S., M.F.-R. and A.M.M.; methodology, Ł.S.; software, Ł.S.; validation, Ł.S.; formal analysis, Ł.S. and A.M.M.; investigation, Ł.S. and A.M.M.; resources, Ł.S.; data curation, Ł.S. and A.M.M.; writing - original draft preparation, Ł.S. and A.M.M.; writing - review and editing, Ł.S., M.F.-R. and A.M.M.; visualisation, Ł.S. and A.M.M.; supervision, Ł.S. and M.F.-R.; project administration, Ł.S.; funding acquisition, Ł.S.

Oświadczenie współautora publikacji

Jako współautor publikacji pt.:

"Isosymmetric Phase Transitions in Crystals: From Subtle Rearrangements to Functional Properties", *opublikowanej w czasopiśmie Crystals (2025, tom 15, numer 9, artykuł 807),* https://doi.org/10.3390/cryst15090807
Autorzy: Anna Maria Mazurek, Monika Franczak-Rogowska and Łukasz Szeleszczuk

Wyrażam zgodę na włączenie tej publikacji do zbioru powiązanych tematycznie artykułów naukowych, stanowiących część pracy doktorskiej przygotowanej przez mgr farm. Annę Marię Mazurek.

Jednocześnie potwierdzam, że następujący zakres stanowi mój wkład w publikację: koncepcja, Ł.S., M.F.-R. oraz A.M.M.; metodologia, Ł.S.; oprogramowanie, Ł.S.; walidacja, Ł.S.; analiza formalna, Ł.S. oraz A.M.M.; badania, Ł.S. oraz A.M.M.; zasoby, Ł.S.; opracowanie danych, Ł.S. oraz A.M.M.; pisanie – przygotowanie pierwotnej wersji manuskryptu, Ł.S. oraz A.M.M.; pisanie - redakcja i korekta manuskryptu, Ł.S., M.F.-R. oraz A.M.M.; wizualizacja, Ł.S. oraz A.M.M.; nadzór, Ł.S. oraz M.F.-R.; zarządzanie projektem, Ł.S.; pozyskiwanie finansowania, Ł.S.

28.04.2026
Date / Data

Franczak-Rogowska
Legible signature / Czytelny podpis

10.2. Publication No. 2

applied sciences

MDPI

Article

Predicting the Pressure-Induced Isosymmetric Phase Transition of Sulfamic Acid by Applying Periodic Density Functional Theory Calculations

Anna Maria Mazurek [1], Monika Franczak-Rogowska [2] and Łukasz Szeleszczuk [1,*]

[1] Department of Organic and Physical Chemistry, Medical University of Warsaw, 1 Banacha Str., 02-097 Warsaw, Poland; anna_m_mazurek@o2.pl
[2] Department of Drug Chemistry, Pharmaceutical and Biomedical Analysis, Medical University of Warsaw, 1 Banacha Str., 02-097 Warsaw, Poland; monika.franczak-rogowska@wum.edu.pl
* Correspondence: lukasz.szeleszczuk@wum.edu.pl; Tel.: +48-501-255-121

Abstract: Sulfamic acid (SA) is extensively utilised in industry as a component in the production of flameproof materials, a catalyst for swift and highly efficient synthesis, in dye and pigment manufacturing processes, or as herbicide. Under ambient conditions, this compound exists as a solid in zwitterionc form, undergoing pressure-induced isosymmetric polymorphic phase transition (IPT), starting at approximately 10.0 GPa. In this work, multiple computational approaches were used to predict and describe this transition. While geometry optimisation at an increased pressure using periodic DFT-level calculations have not resulted in the anticipated IPT, the comparison of the experimental and theoretical Raman spectra confirmed this transformation. Thermodynamic calculations enabled the comparison of the stability of the modelled phases and explained the experimental observations. Ab initio molecular dynamics simulations revealed the mechanisms behind the observed transition. This work presents a complex methodology that can be successfully used to predict the IPT of molecular crystals.

Keywords: sulfamic acid; DFT; CASTEP; aiMD; isosymmetric phase transition; polymorphism

check for updates

Academic Editor: Abdeltif Amrane

Received: 6 March 2025
Revised: 8 April 2025
Accepted: 9 April 2025
Published: 10 April 2025

Citation: Mazurek, A.M.; Franczak-Rogowska, M.; Szeleszczuk, Ł. Predicting the Pressure-Induced Isosymmetric Phase Transition of Sulfamic Acid by Applying Periodic Density Functional Theory Calculations. *Appl. Sci.* **2025**, *15*, 4185. https://doi.org/10.3390/app15084185

Copyright: © 2025 by the authors. Licensee MDPI, Basel, Switzerland. This article is an open access article distributed under the terms and conditions of the Creative Commons Attribution (CC BY) license (https://creativecommons.org/licenses/by/4.0/).

1. Introduction

Polymorphisms, defined as the property of a substance to manifest in two or more crystalline phases with distinct molecular arrangements or conformations in the crystal lattice, are a phenomenon of significant relevance in applied sciences [1–3]. Molecular-level changes among polymorphs can result in distinct properties, including hygroscopicity, solubility, thermal stability, release rate, hardness, and chemical reactivity [4].

Since its inception, chemistry has predominantly utilised temperature to generate or alter materials; nevertheless, the application of pressure above a few tens of atmospheres for similar reasons has been infrequently recorded.

The application of high pressure has demonstrated efficacy in uncovering fresh states in solid-state materials, exemplified by the transformation of graphite into diamond [5]. Under increased pressure, the organisation of both inter- and intramolecular contacts can often be altered, new hydrogen bonds can form, and existing ones can be broken or symmetrized.

Pressure-induced phase transitions often manifest in one of three forms: a direct transition between higher- and lower-symmetry space groups (type I), a transition including a low-symmetry state linking higher-symmetry initial and final structures (type II), or a more complex transformation process (type III).

Isosymmetric structural phase transitions (IPT, type 0), characterised by the absence of alterations in the occupation of Wyckoff positions, the atom count in the unit cell, and the space group symmetry, are rather rare [6]. Nonetheless, there exist several notable and newly identified instances of such transitions; sodium oxalate [7], 1,3-cyclohexanedione [8], L-serine [9], chlorothiazide [10], biurea [11], and glycylglycine [12] are just some of the well-known examples.

Density functional theory (DFT) methods are frequently applied to model the structure and properties of organic materials and compounds.

The distinctiveness of each polymorphic form primarily arises from both short- and long-range intermolecular interactions. Consequently, DFT-based approaches modelling a single molecule in vacuum or solution were deemed insufficient and imprecise for investigating polymorphism-related events. Although "single molecule" methods are typically effective in various areas of sciences, such as investigating drug–biomolecule interactions or predicting complex formation, the study on molecular crystals necessitated the use of alternative calculations, often referred to as "periodic DFT calculations" [13]. The term "periodic" abbreviates "performed under periodic boundary conditions", a critical prerequisite for precise crystal modelling. Moreover, in these computations, pseudopotentials are commonly employed to depict an effective interaction that approximates the potential encountered by valence electrons. Furthermore, plane wave-basis sets are usually utilised in lieu of localised ones.

Sulfamic acid (SA) is the derivative of sulfuric acid and serves as a model for investigating the properties of hydrogen-bonded molecular crystals under severe circumstances. This classical chemical is extensively utilised in industry and has garnered significant interest owing to its broad applications and distinctive features. For example, it is an acidic cleaning agent and can be utilised as a component in the production of flameproof materials [14]. Simultaneously, the steady characteristics of SA render it a standard substance for nonaqueous titrimetric analysis [15]. The most renowned application of SA is its role as a catalyst for swift and highly efficient synthesis [16]. It is important to acknowledge that SA exists as a zwitterion, $NH_3^+SO_3^-$, in the solid state under ambient conditions. The zwitterionic characteristic of SA not only results in distinctive physical qualities, such as a high melting point of around 205 °C, unlike other sulfonic acids, but also enables it to function as a recyclable catalyst, which may be reused via straightforward filtration and washing. Given its wide-ranging applications, SA is indispensable for use in harsh environments.

The crystal structure of SA has been thoroughly analysed under ambient conditions. SA crystallises in the orthorhombic space group P*bca* with Z′ = 1 and Z = 8. In the ICSD database, four similar structures of SA can be found, with the most recently published ones obtained from X-ray diffraction and characterised by the following cell parameters: a = 8.034(1) Å, b = 8.020(1) Å, c = 9.236(2) Å; and neutron diffraction with the following cell parameters: a = 8.036(3) Å, b = 8.025(3) Å, c = 9.236(5) Å [17]. Despite the small size of SA molecules, the hydrogen bonding arrangement in its crystal lattice is quite complex. In the solid state, SA exists in the form of zwitterions, characterised by anti-periplanar conformation. Both ends of this molecule participate in independent hydrogen bonding with neighbouring molecules; the NH_3^+ group is surrounded by five oxygen atoms at short interatomic distances (about 2.79–2.95 Å), but only three of those oxygens are directly implicated in hydrogen bonding. It should be also noted that the shortest N-O distance is not in the direction of any hydrogen atom. The zwitterionic form of SA, which boosts the intermolecular electrostatic interactions, and presence of multiple strong H-bonds, results in distinctive physical features of this compound, including a high melting point of around 205 °C, unlike other sulfonic acids (Figure 1).

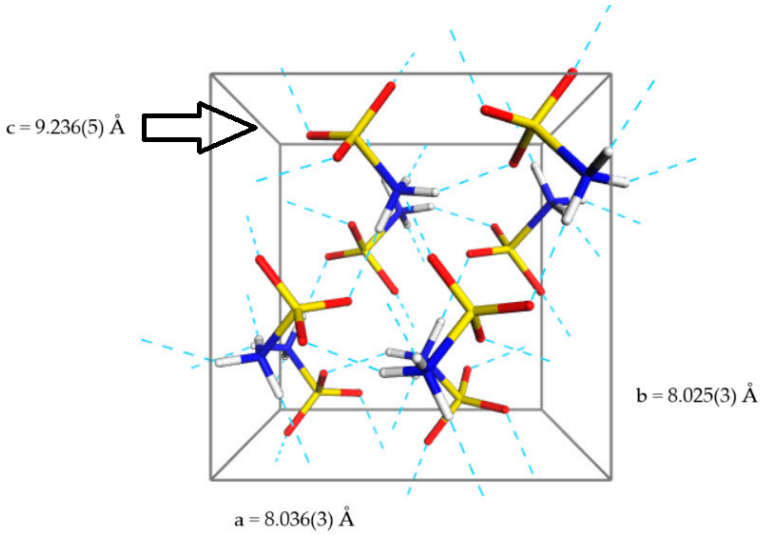

Figure 1. Unit cell of SA in a perspective projection. Blue dashed lines represent the hydrogen bonds.

Recently, it has been discovered experimentally that SA undergoes pressure-induced IPT, resulting in the abrupt decrease in "c" and increase in "a" and "b" unit cell lengths (Figure 2) [18]. The authors of [18] have used Raman spectroscopy to additionally characterise this transition of initial Phase I into newly discovered Phase II, starting at approximately 10.0 GPa. Although the authors of [18] have performed the Rietveld refinement of the powder pattern of Phase II recorded at 13.7 GPa, they have not published nor deposited in a database the final coordinates after refinement, presenting the structure of Phase II solely in a form of a Figure (Figure 9 in [18]) and the unit cell dimensions resulting from the analysis of the PXRD patterns.

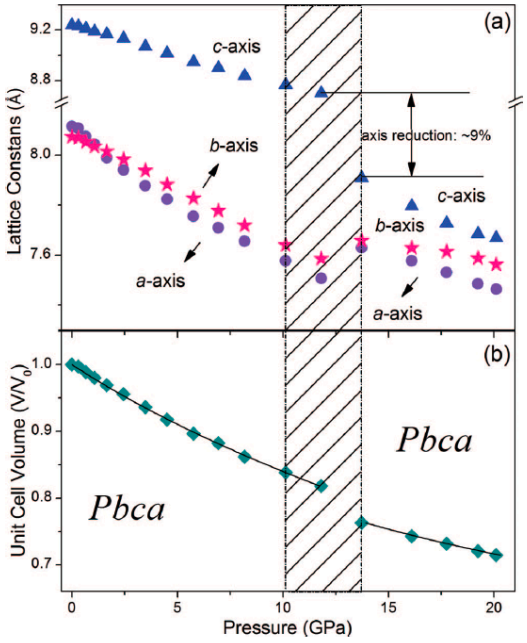

Figure 2. Compression of (**a**) lattice constants and (**b**) unit cell volume of SA with respect to pressure. Shadow represents the phase transition region. Reprinted from [18], with the permission of AIP Publishing.

As we have shown in a recent review [19], computational methods developed to mimic the solid state are typically calibrated using structural data at an ambient pressure, making their application to high-pressure scenarios a significant challenge for validating

their computational accuracy. Nonetheless, quantum chemical calculations, particularly utilizing the density functional theory (DFT), have consistently demonstrated their efficacy as a valuable instrument for predicting properties that can subsequently be validated by experimentalists, as well as elucidating, at the molecular level, the findings of high-pressure experiments.

On the one hand, the application of high pressure can result in the formation of the new phase, which makes this approach a tempting direction for widespread exploration and application. On the other hand, high-pressure experiments are experimentally demanding; therefore, the methods that can be accurately used to guide those experiments and predict their outcomes are highly anticipated. Therefore, the aim of this work was to assess if the periodic DFT methods can predict the pressure-induced polymorphic phase transition of SA, describe the thermodynamic aspects of this transformation and explain the differences in the Raman spectra observed experimentally.

2. Materials and Methods

Calculations at the density functional theory (DFT) level, in particular enthalpy minimisation, phonon dispersion, density of states, ab initio molecular dynamics (aiMD), and Raman-active vibrations, were conducted using the CASTEP [20] program integrated within the Materials Studio 2020 software (Materials Studio CASTEP version 2020), employing the plane wave pseudopotential formalism. On-the-fly-generated (OTFG) norm-conserving pseudopotentials (H_2017R2ncp.otfg for H, N_2017R2ncp.otfg for N, O_2019ncp.otfg for O, S_2017R2ncp.otfg for S) were obtained utilizing the Koelling–Harmon scalar relativistic method.

2.1. DFT Functionals and Dispersion Correction Methods

The complete list of the DFT functionals and dispersion corrections used in this study is presented in Table 1.

Table 1. DFT-based computational methods used in this study.

No.	Approximation	Functional	Dispersion Correction	References
1	GGA	PBE	TS	[21,22]
2	GGA	PBE	Grimme	[21,23]
3	GGA	PBE	MBD*	[21,24]
4	GGA	PBE	n/a	[21]
5	GGA	RPBE	TS	[22,25]
6	GGA	RPBE	n/a	[25]
7	GGA	PW91	TS	[22,26]
8	GGA	PW91	OBS	[26,27]
9	GGA	PW91	n/a	[26]
10	GGA	WC	n/a	[28]
11	GGA	PBESOL	TS	[22,29]
12	GGA	PBESOL	n/a	[29]
13	GGA	BLYP	TS	[22,30,31]
14	GGA	BLYP	Grimme	[23,30,31]
15	GGA	BLYP	n/a	[30,31]
16	meta-GGA	RSCAN	n/a	[32,33]

2.2. Geometry Optimisation

Geometry optimisation was carried out using the limited-memory Broyden−Fletcher−Goldfarb−Shanno (LBFGS) optimisation algorithm and smart method for finite-basis set correction. The kinetic energy cutoff for the plane waves (E_{cut}) was optimised and set to

1020 eV. The Monkhorst–Pack k-points used for sampling the Brillouin zone integration of the primitive cell were adjusted to maintain separation lower than 0.07 $Å^{-1}$.

The experimental crystal structure of sulfamic acid (ref. code ICSD_802 [17]) from the Inorganic Crystal Structure Database (ICSD) served as the initial structure for calculations. Two approaches for geometry optimisation were employed: "full + cell", wherein all atomic positions and cell parameters are relaxed, and "full", in which all atomic positions are optimised but the cell parameters are fixed at experimental values. The convergence criteria applied were 5×10^{-6} eV/atom for energy, 1×10^{-2} eV/Å for interatomic forces, 2×10^{-2} GPa for stresses, and 5×10^{-4} Å for displacements. The fixed-basis set quality approach was employed for cell optimisation calculations, with a limit of 5×10^{-7} eV/atom for SCF.

2.3. Thermodynamic Parameters and Raman Activity Calculations

Phonon frequencies were obtained using the diagonalisation of dynamical matrices computed using linear response techniques, known also as density functional perturbation theory (DFPT). DFPT is the primary ab initio technique utilised for phonon computations. This method is different from the direct method, as DFPT calculates the change in the Hamiltonian due to a specific perturbation in charge density or wavefunction, rather than actually displacing atoms as in a direct method. The q-point separation parameter, denoting the mean distance between Monkhorst–Pack mesh q-points utilised in real space dynamical matrix computations, was established at 0.05 $Å^{-1}$. The convergence criterion for the force constants during a phonon properties calculation was established at 1×10^{-5} eV/$Å^2$. This model was utilised to compute band structure, density of states (DOS), phonon spectrum, and phonon density of states (phonon DOS) features. For the dispersion calculations the distance between q-vectors along the reciprocal space trajectory was established at 0.015 $Å^{-1}$. The DOS calculations employed a $3 \times 3 \times 3$ Monkhorst–Pack k-points grid, yielding a q-vector separation of 0.04 $Å^{-1}$.

The outcomes of a phonon spectra calculation were utilised to ascertain, within the quasi-harmonic approximation, zero-point vibrational energy (Ezp), entropy (S), Gibbs free energy (G), and enthalpy (H) as functions of temperature, employing Equations (1)–(4) formulated by Baroni et al. [33]. In the equation, ω represents phonon frequency, F(ω) indicates the vibrational density of states for a phonon spectrum, Etot symbolises the total electronic energy at absolute zero, k is Boltzmann's constant, and $\hbar$ is Dirac's constant.

$$E_{zp} = \frac{1}{2}\int F(\omega)\hbar\omega d\omega \quad (1)$$

$$S(T) = k\left\{\int \frac{\frac{\hbar\omega}{kT}}{\exp\left(\frac{\hbar\omega}{kT}\right)-1}F(\omega)d\omega - \int F(\omega)\ln\left[1-\exp\left(-\frac{\hbar\omega}{kT}\right)\right]d\omega\right\} \quad (2)$$

$$G(T) = E_{tot} + E_{zp} + kT\int F(\omega)\ln\left[1-\exp\left(-\frac{\hbar\omega}{kT}\right)\right]d\omega + pV \quad (3)$$

$$H = G + TS \quad (4)$$

Activities for Raman vibrations were calculated with the required convergence for the second-order response to the electric field set as 1.0×10^{-5} $Å^3$ and with the finite displacement method has been used to calculate Raman intensities. CASTEP analysis was used to construct Raman-mode intensities for a given temperature (298 K) and laser wavelength (532 nm) from calculated activities. No imaginary frequencies for both Phase I and Phase II were observed at 20.1 GPa.

2.4. Ab Initio Molecular Dynamic (aiMD) Simulations

Born–Oppenheimer ab initio molecular dynamic (aiMD) simulations [34] were conducted in CASTEP utilising an NPT ensemble, kept at a constant temperature of 298 K and pressures of either 1.01325×10^{-4} or 20.1 GPa, employing a Nosé thermostat, Parrinello barostat, and PBE TS functional. The kinetic energy cutoff for the plane waves (Ecut) was established at 1020 eV, and the integration time step was set to 0.5 fs. No symmetry requirements were imposed during the simulations. The simulation duration was established at 9 ps. A limit of 5×10^{-7} eV/atom for SCF was employed. It should be noted that CASTEP does not require user-defined convergence criteria for energy/forces during dynamics, relying instead on adaptive algorithms.

3. Results

3.1. Geometry Optimisation of SA at 1 atm and 20.1 GPa

The first stage of this work consisted of geometry optimisation, including the all atom positions and unit cell dimensions of SA Phase I at 1 atm and 20.1 GPa.

Optimisation at 1 atm was performed for two reasons: first, to perform the benchmark of the available functionals (Table 1), by comparing the unit cell dimensions of calculated and experimentally recorded crystal structures; and second, to choose the most accurate method for the further calculations such as phonon DOS and aiMD. It is well known that the choice of the DFT functional can significantly affect the final results, both in non-periodic and periodic calculations. The obtained results (Table 2) confirm this statement, revealing major differences among the results obtained using various approaches. For example, the calculated unit cell dimensions differ by more than 1Å, a: 9.222 Å for RPBE and 7.993 Å for PBESOL, which is a significant difference as it corresponds to more than 10% of the experimentally determined value. Also, some functionals (i.e., RPBE, BLYP) significantly overestimated the unit cell dimensions; however, adding the dispersion correction generally increased the accuracy of the results. The meta-GGA functional, RSCAN is located at the higher rung of the so-called Jacob's ladder of the density functional theory, with each rung generally leading to approximations with better accuracy. However, in this case, the values obtained using RSCAN were found to be underestimated. The accuracy of the PBESOL functional, designed to improve the results obtained for the solid materials, was lower than original PBE. Interestingly, in most of the cases, the calculated "c" unit cell length was larger than the experimentally obtained one, being also the one that undergoes rapid decrease upon IPT (Figure 2).

The second step of this work was the geometry optimisation ad 20.1 GPa using the experimentally obtained crystal structure of Phase I as the initial structure. According to the experimental results [18], Phase I does not exist at this pressure; therefore, the phase transition of Phase I into Phase II during the geometry optimisation was anticipated, as observed in our earlier works [37,38]. However, no such transition was observed this time, regardless of the method used (Table 3). The experimentally determined "c" length of Phase II at 20.1 GPa was 7.68 Å, while in the calculations, the values higher by about 1.0 Å (13%) were obtained. However, the obtained values were not just the inaccurate predictions of Phase II. A comparative analysis of Figure 2 and Table 3 indicated that the obtained values (a = 7.249 Å, b = 7.376 Å, c = 8.489 Å, V = 453.9 Å^3 for PBE TS, Table 3) were close to those that would be characterising Phase I if it did not undergo the IPT, and would have been stable at this elevated pressure, assuming that the compression of the unit cell dimensions continued, as modelled in Figure 2 (a = 7.5 Å, b = 7.7 Å, c = 8.8 Å, V = 508 Å^3).

Table 2. Comparison of experimentally determined (blue) and geometrically optimised unit cell dimensions of SA Phase I at 1 atm.

CCDC Ref. Code/ DFT Functional	Dispersion Correction	a [Å]	b [Å]	c [Å]	V [Å^3]
ICSD_94 [35]		8.066(2)	8.115(2)	9.248(2)	605.3(5)
ICSD_25799 [36]		8.066(1)	8.115(1)	9.255(3)	605.8(2)
ICSD_803 [17]		8.034(1)	8.020(1)	9.236(2)	595.1(2)
ICSD_802 [17]		8.036(3)	8.025(3)	9.236(5)	595.6(5)
PBE	TS	8.090	8.089	9.444	618.0
PBE	Grimme	8.041	8.058	9.377	607.6
PBE	MBD*	8.118	8.084	9.417	618.0
PBE	n/a	8.371	8.188	9.6878	664.0
RPBE	TS	8.093	8.068	9.370	611.8
RPBE	n/a	9.222	8.482	10.137	792.9
PW91	TS	8.094	8.091	9.446	618.6
PW91	OBS	8.096	8.093	9.442	618.6
PW91	n/a	8.374	8.171	9.689	663.0
WC	n/a	8.019	7.985	9.494	607.9
PBESOL	TS	7.933	7.924	9.282	583.5
PBESOL	n/a	7.993	7.971	9.407	599.3
BLYP	TS	8.090	8.018	9.144	593.1
BLYP	Grimme	8.083	8.109	9.363	613.7
BLYP	n/a	8.660	8.340	9.813	708.7
RSCAN	n/a	7.983	8.016	9.327	596.9

Table 3. Comparison of the experimentally determined (blue, a = 7.46 Å, b = 7.57 Å, c = 7.68 Å, V = 433.7 Å^3) and geometrically optimised unit cell dimensions of SA at 20.1 GPa.

DFT Functional	Dispersion Correction	a [Å]	b [Å]	c [Å]	V [Å^3]
Experimental Phase II, determined at 20.1 GPa from [18]		7.46	7.57	7.68	433.7
PBE	TS	7.249	7.376	8.489	453.9
PBE	Grimme	7.213	7.364	8.510	452.0
PBE	MBD*	7.227	7.365	8.474	451.1
PBE	n/a	7.268	7.402	8.548	459.8
RPBE	TS	7.167	7.315	8.310	435.6
RPBE	n/a	7.356	7.493	8.648	476.6
PW91	TS	7.248	7.369	8.488	453.3
PW91	OBS	7.248	7.369	8.488	453.4
PW91	n/a	7.261	7.394	8.538	458.4
WC	n/a	7.170	7.304	8.446	442.3
PBESOL	TS	7.152	7.284	8.420	438.7
PBESOL	n/a	7.167	7.304	8.452	442.5
BLYP	TS	7.166	7.298	8.380	438.3
BLYP	Grimme	7.267	7.410	8.548	460.4
BLYP	n/a	7.362	7.476	8.596	473.1
RSCAN	n/a	7.195	7.336	8.432	445.1

These results could indicate two possible scenarios. First, the energy barrier between Phase I and II is too large to be overcome during the geometry optimisation [37,38]. Second, the experimentally observed Phase II is, for some reason, not a DFT minimum at 20.1 GPa. Therefore, to verify these hypotheses, calculations of geometry optimisation at 20.1 GPa were repeated, but this time using the Phase II as the initial structure (Table S1). No

significant differences were observed, indicating that the choice of either Phase I or Phase II initially for calculations had no influence on the results received. This excluded the first hypothesis, as starting with the experimental Phase II structure initially for calculations should not require overcoming the energy barrier during the geometry optimisation if it was indeed the DFT minimum.

Another set of geometry optimisation calculations at 20.1 GPa was performed using again the experimental structure of Phase II as the initial, but this time allowing only for the atomic positions to relax, with unit cell dimensions constrained to their experimental values. Since the authors of [18] did not deposit the crystal structure of Phase II, Phase II was created by us using the experimental structure of Phase I and changing the values of the unit cell dimensions to those presented in [18]. This approach was deemed justified as it has been determined experimentally that Phase I and Phase II exist in the same space group: P*bca*, with Z′ = 1 and Z = 8. Additionally, since the conformational space of SA was very limited, we could assume that the same anti-periplanar conformation was present in both forms. Additionally, although the authors of [18] did not deposit the crystal structure of Phase II, they compared both phases in Figure 9 of [18], revealing that no major changes in the molecular structure occurred during IPT. Finally, as during geometry optimisation, all atom positions were relaxed, and molecular properties (distance, angles, torsions) were optimised to reach the lowest enthalpy conformation. Then, the energy of Phase I and Phase II was compared (Table 4).

Table 4. Energy differences between Phase II and Phase I of SA optimised at 20.1 GPa. Unit cell dimensions of Phase II were fixed to their experimental values, while unit cell dimensions of Phase I were optimised.

DFT Functional	Dispersion Correction	ΔE Phase II—Phase I [kJ/mol]
PBE	TS	14.46
PBE	Grimme	13.33
PBE	MBD*	12.73
PBE	n/a	16.74
RPBE	TS	5.75
RPBE	n/a	26.69
PW91	TS	14.03
PW91	OBS	14.03
PW91	n/a	16.14
WC	n/a	12.03
PBESOL	TS	11.36
PBESOL	n/a	12.22
BLYP	TS	8.50
BLYP	Grimme	16.23
BLYP	n/a	24.59
RSCAN	n/a	11.04

Analysis of the results presented in Table 4 revealed that at 20.1 GPa Phase I was energetically preferable (ΔE > 0). Since the results of the DFT calculations may depend on the choice of the DFT functional, a large variety of methods (functional + dispersion correction) were used in this study to validate if the sign of ΔE will depend in the choice of the method. The positive value of ΔE between Phase II and Phase I of dozen kJ/mol was obtained, regardless of the method used. It was confirmed that functional/dispersion choice does not alter the conclusion that Phase I is higher in energy. This explained why the optimisation of Phase I at 20.1 GPa did not result in the phase transition and why the

optimisation of Phase II at 20.1 GPa ended with its transformation to Phase I, which is in disagreement with the experimental results.

The comparison of the molecular and crystal structures of Phase I and Phase II is presented in Figure 3. No major differences were observed between the molecular structures of SA zwitterions, and the values of angles were preserved while the differences in the bond lengths were lower than 0.02 Å (Figure 3A). In both forms, the SA crystal structure was stabilised by a dense network of hydrogen bonds. The comparison of the H-bonding between Phase I and Phase II (Figure 3C) revealed that while the number of hydrogen bonds was preserved, their lengths were altered. Some H-bonds of Phase II were longer (i.e., 1.680 Å vs. 1.580 Å) while the other were shorter (i.e., 2.003 Å vs. 2.265 Å) than the corresponding ones of Phase I. Moreover, the phase transition resulted in alterations in the intermolecular S–N distances between the neighboring molecules (Figure 3D). While some of those S–N distances remained unchanged (5.280 vs. 5.283 Å), the other ones were significantly shortened (i.e., 3.575 vs. 3.799 Å). This confirms that transition results from anisotropic compression and sliding of the molecules among the specific direction. Overall, Phases I and I are clearly different from each other (Figure 3B).

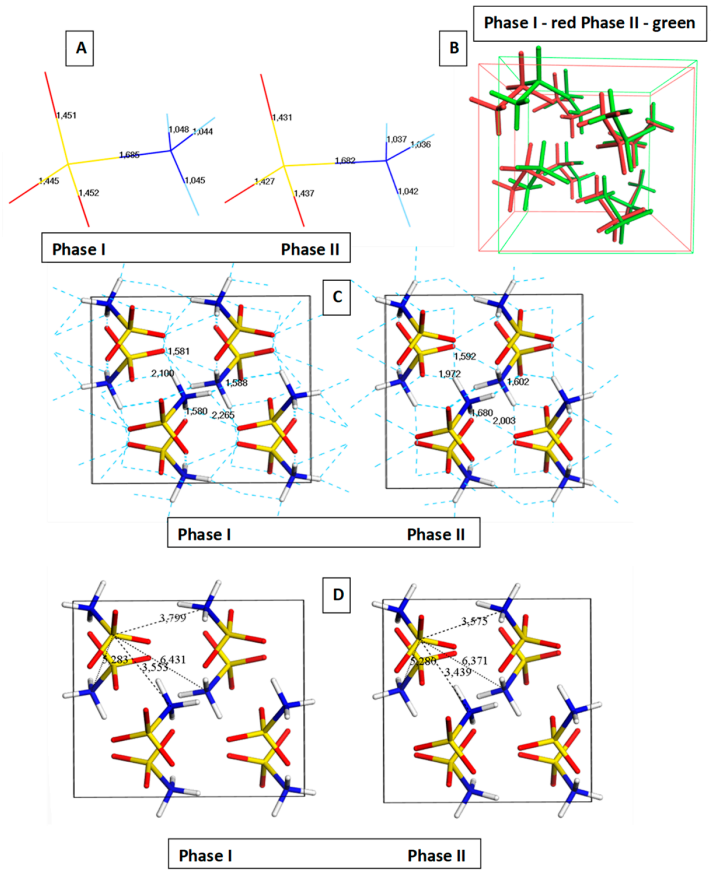

Figure 3. Comparison of the molecular and crystal structures of Phases I and II optimised at 20.1 GPa, showing the structural differences resulting from polymorphic transitions. (**A**) Comparison of bond lengths; (**B**) superimposed unit cells; (**C**) comparison of H-bonding network and lengths of the H-bonds present in the unit cells; (**D**) comparison of the intermolecular S–N distances.

3.2. Raman Spectra Calculations and Comparison with Experiment

Although the geometry optimisation of Phase I at 20.1. GPa did not result in the anticipated IPT, this did not discourage us from continuing our research. Since apart from XRD Raman spectrometry was also used to describe the IPT of SA [18], we decided to calculate the Raman spectra of Phase I at 1 atm and 20.1 GPa, as well as Phase II at

20.1 GPa. Here, it should be noted that in order to obtain the Raman spectra of Phase II at 20.1 GPa, we could not optimise the unit cell dimensions, as it resulted in its transition to Phase I (Table S1). Therefore, for that purpose, we performed the optimisation of Phase II at 20.1 GPa with the constrained unit cell dimensions using the same approach described above (Table 4). Then, the calculated (at 1 atm and 20.1 GPa) Raman spectra were compared with the experimental ones, recorded in the pressure range of 1 atm–18.9 GPa (Figure 4).

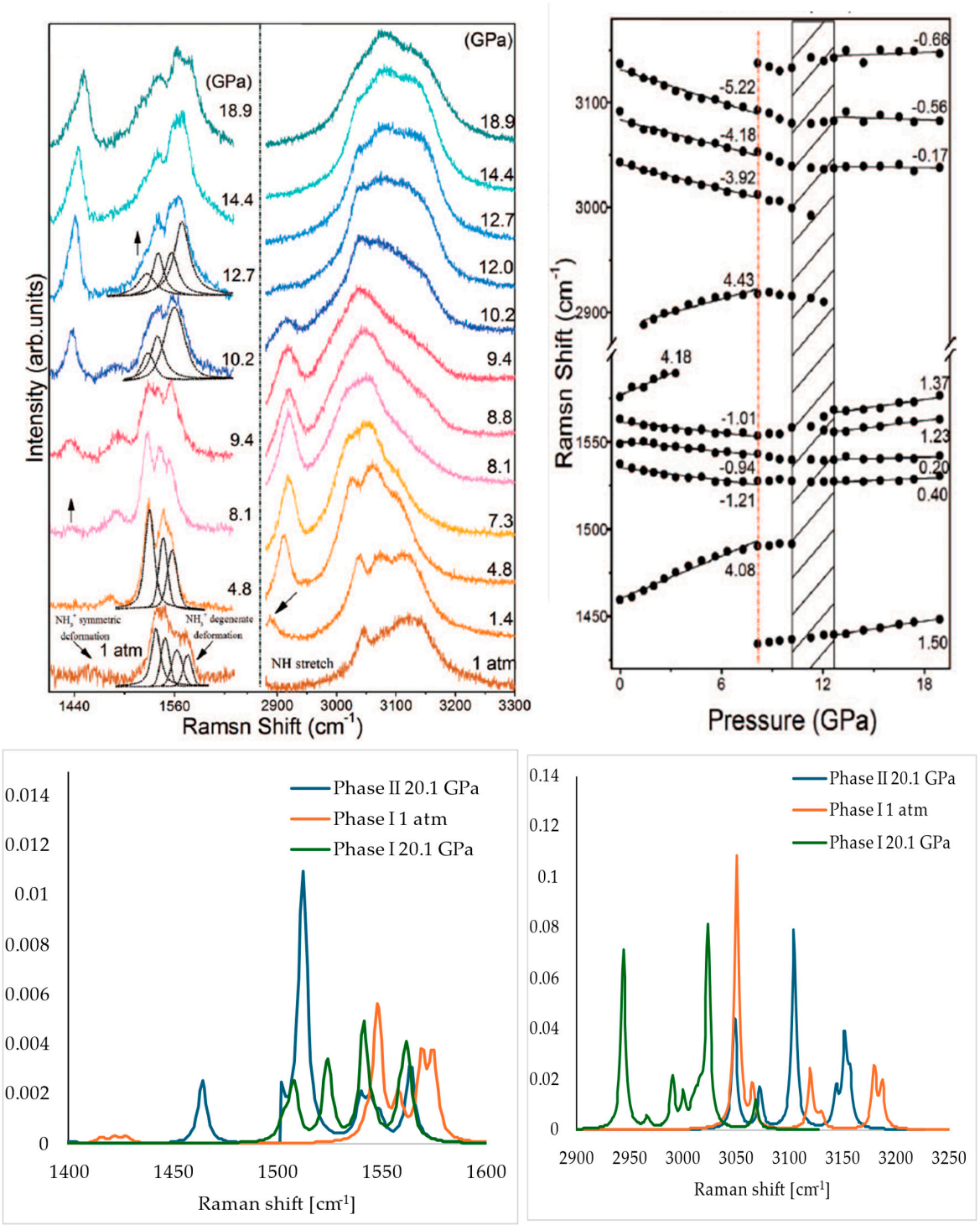

Figure 4. Comparison of experimental (**top**) (recorded in the pressure range 1 atm–18.9 GPa) and theoretical (**bottom**) (calculated at 1 atm and 20.1 GPa) Raman spectra of SA. Reprinted from [18], with the permission of AIP Publishing.

Analysis of the spectra recorded and calculated at 1 atm, within the 1400–1600 cm^{-1} range, revealed the presence of the low-intensity overlapping peaks at 1440 cm^{-1}. Also, for both experimental and theoretical spectra, four peaks were observed in the 1540–1580 cm^{-1} range. In the 2900–3300 cm^{-1} region, the peaks in the experimental spectrum were more overlapping; however, both for experimental and theoretical spectra, few peaks were observed, with the most intensive one at c.a. 3050 cm^{-1}. Overall, good agreement between the experimental and calculated Raman spectra of Phase I at 1 atm was observed, with the differences between the corresponding peaks lower than 50 cm^{-1}.

Analysis of the theoretical spectra of Phase I and Phase II at 20.1 GPa revealed some major differences among them. In the 1400–1600 cm^{-1} range, in the theoretical spectrum of Phase II, a peak can be observed at 1455 cm^{-1}, which was absent in the spectrum of Phase I. This peak was also observed in the experimental spectra recorded at a higher pressure, and was associated by the authors of [18] with the formation of the new Phase II. Additionally, the theoretical spectra of Phase I and II differed substantially in the 2900–3250 cm^{-1} region. For example, solely in the spectrum of Phase I, the intensive peak was observed at 2950 cm^{-1}. This peak was observed experimentally at 1 atm, but disappeared at a higher pressure due to the phase transition. In the experimental spectrum, the overlapping peaks were observed in the 3000–3200 cm^{-1} region. Also, a couple of peaks in the theoretical spectrum of Phase II were present in this range. On the contrary, the peaks in the theoretical spectrum of Phase I at 20.1 GPa were characterised by lower wavenumbers in the range of 2920–3200 cm^{-1}.

In conclusion, the comparative analysis of the experimental and theoretical Raman spectra revealed the good agreement between the experimental spectrum recorded at a higher pressure and spectrum of Phase II calculated at 20.1 GPa, with the differences between the corresponding peaks being lower than 50 cm^{-1}.

This confirmed that the modelled structure of Phase II at 20.1 GPa was observed experimentally, but the questioned remained on the stability of this form, taking into account its higher lattice energy, in comparison to Phase I (Table 4). To answer this question, we calculated and compared the thermodynamic properties of Phase I and Phase II.

3.3. Thermodynamic Paramater Calculations

Although the phonon dispersion and density of states calculations are quite computationally demanding, they can be very informative as they allow for calculating the thermodynamic properties to assess the stability of the analysed polymorphic forms. The differences (Δ, Phase I–Phase II) between the chosen thermodynamic properties, including Gibbs free energy (ΔG), enthalpy (ΔH), and temperature times entropy (TΔS) of the structures modelled using PBE TS functional at 20.1 GPa, with respect to the temperature, are presented in Figure 5.

The positive values of ΔG in the whole range of T indicate the higher thermodynamic stability of Phase II at 20.1 GPa, which is in agreement with the experimental observations. In addition, the differences at the level of a few kJ/mol were reasonable, as the lattice energy differences between experimentally observed polymorphs were usually less than 4.2 kJ/mol (1 kcal/mol) per molecule, but could be even lower than 1 kJ/mol [39]. The higher thermodynamic stability of Phase II at 20.1 GPa was a result of both entropic (S) and enthalpic (H) contributions, as Phase II is characterised by higher S and lower H in the whole region of studied temperatures than Phase I.

Thermodynamic analysis explains the experimentally observed IPT and highlights the important role of phonon DOS calculations required for the thermodynamic analysis, as the analysis of solely lattice energies can be misleading and does not reflect the true order of the stability of polymorphs.

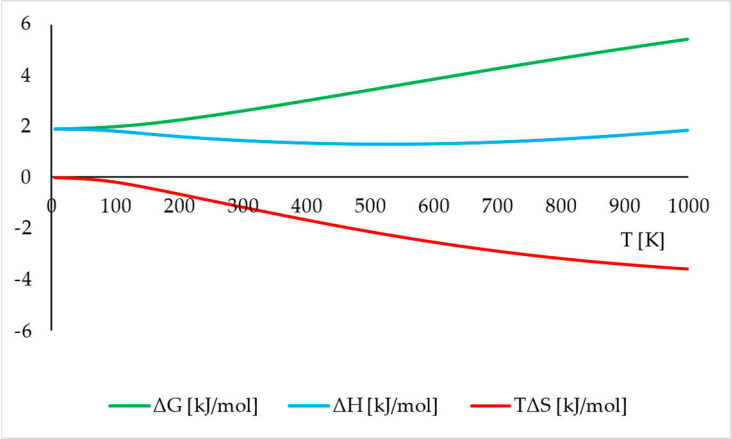

Figure 5. Differences (Phase I–Phase II) between the thermodynamic parameters: Gibbs free energy (ΔG), enthalpy (ΔH), and temperature times entropy (TΔS) of the structures modelled using PBE TS functional at 20.1 GPa, with respect to the temperature.

3.4. Molecular Dynamics Simulations

Molecular dynamics (MD) simulations can be very useful in the computational analysis of complex phenomena such as polymorphic phase transitions. The kinetic energy, associated with the non-zero T, added to the system, may allow for overcoming the potential energy barriers between the forms. Moreover, it allows for including the entropic contributions, which are neglected at 0 K.

To check the dynamic stability of SA, we conducted MD simulations at both 1 atm and 20.1 GPa using the Phase I as the initial (Figure 6).

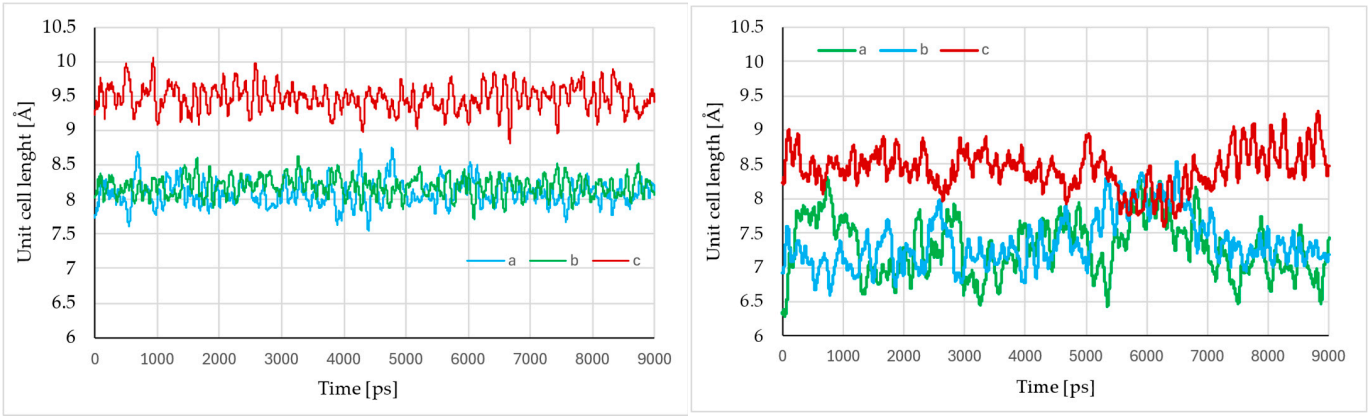

Figure 6. Evolution of the unit cell parameters during the aiMD simulations at 1 atm (**left**) and 20.1 GPa (**right**).

At 1 atm, no major changes in the unit cell dimensions were being observed, apart from oscillations resulting from lattice dynamics. The average values of the unit cell lengths were close to those obtained from geometry optimisation and simultaneously to the recorded experimental values.

However, at 20.1 GPa, the increase in the amplitude of the oscillations was being observed. Additionally, at c.a. 6 ns of simulation time, the significant increase in the lengths of "a" and "b" with the simultaneous decrease in "c" was being observed, which indicated the IPT and formation of Phase II (Figure 2). Nevertheless, Phase II was only present during the short period of the simulation time, and the backward transition to Phase I was being observed at the end of simulation.

As the unit cell dimensions at 6 ns of aiMD simulation resembled those of Phase II, we used the snapshot from the trajectory, recorded at 6 ns, and optimised it at 20.1 GPa. The results were compared with those obtained for Phase I and Phase II using the same computational method (Table 5).

Table 5. Comparison between Phase I and Phase II, and snapshot taken at 6 ns of aiMD of SA optimised at 20.1 GPa using the PBE TS method. Unit cell dimensions of Phase II were fixed to their experimental values while unit cell dimensions of Phase I and "6 ns" were optimised. All atoms positions were optimised as well for all three structures. E stands for relative energy, with reference to the energy of Phase I.

Structure	a [Å]	b [Å]	c [Å]	α [°]	β [°]	γ [°]	V [Å^3]	E [kJ/mol]
Phase I	7.249	7.376	8.489	90.0	90.0	90.0	453.9	0
Phase II	7.460	7.570	7.680	90.0	90.0	90.0	433.7	14.46
6ns	7.446	7.193	8.529	89.6	90.8	79.7	449.5	37.29

Optimisation of the 6 ns structure resulted in the local minimum, as its energy was higher than those of Phase I and Phase II. Moreover, the space group of 6 ns was not preserved and changed from P*bca* to P*1*.

As the intramolecular H-bonds between the $-NH_3^+$ groups and oxygen atoms were the main forces stabilising the structure of SA (Figure 7), we analysed the length distribution (Figure 8) and length evolution (Figures 9 and 10) of the representative bond during the MD simulations at the two studied pressures (1 atm and 20.1 GPa).

Analysis of the length distribution at 1 atm (Figure 8) indicates the presence of two peaks. First, more intensive, confirms the presence of strong, stable H-bond, with an approximate length of 1.7 Å. During the MD simulations the rotation of the $-NH_3^+$ group is being observed, it is possible for the H atoms of a particular group to switch positions (i.e., 2–4 ns, Figure 9), which results in the larger distance of the tracked H atom from the O atom, and consequently, the presence of the second peak at 3.0 Å is shown in Figure 8.

The analysis of the H-bonds during the simulation at 20.1 GPa reveals their completely different behaviour. The reasonable distance, for an H-bond, was observed only during the initial stage of simulation (Figure 10), while during the rest of it, the observed $-NH_3^+ \cdots O$ distance increased and fluctuated. This indicates that the H-bonds were being broken, which resulted in the experimentally observed IPT.

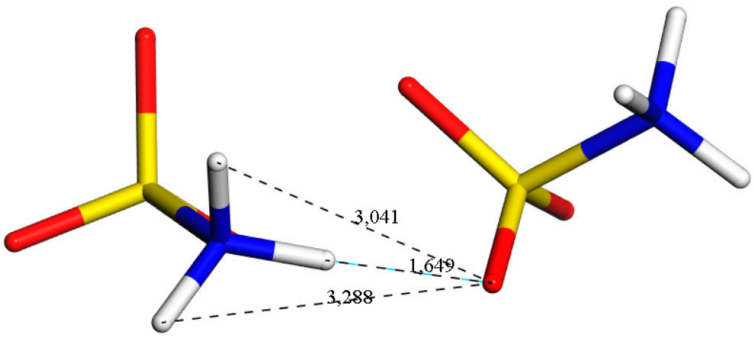

Figure 7. Fragment of the crystal structure of Phase I optimised at 1 atm. H-bond (black–blue dashed line, 1.649 Å), and the distances between the other two H atoms of $-NH_3^+$ group and oxygen atom from the neighbouring molecule. The H-bond length analysis during the aiMD simulations is presented in Figures 8–10.

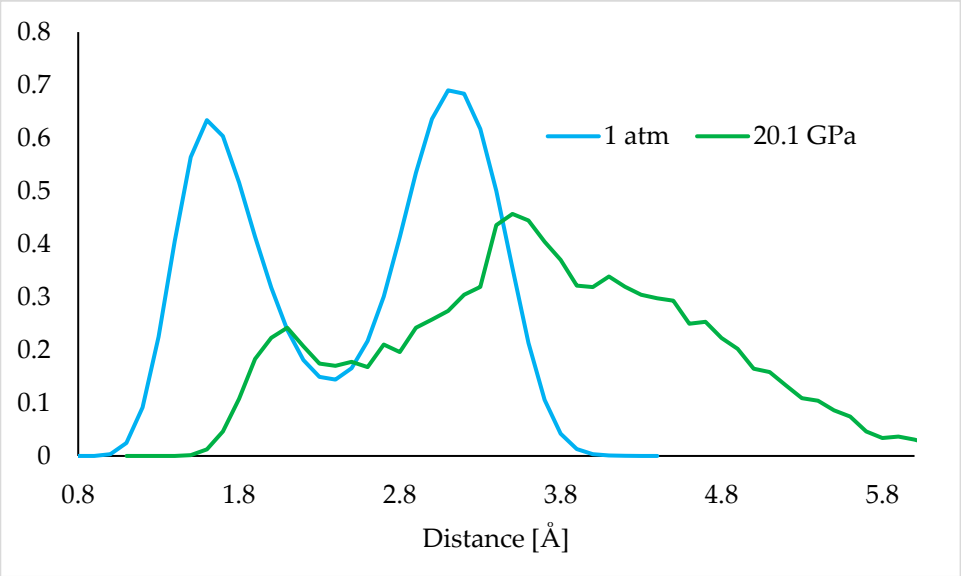

Figure 8. Length distribution of the H-bond during the aiMD simulations at 1 atm (blue) and 20.1 GPa (green).

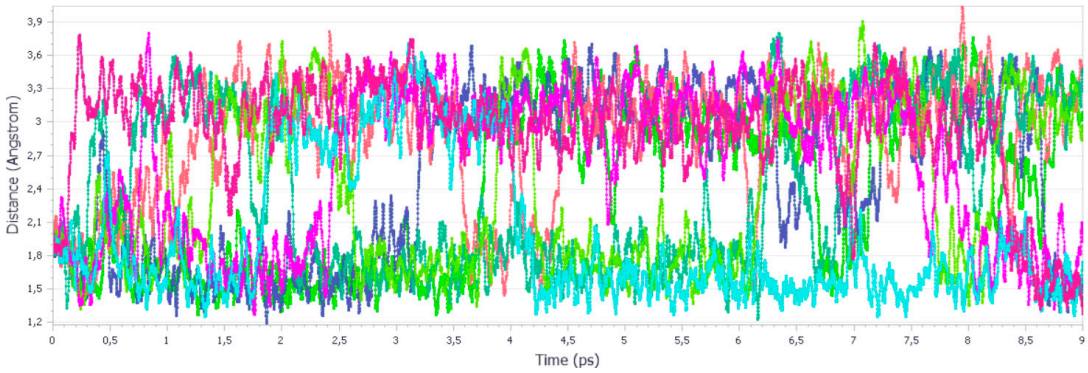

Figure 9. Length evolution of the H-bonds during the aiMD simulations at 1 atm. Different colors represent the unique H-bonds within the unit cell.

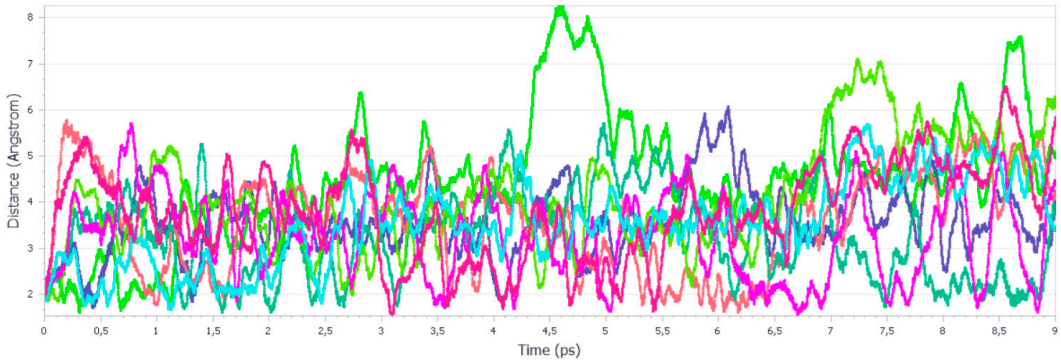

Figure 10. Length evolution of the H-bonds during the aiMD simulations at 20.1 GPa. Different colors represent the unique H-bonds within the unit cell.

The structural differences between Phase I and Phase II, as well as the molecular mechanism responsible for this transition, were already described in details in [18]. Based on the experimental results, the authors deduced the mechanism of the phase change as follows. Under ambient conditions, hydrogen bonding and electrostatic interactions are the predominant forces within SA. The transition of SA under high pressure is anticipated to arise from the cooperativity of these two interactions. As pressure escalates, the distances

between molecules diminish. Hydrogen bonding and electrostatic interactions between the adjacent SO_3^- and NH_3^+ groups are intensified, leading to an increase in the total Gibbs free energy. Thus, to maintain structural equilibrium, clusters of SO_3^- and NH_3^+ begin to deform beyond 8.1 GPa, accompanied by the formation of new hydrogen bonds. Upon additional compression between 10.1 and 12.7 GPa, the structure can no longer accommodate the rising free energy, prompting SA to transition to a new conformation to minimise the free energy. Pressure causes relative sliding movements between adjacent molecular chains in SA, accompanied by the reconfiguration of hydrogen bonding and the intensification of electrostatic interactions. Nevertheless, the phase change does not cause an obvious breakdown of the structure. Following the relative displacement of the molecules, the high-pressure structure retains a resemblance to the ambient structure. Despite a sudden alteration in unit cell characteristics, the high-pressure phase can maintain the same symmetry as the ambient phase. As a result, SA undergoes an isosymmetric transition at an elevated pressure. Phase II can be seen as the outcome of the relative displacement between adjacent hydrogen-bonded molecular chains of Phase I. The apparent direction of the slippage is just along the c-axis. The c-axis exhibits a significant contraction following the phase shift. Concurrently, the movement between the molecules results in a slight elongation of a- and b-axes. Moreover, in the ab plane, the angle of intersection between two SA molecules diminishes, corroborating our assertion that Phase II is more compact than Phase I. The tight structure of Phase II renders the hydrogen-bonded network challenging to compress under high pressure.

4. Conclusions

In this work, we analysed the IPT of SA using multiple diverse computational approaches, comparing the obtained theoretical results with the corresponding experimental ones. Despite the high accuracy of the calculations of unit cell dimensions of Phase I at 1 atm, the optimisation of SA at 20.1 GPa did not result in the anticipated IPT. At this pressure, Phase II was characterised by a higher lattice energy than Phase I. However, the simulation of Raman spectra indicated the greater compliance between the theoretical spectrum of Phase II with the experimental results than that of Phase I. The thermodynamic calculations revealed that Phase II is characterised by a lower G and H, and higher S than Phase I, which indicates the higher thermodynamic stability of Phase II at an elevated pressure. No major changes were observed during the MD simulations at 1 atm; however, at 20.1 GPa, significant changes in both unit cell dimensions, as well as in the H-bond lattice were observed, indicating the instability of Phase I and pointing to the anticipated IPT.

Thermodynamic analysis explains the experimentally observed IPT and highlights the important role of phonon DOS calculations required for the thermodynamic analysis, as the analysis of solely lattice energies can be misleading and does not reflect the true order of stability of polymorphs. However, it should also be noticed that the kinetic factors play a significant role in the stability and rate of polymorphic phase transition, determining i.e., the order and constant of this transformation. To our knowledge, kinetic effects have yet to be examined in crystal structure prediction simulations conducted at a fully first-principles level. However, this is only attributable to the deficiency of requisite processing power to do these calculations. Future studies should, therefore, include the prediction of the transition state between Phase I and Phase II, which would allow for calculating the free energy barrier and, subsequently, the kinetic constant (k). While calculation of the kinetic aspects of this transition is computationally expensive, it would allow for observing the energy barriers and reaction pathways, contributing to a more complete understanding of this phenomenon.

In conclusion, the answer to the question stated in the title of this work is positive; however, the prediction of IPT is not a straightforward task and requires careful analysis. This work points on several aspects, such as thermodynamic calculations and MD simulations that, despite their high computational costs, should be taken into account when analysing phenomena such as polymorphic phase transitions.

Additionally, it should be noted that while in [18] a detailed crystallographic and Raman analysis of the studied IPT were conducted, additional SCXRD or ssNMR experiments could provide more information on this phenomenon.

Supplementary Materials: The following supporting information can be downloaded at: https://www.mdpi.com/article/10.3390/app15084185/s1, Table S1. Comparison of the results of calculations of "full + cell" geometry optimisation at 20.1 GPa obtained using the initial structures of Phase I ICSD_802 and Phase II, created using the experimental structure of Phase I and changing the values of the unit cell dimensions to those presented in [18], as described in Section 3.1.

Author Contributions: Conceptualisation, Ł.S., M.F.-R. and A.M.M.; methodology, Ł.S.; software, Ł.S.; validation, Ł.S.; formal analysis, Ł.S. and A.M.M.; investigation, Ł.S. and A.M.M.; resources, Ł.S.; data curation, Ł.S. and A.M.M.; writing—original draft preparation, Ł.S. and A.M.M.; writing—review and editing, Ł.S., M.F.-R. and A.M.M.; visualisation, Ł.S. and A.M.M.; supervision, Ł.S. and M.F.-R.; project administration, Ł.S.; funding acquisition, Ł.S. All authors have read and agreed to the published version of the manuscript.

Funding: This research received no external funding.

Institutional Review Board Statement: Not applicable.

Informed Consent Statement: Not applicable.

Data Availability Statement: The raw data supporting the conclusions of this article will be made available by the authors on request.

Conflicts of Interest: The authors declare no conflicts of interest.

References

1. Şaşmaz, A.; Kılıç, A.D.; Konakçı, N. Chemical and Thermal Changes in $Mg_3Si_2O_5(OH)_4$ Polymorph Minerals and Importance as an Industrial Material. *Appl. Sci.* **2024**, *14*, 10298. [CrossRef]
2. Wilińska, J.; Turek, A.; Rech, J.; Janeczek, H.; Pastusiak, M.; Kordyka, A.; Borecka, A.; Kobielarz, M.; Kasperczyk, J. Hot Melt Extrusion as a Formulation Method of Terpolymer Rods with Aripiprazole: A Preliminary Study. *Appl. Sci.* **2023**, *13*, 9521. [CrossRef]
3. Takajo, D.; Sudoh, K. Stability of Two-Dimensional Polymorphs for 10,12-Pentacosadyn-1-ol on Graphite Investigated by SPM. *Appl. Sci.* **2018**, *8*, 503. [CrossRef]
4. Braga, D.; Casali, L.; Grepioni, F. The Relevance of Crystal Forms in the Pharmaceutical Field: Sword of Damocles or Innovation Tools? *Int. J. Mol. Sci.* **2022**, *23*, 9013. [CrossRef] [PubMed]
5. Chen, C.; Li, Y.; Guo, D.; Ke, C.; Fan, D.; Lu, S.; Li, X.; Jiang, M.; Hu, X. Monodispersed Transition Metals Induced Ordinary-Pressure Phase Transformation from Graphite to Diamond: A First-Principles Calculation. *ACS Appl. Mater. Interfaces* **2023**, *15*, 30684–30691. [CrossRef]
6. Christy, A.G. Isosymmetric structural phase transitions: Phenomenology and examples. *Acta Crystallogr. Sect. B Struct. Sci.* **1995**, *51*, 753–757. [CrossRef]
7. Goryainov, S.V.; Boldyreva, E.V.; Smirnov, M.B.; Ahsbahs, H.; Chernyshev, V.V.; Weber, H.P. Isosymmetric Reversible Pressure-Induced Phase Transition in Sodium Oxalate at 3.8 GPa. *Dokl. Phys. Chem.* **2003**, *390*, 154–157. [CrossRef]
8. Szafrański, M.; Czarnecki, P.; Katrusiak, A.; Habrylo, S. DTA investigation of phase transitions in 1,3-cyclohexanedione under high pressures. *Solid State Commun.* **1992**, *82*, 277–281. [CrossRef]
9. Fisch, M.; Lanza, A.; Boldyreva, E.; Macchi, P.; Casati, N. Kinetic control of high-pressure solid-state phase transitions: A case study on L-Serine. *J. Phys. Chem. C* **2015**, *119*, 18611–18617. [CrossRef]
10. Oswald, I.D.H.; Lennie, A.R.; Pulham, C.R.; Shankland, K. High-pressure structural studies of the pharmaceutical, chlorothiazide. *CrystEngComm* **2010**, *12*, 2533. [CrossRef]

11. Bull, C.L.; Funnell, N.P.; Ridley, C.J.; Pulham, C.R.; Coster, P.; Tellam, J.P.; Marshall, W.G. Pressure-Induced Isosymmetric Phase Transition in Biurea. *CrystEngComm* **2019**, *21*, 5872–5881. [CrossRef]
12. Clarke, S.M.; Steele, B.A.; Kroonblawd, M.P.; Zhang, D.; Kuo, I.-F.W.; Stavrou, E. An Isosymmetric High-Pressure Phase Transition in α-Glycylglycine: A Combined Experimental and Theoretical Study. *J. Phys. Chem. B* **2019**, *124*, 1–10. [CrossRef] [PubMed]
13. Mazurek, A.H.; Szeleszczuk, Ł.; Pisklak, D.M. Periodic DFT Calculations—Review of Applications in the Pharmaceutical Sciences. *Pharmaceutics* **2020**, *12*, 415. [CrossRef]
14. Spillane, W.; Malaubier, J.-B. Sulfamic Acid and Its N- and O-Substituted Derivatives. *Chem. Rev.* **2014**, *114*, 2507–2586. [PubMed]
15. Caso, M.M.; Cefola, M. The use of sulfamic acid as a primary standard in nonaqueous titrimetry. *Anal. Chim. Acta* **1959**, *21*, 205–214. [CrossRef]
16. Rajitha, B.; Kumar, B.S.; Reddy, Y.T.; Reddy, P.N.; Sreenivasulu, N. Sulfamic acid: A novel and efficient catalyst for the synthesis of aryl-14H-dibenzo[a.j]xanthenes under conventional heating and microwave irradiation. *Tetrahedron Lett.* **2005**, *46*, 8691–8693. [CrossRef]
17. Bats, J.W.; Coppens, P.; Koetzle, T.F. The Experimental Charge Density in Sulfur-Containing Molecules: A Study of the Deformation Electron Density in Sulfamic Acid at 78 K by X-ray and Neutron Diffraction. *Acta Cryst.* **1977**, *B33*, 37–45. [CrossRef]
18. Li, Q.; Li, S.; Wang, K.; Li, X.; Liu, J.; Liu, B.; Zou, G.; Zou, B. Pressure-induced isosymmetric phase transition in sulfamic acid: A combined Raman and x-ray diffraction study. *J. Chem. Phys.* **2013**, *138*, 214505. [CrossRef]
19. Napiórkowska, E.; Milcarz, K.; Szeleszczuk, Ł. Review of Applications of Density Functional Theory (DFT) Quantum Mechanical Calculations to Study the High-Pressure Polymorphs of Organic Crystalline Materials. *Int. J. Mol. Sci.* **2023**, *24*, 14155. [CrossRef]
20. Clark, S.J.; Segall, M.D.; Pickard, C.J.; Hasnip, P.J.; Probert, M.J.; Refson, K.; Payne, M.C. First principles methods using CASTEP. Z. Kristallogr. *Cryst. Mater.* **2005**, *220*, 567–570.
21. Perdew, J.P.; Burke, K.; Ernzerhof, M. Generalized Gradient Approximation Made Simple. *Phys. Rev. Lett.* **1996**, *77*, 3865–3868. [CrossRef]
22. Tkatchenko, A.; Scheffler, M. Accurate Molecular Van Der Waals Interactions from Ground-State Electron Density and Free-Atom Reference Data. *Phys. Rev. Lett.* **2009**, *102*, 073005. [CrossRef] [PubMed]
23. Grimme, S. Semiempirical GGA-type density functional constructed with a long-range dispersion correction. *J. Comput. Chem.* **2006**, *27*, 1787–1799. [CrossRef] [PubMed]
24. Ambrosetti, A.; Reilly, A.M.; DiStasio, R.A., Jr.; Tkatchenko, A. Long-range correlation energy calculated from coupled atomic response functions. *J. Chem. Phys.* **2014**, *140*, 18A508. [CrossRef] [PubMed]
25. Hammer, B.; Hansen, L.B.; Nørskov, J.K. Improved adsorption energetics within density-functional theory using revised Perdew–Burke–Ernzerhof functionals. *Phys. Rev. B* **1999**, *59*, 7413–7421. [CrossRef]
26. Perdew, J.P.; Chevary, J.A.; Vosko, S.H.; Jackson, K.A.; Pederson, M.R.; Singh, D.J.; Fiolhais, C. Atoms, molecules, solids, and surfaces: Applications of the generalized gradient approximation for exchange and correlation. *Phys. Rev. B* **1992**, *46*, 6671–6687. [CrossRef]
27. Ortmann, F.; Bechstedt, F.; Schmidt, W.G. Semiempirical van der Waals correction to the density functional description of solids and molecular structures. *Phys. Rev. B* **2006**, *73*, 205101. [CrossRef]
28. Wu, Z.; Cohen, R.E. More accurate generalized gradient approximation for solids. *Phys. Rev. B* **2006**, *73*, 235116. [CrossRef]
29. Perdew, J.P.; Ruzsinszky, A.; Csonka, G.I.; Vydrov, O.A.; Scuseria, G.E.; Constantin, L.A.; Zhou, X.; Burke, K. Restoring the Density-Gradient Expansion for Exchange in Solids and Surfaces. *Phys. Rev. Lett.* **2008**, *100*, 136406. [CrossRef]
30. Becke, A.D. Density-functional exchange-energy approximation with correct asymptotic behavior. *Phys. Rev. A* **1988**, *38*, 3098–3100. [CrossRef]
31. Lee, C.; Yang, W.; Parr, R.G. Development of the Colle-Salvetti correlation-energy formula into a functional of the electron density. *Phys. Rev. B* **1988**, *37*, 785–789. [CrossRef] [PubMed]
32. Bartók, A.P.; Yates, J.R. Regularized SCAN functional. *J. Chem. Phys.* **2019**, *150*, 161101. [CrossRef]
33. Baroni, S.; de Gironcoli, S.; Dal Corso, A.; Giannozzi, P. Phonons and related crystal properties from density-functional perturbation theory. *Rev. Mod. Phys.* **2001**, *73*, 515–532. [CrossRef]
34. Arias, T.A.; Payne, M.C.; Joannopoulos, J.D. Ab initio molecular dynamics: Analytically continued energy functionals and insights into iterative solutions. *Phys. Rev. Lett.* **1992**, *69*, 1077–1080. [CrossRef] [PubMed]
35. Cameron, A.F.; Duncanson, F.D. Refinement of sulphamic acid. Acta Crystallogr. *Sect. B Struct. Sci.* **1976**, *32*, 1563–1564. [CrossRef]
36. Osaki, K.; Tadokoro, H.; Nitta, I. Structure of Sulphamic Acid Molecule from a Three-dimensional Fourier Analysis. *Bull. Chem. Soc. Jpn.* **1955**, *28*, 524–528. [CrossRef]
37. Szeleszczuk, Ł.; Mazurek, A.H.; Milcarz, K.; Napiórkowska, E.; Pisklak, D.M. Can We Predict the Isosymmetric Phase Transition? Application of DFT Calculations to Study the Pressure Induced Transformation of Chlorothiazide. *Int. J. Mol. Sci.* **2021**, *22*, 10100. [CrossRef]

38. Mazurek, A.; Szeleszczuk, Ł.; Pisklak, D.M. Can We Predict the Pressure Induced Phase Transition of Urea? Application of Quantum Molecular Dynamics. *Molecules* **2020**, *25*, 1584. [CrossRef]
39. Cruz-Cabeza, A.J.; Reutzel-Edens, S.M.; Bernstein, J. Facts and fictions about polymorphism. *Chem. Soc. Rev.* **2015**, *44*, 8619–8635. [CrossRef]

Disclaimer/Publisher's Note: The statements, opinions and data contained in all publications are solely those of the individual author(s) and contributor(s) and not of MDPI and/or the editor(s). MDPI and/or the editor(s) disclaim responsibility for any injury to people or property resulting from any ideas, methods, instructions or products referred to in the content.

Article

Predicting the Pressure-Induced Isosymmetric Phase Transition of Sulfamic Acid by Applying Periodic Density Functional Theory Calculations

Anna Maria Mazurek [1], Monika Franczak-Rogowska [2] and Łukasz Szeleszczuk [1,*]

[1] Department of Organic and Physical Chemistry, Medical University of Warsaw, 1 Banacha Str., 02-097 Warsaw, Poland; anna_m_mazurek@o2.pl
[2] Department of Drug Chemistry, Pharmaceutical and Biomedical Analysis, Medical University of Warsaw, 1 Banacha Str., 02-097 Warsaw, Poland; monika.franczak-rogowska@wum.edu.pl
* Correspondence: lukasz.szeleszczuk@wum.edu.pl; Tel.: +48 501 255 121

Table S1. Comparison of the results of calculations of "full+cell" geometry optimization at 20.1 GPa obtained using the as initial structures of Phase I ICSD_802 and Phase II, created using the experimental structure of Phase I and changing the values of the unit cell dimensions to those presented in [18], as described in the 3.1. section.

		Phase I used as initial				Phase II used as initial				Phase II – Phase I				
DFT functional	**Dispersion correction**	**a [Å]**	**b [Å]**	**c [Å]**	**V [Å³]**	**a [Å]**	**b [Å]**	**c [Å]**	**V [Å³]**	**Δa [Å]**	**Δb [Å]**	**Δc [Å]**	**ΔV [Å³]**	**ΔE* [kJ/mol]**
PBE	TS	7.248949	7.375992	8.488876	453.884833	7.247604	7.37771	8.493029	454.12838	-0.001345	0.001718	0.004153	0.24354648	0.0048
PBE	Grimme	7.212575	7.363996	8.510022	451.995977	7.214635	7.365026	8.509725	452.172529	0.00206	0.00103	-0.000297	0.17655282	0.0012
PBE	MBD*	7.226844	7.36537	8.474166	451.066128	7.228524	7.36577	8.475041	451.242076	0.00168	0.0004	0.000875	0.17594829	0.0144
PBE	n/a	7.267552	7.402163	8.548063	459.848217	7.269506	7.403403	8.549187	460.109401	0.001954	0.00124	0.001124	0.26118419	0.0048
RPBE	TS	7.166354	7.315016	8.30951	435.601085	7.167951	7.315058	8.311321	435.795617	0.001597	4.2E-05	0.001811	0.19453191	0.0072
RPBE	n/a	7.356077	7.49266	8.647747	476.634273	7.354932	7.494851	8.650991	476.878261	-0.001145	0.002191	0.003244	0.24398826	0.0036
PW91	TS	7.248146	7.368973	8.487849	453.347832	7.247862	7.369973	8.490971	453.558354	-0.000284	0.001	0.003122	0.21052195	0.0060
PW91	OBS	7.247881	7.369142	8.488238	453.36243	7.246904	7.370438	8.491594	453.560293	-0.000977	0.001296	0.003356	0.19786262	0.0036
PW91	n/a	7.261196	7.394089	8.537517	458.378686	7.260977	7.396033	8.538876	458.558352	-0.000219	0.001944	0.001359	0.1796667	0.0048
WC	n/a	7.169666	7.304308	8.446465	442.336716	7.170763	7.303291	8.448931	442.471943	0.001097	-0.001017	0.002466	0.13522764	0.0000
PBESOL	TS	7.152361	7.284258	8.419974	438.677638	7.153992	7.284166	8.420818	438.816112	0.001631	-9.2E-05	0.000844	0.13847437	0.0024
PBESOL	n/a	7.16717	7.304333	8.452671	442.50913	7.16856	7.305238	8.452569	442.644445	0.00139	0.000905	-0.000102	0.13531572	0.0012
BLYP	TS	7.166023	7.298286	8.380631	438.304364	7.166148	7.300738	8.380891	438.472872	0.000125	0.002452	0.00026	0.16850763	0.0012
BLYP	Grimme	7.267476	7.410279	8.548107	460.349966	7.270444	7.411486	8.546725	460.538515	0.002968	0.001207	-0.001382	0.18854906	0.0060
BLYP	n/a	7.361784	7.476496	8.59559	473.10427	7.358852	7.479695	8.598443	473.275229	-0.002932	0.003199	0.002853	0.17095857	0.0060
RSCAN	n/a	7.194811	7.336458	8.432219	445.089863	7.196491	7.33529	8.433352	445.182724	0.00168	-0.001168	0.001133	0.09286137	0.0012

Publication co-author statement

As a co-author of the publication entitled:

"Predicting the Pressure-Induced Isosymmetric Phase Transition of Sulfamic Acid by Applying Periodic Density Functional Theory Calculations", *published in Applied Sciences (2025, Volume 15, Issue 8, Article 4185),* https://doi.org/10.3390/app15084185
Authors: Anna Maria Mazurek, Monika Franczak-Rogowska and Łukasz Szeleszczuk

I agree to include this publication into a collection of thematically related publications forming a doctoral dissertation prepared by mgr farm. Anna Maria Mazurek.

Additionally, I declare my contribution to the publication as follows: conceptualisation, Ł.S., M.F.-R. and A.M.M.; methodology, Ł.S.; software, Ł.S.; validation, Ł.S.; formal analysis, Ł.S. and A.M.M.; investigation, Ł.S. and A.M.M.; resources, Ł.S.; data curation, Ł.S. and A.M.M.; writing - original draft preparation, Ł.S. and A.M.M.; writing - review and editing, Ł.S., M.F.-R. and A.M.M.; visualisation, Ł.S. and A.M.M.; supervision, Ł.S. and M.F.-R.; project administration, Ł.S.; funding acquisition, Ł.S.

Oświadczenie współautora publikacji

Jako współautor publikacji pt.:

"Predicting the Pressure-Induced Isosymmetric Phase Transition of Sulfamic Acid by Applying Periodic Density Functional Theory Calculations", *opublikowanej w czasopiśmie Applied Sciences (2025, tom 15, numer 8, artykuł 4185),*
https://doi.org/10.3390/app15084185
Autorzy: Anna Maria Mazurek, Monika Franczak-Rogowska and Łukasz Szeleszczuk

Wyrażam zgodę na włączenie tej publikacji do zbioru powiązanych tematycznie artykułów naukowych, stanowiących część pracy doktorskiej przygotowanej przez mgr farm. Annę Marię Mazurek.

Jednocześnie potwierdzam, że następujący zakres stanowi mój wkład w publikację: koncepcja, Ł.S., M.F.-R. oraz A.M.M.; metodologia, Ł.S.; oprogramowanie, Ł.S.; walidacja, Ł.S.; analiza formalna, Ł.S. oraz A.M.M.; badania, Ł.S. oraz A.M.M.; zasoby, Ł.S.; opracowanie danych, Ł.S. oraz A.M.M.; pisanie – przygotowanie pierwotnej wersji manuskryptu, Ł.S. oraz A.M.M.; pisanie - redakcja i korekta manuskryptu, Ł.S., M.F.-R. oraz A.M.M.; wizualizacja, Ł.S. oraz A.M.M.; nadzór, Ł.S. oraz M.F.-R.; zarządzanie projektem, Ł.S.; pozyskiwanie finansowania, Ł.S.

28.04.2026
Date / Data

Anna Mazurek
Legible signature / Czytelny podpis

Publication co-author statement

As a co-author of the publication entitled:

"Predicting the Pressure-Induced Isosymmetric Phase Transition of Sulfamic Acid by Applying Periodic Density Functional Theory Calculations", *published in Applied Sciences (2025, Volume 15, Issue 8, Article 4185),* https://doi.org/10.3390/app15084185
Authors: Anna Maria Mazurek, Monika Franczak-Rogowska and Łukasz Szeleszczuk

I agree to include this publication into a collection of thematically related publications forming a doctoral dissertation prepared by mgr farm. Anna Maria Mazurek.

Additionally, I declare my contribution to the publication as follows: conceptualisation, Ł.S., M.F.-R. and A.M.M.; methodology, Ł.S.; software, Ł.S.; validation, Ł.S.; formal analysis, Ł.S. and A.M.M.; investigation, Ł.S. and A.M.M.; resources, Ł.S.; data curation, Ł.S. and A.M.M.; writing - original draft preparation, Ł.S. and A.M.M.; writing - review and editing, Ł.S., M.F.-R. and A.M.M.; visualisation, Ł.S. and A.M.M.; supervision, Ł.S. and M.F.-R.; project administration, Ł.S.; funding acquisition, Ł.S.

Oświadczenie współautora publikacji

Jako współautor publikacji pt.:

"Predicting the Pressure-Induced Isosymmetric Phase Transition of Sulfamic Acid by Applying Periodic Density Functional Theory Calculations", *opublikowanej w czasopiśmie Applied Sciences (2025, tom 15, numer 8, artykuł 4185),*
https://doi.org/10.3390/app15084185
Autorzy: Anna Maria Mazurek, Monika Franczak-Rogowska and Łukasz Szeleszczuk

Wyrażam zgodę na włączenie tej publikacji do zbioru powiązanych tematycznie artykułów naukowych, stanowiących część pracy doktorskiej przygotowanej przez mgr farm. Annę Marię Mazurek.

Jednocześnie potwierdzam, że następujący zakres stanowi mój wkład w publikację: koncepcja, Ł.S., M.F.-R. oraz A.M.M.; metodologia, Ł.S.; oprogramowanie, Ł.S.; walidacja, Ł.S.; analiza formalna, Ł.S. oraz A.M.M.; badania, Ł.S. oraz A.M.M.; zasoby, Ł.S.; opracowanie danych, Ł.S. oraz A.M.M.; pisanie – przygotowanie pierwotnej wersji manuskryptu, Ł.S. oraz A.M.M.; pisanie - redakcja i korekta manuskryptu, Ł.S., M.F.-R. oraz A.M.M.; wizualizacja, Ł.S. oraz A.M.M.; nadzór, Ł.S. oraz M.F.-R.; zarządzanie projektem, Ł.S.; pozyskiwanie finansowania, Ł.S.

28.04.2026
Date / Data

Szeleszczuk
Legible signature / Czytelny podpis

Publication co-author statement

As a co-author of the publication entitled:

"Predicting the Pressure-Induced Isosymmetric Phase Transition of Sulfamic Acid by Applying Periodic Density Functional Theory Calculations", *published in Applied Sciences (2025, Volume 15, Issue 8, Article 4185),* https://doi.org/10.3390/app15084185
Authors: Anna Maria Mazurek, Monika Franczak-Rogowska and Łukasz Szeleszczuk

I agree to include this publication into a collection of thematically related publications forming a doctoral dissertation prepared by mgr farm. Anna Maria Mazurek.

Additionally, I declare my contribution to the publication as follows: conceptualisation, Ł.S., M.F.-R. and A.M.M.; methodology, Ł.S.; software, Ł.S.; validation, Ł.S.; formal analysis, Ł.S. and A.M.M.; investigation, Ł.S. and A.M.M.; resources, Ł.S.; data curation, Ł.S. and A.M.M.; writing - original draft preparation, Ł.S. and A.M.M.; writing - review and editing, Ł.S., M.F.-R. and A.M.M.; visualisation, Ł.S. and A.M.M.; supervision, Ł.S. and M.F.-R.; project administration, Ł.S.; funding acquisition, Ł.S.

Oświadczenie współautora publikacji

Jako współautor publikacji pt.:

"Predicting the Pressure-Induced Isosymmetric Phase Transition of Sulfamic Acid by Applying Periodic Density Functional Theory Calculations", *opublikowanej w czasopiśmie Applied Sciences (2025, tom 15, numer 8, artykuł 4185),*
https://doi.org/10.3390/app15084185
Autorzy: Anna Maria Mazurek, Monika Franczak-Rogowska and Łukasz Szeleszczuk

Wyrażam zgodę na włączenie tej publikacji do zbioru powiązanych tematycznie artykułów naukowych, stanowiących część pracy doktorskiej przygotowanej przez mgr farm. Annę Marię Mazurek.

Jednocześnie potwierdzam, że następujący zakres stanowi mój wkład w publikację: koncepcja, Ł.S., M.F.-R. oraz A.M.M.; metodologia, Ł.S.; oprogramowanie, Ł.S.; walidacja, Ł.S.; analiza formalna, Ł.S. oraz A.M.M.; badania, Ł.S. oraz A.M.M.; zasoby, Ł.S.; opracowanie danych, Ł.S. oraz A.M.M.; pisanie – przygotowanie pierwotnej wersji manuskryptu, Ł.S. oraz A.M.M.; pisanie - redakcja i korekta manuskryptu, Ł.S., M.F.-R. oraz A.M.M.; wizualizacja, Ł.S. oraz A.M.M.; nadzór, Ł.S. oraz M.F.-R.; zarządzanie projektem, Ł.S.; pozyskiwanie finansowania, Ł.S.

28.04.2026
Date / Data

Franczak-Rogowska
Legible signature / Czytelny podpis

10.3. Publication No. 3

crystals

MDPI

Article

Periodic DFT Investigation of Isosymmetric Alpha–Beta Phase Transition in Resorcinol Under Ambient and High Pressure

Anna Maria Mazurek [1], Monika Franczak-Rogowska [2] and Łukasz Szeleszczuk [1,*]

[1] Department of Organic and Physical Chemistry, Medical University of Warsaw, 1 Banacha Str., 02-097 Warsaw, Poland; anna.mazurek1@wum.edu.pl
[2] Department of Drug Chemistry, Pharmaceutical and Biomedical Analysis, Medical University of Warsaw, 1 Banacha Str., 02-097 Warsaw, Poland; monika.franczak-rogowska@wum.edu.pl
* Correspondence: lukasz.szeleszczuk@wum.edu.pl; Tel.: +48-501-255-121

Abstract

Isosymmetric phase transitions driven by subtle hydrogen-bond rearrangements remain challenging for periodic density functional theory (DFT), particularly when energy differences between polymorphs are small. Resorcinol represents an interesting case in which the α and β polymorphs crystallize in the same space group and differ primarily in hydroxyl orientation and hydrogen-bond topology. In this work, the α–β phase transition was systematically investigated using periodic DFT calculations under ambient and elevated pressure. A broad set of exchange–correlation functionals combined with different dispersion corrections was benchmarked against experimental structural and energetic data. Dispersion-corrected methods were essential for reproducing lattice parameters and the pressure-induced inversion of stability. PBESOL with Tkatchenko–Scheffler dispersion provided the most consistent agreement with the experiment and was therefore used for phonon and ab initio molecular dynamics simulations. Phonon-derived thermodynamic analysis revealed a delicate enthalpy–entropy balance governing the transition, strongly affected by pressure. Dynamical simulations confirmed the instability of the α phase under compression, demonstrating the cooperative nature of this hydrogen-bond-driven isosymmetric transformation.

Keywords: resorcinol polymorphism; isosymmetric phase transition; periodic DFT; phonon thermodynamics; hydrogen bonding; high-pressure crystallography; ab initio molecular dynamics

Check for updates

Academic Editors: Tarciso Silva Andrade-Filho, Rodrigo Gester and Mateus Ribeiro Lage

Received: 6 March 2026
Revised: 20 March 2026
Accepted: 21 March 2026
Published: 23 March 2026

Copyright: © 2026 by the authors. Licensee MDPI, Basel, Switzerland. This article is an open access article distributed under the terms and conditions of the Creative Commons Attribution (CC BY) license.

1. Introduction

Polymorphism remains one of the central challenges in solid-state chemistry and materials science, particularly in systems where subtle structural rearrangements lead to pronounced changes in physical properties [1]. In molecular crystals, even small variations in molecular conformation or hydrogen-bond topology may alter density, compressibility, vibrational spectra, or thermodynamic stability [2]. Among the various types of solid-state transformations, isosymmetric phase transitions (IPTs) are especially intriguing [3]. In such transitions, substantial structural reorganization occurs without a change in the crystallographic space group, which complicates both their experimental detection and theoretical prediction [4,5].

Resorcinol (benzene-1,3-diol) represents a classical and extensively studied model system for investigating polymorphism and hydrogen-bond-driven phase transitions [6–10]. At ambient pressure, it crystallizes in two polymorphic forms, α and β, both adopting the

orthorhombic space group $Pna2_1$ with Z = 4 and Z′ = 1 (Figure 1). Despite sharing identical symmetry and the same number of symmetry-independent molecules, the two phases differ markedly in molecular conformation and hydrogen-bond arrangement. In the α-form, the molecule adopts the anti–anti conformation, whereas in the β-form one hydroxyl group rotates, yielding an anti–syn arrangement (Figure 2). This conformational change is directly coupled to a reorganization of the O–H···O hydrogen-bond network, transforming the three-dimensional spiral-like motif characteristic of the α-phase into distinct chain-like arrangements in the β-phase.

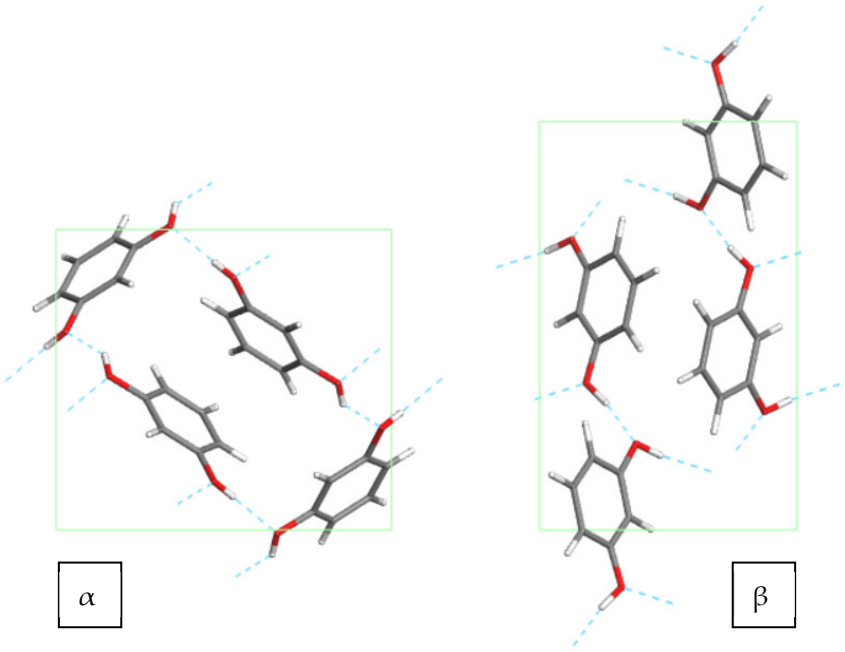

Figure 1. Crystal structures of α (RESORA19) and β (RESORA24) polymorphs of resorcinol.

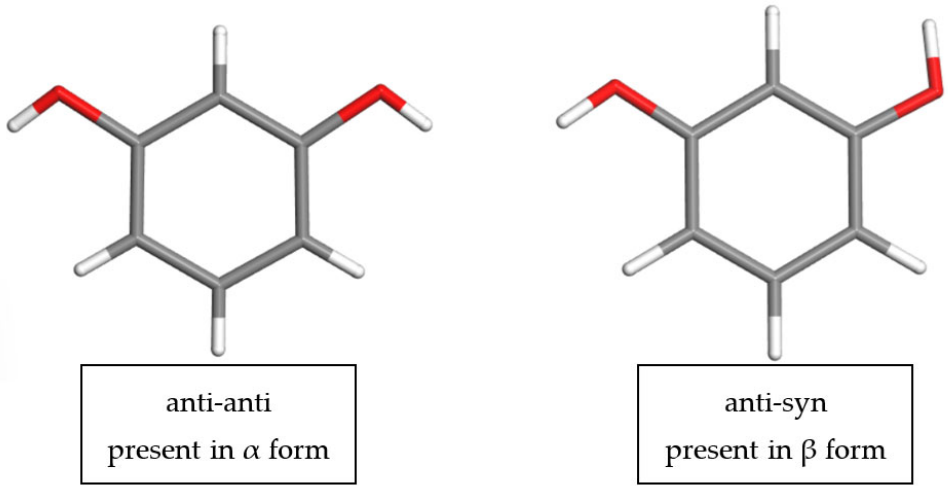

Figure 2. Molecular conformations of resorcinol: anti–anti, present in α form (RESORA19) and anti–syn, present in β form (RESORA24).

The α to β transformation is induced by temperature at an ambient pressure and by compression at room temperature (Figure 3) [8–10]. Thermodynamic studies have shown that the transition temperature is approximately 365–370 K, accompanied by a relatively small enthalpy and entropy change, consistent with the retention of the same space group. High-pressure experiments further demonstrated that the α-phase can transform into β at around 0.4–0.5 GPa, although significant hysteresis and kinetic effects have been reported.

Additional high-pressure polymorphs have also been proposed at elevated pressures. The complexity of the resorcinol phase diagram, including the coexistence regions and strong dependence on compression rate, makes it a demanding test case for computational modeling [6,7].

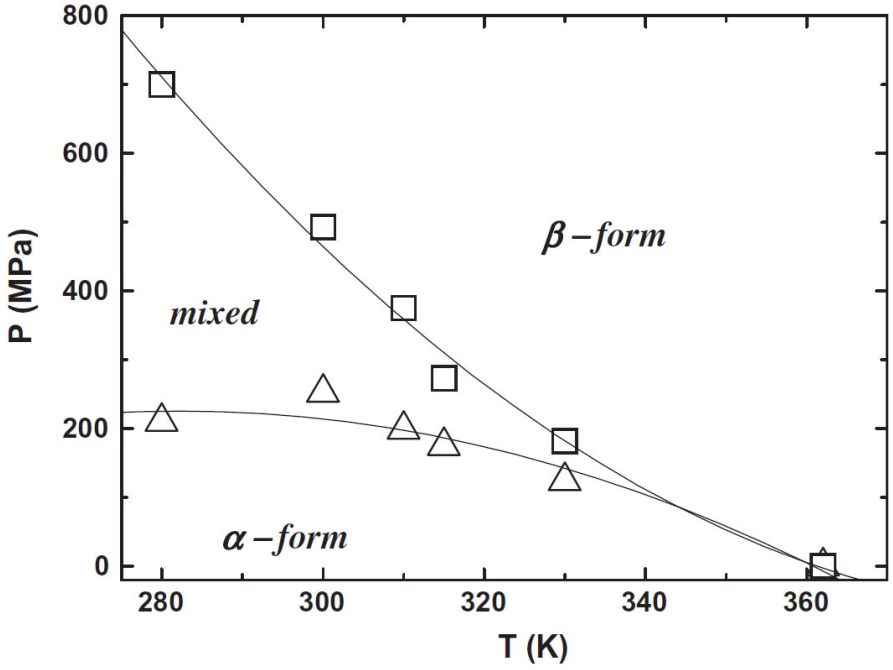

Figure 3. Phase diagram of resorcinol. Reprinted from [8], with permission from Elsevier.

From an experimental perspective, the two polymorphs of resorcinol can be distinguished using several complementary techniques under ambient conditions. Solid-state NMR spectroscopy is expected to be particularly sensitive to the differences in local hydrogen-bond environments and molecular conformations present in the α and β structures, which would lead to distinct ^{13}C and ^{1}H ssNMR spectra [8]. In addition, vibrational spectroscopies such as Raman and infrared spectroscopy have previously been shown to provide characteristic signatures of the two polymorphs, reflecting differences in lattice modes and hydrogen-bonding interactions. X-ray diffraction remains the most direct method for structural identification, as the α and β phases exhibit distinct unit-cell metrics and packing arrangements.

From a theoretical perspective, the α/β-resorcinol system poses a particularly stringent challenge. Because both polymorphs are isosymmetric and differ primarily in the orientation of hydroxyl hydrogen atoms and in subtle intermolecular rearrangements, the energy differences between them are small and highly sensitive to the treatment of dispersion interactions and hydrogen bonding. Standard geometry optimization alone is often insufficient to capture the correct relative stability. Accurate prediction requires not only reliable exchange–correlation functionals and dispersion corrections, but also analysis of pressure-dependent enthalpies, vibrational contributions, and, in some cases, dynamical effects beyond the static 0 K approximation.

In recent years, periodic density functional theory (DFT) calculations have become a powerful tool for investigating polymorphism in molecular crystals [11]. When performed under periodic boundary conditions with appropriate dispersion corrections, DFT enables simultaneous optimization of lattice parameters and atomic positions, evaluation of pressure-dependent enthalpy landscapes, phonon spectra, and thermodynamic functions. Moreover, ab initio molecular dynamics (aiMD) simulations provide access to finite-temperature behavior and potential mechanisms of structural reorganization [12–16].

However, the predictive power of periodic DFT for isosymmetric transitions remains system-dependent and requires careful benchmarking [3].

The aim of the present study is to systematically investigate the isosymmetric α/β phase transition of resorcinol using periodic DFT calculations. A broad range of exchange–correlation functionals and dispersion correction schemes is assessed in terms of their ability to reproduce experimental structural parameters and to predict the correct pressure-dependent stability ordering of the two polymorphs. Enthalpy–pressure relationships, phonon analyses, and dynamical simulations are employed to elucidate the mechanism of the conformational and hydrogen-bond rearrangement underlying the transition. By using resorcinol as a benchmark system, this work seeks to evaluate the reliability and limitations of periodic DFT in modeling subtle, hydrogen-bond-driven isosymmetric phase transitions in molecular crystals.

2. Materials and Methods

The density functional theory (DFT) calculations, including enthalpy minimization, phonon dispersion analysis, density of states evaluation, and ab initio molecular dynamics (aiMD), were performed with the CASTEP module [17] available in Materials Studio 2020 (CASTEP version 2020). The simulations employed a plane-wave pseudopotential approach, using on-the-fly generated (OTFG) norm-conserving pseudopotentials (H_2017R2ncp.otfg for hydrogen, O_2019ncp.otfg for oxygen, and C_2017R2ncp.otfg for carbon), generated via the Koelling–Harmon scalar relativistic scheme.

2.1. DFT Functionals and Dispersion Correction Methods

The complete list of the DFT functionals and dispersion corrections used in this study is presented in Table 1.

Table 1. DFT-based computational methods used in this study.

No.	Approximation	Functional	Dispersion Correction	References
1	GGA	PBE	TS	[18,19]
2	GGA	PBE	Grimme	[18,20]
3	GGA	PBE	MBD*	[18,21]
4	GGA	PBE	n/a	[18]
5	GGA	RPBE	TS	[19,22]
6	GGA	RPBE	n/a	[22]
7	GGA	PW91	TS	[19,23,24]
8	GGA	PW91	OBS	[23–25]
9	GGA	PW91	n/a	[23,24]
10	GGA	WC	n/a	[26]
11	GGA	PBESOL	TS	[19,27]
12	GGA	PBESOL	n/a	[27]
13	GGA	BLYP	TS	[19,28,29]
14	GGA	BLYP	Grimme	[20,28,29]
15	GGA	BLYP	n/a	[28,29]
16	meta-GGA	RSCAN	n/a	[30]

2.2. Geometry Optimization

Geometry optimizations were performed using the limited-memory Broyden–Fletcher–Goldfarb–Shanno (LBFGS) algorithm, combined with the smart finite-basis set correction method. The plane-wave kinetic energy cutoff (E_{cut}) was first optimized and then fixed at 1020 eV. Brillouin zone sampling of the primitive cell was carried out with Monkhorst–Pack k-point grids selected to keep the spacing below 0.07 $Å^{-1}$.

As starting geometries, the experimental crystal structures of the α-polymorph (refcodes RESORA19) and β-polymorph (refcode RESORA24) of resorcinol, obtained from the Cambridge Structural Database (CSD), were used. Optimizations employed the "full + cell" scheme, allowing relaxation of both atomic coordinates and lattice parameters. Convergence thresholds were set to 5×10^{-6} eV/atom for total energy, 1×10^{-2} eV/Å for forces, 2×10^{-2} GPa for stress, and 5×10^{-4} Å for atomic displacements. For cell optimization, a fixed-basis set quality approach was applied, with the self-consistent field (SCF) tolerance set to 5×10^{-7} eV/atom.

2.3. Thermodynamic Parameters Calculations

Phonon frequencies were determined through diagonalization of dynamical matrices obtained via linear response methods, specifically density functional perturbation theory (DFPT). DFPT serves as the principal ab initio approach for phonon calculations and differs from the direct method in that it evaluates the variations in the Hamiltonian resulting from a defined perturbation in the charge density or wavefunction, rather than introducing explicit atomic displacements. For real-space dynamical matrix calculations, the q-point spacing parameter, representing the average distance between Monkhorst–Pack mesh points, was set to 0.05 $Å^{-1}$. The force constants in phonon property calculations were converged to 1×10^{-5} eV/$Å^2$. This framework was employed to evaluate band structure, density of states (DOS), phonon dispersion relations, and the phonon density of states (phonon DOS). In dispersion computations, the interval between q-vectors along the reciprocal space path was fixed at 0.015 $Å^{-1}$. DOS calculations used a $3 \times 3 \times 3$ Monkhorst–Pack k-point mesh, corresponding to a q-vector spacing of 0.04 $Å^{-1}$.

The outcomes of a phonon spectra calculation were utilized to ascertain, within the quasi-harmonic approximation, zero-point vibrational energy (Ezp), entropy (S), Gibbs free energy (G), and enthalpy (H) as functions of temperature, employing Equations (1)–(4) formulated by Baroni et al. [31]. In the equation, ω represents phonon frequency, F(ω) indicates the vibrational density of states for a phonon spectrum, Etot symbolizes the total electronic energy at absolute zero, k is Boltzmann's constant, and ħ is Dirac's constant.

$$E_{zp} = \frac{1}{2}\int F(\omega)\hbar\omega d\omega \quad (1)$$

$$S(T) = k\left\{\int \frac{\frac{\hbar\omega}{kT}}{\exp\left(\frac{\hbar\omega}{kT}\right)-1}F(\omega)d\omega - \int F(\omega)\ln\left[1-\exp\left(-\frac{\hbar\omega}{kT}\right)\right]d\omega\right\} \quad (2)$$

$$G(T) = E_{tot} + E_{zp} + kT\int F(\omega)\ln\left[1-\exp\left(-\frac{\hbar\omega}{kT}\right)\right]d\omega + pV \quad (3)$$

$$H = G + TS \quad (4)$$

2.4. Ab Initio Molecular Dynamics (aiMD) Simulations

Born–Oppenheimer ab initio molecular dynamics (aiMD) simulations [32] were performed in CASTEP using an NPT ensemble, maintaining a temperature of 298 K and pressures of either 1 atm or 2.5 GPa. Temperature and pressure control were achieved via a Nosé thermostat and a Parrinello barostat, respectively, with the PBESOL/TS functional/dispersion correction applied throughout. The plane-wave kinetic energy cutoff (E_{cut}) was fixed at 1020 eV, and the integration step was set to 0.5 fs. No symmetry constraints were enforced during the runs. Each simulation spanned 5 ps, with a self-consistent field (SCF) convergence limit of 5×10^{-7} eV/atom. The ab initio molecular dynamics simulations were computationally demanding due to the size of the periodic system and the plane-wave basis set used; typical trajectories required several tens of thousands of

self-consistent field evaluations and were performed on a high-performance computing cluster using parallel MPI execution.

3. Results and Discussion

Before addressing the mechanistic aspects of the pressure-induced transformation, it was necessary to establish a reliable computational framework capable of accurately describing the crystal structures and relative energetics of the α and β polymorphs. In systems such as resorcinol, where both phases share the same space group and differ primarily in the orientation of hydroxyl groups, the energetic differences governing phase stability are subtle and typically fall within a few kcal/mol [6–10]. Under such circumstances, the choice of exchange–correlation functional and dispersion treatment becomes critical [11].

Moreover, the transformation between the α and β forms occurs under moderate pressure, and therefore the selected theoretical approach must not only reproduce the ambient-pressure crystal structures but also provide a physically meaningful description of their response to compression. Since the IPT mechanism investigated in this work involves delicate changes in hydrogen-bond topology and intermolecular packing efficiency, any systematic bias in lattice parameters or cohesive energies could lead to incorrect predictions of phase stability.

For these reasons, the study begins with a systematic benchmark of a broad range of GGA and meta-GGA functionals combined with different dispersion correction schemes. The objective of this analysis was to identify a computational setup that simultaneously reproduces (i) experimental unit-cell metrics at 1 atm, (ii) structural compression trends at elevated pressure, and (iii) the experimentally observed inversion of α/β stability under pressure.

3.1. Benchmark of DFT Functionals at Ambient and Elevated Pressure

The performance of the tested exchange–correlation functionals and dispersion schemes was first assessed through comparison of optimized lattice parameters and unit-cell volumes with experimental data for both polymorphs at 1 atm and 2.5 GPa (Tables 2 and 3)

Table 2. Results of the geometry optimization of resorcinol α polymorph.

Pressure		1 atm				2.5 GPa			
		a [Å]	**b [Å]**	**c [Å]**	**V [Å^3]**	**a [Å]**	**b [Å]**	**c [Å]**	**V [Å^3]**
Experimental α		10.550	9.570	5.669	572.4	9.989	8.606	5.543	476.5
PBE	TS	10.431	9.424	5.607	551.2	10.029	8.839	5.406	479.2
PBE	Grimme	10.393	9.150	5.613	533.8	9.969	8.396	5.508	461.0
PBE	MBD*	10.363	9.325	5.562	537.5	9.978	8.676	5.409	468.3
PBE	n/a	11.039	9.897	5.925	647.3	10.212	9.100	5.507	511.7
RPBE	TS	10.427	9.350	5.637	549.6	9.813	8.153	5.335	426.9
RPBE	n/a	11.634	10.465	6.324	770.0	10.484	9.500	5.584	556.1
PW91	TS	10.484	9.523	5.593	558.4	10.037	8.896	5.401	482.2
PW91	OBS	10.487	9.529	5.589	558.5	10.036	8.895	5.402	482.2
PW91	n/a	11.054	9.914	5.947	651.8	10.208	9.088	5.503	510.5
WC	n/a	10.711	9.646	5.835	602.8	10.049	8.765	5.451	480.1
PBESOL	TS	10.358	9.323	5.497	530.9	9.916	8.565	5.391	457.9
PBESOL	n/a	10.600	9.508	5.741	578.6	10.019	8.711	5.452	475.8
BLYP	TS	10.183	8.879	5.514	498.5	9.799	8.083	5.372	425.5
BLYP	Grimme	10.393	8.970	5.628	524.6	10.032	8.284	5.538	460.3
BLYP	n/a	11.511	10.210	6.245	733.9	10.396	9.307	5.577	539.6
RSCAN	n/a	10.564	9.477	5.743	575.0	10.071	8.600	5.514	477.6

Table 3. Results of the geometry optimization of resorcinol β polymorph.

Pressure		1 atm				2.5 GPa			
		a [Å]	**b [Å]**	**c [Å]**	**V [Å^3]**	**a [Å]**	**b [Å]**	**c [Å]**	**V [Å^3]**
Experimental β		7.927	12.613	5.521	551.9	7.616	12.017	5.238	479.3
PBE	TS	7.748	12.574	5.388	524.9	7.269	12.472	5.168	468.5
PBE	Grimme	7.769	12.495	5.338	518.2	7.117	12.610	5.049	453.1
PBE	MBD*	7.916	12.286	5.380	523.2	7.422	12.374	5.022	461.3
PBE	n/a	8.260	12.171	6.638	667.3	7.625	12.486	5.230	497.9
RPBE	TS	7.959	12.851	5.126	524.4	6.886	12.953	4.827	430.5
RPBE	n/a	8.728	12.401	7.120	770.6	7.906	12.628	5.434	542.5
PW91	TS	7.818	12.537	5.439	533.1	7.356	12.464	5.136	470.9
PW91	OBS	7.823	12.532	5.442	533.5	7.358	12.465	5.136	471.0
PW91	n/a	8.222	12.061	6.832	677.5	7.621	12.475	5.224	496.6
WC	n/a	7.995	11.794	6.833	644.2	7.418	12.372	5.105	468.5
PBESOL	TS	7.731	12.304	5.389	512.6	7.285	12.350	5.008	450.5
PBESOL	n/a	8.063	12.105	6.142	599.5	7.383	12.355	5.102	465.4
BLYP	TS	7.611	12.618	4.972	477.5	7.148	12.621	4.739	427.5
BLYP	Grimme	7.670	12.694	5.185	504.8	7.087	12.721	5.013	452.0
BLYP	n/a	8.440	11.943	7.600	766.1	7.881	12.578	5.266	521.9
RSCAN	n/a	8.010	12.339	5.610	554.4	7.209	12.434	5.192	465.4

At ambient pressure, dispersion-free functionals systematically overestimate the unit-cell volumes of both polymorphs. For the α-form, the experimental volume of 572.4 Å^3 is reproduced reasonably well only when dispersion corrections are included, whereas PBE without dispersion yields 647.3 Å^3 and RPBE and BLYP without dispersion expand the cell even further, reaching values close to 770 Å^3. An analogous trend is observed for the β-form, where the experimental volume of 551.9 Å^3 contrasts sharply with the 770.6 Å^3 predicted by dispersion-free RPBE. These results clearly demonstrate that long-range dispersion interactions are indispensable for an accurate description of the molecular packing in resorcinol, despite the presence of strong hydrogen bonds. The obtained lattice parameters are also consistent with previous periodic DFT studies of resorcinol. In particular, Beran and co-workers [7] reported values of a = 10.45 Å, b = 9.40 Å, and c = 5.65 Å for α-resorcinol using the B86bPBE-XDM method with quasi-harmonic corrections, in excellent agreement with the experiment.

Among the dispersion-corrected approaches, PBE-TS, PW91-TS, PBESOL-TS, and PBE-MBD* provide unit-cell volumes that are moderately underestimated relative to the experiment, typically within several percent. This level of agreement is consistent with the known tendency of GGA-based functionals combined with pairwise dispersion corrections to slightly overbind molecular crystals. The overall structural trends, including the anisotropy of lattice parameters, are nevertheless well reproduced.

Upon compression to 2.5 GPa, the experimentally observed reduction of the α-phase volume from 572.4 to 476.5 Å^3 and of the β-phase from 551.9 to 479.3 Å^3 is qualitatively captured by all dispersion-corrected methods. However, the magnitude of compression varies significantly depending on the functional. For example, RPBE-TS predicts an excessively contracted α-structure at 2.5 GPa with V = 426.9 Å^3, indicating overbinding under pressure, whereas PBE-TS, PW91-TS, and PBESOL-TS yield volumes much closer to the experiment. Dispersion-free approaches remain inconsistent, often combining residual overexpansion with distorted lattice metrics. The relative stability of the polymorphs provides a more stringent benchmark (Table 4).

Table 4. Energy difference between the polymorphs of resorcinol.

		Energy Difference α-β [kcal/mol]	
		1 atm.	**2.5 GPa**
PBE	TS	−0.14	4.80
PBE	Grimme	−3.92	−1.42
PBE	MBD*	−2.90	1.42
PBE	n/a	−2.03	0.21
RPBE	TS	−0.67	−3.15
RPBE	n/a	−0.34	1.23
PW91	TS	−0.51	4.43
PW91	OBS	−0.52	4.43
PW91	n/a	−1.64	−0.14
WC	n/a	−2.61	−2.81
PBESOL	TS	−1.74	0.91
PBESOL	n/a	−4.28	−2.16
BLYP	TS	−0.70	−2.63
BLYP	Grimme	−2.34	0.61
BLYP	n/a	0.96	1.81
RSCAN	n/a	−4.01	0.84

At 1 atm, most dispersion-corrected functionals predict the α-form to be marginally more stable, with energy differences on the order of fractions of a kcal/mol to several kcal/mol. For instance, PBE-TS yields ΔE(α–β) = −0.14 kcal/mol, PW91-TS −0.51 kcal/mol, and PBESOL-TS −1.74 kcal/mol, all consistent with the experimental predominance of α at low pressure [9]. In contrast, certain dispersion-free treatments invert this ordering, as exemplified by BLYP without dispersion, which predicts the β-form to be more stable at ambient conditions.

At 2.5 GPa the energetic landscape changes considerably. Experimentally, β becomes favored above approximately 0.5 GPa [9], and only a subset of functionals reproduce this pressure-induced inversion. PBE-TS predicts a substantial stabilization of β at 2.5 GPa, with ΔE(α–β) = +4.80 kcal/mol, while PW91-TS gives +4.43 kcal/mol and PBESOL-TS +0.91 kcal/mol. Other approaches either exaggerate the stabilization or fail to reproduce the correct trend, reflecting the delicate energetic balance governing this IPT-type transformation.

The broad spread of energy differences, ranging from strongly negative to strongly positive values depending on the functional and pressure, highlights the exceptional sensitivity of this system to the treatment of exchange–correlation and dispersion interactions. Since the α and β polymorphs share the same space group and differ primarily in the orientation of hydroxyl hydrogens, their relative stability is controlled by subtle variations in hydrogen-bond geometry and intermolecular dispersion contacts. Consequently, resorcinol represents a particularly demanding test case for periodic DFT, where energy differences of only a few kcal/mol determine the occurrence of a pressure-induced conformational phase transition. On the basis of the structural agreement and the physically consistent description of the pressure-induced stability inversion, PBE-TS and PBESOL-TS were selected for subsequent phonon calculations, whereas PBESOL-TS, providing a balanced description of both structure and energetics under compression, was employed in the ab initio molecular dynamics simulations.

3.2. Conformational Perturbation Within a Fixed Packing Motif

Having established a reliable computational framework, we next addressed a more fundamental question related to the nature of the α/β transformation. Since both polymorphs share the same space group and differ primarily in the orientation of the hydroxyl

hydrogens, it is tempting to interpret the phase transition as a simple conformational switch within a nearly identical packing arrangement. To test this hypothesis explicitly, a set of constrained starting models was constructed in which the experimental β structure was manually modified by changing the orientation of one hydroxyl hydrogen to enforce the anti–anti conformation characteristic of the α form, while initially preserving the β lattice parameters. These artificially generated structures, denoted α′ (Figure 4), were subsequently fully relaxed without symmetry constraints at 1 atm (Table 5) and 2.5 GPa (Table 6).

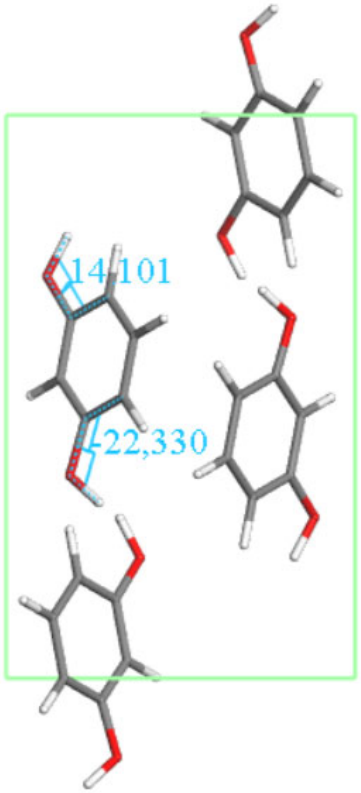

Figure 4. Three-dimensional representation of the α′ configuration obtained by imposing the anti–anti conformation within the β-derived packing framework prior to full relaxation.

This procedure does not correspond to a realistic transformation pathway; rather, it probes whether the α-type molecular conformation can be stabilized within the packing framework of β, or whether the system intrinsically relaxes back to the β topology.

At both pressures, no case was found in which the imposed anti–anti arrangement remained stable after full relaxation. In several instances, the structure reverted to the anti–syn configuration, effectively recovering the β polymorph, as indicated by the "a–s" designation in the final column. In the majority of cases, however, relaxation led to higher-energy stationary points characterized by a loss of molecular planarity, where one of the hydroxyl hydrogens moved out of the aromatic plane. Such geometries are not observed experimentally, as both α and β polymorphs exhibit fully planar molecular conformations.

The energetic penalty associated with these distorted configurations is substantial, typically on the order of 20–30 kcal/mol relative to the stable polymorphs. Even without phonon analysis, this large energy separation strongly suggests that these structures represent unfavorable local minima rather than physically relevant competing phases. Their systematic appearance nevertheless provides important insight: when the anti–anti conformation is forced into the β packing environment, the system is unable to reorganize into a true α-like arrangement. Instead, it either relaxes back to β or escapes toward a geometrically distorted configuration that relieves local strain at the expense of planarity.

Table 5. Results of the geometry optimization (1 atm) of resorcinol α′ form, created based on the experimental β form (RESORA24), preserving its unit-cell dimensions, but with conformation changed to anti–anti.

Functional	Dispersion Correction	a [Å]	b [Å]	c [Å]	V [Å^3]	Eα	Eβ	Eα′	Conf *
	Experimental α	10.550	9.570	5.669	572.4				a-a
	Experimental β	7.927	12.613	5.521	551.9				a-s
PBE	TS	7.742	12.571	5.390	524.6	0.00	0.14	0.12	a-s
PBE	Grimme	7.776	12.506	5.324	517.7	0.00	3.92	3.91	a-s
PBE	MBD*	9.495	13.136	4.186	522.1	0.00	2.90	24.97	x
PBE	n/a	8.259	12.161	6.646	667.5	0.00	2.03	2.04	a-s
RPBE	TS	9.398	13.401	3.733	470.1	0.00	0.67	5.41	x
RPBE	n/a	4.973	12.793	12.070	767.8	0.00	0.34	12.04	x
PW91	TS	7.834	12.556	5.421	533.3	0.00	0.51	0.54	a-s
PW91	OBS	7.830	12.555	5.424	533.3	0.00	0.52	0.52	a-s
PW91	n/a	8.231	12.079	6.774	673.5	0.00	1.64	1.63	a-s
WC	n/a	9.459	12.847	5.512	669.8	0.00	2.61	29.14	x
PBESOL	TS	9.624	13.179	3.938	499.5	0.00	1.74	27.45	x
PBESOL	n/a	9.223	13.010	4.903	588.3	0.00	4.28	30.84	x
BLYP	TS	7.088	13.105	5.114	475.0	0.00	0.70	24.48	x
BLYP	Grimme	7.726	12.681	5.157	505.3	0.00	2.34	2.37	a-s
BLYP	n/a	9.953	11.295	7.372	828.8	0.96	0.00	27.54	x
RSCAN	n/a	8.020	12.312	5.702	563.1	0.00	4.01	4.05	a-s

* Eα, Eβ, Eα′—relative energies of the studied form [kcal/mol]. Conf-conformation: anti–syn (a-s), anti–anti (a-a), with H atom out of plane—x.

Table 6. Results of the geometry optimization (2.5 GPa) of resorcinol α′ form, created based on the experimental β form (RESORA24), preserving its unit-cell dimensions, but with conformation changed to anti–anti.

Functional	Dispersion Correction	a [Å]	b [Å]	c [Å]	V [Å^3]	Eα	Eβ	Eα′	Conf *
	Experimental α	9.989	8.606	5.543	476.5				a-a
	Experimental β	7.616	12.017	5.238	479.3				a-s
PBE	TS	6.834	10.743	6.391	469.2	4.80	0.00	22.80	x
PBE	Grimme	6.280	12.739	5.566	445.2	0.00	1.42	30.76	x
PBE	MBD*	7.062	10.490	6.250	463.0	1.42	0.00	21.38	x
PBE	n/a	9.735	13.238	3.799	489.5	0.21	0.00	21.52	x
RPBE	TS	6.213	13.000	5.168	417.4	0.00	3.15	17.35	x
RPBE	n/a	7.947	12.621	5.411	542.8	1.23	0.00	0.00	a-s
PW91	TS	6.596	12.609	5.637	468.8	4.43	0.00	32.44	x
PW91	OBS	6.585	12.603	5.650	468.9	4.43	0.00	32.44	x
PW91	n/a	9.705	13.233	3.796	487.5	0.00	0.14	22.42	x
WC	n/a	9.458	13.134	3.648	453.1	0.00	2.81	26.51	x
PBESOL	TS	6.452	12.655	5.423	442.7	0.91	0.00	34.76	x
PBESOL	n/a	7.064	12.696	5.212	467.4	0.00	2.16	37.81	x
BLYP	TS	6.193	13.025	5.194	418.9	0.00	2.63	22.62	x
BLYP	Grimme	6.241	12.826	5.539	443.3	0.61	0.00	27.95	x
BLYP	n/a	7.893	12.569	5.260	521.8	1.82	0.01	0.00	a-s
RSCAN	n/a	9.713	12.996	3.591	453.3	0.84	0.00	16.72	x

* Eα, Eβ, Eα′—relative energies of the studied form [kcal/mol]. Conf-conformation: anti–syn (a-s), anti–anti (a-a), with H atom out of plane—x.

The same qualitative behavior persists under compression at 2.5 GPa. The imposed anti–anti geometry does not become stabilized by pressure within the β framework, despite the experimentally observed pressure-induced stabilization of β relative to α. This observation indicates that the phase transition cannot be interpreted as a simple local proton

reorientation within a rigid lattice. Rather, the molecular conformation and intermolecular packing are strongly coupled degrees of freedom.

For completeness, the reverse procedure, namely attempting to generate β-like structures from the α framework by selectively rotating one hydroxyl hydrogen, was also examined (Tables S1–S4, Supporting Information). In this case two distinct hydrogen choices are possible, leading to additional metastable solutions, yet the overall conclusion remains unchanged: neither polymorph can be obtained from the other by a purely local conformational perturbation without cooperative rearrangement of the crystal packing.

Taken together, these results demonstrate that the α/β transformation in resorcinol is not governed by an isolated intramolecular rotation but represents a collective reorganization of hydrogen-bond topology and dispersion-stabilized packing contacts. The failure to stabilize α′ within the β lattice provides direct computational evidence that the IPT involves a cooperative lattice response rather than a trivial conformational flip.

3.3. Phonon-Derived Thermodynamics of the α to β Transformation

To move beyond static lattice energies and directly address the thermodynamic driving force of the α to β transformation, phonon calculations were performed and vibrational contributions were incorporated within the quasi-harmonic approximation. Figure 5 presents the temperature dependence of the enthalpy difference ΔH, entropy contribution TΔS, and Gibbs free energy difference ΔG between the two polymorphs at 1 atm and 2.5 GPa, obtained using PBE/TS and PBESOL/TS.

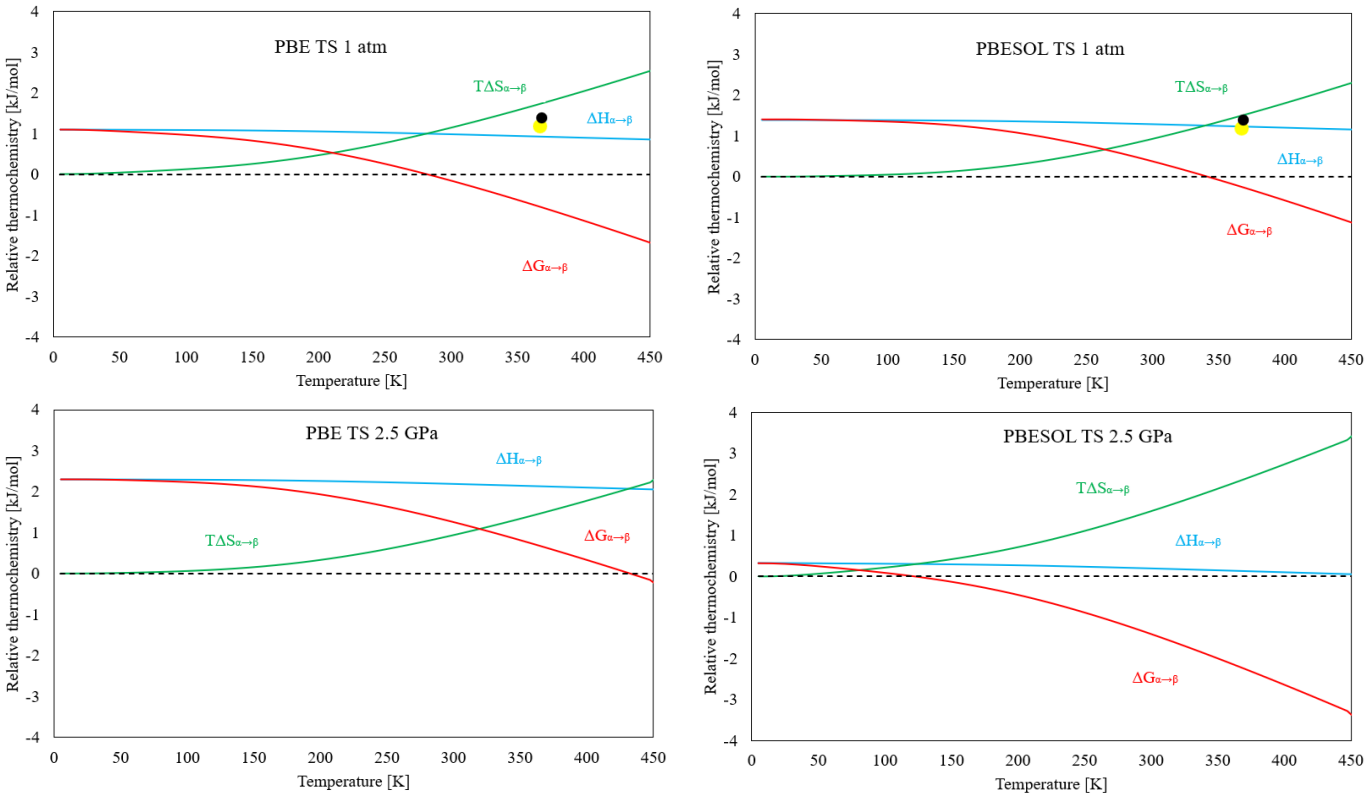

Figure 5. Relative enthalpy, entropy (−TΔS), and Gibbs free energy differences for the α to β phase change (in kJ/mol) using PBE/TS and PBESOL/TS approaches, at 1 atm and 2.5 GPa. The yellow [33] and black [34] points represent the literature data on the enthalpy of this transition.

At 1 atm, the calculated enthalpy differences can be directly compared with experimental calorimetric ΔH values (black and yellow markers in Figure 5). The PBESOL/TS results are clearly closer to the experiment, both in magnitude and in overall temperature trend,

whereas PBE/TS systematically overestimates the enthalpic offset between α and β. This behavior is consistent with the structural benchmark discussed earlier: since PBESOL/TS provides a more balanced description of lattice parameters and cohesive energies, the derived phonon spectra and vibrational thermodynamics are likewise more reliable. In systems such as resorcinol, where the polymorphs differ mainly in hydrogen-bond topology and subtle packing effects, small structural inaccuracies directly translate into significant errors in vibrational free energy.

The temperature evolution of ΔG at 1 atm shows the expected competition between a positive enthalpy term and an increasing entropy contribution. As temperature rises, the TΔS term progressively compensates the enthalpic penalty, leading to a crossing point where ΔG = 0. PBESOL/TS predicts this balance at a temperature closer to the experimental transition region, whereas PBE/TS shifts the crossing to a higher temperature. This indicates that PBESOL/TS captures the relative vibrational entropy of the two polymorphs more accurately, particularly the contribution of low-frequency lattice modes that are highly sensitive to intermolecular interactions.

The difference between the two functionals becomes even more pronounced at 2.5 GPa. Under compression, PBESOL/TS predicts that the β form becomes thermodynamically favored already at a low temperature, with the ΔG crossing occurring around 125 K. This implies that at room temperature the β polymorph is clearly stabilized, in agreement with experimental observations that pressure favors β over α. In contrast, PBE/TS delays the ΔG crossing to approximately 425 K, which would imply persistence of α stability far above ambient temperatures. Such behavior is inconsistent with the known pressure-induced stabilization of β and suggests that PBE/TS overestimates the enthalpic stability of α or underestimates the entropy gain associated with β under compression.

The enthalpy curves at 2.5 GPa further illustrate this difference. PBESOL/TS yields a relatively small positive ΔH that can be readily compensated by vibrational entropy, whereas PBE/TS maintains a larger enthalpic separation across the temperature range. Since the α and β polymorphs are isosymmetric and differ primarily in hydroxyl orientation, the transformation is governed by subtle changes in hydrogen-bond geometry and collective lattice modes. The improved performance of PBESOL/TS therefore likely reflects its more accurate description of intermolecular forces and pressure-dependent lattice stiffness, which directly influence low-frequency phonon modes and hence vibrational entropy.

Overall, Figure 5 demonstrates that the α to β transformation in resorcinol is not driven purely by electronic energy differences but results from a delicate balance between enthalpy and vibrational entropy that is strongly pressure-dependent. Among the tested approaches, PBESOL/TS provides the most consistent agreement with experimental enthalpy data at 1 atm and correctly reproduces the pressure-induced stabilization of β at 2.5 GPa. This validates its selection as the reference method for subsequent dynamical simulations.

3.4. Ab Initio Molecular Dynamics Under Ambient and High Pressure

To complement the static and phonon-based thermodynamic analysis, Born–Oppenheimer ab initio molecular dynamics simulations were performed at 298 K under 1 atm and 2.5 GPa using the PBESOL/TS functional. The time evolution of the unit-cell parameters during the 5 ps simulations is shown in Figure 6, where the dashed horizontal lines indicate experimental lattice constants.

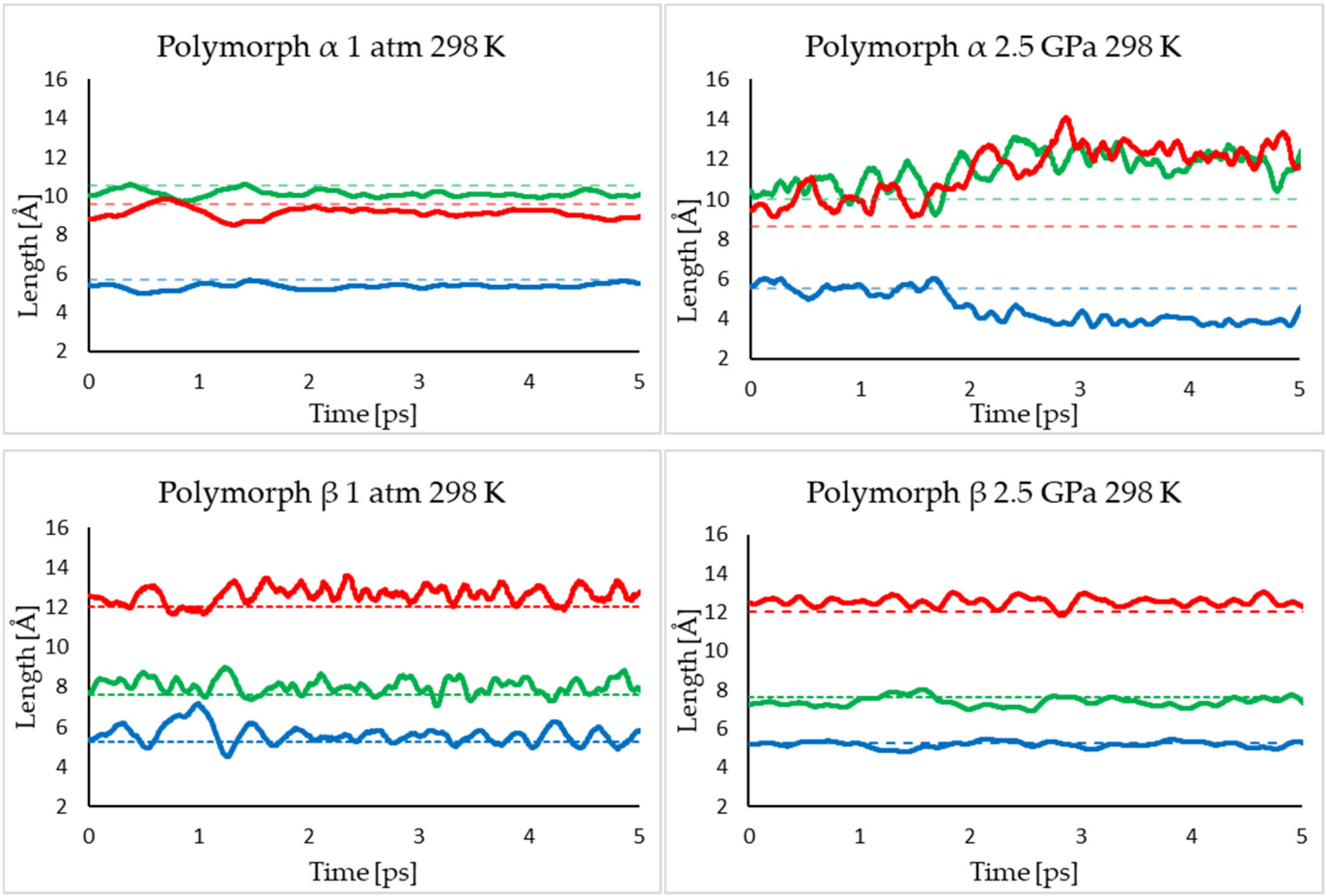

Figure 6. Evolution of the unit-cell parameters during the aiMD simulations at 1 atm (**left**) and 2.5 GPa (**right**) of α (**top**) and β (**bottom**) resorcinol at 298 K. Green: a length; red: b length; blue: c length. Horizontal dashed lines represent the experimental values.

At 1 atm, the α polymorph remains structurally stable throughout the entire simulation. The lattice parameters fluctuate around their experimental values with only minor thermal oscillations, and no systematic drift is observed. This behavior is fully consistent with the thermodynamic analysis, which identified α as the stable form at an ambient pressure. The absence of any progressive distortion or cell deformation confirms that the optimized structure corresponds to a genuine minimum on the free-energy surface with these conditions.

The β polymorph at 1 atm also remains dynamically stable during the simulation, although noticeably larger fluctuations are present, particularly in the b lattice parameter. These enhanced oscillations are consistent with the fact that β is thermodynamically less favored at an ambient pressure. Nevertheless, no structural collapse, symmetry breaking, or systematic cell distortion occurs, indicating that β corresponds to a metastable but well-defined local minimum under these conditions.

The situation changes markedly for the α polymorph at 2.5 GPa. After approximately 2 ps of simulation time, a clear deviation of the lattice parameters from their initial equilibrium values becomes apparent. The cell begins to distort, and the parameters progressively depart from the experimental reference lines. This behavior indicates a loss of mechanical stability under compression and is consistent with experimental observations that α is not the favored phase at an elevated pressure. In contrast to the moderate oscillations observed for β at 1 atm, the deviations for α at 2.5 GPa are systematic rather than purely thermal,

suggesting that the structure is evolving toward a different region of configuration space rather than simply sampling around a stable minimum.

By comparison, the β polymorph at 2.5 GPa remains dynamically stable. The lattice parameters fluctuate narrowly around the experimental high-pressure values, with no evidence of long-term drift or structural destabilization. The close correspondence between simulated and experimental cell metrics confirms that β represents the thermodynamically and mechanically preferred structure at this pressure.

Taken together, the aiMD simulations provide dynamic confirmation of the conclusions drawn from static and phonon-based analyses. While static energy differences and Gibbs free energy curves predict the pressure-induced stabilization of β, the molecular dynamics simulations demonstrate that α loses structural stability under compression at room temperature, whereas β remains robust. The fact that the instability of α at 2.5 GPa emerges spontaneously during the simulation, without any imposed perturbation, strongly supports the interpretation that the α to β transformation involves cooperative lattice rearrangement rather than a purely local conformational change.

The present study should therefore be regarded as a first step toward a more detailed mechanistic understanding of the α–β transition in crystalline resorcinol, providing a computational framework that may facilitate future investigations of the transformation pathway and cooperative hydrogen-bond rearrangements.

4. Conclusions

In this study, the isosymmetric α/β phase transition of resorcinol was systematically investigated using periodic density functional theory calculations combined with phonon-based thermodynamic analysis and ab initio molecular dynamics simulations. The results demonstrate that this system constitutes a stringent benchmark for computational modeling due to the small energy differences and subtle structural variations governing its polymorphic behavior. Benchmarking across a wide range of exchange–correlation functionals confirmed that dispersion interactions are indispensable for accurately reproducing experimental lattice parameters and relative stability. Among the tested approaches, PBESOL combined with Tkatchenko–Scheffler dispersion provided the most balanced description of structural metrics and pressure-induced stability inversion, and proved essential for reliable thermodynamic predictions. Artificial conformational perturbation tests showed that the α and β polymorphs cannot be interconverted by a simple local hydroxyl rotation within a fixed packing framework. Instead, the transformation requires cooperative rearrangement of hydrogen-bond topology and intermolecular contacts, underscoring the collective nature of this isosymmetric transition. Phonon-derived Gibbs free energy calculations revealed that the α to β transition is governed by a delicate enthalpy–entropy balance that is strongly pressure-dependent. Ab initio molecular dynamics simulations further confirmed the dynamical instability of the α phase under compression, while the β phase remains structurally robust at 2.5 GPa. Overall, resorcinol emerges as a demanding yet informative model system for evaluating the reliability of periodic DFT in describing hydrogen-bond-driven isosymmetric phase transitions in molecular crystals.

Supplementary Materials: The following supporting information can be downloaded at: https://www.mdpi.com/article/10.3390/cryst16030215/s1, Table S1: Results of the geometry optimization (1 atm) of resorcinol β′ form, created based on the experimental α form (RESORA19), preserving its unit-cell dimensions, but with conformation changed to anti–syn by moving the initial position of H2; Table S2: Results of the geometry optimization (1 atm) of resorcinol β′ form, created based on the experimental α form (RESORA19), preserving its unit-cell dimensions, but with conformation changed to anti–syn by moving the initial position of H2; Table S3: Results of the geometry optimization (1 atm) of resorcinol β″ form, created based on the experimental α form (RESORA19), preserving

its unit-cell dimensions, but with conformation changed to anti–syn by moving the initial position of H1; Table S4: Results of the geometry optimization (2.5 GPa) of resorcinol β″ form, created based on the experimental α form (RESORA19), preserving its unit-cell dimensions, but with conformation changed to anti–syn by moving the initial position of H1.

Author Contributions: Conceptualization, Ł.S., M.F.-R. and A.M.M.; methodology, Ł.S.; software, Ł.S.; validation, Ł.S.; formal analysis, Ł.S. and A.M.M.; investigation, Ł.S. and A.M.M.; resources, Ł.S.; data curation, Ł.S. and A.M.M.; writing—original draft preparation, Ł.S. and A.M.M.; writing—review and editing, Ł.S., M.F.-R. and A.M.M.; visualization, Ł.S. and A.M.M.; supervision, Ł.S. and M.F.-R.; project administration, Ł.S.; funding acquisition, Ł.S. All authors have read and agreed to the published version of the manuscript.

Funding: This research received no external funding.

Data Availability Statement: The raw data supporting the conclusions of this article will be made available by the authors on request.

Conflicts of Interest: The authors declare no conflicts of interest.

References

1. Yan, T.; Xi, D.; Fang, Q.; Zhang, Y.; Wang, J.; Wang, X. High-Pressure Polymorphism in Hydrogen-Bonded Crystals: A Concise Review. *Crystals* **2022**, *12*, 739. [CrossRef]
2. Tao, Y.; Gao, Y.; Zhang, B.; Hu, K.; Xie, Y.; Zhang, L.; Yang, S.; Lu, Y. Advances in Quantitative Analytical Methods for Solid Drugs. *Crystals* **2025**, *15*, 38. [CrossRef]
3. Mazurek, A.M.; Franczak-Rogowska, M.; Szeleszczuk, Ł. Isosymmetric Phase Transitions in Crystals: From Subtle Rearrangements to Functional Properties. *Crystals* **2025**, *15*, 807. [CrossRef]
4. Szeleszczuk, Ł.; Mazurek, A.H.; Milcarz, K.; Napiórkowska, E.; Pisklak, D.M. Can We Predict the Isosymmetric Phase Transition? Application of DFT Calculations to Study the Pressure Induced Transformation of Chlorothiazide. *Int. J. Mol. Sci.* **2021**, *22*, 10100. [CrossRef]
5. Mazurek, A.M.; Franczak-Rogowska, M.; Szeleszczuk, Ł. Predicting the Pressure-Induced Isosymmetric Phase Transition of Sulfamic Acid by Applying Periodic Density Functional Theory Calculations. *Appl. Sci.* **2025**, *15*, 4185. [CrossRef]
6. Druzbicki, K.; Mikuli, E.; Pałka, N.; Zalewski, S.; Ossowska-Chruściel, M.D. Polymorphism of Resorcinol Explored by Complementary Vibrational Spectroscopy (FT-RS, THz-TDS, INS) and First-Principles Solid-State Computations (Plane-Wave DFT). *J. Phys. Chem. B* **2015**, *119*, 1681–1695. [CrossRef] [PubMed]
7. Cook, C.; McKinley, J.L.; Beran, G.J.O. Modeling the α- and β-Resorcinol Phase Boundary via Combination of Density Functional Theory and Density Functional Tight Binding. *J. Chem. Phys.* **2021**, *154*, 134109. [CrossRef]
8. Kichanov, S.E.; Kozlenko, D.P.; Bilski, P.; Wąsicki, J.; Nawrocik, W.; Medek, A.; Hancock, B.C.; Lukin, E.V.; Lathe, C.; Dubrovinsky, L.S.; et al. The Polymorphic Phase Transformations in Resorcinol at High Pressure. *J. Mol. Struct.* **2011**, *1006*, 337–343. [CrossRef]
9. Safari, F.; Olejniczak, A.; Katrusiak, A. Pressure-Dependent Crystallization Preference of Resorcinol Polymorphs. *Cryst. Growth Des.* **2019**, *19*, 5629–5635. [CrossRef]
10. Safari, F.; Katrusiak, A. High-Pressure Polymorphs Nucleated and Stabilized by Rational Doping under Ambient Conditions. *J. Phys. Chem. C* **2021**, *125*, 23501–23509. [CrossRef]
11. Mazurek, A.H.; Szeleszczuk, Ł.; Pisklak, D.M. Periodic DFT Calculations—Review of Applications in the Pharmaceutical Sciences. *Pharmaceutics* **2020**, *12*, 415. [CrossRef] [PubMed]
12. Arkhipin, A.S.; Pisch, A.; Uspenskaya, I.A.; Jakse, N. A Molecular Dynamics Simulation Study of Crystalline and Liquid MgO. *Ceramics* **2024**, *7*, 1187–1203. [CrossRef]
13. Ludt, C.; Meyer, D.C.; Zschornak, M. Ferroelectric Phase Transition in Barium Titanate Revisited with Ab Initio Molecular Dynamics. *Materials* **2024**, *17*, 1023. [CrossRef]
14. Gal, J. ab Initio DFT and MD Simulations Serving as an Anchor for Correcting Melting Curves Reported by DAC and SW Experiments—Some Transition Metals as Illustrative Examples. *Crystals* **2023**, *13*, 1263. [CrossRef]
15. Tachikawa, H. Molecular Design of H2 Storage/Release Devices: A Direct Ab Initio MD Study. *Nanomaterials* **2025**, *15*, 1498. [CrossRef]
16. Kalchevski, D.A.; Trifonov, D.V.; Kolev, S.K.; Aleksandrov, H.A.; Dimov, D.A.; Popov, V.N.; Milenov, T.I. Ab Initio MD Study of the Mechanism of Carbonization of Si(001) Surfaces with Methane at High Temperatures. *Coatings* **2025**, *15*, 427. [CrossRef]
17. Clark, S.J.; Segall, M.D.; Pickard, C.J.; Hasnip, P.J.; Probert, M.J.; Refson, K.; Payne, M.C. First principles methods using CASTEP. *Z. Krist. Cryst. Mater.* **2005**, *220*, 567–570. [CrossRef]

18. Perdew, J.P.; Burke, K.; Ernzerhof, M. Generalized Gradient Approximation Made Simple. *Phys. Rev. Lett.* **1996**, *77*, 3865–3868. [CrossRef]
19. Tkatchenko, A.; Scheffler, M. Accurate Molecular Van Der Waals Interactions from Ground-State Electron Density and Free-Atom Reference Data. *Phys. Rev. Lett.* **2009**, *102*, 073005. [CrossRef]
20. Grimme, S. Semiempirical GGA-type density functional constructed with a long-range dispersion correction. *J. Comput. Chem.* **2006**, *27*, 1787–1799. [CrossRef] [PubMed]
21. Ambrosetti, A.; Reilly, A.M.; DiStasio, R.A., Jr.; Tkatchenko, A. Long-range correlation energy calculated from coupled atomic response functions. *J. Chem. Phys.* **2014**, *140*, 18A508. [CrossRef]
22. Hammer, B.; Hansen, L.B.; Nørskov, J.K. Improved adsorption energetics within density-functional theory using revised Perdew–Burke–Ernzerhof functionals. *Phys. Rev. B* **1999**, *59*, 7413–7421. [CrossRef]
23. Perdew, J.P.; Wang, Y. Accurate and simple analytic representation of the electron-gas correlation energy. *Phys. Rev. B* **1992**, *45*, 13244–13249. [CrossRef]
24. Perdew, J.P.; Chevary, J.A.; Vosko, S.H.; Jackson, K.A.; Pederson, M.R.; Singh, D.J.; Fiolhais, C. Atoms, molecules, solids, and surfaces: Applications of the generalized gradient approximation for exchange and correlation. *Phys. Rev. B* **1992**, *46*, 6671–6687. [CrossRef] [PubMed]
25. Ortmann, F.; Bechstedt, F.; Schmidt, W.G. Semiempirical van der Waals correction to the density functional description of solids and molecular structures. *Phys. Rev. B* **2006**, *73*, 205101. [CrossRef]
26. Wu, Z.; Cohen, R.E. More accurate generalized gradient approximation for solids. *Phys. Rev. B* **2006**, *73*, 235116. [CrossRef]
27. Perdew, J.P.; Ruzsinszky, A.; Csonka, G.I.; Vydrov, O.A.; Scuseria, G.E.; Constantin, L.A.; Zhou, X.; Burke, K. Restoring the Density-Gradient Expansion for Exchange in Solids and Surfaces. *Phys. Rev. Lett.* **2008**, *100*, 136406. [CrossRef]
28. Becke, A.D. Density-functional exchange-energy approximation with correct asymptotic behavior. *Phys. Rev. A* **1988**, *38*, 3098–3100. [CrossRef]
29. Lee, C.; Yang, W.; Parr, R.G. Development of the Colle-Salvetti correlation-energy formula into a functional of the electron density. *Phys. Rev. B* **1988**, *37*, 785–789. [CrossRef] [PubMed]
30. Bartók, A.P.; Yates, J.R. Regularized SCAN functional. *J. Chem. Phys.* **2019**, *150*, 161101. [CrossRef] [PubMed]
31. Baroni, S.; de Gironcoli, S.; Dal Corso, A.; Giannozzi, P. Phonons and related crystal properties from density-functional perturbation theory. *Rev. Mod. Phys.* **2001**, *73*, 515–532. [CrossRef]
32. Arias, T.A.; Payne, M.C.; Joannopoulos, J.D. Ab initio molecular dynamics: Analytically continued energy functionals and insights into iterative solutions. *Phys. Rev. Lett.* **1992**, *69*, 1077–1080. [CrossRef] [PubMed]
33. Bret-Dibat, P.; Lichanot, A. Propriétés Thermodynamiques des Isomères de Position de Benzènes Disubstitués en Phase Condensée. *Thermochim. Acta* **1989**, *147*, 261–271. [CrossRef]
34. Ebisuzaki, Y.; Askari, L.H.; Bryan, A.M.; Nicol, M.F. Phase Transitions in Resorcinol. *J. Chem. Phys.* **1987**, *87*, 6659–6664. [CrossRef]

Disclaimer/Publisher's Note: The statements, opinions and data contained in all publications are solely those of the individual author(s) and contributor(s) and not of MDPI and/or the editor(s). MDPI and/or the editor(s) disclaim responsibility for any injury to people or property resulting from any ideas, methods, instructions or products referred to in the content.

Supporting Information

Periodic DFT Investigation of the Isosymmetric Alpha–Beta Phase Transition in Resorcinol Under Ambient and High Pressure

Anna Maria Mazurek [1], Monika Franczak-Rogowska [2] and Łukasz Szeleszczuk [1,*]

[1] Department of Organic and Physical Chemistry, Medical University of Warsaw, 1 Banacha Str., 02-097 Warsaw, Poland; anna.mazurek1@wum.edu.pl
[2] Department of Drug Chemistry, Pharmaceutical and Biomedical Analysis, Medical University of Warsaw, 1 Banacha Str., 02-097 Warsaw, Poland; monika.franczak-rogowska@wum.edu.pl
* Correspondence: lukasz.szeleszczuk@wum.edu.pl; Tel.: +48-501-255-121

Table S1. Results of the geometry optimization (1 atm) of resorcinol β′ form, created based on the experimental α form (RESORA19), preserving its unit cell dimensions, but with conformation changed to anti-syn by moving the initial position of H2.

Functional	Dispression correction	a [Å]	b [Å]	c [Å]	V [Å^3]	Eα	Eβ	Eβ′	Conf*
Experimental α		10.550	9.570	5.669	572.4				a-a
Experimental β		7.927	12.613	5.521	551.9				a-s
PBE	TS	9.813	10.708	5.046	530.2	0.00	0.14	30.93	x
PBE	Grimme	11.426	8.310	5.647	536.2	0.00	3.92	34.39	x
PBE	MBD*	10.707	9.924	4.977	528.8	0.00	2.90	33.80	x
PBE	n/a	12.174	9.502	5.953	688.7	0.00	2.03	30.49	x
RPBE	TS	9.109	10.869	5.317	526.4	0.00	0.67	20.97	x
RPBE	n/a	.	.	.	.	0.00	0.34	.	y
PW91	TS	10.437	10.379	5.044	546.3	0.00	0.51	32.76	x
PW91	OBS	10.205	10.505	5.068	543.2	0.00	0.52	32.58	x
PW91	n/a	13.689	6.700	9.428	864.7	0.00	1.64	28.95	x
WC	n/a	.	.	.	.	0.00	2.61	.	y
PBESOL	TS	11.295	8.511	5.584	536.8	0.00	1.74	41.63	x
PBESOL	n/a	10.944	10.041	5.223	573.9	0.00	4.28	41.04	x
BLYP	TS	9.987	10.018	4.712	471.4	0.00	0.70	22.07	x
BLYP	Grimme	11.332	8.241	5.607	523.6	0.00	2.34	32.02	x
BLYP	n/a	.	.	.	.	0.96	0.00	.	y
RSCAN	n/a	11.886	8.717	5.694	590.0	0.00	4.01	32.89	x

Eα, Eβ, Eβ′ – relative energies of the studied form [kcal/mol]. Conf-conformation: anti-syn (a-s), syn-syn (s-s), with H atom out of plane – x; y – optimization didn't converge.

Table S2. Results of the geometry optimization (1 atm) of resorcinol β′ form, created based on the experimental α form (RESORA19), preserving its unit cell dimensions, but with conformation changed to anti-syn by moving the initial position of H2.

Functional	Dispression correction	a [Å]	b [Å]	c [Å]	V [Å^3]	Eα	Eβ	Eβ′	Conf*
	Experimental α	9.989	8.606	5.543	476.5				a-a
	Experimental β	7.616	12.017	5.238	479.3				a-s
PBE	TS	10.586	8.274	5.422	474.9	4.80	0.00	37.85	x
PBE	Grimme	10.634	7.917	5.450	458.8	0.00	1.42	33.96	x
PBE	MBD*	10.719	8.154	5.320	465.0	1.42	0.00	37.23	x
PBE	n/a	11.104	8.373	5.515	512.7	0.21	0.00	35.78	x
RPBE	TS	10.621	7.801	5.104	422.9	0.00	3.15	21.84	x
RPBE	n/a	10.270	10.494	5.113	551.1	1.23	0.00	27.18	x
PW91	TS	10.615	8.317	5.412	477.8	4.43	0.00	38.61	x
PW91	OBS	10.617	8.318	5.411	477.9	4.43	0.00	38.60	x
PW91	n/a	11.098	8.344	5.524	511.5	0.00	0.14	36.74	x
WC	n/a	10.847	8.026	5.476	476.8	0.00	2.81	43.55	x
PBESOL	TS	10.663	8.068	5.304	456.3	0.91	0.00	42.32	x
PBESOL	n/a	10.794	8.025	5.459	472.9	0.00	2.16	43.32	x
BLYP	TS	10.591	7.870	5.105	425.5	0.00	2.63	27.30	x
BLYP	Grimme	10.568	7.923	5.457	456.9	0.61	0.00	31.92	x
BLYP	n/a	10.125	10.352	5.025	526.7	1.82	0.01	30.59	a-s
RSCAN	n/a	10.704	8.099	5.492	476.1	0.84	0.00	34.23	x

Eα, Eβ, Eβ′ – relative energies of the studied form [kcal/mol]. Conf-conformation: anti-syn (a-s), syn-syn (s-s), with H atom out of plane – x.

Table S3. Results of the geometry optimization (1 atm) of resorcinol β'' form, created based on the experimental α form (RESORA19), preserving its unit cell dimensions, but with conformation changed to anti-syn by moving the initial position of H1.

Functional	Dispression correction	a [Å]	b [Å]	c [Å]	V [Å^3]	Eα	Eβ	Eβ''	Conf*
Experimental α		10.550	9.570	5.669	572.4				a-a
Experimental β		7.927	12.613	5.521	551.9				a-s
PBE	TS	9.477	11.558	5.219	571.6	0.00	0.14	30.74	x
PBE	Grimme	9.560	11.151	5.200	554.3	0.00	3.92	30.81	x
PBE	MBD*	9.192	11.767	5.112	552.9	0.00	2.90	31.95	x
PBE	n/a	9.934	13.240	5.735	754.3	0.00	2.03	27.73	x
RPBE	TS	9.065	10.793	5.301	518.7	0.00	0.67	20.42	x
RPBE	n/a	.	.	.	.	0.00	0.34	.	y
PW91	TS	9.579	11.705	5.175	580.3	0.00	0.51	31.67	x
PW91	OBS	9.581	11.715	5.172	580.5	0.00	0.52	31.66	x
PW91	n/a	8.248	12.062	6.817	678.2	0.00	1.64	1.66	a-s
WC	n/a	.	.	.	.	0.00	2.61	.	y
PBESOL	TS	9.357	11.634	5.005	544.8	0.00	1.74	37.99	x
PBESOL	n/a	10.051	11.821	5.123	608.6	0.00	4.28	34.38	x
BLYP	TS	8.914	10.726	5.241	501.1	0.00	0.70	24.87	x
BLYP	Grimme	9.137	11.233	5.288	542.8	0.00	2.34	29.69	x
BLYP	n/a	.	.	.	.	0.96	0.00	.	y
RSCAN	n/a	10.060	11.041	5.357	595.1	0.00	4.01	27.04	x

Eα, Eβ, Eβ'' – relative energies of the studied form [kcal/mol]. Conf-conformation: anti-syn (a-s), syn-syn (s-s), with H atom out of plane – x; y – optimization didn't converge.

Table S4. Results of the geometry optimization (2.5 GPa) of resorcinol β'' form, created based on the experimental α form (RESORA19), preserving its unit cell dimensions, but with conformation changed to anti-syn by moving the initial position of H1.

Functional	Dispression correction	a [Å]	b [Å]	c [Å]	V [Å^3]	Eα	Eβ	Eβ''	Conf*
	Experimental α	9.989	8.606	5.543	476.5				a-a
	Experimental β	7.616	12.017	5.238	479.3				a-s
PBE	TS	8.860	10.848	5.134	493.5	4.80	0.00	43.38	x
PBE	Grimme	8.591	10.520	5.271	476.3	0.00	1.42	38.89	x
PBE	MBD*	8.742	10.939	5.040	482.0	1.42	0.00	40.15	x
PBE	n/a	9.093	11.094	5.159	520.4	0.21	0.00	34.35	x
RPBE	TS	8.377	10.234	5.116	438.6	0.00	3.15	26.06	x
RPBE	n/a	9.284	11.399	5.371	568.4	1.23	0.00	29.94	x
PW91	TS	8.902	10.997	5.058	495.1	4.43	0.00	43.46	x
PW91	OBS	8.894	11.007	5.058	495.2	4.43	0.00	43.47	x
PW91	n/a	9.117	11.135	5.116	519.4	0.00	0.14	34.84	x
WC	n/a	8.933	10.959	4.996	489.0	0.00	2.81	40.43	x
PBESOL	TS	8.716	10.397	5.148	466.5	0.91	0.00	45.06	x
PBESOL	n/a	8.930	10.871	5.007	486.1	0.00	2.16	41.01	x
BLYP	TS	8.326	10.218	5.199	442.3	0.00	2.63	33.45	x
BLYP	Grimme	10.044	8.276	5.533	459.9	0.61	0.00	0.59	a-a
BLYP	n/a	9.323	11.299	5.199	547.6	1.82	0.01	33.47	x
RSCAN	n/a	8.822	10.653	5.212	489.8	0.84	0.00	33.87	x

Eα, Eβ, Eβ'' – relative energies of the studied form [kcal/mol]. Conf-conformation: anti-syn (a-s), syn-syn (s-s), with H atom out of plane – x.

Publication co-author statement

As a co-author of the publication entitled:

"Periodic DFT Investigation of Isosymmetric Alpha–Beta Phase Transition in Resorcinol Under Ambient and High Pressure", *published in Crystals (2026, Volume 16, Issue 3, Article 215),* https://doi.org/10.3390/cryst16030215
Authors: Anna Maria Mazurek, Monika Franczak-Rogowska and Łukasz Szeleszczuk

I agree to include this publication into a collection of thematically related publications forming a doctoral dissertation prepared by mgr farm. Anna Maria Mazurek.

Additionally, I declare my contribution to the publication as follows: conceptualisation, Ł.S., M.F.-R. and A.M.M.; methodology, Ł.S.; software, Ł.S.; validation, Ł.S.; formal analysis, Ł.S. and A.M.M.; investigation, Ł.S. and A.M.M.; resources, Ł.S.; data curation, Ł.S. and A.M.M.; writing - original draft preparation, Ł.S. and A.M.M.; writing - review and editing, Ł.S., M.F.-R. and A.M.M.; visualisation, Ł.S. and A.M.M.; supervision, Ł.S. and M.F.-R.; project administration, Ł.S.; funding acquisition, Ł.S.

Oświadczenie współautora publikacji

Jako współautor publikacji pt.:

"Periodic DFT Investigation of Isosymmetric Alpha–Beta Phase Transition in Resorcinol Under Ambient and High Pressure", *opublikowanej w czasopiśmie Crystals (2026, tom 16, numer 3, artykuł 215),* https://doi.org/10.3390/cryst16030215
Autorzy: Anna Maria Mazurek, Monika Franczak-Rogowska and Łukasz Szeleszczuk

Wyrażam zgodę na włączenie tej publikacji do zbioru powiązanych tematycznie artykułów naukowych, stanowiących część pracy doktorskiej przygotowanej przez mgr farm. Annę Marię Mazurek.

Jednocześnie potwierdzam, że następujący zakres stanowi mój wkład w publikację: koncepcja, Ł.S., M.F.-R. oraz A.M.M.; metodologia, Ł.S.; oprogramowanie, Ł.S.; walidacja, Ł.S.; analiza formalna, Ł.S. oraz A.M.M.; badania, Ł.S. oraz A.M.M.; zasoby, Ł.S.; opracowanie danych, Ł.S. oraz A.M.M.; pisanie – przygotowanie pierwotnej wersji manuskryptu, Ł.S. oraz A.M.M.; pisanie - redakcja i korekta manuskryptu, Ł.S., M.F.-R. oraz A.M.M.; wizualizacja, Ł.S. oraz A.M.M.; nadzór, Ł.S. oraz M.F.-R.; zarządzanie projektem, Ł.S.; pozyskiwanie finansowania, Ł.S.

28.04.2026
Date / Data

Anna Mazurek
Legible signature / Czytelny podpis

Publication co-author statement

As a co-author of the publication entitled:

"Periodic DFT Investigation of Isosymmetric Alpha–Beta Phase Transition in Resorcinol Under Ambient and High Pressure", *published in Crystals (2026, Volume 16, Issue 3, Article 215),* https://doi.org/10.3390/cryst16030215
Authors: Anna Maria Mazurek, Monika Franczak-Rogowska and Łukasz Szeleszczuk

I agree to include this publication into a collection of thematically related publications forming a doctoral dissertation prepared by mgr farm. Anna Maria Mazurek.

Additionally, I declare my contribution to the publication as follows: conceptualisation, Ł.S., M.F.-R. and A.M.M.; methodology, Ł.S.; software, Ł.S.; validation, Ł.S.; formal analysis, Ł.S. and A.M.M.; investigation, Ł.S. and A.M.M.; resources, Ł.S.; data curation, Ł.S. and A.M.M.; writing - original draft preparation, Ł.S. and A.M.M.; writing - review and editing, Ł.S., M.F.-R. and A.M.M.; visualisation, Ł.S. and A.M.M.; supervision, Ł.S. and M.F.-R.; project administration, Ł.S.; funding acquisition, Ł.S.

Oświadczenie współautora publikacji

Jako współautor publikacji pt.:

"Periodic DFT Investigation of Isosymmetric Alpha–Beta Phase Transition in Resorcinol Under Ambient and High Pressure", *opublikowanej w czasopiśmie Crystals (2026, tom 16, numer 3, artykuł 215),* https://doi.org/10.3390/cryst16030215
Autorzy: Anna Maria Mazurek, Monika Franczak-Rogowska and Łukasz Szeleszczuk

Wyrażam zgodę na włączenie tej publikacji do zbioru powiązanych tematycznie artykułów naukowych, stanowiących część pracy doktorskiej przygotowanej przez mgr farm. Annę Marię Mazurek.

Jednocześnie potwierdzam, że następujący zakres stanowi mój wkład w publikację: koncepcja, Ł.S., M.F.-R. oraz A.M.M.; metodologia, Ł.S.; oprogramowanie, Ł.S.; walidacja, Ł.S.; analiza formalna, Ł.S. oraz A.M.M.; badania, Ł.S. oraz A.M.M.; zasoby, Ł.S.; opracowanie danych, Ł.S. oraz A.M.M.; pisanie – przygotowanie pierwotnej wersji manuskryptu, Ł.S. oraz A.M.M.; pisanie - redakcja i korekta manuskryptu, Ł.S., M.F.-R. oraz A.M.M.; wizualizacja, Ł.S. oraz A.M.M.; nadzór, Ł.S. oraz M.F.-R.; zarządzanie projektem, Ł.S.; pozyskiwanie finansowania, Ł.S.

28.04.2026
Date / Data

Szeleszczuk
Legible signature / Czytelny podpis

Publication co-author statement

As a co-author of the publication entitled:

"Periodic DFT Investigation of Isosymmetric Alpha–Beta Phase Transition in Resorcinol Under Ambient and High Pressure", *published in Crystals (2026, Volume 16, Issue 3, Article 215),* https://doi.org/10.3390/cryst16030215
Authors: Anna Maria Mazurek, Monika Franczak-Rogowska and Łukasz Szeleszczuk

I agree to include this publication into a collection of thematically related publications forming a doctoral dissertation prepared by mgr farm. Anna Maria Mazurek.

Additionally, I declare my contribution to the publication as follows: conceptualisation, Ł.S., M.F.-R. and A.M.M.; methodology, Ł.S.; software, Ł.S.; validation, Ł.S.; formal analysis, Ł.S. and A.M.M.; investigation, Ł.S. and A.M.M.; resources, Ł.S.; data curation, Ł.S. and A.M.M.; writing - original draft preparation, Ł.S. and A.M.M.; writing - review and editing, Ł.S., M.F.-R. and A.M.M.; visualisation, Ł.S. and A.M.M.; supervision, Ł.S. and M.F.-R.; project administration, Ł.S.; funding acquisition, Ł.S.

Oświadczenie współautora publikacji

Jako współautor publikacji pt.:

"Periodic DFT Investigation of Isosymmetric Alpha–Beta Phase Transition in Resorcinol Under Ambient and High Pressure", *opublikowanej w czasopiśmie Crystals (2026, tom 16, numer 3, artykuł 215),* https://doi.org/10.3390/cryst16030215
Autorzy: Anna Maria Mazurek, Monika Franczak-Rogowska and Łukasz Szeleszczuk

Wyrażam zgodę na włączenie tej publikacji do zbioru powiązanych tematycznie artykułów naukowych, stanowiących część pracy doktorskiej przygotowanej przez mgr farm. Annę Marię Mazurek.

Jednocześnie potwierdzam, że następujący zakres stanowi mój wkład w publikację: koncepcja, Ł.S., M.F.-R. oraz A.M.M.; metodologia, Ł.S.; oprogramowanie, Ł.S.; walidacja, Ł.S.; analiza formalna, Ł.S. oraz A.M.M.; badania, Ł.S. oraz A.M.M.; zasoby, Ł.S.; opracowanie danych, Ł.S. oraz A.M.M.; pisanie – przygotowanie pierwotnej wersji manuskryptu, Ł.S. oraz A.M.M.; pisanie - redakcja i korekta manuskryptu, Ł.S., M.F.-R. oraz A.M.M.; wizualizacja, Ł.S. oraz A.M.M.; nadzór, Ł.S. oraz M.F.-R.; zarządzanie projektem, Ł.S.; pozyskiwanie finansowania, Ł.S.

28.04.2026
Date / Data

Legible signature / Czytelny podpis

10.4. Publication No. 4

crystals

MDPI

Article

Entropy-Driven Isosymmetric Phase Transition in L-Serine Under Pressure: A Periodic DFT Study

Anna Maria Mazurek [1], Monika Franczak-Rogowska [2] and Łukasz Szeleszczuk [1,*]

[1] Department of Organic and Physical Chemistry, Medical University of Warsaw, 1 Banacha Str., 02-097 Warsaw, Poland; anna.mazurek1@wum.edu.pl
[2] Department of Drug Chemistry, Pharmaceutical and Biomedical Analysis, Medical University of Warsaw, 1 Banacha Str., 02-097 Warsaw, Poland; monika.franczak-rogowska@wum.edu.pl
* Correspondence: lukasz.szeleszczuk@wum.edu.pl; Tel.: +48-501-255-121

Abstract

Understanding pressure-induced isosymmetric phase transitions in molecular crystals requires consideration of both structural and thermodynamic factors, particularly in hydrogen-bonded systems. In this work, periodic density functional theory (DFT) calculations were employed to investigate the pressure-dependent behavior of L-serine and to elucidate the origin of its experimentally observed phase transition between Phase I and Phase IV. Geometry optimizations performed at ambient pressure and 8.8 GPa reproduce the compression of the crystal lattice and the pressure-driven stabilization of Phase IV. However, no spontaneous reorientation of the hydroxyl groups is observed, indicating that the transition is not accessible within a purely static framework. To further explore the stability of the system, a series of modified crystal structures with different hydroxyl group orientations was generated and analyzed, revealing a complex energy landscape at ambient conditions that becomes significantly simplified under compression. Phonon calculations within the quasi-harmonic approximation demonstrate that the experimentally observed Phase I structure is not stabilized by enthalpy but by vibrational entropy, whose contribution increases with temperature. These results show that the phase transition in L-serine is governed by an interplay between lattice energy, hydrogen-bond rearrangement, and vibrational effects, and highlight that an accurate description of polymorphic stability in such systems requires inclusion of both static and dynamic contributions.

Keywords: L-serine; periodic DFT; CASTEP; isosymmetric phase transition; polymorphism

Check for updates

Academic Editor: Jasna Prlić Kardum

Received: 30 March 2026
Revised: 11 April 2026
Accepted: 13 April 2026
Published: 16 April 2026

Copyright: © 2026 by the authors. Licensee MDPI, Basel, Switzerland. This article is an open access article distributed under the terms and conditions of the Creative Commons Attribution (CC BY) license.

1. Introduction

Pressure is a powerful thermodynamic variable that can significantly alter the structural, energetic, and dynamical properties of molecular crystals. While temperature primarily increases molecular motion and entropy, pressure directly modifies intermolecular distances and orientations, often leading to reorganization of hydrogen-bond networks, conformational changes, and the formation of new polymorphic forms. Consequently, high-pressure studies have become an essential tool for probing complex energy landscapes and accessing phases inaccessible under ambient conditions [1–3].

Pressure-induced phase transitions in molecular crystals are commonly classified according to symmetry changes and transformation pathways. Most involve changes in space-group symmetry or unit-cell multiplicity; however, isosymmetric phase transitions (IPTs) represent a rare and conceptually intriguing class of transformations. In IPTs, the

space group, Wyckoff positions, and number of molecules in the unit cell remain unchanged, while discontinuities in lattice parameters, elastic properties, vibrational spectra, or molecular arrangements indicate a phase transition [4,5]. Such transitions challenge classical Landau-type descriptions and require detailed structural and thermodynamic analysis.

IPTs have been reported in a limited number of molecular solids, including glycylglycine [6], L-histidine [7], chlorothiazide [8], biurea [9], and sulfamic acid [10]. In these systems, transitions are driven by subtle cooperative rearrangements of hydrogen-bond networks and electrostatic interactions rather than by symmetry breaking. As a result, IPTs are particularly relevant in hydrogen-bonded crystals, where multiple weak interactions stabilize competing polymorphic forms.

Amino acids constitute an important class of hydrogen-bonded molecular solids and are widely used as model systems for investigating intermolecular interactions, structural flexibility, and phase behavior under varying thermodynamic conditions. In addition to their biological relevance, many amino-acid crystals exhibit functional properties such as nonlinear optical response [11], piezoelectricity [12], and ferroelectric behavior [13], further motivating studies of their structural stability and polymorphism [14].

L-serine ($HOCH_2$–$CH(NH_3^+)$–COO^-) is a prototypical example of such a system. In the solid state, it exists as a zwitterion, forming an extensive three-dimensional hydrogen-bond network involving ammonium, carboxylate, and hydroxyl groups. This network creates a dense yet adaptable crystal structure that is highly sensitive to external pressure, making L-serine a model system for studying pressure-induced polymorphism and kinetic effects.

Under ambient conditions, L-serine crystallizes in the orthorhombic space group $P2_12_12_1$, with one molecule in the asymmetric unit ($Z' = 1$) and four molecules in the unit cell ($Z = 4$) [15,16]. Several crystal structures have been reported in the Cambridge Structural Database, with Phase I characterized by lattice parameters a = 5.6193(14) Å, b = 8.519(3) Å, and c = 9.264(3) Å [17–20]. The structure consists of head-to-tail chains formed by strong N–H···O interactions, interconnected by O–H···O hydrogen bonds, resulting in a cooperative three-dimensional network.

Upon compression, L-serine undergoes a series of pressure-induced phase transitions. Early studies identified high-pressure polymorphs (phases II and III) at approximately 5 and 8 GPa [21,22], both preserving the original space-group symmetry and thus fulfilling the criteria for IPTs. Subsequent synchrotron studies revealed an additional polymorph, Phase IV (Figure 1), which emerges at around 5 GPa under specific compression conditions and remains stable up to at least 9.5 GPa [16]. These transitions are associated with changes in the orientation of the hydroxyl group and cooperative rearrangements of the hydrogen-bond network.

A detailed computational investigation of pressure-induced phase transitions in L-serine polymorphs was previously reported by Rychkov et al. [23], who employed periodic DFT calculations with dispersion corrections and external stress to analyze structural transformations under pressure. In that work, the phase transitions were interpreted primarily in terms of enthalpy changes and volume reduction, with the decrease in unit-cell volume identified as a key macroscopic driving force. At the microscopic level, the mechanism was attributed to overstrain of selected hydrogen bonds, leading to cooperative, martensitic-like transformations.

However, despite the detailed structural and energetic analysis, vibrational contributions to thermodynamic stability were not explicitly considered. As a result, the role of entropy in stabilizing competing polymorphs remained unresolved.

Detailed diffraction studies have shown that the I→II transition involves abrupt changes in lattice parameters and hydrogen-bond rearrangements without symmetry

reduction [21,22], while the II→III transition leads to further densification [21]. Importantly, Phase IV does not evolve from Phase II but originates directly from Phase I under slow compression, whereas rapid compression favors the I→II pathway [16].

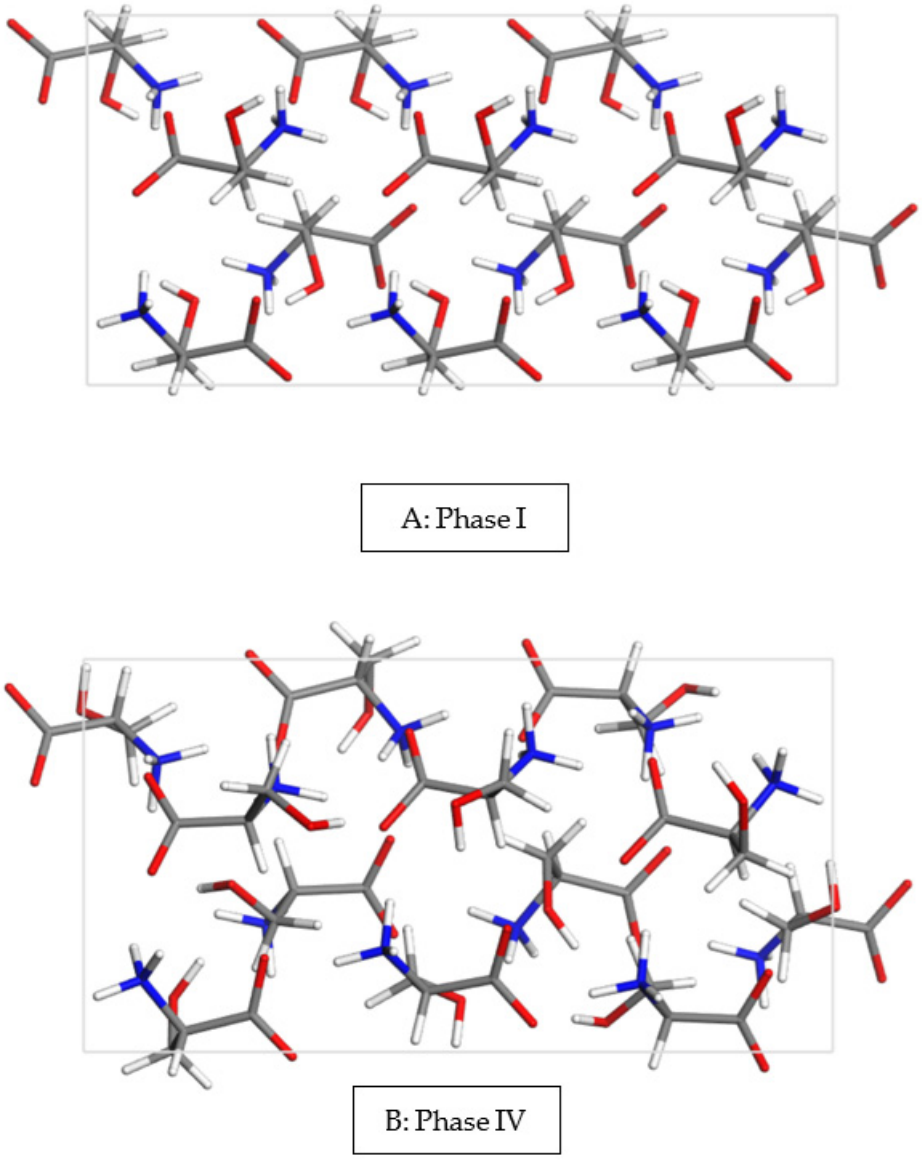

Figure 1. Unit cells of L-serine (**A**) phase I and (**B**) phase IV. Gray: carbon, blue: nitrogen, red: oxygen, white: hydrogen.

These observations highlight the crucial role of kinetic effects in the pressure-induced behavior of L-serine. The sequence and reversibility of phase transitions strongly depend on compression rate and stress conditions, indicating that metastable phases may be trapped under non-equilibrium conditions, while slower compression allows access to alternative pathways [16]. The interpretation of experimental data is complicated by the presence of kinetic control and energy barriers associated with phase transitions, as well as by the limited ability to directly access thermodynamic properties under high-pressure conditions.

Density functional theory (DFT) calculations provide a powerful framework for modeling molecular crystals. In polymorphic systems, structural differences arise from variations in intermolecular interactions, including hydrogen bonding, electrostatics, and dispersion forces [24–26]. Methods based on isolated molecules are therefore insufficient, and accurate description of polymorphism requires explicit treatment of periodic crystal structures [27,28].

Periodic DFT calculations under periodic boundary conditions are now a standard approach for modeling molecular solids, enabling accurate representation of collective intermolecular interactions. The use of plane-wave basis sets and pseudopotentials ensures computational efficiency and systematic convergence, which are essential for studying pressure-dependent structural changes [27–30].

In this work, we extend previous computational studies by explicitly incorporating vibrational contributions to thermodynamic stability through phonon calculations within the quasi-harmonic approximation. This approach allows us to move beyond purely enthalpy-driven interpretations and to evaluate the full Gibbs free energy landscape of L-serine polymorphs under pressure. In particular, we demonstrate that the experimentally observed stability of Phase I under ambient conditions is governed by vibrational entropy, highlighting the importance of dynamic effects in pressure-induced isosymmetric phase transitions.

2. Materials and Methods

Density functional theory (DFT) calculations, including enthalpy minimization, phonon dispersion, and density of states analysis, were performed using the CASTEP code [31] implemented in Materials Studio 2020. All calculations employed the plane-wave pseudopotential formalism. On-the-fly-generated (OTFG) norm-conserving pseudopotentials (H_2017R2ncp.otfg for H, N_2017R2ncp.otfg for N, O_2019ncp.otfg for O, and C_2017R2ncp.otfg for C) were used, generated within the Koelling–Harmon scalar relativistic scheme. External pressure was applied within the periodic DFT framework during geometry optimization by including a stress tensor corresponding to the target pressure, allowing simultaneous relaxation of atomic positions and unit cell parameters under pressure conditions.

2.1. DFT Functionals and Dispersion Correction Methods

The DFT functionals and dispersion corrections utilized in this study are presented in Table 1. Different functional–dispersion combinations were considered in order to assess their relative performance in describing the structural and energetic properties of the system.

Table 1. DFT-based computational methods used in this study.

No.	Approximation	Functional	Dispersion Correction	References
1	GGA	PBE	TS	[32,33]
2	GGA	PBE	GD2	[32,34]
3	GGA	PBE	MBD*	[32,35]
4	GGA	PBE	Not used	[32]
5	GGA	RPBE	TS	[33,36]
6	GGA	RPBE	Not used	[36]
7	GGA	PW91	TS	[33,37,38]
8	GGA	PW91	OBS	[37–39]
9	GGA	PW91	Not used	[37,38]
10	GGA	WC	Not used	[40]
11	GGA	PBESOL	TS	[33,41]
12	GGA	PBESOL	Not used	[41]
13	GGA	BLYP	TS	[33,42,43]
14	GGA	BLYP	GD2	[34,42,43]
15	GGA	BLYP	Not used	[42,43]
16	meta-GGA	RSCAN	Not used	[44]

2.2. Geometry Optimization

Geometry optimizations were performed using the limited-memory Broyden–Fletcher–Goldfarb–Shanno (LBFGS) algorithm with the finite-basis set correction ("smart") scheme. The plane-wave kinetic energy cutoff (E_{cut}) was optimized and set to 1020 eV. Brillouin zone sampling was carried out using Monkhorst–Pack k-point grids, with a spacing below 0.07 $Å^{-1}$.

Experimental crystal structures of L-serine (CSD refcodes LSERIN20 and LSERIN50 were used as initial models. Two optimization schemes were applied: (i) "full + cell", in which both atomic positions and lattice parameters were relaxed, and (ii) "atoms", where only atomic positions were optimized while lattice parameters were fixed at experimental values. All the calculations were done without the space group symmetry constraints.

The convergence criteria were set to 5×10^{-6} eV/atom for total energy, 1×10^{-2} eV/Å for forces, 2×10^{-2} GPa for stress, and 5×10^{-4} Å for atomic displacements. For cell optimization, the fixed-basis set quality approach was employed, with an SCF convergence threshold of 5×10^{-7} eV/atom.

2.3. Thermodynamic Parameters

Phonon frequencies were calculated using density functional perturbation theory (DFPT) via diagonalization of the dynamical matrix. DFPT provides phonon properties by evaluating the response of the electronic structure to perturbations, without the need for explicit atomic displacements. Phonon calculations and thermodynamic properties were obtained using the density functional perturbation theory (DFPT) implementation available in CASTEP, without the use of external software.

The q-point sampling for dynamical matrix calculations was defined by a Monkhorst–Pack grid with a spacing of 0.05 $Å^{-1}$. The convergence threshold for force constants was set to 1×10^{-5} eV/$Å^2$. Phonon dispersion relations, phonon density of states (phonon DOS), and electronic density of states (DOS) were computed based on the optimized structures. For phonon dispersion calculations, the spacing between q-points along the reciprocal-space path was set to 0.015 $Å^{-1}$. DOS calculations were performed using a $3 \times 3 \times 3$ Monkhorst–Pack k-point grid, corresponding to a q-point spacing of 0.04 $Å^{-1}$.

Thermodynamic properties were derived within the quasi-harmonic approximation, including zero-point energy (E_{zp}), entropy (S), Gibbs free energy (G), and enthalpy (H) as functions of temperature, using Equations (1)–(4) reported by Baroni et al. [45]. In these expressions, ω denotes phonon frequency, $F(\omega)$ the phonon density of states, E_{tot} the total electronic energy at 0 K, k the Boltzmann constant, and $\hbar$ the reduced Planck constant.

$$E_{zp} = \frac{1}{2}\int F(\omega)\hbar\omega d\omega \quad (1)$$

$$S(T) = k\left\{\int \frac{\frac{\hbar\omega}{kT}}{\exp\left(\frac{\hbar\omega}{kT}\right)-1}F(\omega)d\omega - \int F(\omega)\ln\left[1-\exp\left(-\frac{\hbar\omega}{kT}\right)\right]d\omega\right\} \quad (2)$$

$$G(T) = E_{tot} + E_{zp} + kT\int F(\omega)\ln\left[1-\exp\left(-\frac{\hbar\omega}{kT}\right)\right]d\omega + pV \quad (3)$$

$$H = G + TS \quad (4)$$

3. Results

3.1. Geometry Optimization of L-serine at 1 Atm and 8.8 GPa

Geometry optimizations of L-serine Phases I and IV were performed at both ambient pressure (1 atm) and 8.8 GPa, including full relaxation of atomic positions and unit cell

parameters. The pressure of 8.8 GPa was selected to correspond to the experimentally relevant high-pressure range in which L-serine polymorphs are observed and to enable direct comparison with available structural data.

To enable direct structural comparison between the two polymorphs, the experimental unit cell of Phase I ($Z' = 1$) was expanded threefold along the a axis to match the supercell representation of Phase IV ($Z' = 3$), resulting in comparable lattice dimensions and molecular arrangements. This type of computational approach, involving optimization of crystal structures at different pressures (including conditions beyond their experimental stability range), has been previously applied in studies of L-serine polymorphs under pressure, where it was used to rationalize phase transition mechanisms and relative stability of different forms [23].

Optimizations at 1 atm served two purposes: (i) benchmarking the performance of different DFT functionals (Table 1) through comparison with experimental unit cell parameters, and (ii) selecting the most reliable method for subsequent calculations, including phonon analysis. As expected, the choice of functional significantly affects the calculated structural parameters.

The results (Table 2) show considerable variation depending on the computational approach. For example, the lattice parameter a ranges from 16.372 Å (RPBE-TS) to 17.569 Å (RPBE without dispersion), corresponding to deviations of nearly 1 Å from the experimental value. Similar trends are observed for the remaining lattice parameters and unit cell volumes. Dispersion corrections systematically improve agreement with experiment, whereas methods without dispersion tend to overestimate intermolecular distances and unit cell volumes. Among the tested approaches, the meta-GGA functional RSCAN provides the best agreement with experimental data. A comparison between experimental Phase IV data at 6.64 GPa and structures optimized at 1 atm is provided in Table 3.

Table 2. Comparison of experimentally determined and geometrically optimized unit cell dimensions of L-serine Phase I at 1 atm.

CCDC Ref. Code/DFT Functional	Dispersion Correction	a [Å]	b [Å]	c [Å]	V [Å^3]
CSD_LSERIN20		16.858 [1]	8.519(3)	9.264(3)	1358.9
PBE	TS	16.906	8.489	9.469	1303.2
PBE	GD2	16.969	8.433	9.106	1340.6
PBE	MBD*	16.937	8.497	9.316	1470.2
PBE	Not used	17.087	8.738	9.847	1295.5
RPBE	TS	16.372	8.814	8.978	1859.2
RPBE	Not used	17.569	10.510	10.069	1365.0
PW91	TS	16.918	8.479	9.515	1364.9
PW91	OBS	16.918	8.481	9.513	1469.5
PW91	Not used	17.076	8.717	9.872	1365.5
WC	Not used	16.808	8.459	9.605	1286.7
PBESOL	TS	16.662	8.364	9.233	1343.0
PBESOL	Not used	16.784	8.439	9.481	1244.1
BLYP	TS	16.508	8.740	8.623	1292.8
BLYP	GD2	17.141	8.507	8.866	1591.5
BLYP	Not used	17.372	9.075	10.095	1327.1
RSCAN	Not used	16.825	8.519	9.259	1358.9

[1] The value was multiplied by three to enable direct comparison with the L-serine phase IV crystal lattice.

Geometry optimizations were subsequently performed under high-pressure conditions (8.8 GPa) for both polymorphs (Tables 4 and 5). The calculated structures reproduce the experimentally observed lattice compression, with all unit cell parameters decreasing relative to ambient conditions. The compression is anisotropic, reflecting the directional

character of the hydrogen-bond network, with the most pronounced contraction observed along the c axis.

Table 3. Comparison of experimentally determined at 6.64 GPa and geometrically optimized at 1 atm unit cell dimensions of L-serine Phase IV.

CCDC Ref. Code/DFT Functional	Dispersion Correction	a [Å]	b [Å]	c [Å]	V [Å^3]
CSD_LSERIN50		16.09873(5)	8.42773(2)	8.04459(7)	1091.5
PBE	TS	16.306	9.110	9.197	1366.1
PBE	GD2	16.534	8.751	8.850	1280.5
PBE	MBD*	16.297	9.090	9.123	1351.5
PBE	Not used	16.593	9.390	10.080	1570.4
RPBE	TS	16.331	8.662	8.774	1241.0
RPBE	Not used	16.772	9.655	10.766	1743.3
PW91	TS	16.279	9.164	9.291	1386.0
PW91	OBS	16.281	9.161	9.291	1385.8
PW91	Not used	16.577	9.384	10.119	1574.1
WC	Not used	16.391	9.218	9.930	1500.2
PBESOL	TS	16.131	8.995	9.021	1308.8
PBESOL	Not used	16.123	9.263	9.585	1431.4
BLYP	TS	16.407	8.614	8.459	1195.4
BLYP	GD2	16.672	8.724	8.742	1271.5
BLYP	Not used	16.777	9.516	10.551	1684.4
RSCAN	Not used	16.317	8.898	9.110	1322.7

Table 4. Comparison of experimentally determined and geometrically optimized unit cell dimensions of L-serine Phase I at 8.8 GPa.

CCDC Ref. Code/DFT Functional	Dispersion Correction	a [Å]	b [Å]	c [Å]	V [Å^3]
L-Ser I		16.05096 [1]	8.1594	8.33669	1091.8
PBE	TS	16.277	8.061	8.366	1097.7
PBE	GD2	16.289	8.032	8.228	1076.6
PBE	MBD*	16.232	8.078	8.273	1084.7
PBE	Not used	16.327	8.194	8.422	1126.7
RPBE	TS	16.057	7.755	7.828	974.6
RPBE	Not used	16.529	8.303	8.618	1182.8
PW91	TS	16.242	8.082	8.350	1096.1
PW91	OBS	16.241	8.084	8.350	1096.2
PW91	Not used	16.308	8.191	8.406	1123.0
WC	Not used	16.115	8.085	8.268	1077.2
PBESOL	TS	15.443	8.420	8.128	1057.0
PBESOL	Not used	16.105	8.088	8.270	1077.2
BLYP	TS	16.438	7.703	7.924	1003.3
BLYP	GD2	16.408	8.040	8.237	1086.6
BLYP	Not used	16.502	8.289	8.516	1164.9
RSCAN	Not used	16.162	8.084	8.267	1080.2

[1] The value was multiplied by three to enable direct comparison with the L-serine phase IV crystal lattice.

Importantly, no spontaneous reorientation of the hydroxyl groups was observed during geometry optimization. Phase I optimized at 8.8 GPa retained its original hydroxyl orientation, with no transition toward the configuration characteristic of Phase IV. Likewise, Phase IV structures preserved their initial hydroxyl arrangement. This indicates that the hydroxymethyl rotation associated with the phase transition is not accessible within a purely static DFT framework and suggests the presence of an energy barrier separating the two configurations.

Table 5. Comparison of experimentally determined and geometrically optimized unit cell dimensions of L-serine Phase IV at 8.8 GPa.

CCDC Ref. Code/DFT Functional	Dispersion Correction	a [Å]	b [Å]	c [Å]	V [Å^3]
L-Ser IV		16.01396	8.34378	7.93006	1091.8
PBE	TS	15.943	8.296	8.084	1069.3
PBE	GD2	15.972	8.232	7.976	1048.6
PBE	MBD*	15.941	8.257	8.020	1055.7
PBE	Not used	16.044	8.371	8.156	1095.4
RPBE	TS	15.647	8.106	7.646	969.8
RPBE	Not used	16.216	8.521	8.351	1153.9
PW91	TS	15.941	8.290	8.074	1067.1
PW91	OBS	15.943	8.289	8.074	1067.0
PW91	Not used	16.033	8.359	8.140	1091.0
WC	Not used	15.864	8.239	7.984	1043.5
PBESOL	TS	15.810	8.182	7.920	1024.5
PBESOL	Not used	15.867	8.240	7.986	1044.1
BLYP	TS	15.739	8.169	7.673	986.5
BLYP	GD2	16.075	8.260	7.976	1059.0
BLYP	Not used	16.204	8.475	8.254	1133.5
RSCAN	Not used	15.893	8.239	8.005	1048.1

Such behavior is consistent with experimental observations, which attribute the phase transition to cooperative rearrangements of hydroxymethyl groups and the hydrogen-bond network. These collective processes likely involve overcoming an energy barrier and cannot be captured by standard geometry optimization alone. Therefore, while static DFT calculations correctly reproduce the pressure-dependent stability of the polymorphs, additional approaches, such as phonon-based thermodynamic analysis, are required to fully describe the mechanism of the isosymmetric phase transition.

Further insight into the relative stability of the two polymorphs was obtained from the calculated energy differences between Phase I and Phase IV (Tables 6 and 7). At ambient pressure, all computational approaches yield negative values of ΔE (Phase I—Phase IV), confirming that Phase I is energetically more stable than Phase IV. This is consistent with experimental observations, where Phase I is the only stable polymorph under ambient conditions.

Table 6. Energy differences between Phase I and Phase IV of L-serine optimized at 1 atm.

DFT Functional	Dispersion Correction	ΔE Phase I—Phase IV [kJ/mol]
PBE	TS	−138.36
PBE	GD2	−149.09
PBE	MBD*	−153.93
PBE	Not used	−51.56
RPBE	TS	−107.59
RPBE	Not used	−48.20
PW91	TS	−128.46
PW91	OBS	−128.41
PW91	Not used	−42.26
WC	Not used	−40.90
PBESOL	TS	−110.38
PBESOL	Not used	−82.98
BLYP	TS	−83.12
BLYP	GD2	−148.56
BLYP	Not used	−25.62
RSCAN	Not used	−183.55

Table 7. Energy differences between Phase I and Phase IV of L-serine optimized at 8.8 GPa.

DFT Functional	Dispersion Correction	ΔE Phase I—Phase IV [kJ/mol]
PBE	TS	30.61
PBE	GD2	0.37
PBE	MBD*	6.43
PBE	Not used	−31.79
RPBE	TS	63.40
RPBE	Not used	−72.58
PW91	TS	22.93
PW91	OBS	23.00
PW91	Not used	−26.77
WC	Not used	18.17
PBESOL	TS	34.20
PBESOL	Not used	22.47
BLYP	TS	145.16
BLYP	GD2	−0.48
BLYP	Not used	−52.71
RSCAN	Not used	−23.36

Under elevated pressure, however, this relationship changes markedly. As shown in Table 7, many dispersion-corrected methods predict positive ΔE values at 8.8 GPa, indicating that Phase IV becomes energetically favored under compression. In several cases, ΔE approaches zero, suggesting that the two polymorphs become nearly isoenergetic in the high-pressure regime. Such small energy differences are characteristic of molecular crystal polymorphs, where competing structures often differ in stability by only a few kJ/mol, making their relative stability highly sensitive to external conditions such as pressure and temperature.

The lattice energy differences between Phase I and Phase IV of L-serine, calculated as a function of pressure using the PBE-TS functional (Figure 2, Table S1), reveal a clear pressure-dependent trend in their relative stability. At low pressures, ΔE values are strongly negative, indicating that Phase I is thermodynamically favored. With increasing pressure, the magnitude of ΔE decreases, reflecting a gradual reduction in the energetic preference for Phase I.

This trend suggests that intermolecular interactions stabilizing Phase IV become progressively more favorable under compression, likely due to pressure-induced rearrangement of the hydrogen-bond network and improved molecular packing efficiency.

A key feature of this behavior is the sign inversion of ΔE between 6.8 and 7.2 GPa, marking the point at which Phase IV becomes energetically more stable than Phase I. This pressure range is in reasonable agreement with experimental observations, which place the onset of Phase IV under slow compression at approximately 5.4–5.8 GPa [16], although the transition is shifted to slightly higher pressures in the calculations.

Such a crossing of lattice energies is commonly interpreted as computational evidence of a pressure-induced phase transition, corresponding to the inversion of thermodynamic stability between the two polymorphs. The gradual nature of the ΔE variation indicates that the transformation is driven by continuous changes in intermolecular interactions rather than an abrupt structural rearrangement. The difference between the calculated and experimental transition pressure (approximately 1 GPa) is within the typical accuracy of periodic DFT methods for molecular crystals [46–48]. This discrepancy may arise from the approximate nature of exchange–correlation functionals, limitations in dispersion corrections, and the neglect of anharmonic effects. In addition, experimental conditions

such as non-hydrostatic stress and kinetic barriers may influence the observed transition pressure.

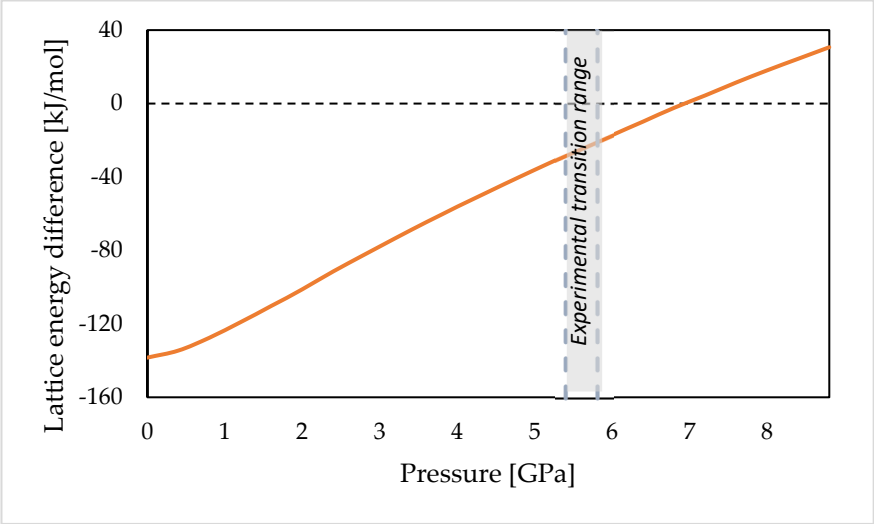

Figure 2. Pressure dependence of the lattice energy difference between Phase I and Phase IV of L-serine calculated using the PBE-TS functional. The zero reference corresponds to the equal lattice energy of Phase I and IV. The gray shaded region (5.4–5.8 GPa) indicates the experimentally observed pressure range of the onset of Phase IV under slow compression conditions, as reported by Fisch et al. [16].

The next stage of this study involved the optimization of modified L-serine crystal structures derived from the experimentally determined Phases I and IV. The initial cell parameters were retained, while the orientation of the hydroxyl groups within the $–CH_2OH$ side chains of selected molecules in the lattice was systematically varied. Multiple configurations were generated by altering hydroxyl group orientations while preserving the overall crystal packing and lattice topology. These configurations were subsequently subjected to full geometry optimization. This approach was designed to reproduce the experimentally observed structural differences between the polymorphs and to assess whether the pressure-induced IPT could be captured computationally through cooperative reorientation of the hydroxyl groups.

The generated configurations were defined by the orientation of the hydroxyl group in each molecule within the crystal lattice. Orientations were described with respect to the crystallographic axes, taking the a axis as horizontal and the b axis as vertical when viewed along the c direction. The configurations were constructed based on three reference molecules within the structural motif, whose hydroxyl groups could adopt three possible orientations: up, left, or right. These were denoted as U, L, and R, respectively (Figure 3). For Phase IV ($Z' = 3$), this leads to a total of $3^3 = 27$ possible configurations, corresponding to all combinations of hydroxyl group orientations in the three symmetry-independent molecules. Each configuration was labeled using a three-letter code reflecting the orientations of the hydroxyl groups in the reference molecules, hereafter referred to as the configuration label.

To examine the relative stability of the generated configurations, lattice energy differences were evaluated at both ambient pressure (1 atm) and elevated pressure (8.8 GPa), as summarized in Tables 8 and 9. At 1 atm, all energies were referenced to the experimentally observed Phase I configuration (UUU), whereas at 8.8 GPa the values were calculated relative to the Phase IV configuration (URL). The complete set of optimized structural parameters and total energies is provided in Tables S1 and S2.

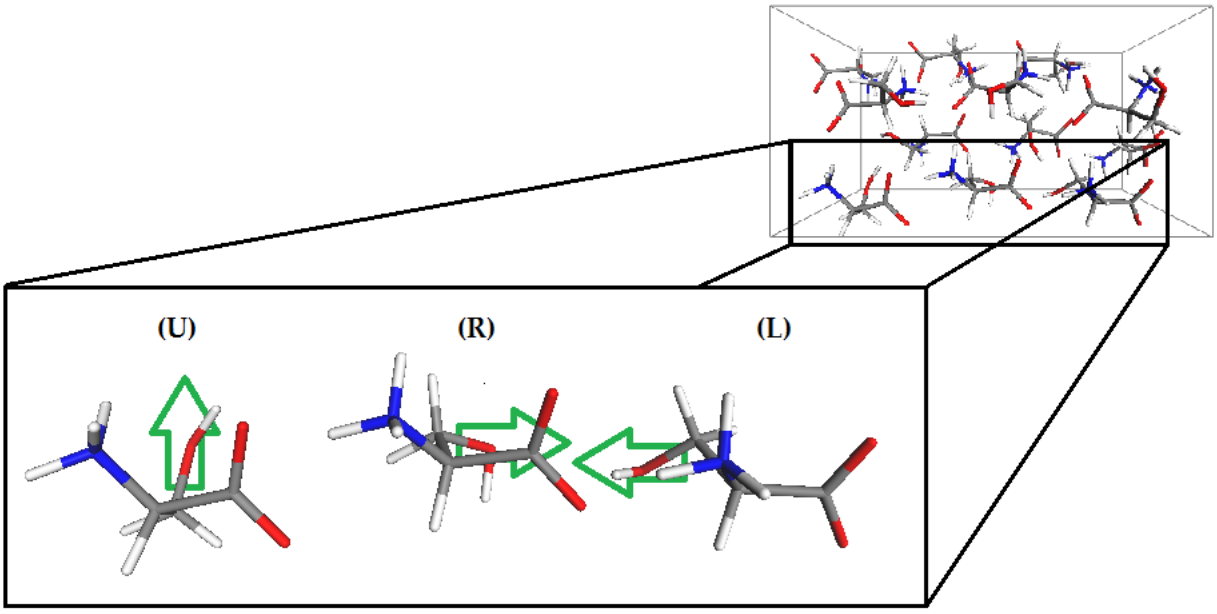

Figure 3. The asymmetric unit of L-serine phase IV with defined hydroxyl group orientation URL: Up (U), Right (R), Left (L).

Table 8. Energy differences between Phase I (UUU) and configurations derived from Phase I and IV of L-serine optimized using PBE TS functional at 1 atm. Negative values are bolded.

Label	ΔE Configuration Derived from Phase I—Phase I (UUU) [kJ/mol]	ΔE Configuration Derived from Phase IV—Phase I (UUU) [kJ/mol]
UUU	0.00	81.76
UUR	79.68	47.12
UUL	**−15.41**	**−22.98**
URU	19.06	171.99
URR	151.72	106.47
URL	3.15	138.38
ULU	36.50	**−29.20**
ULR	115.55	127.26
ULL	11.66	40.47
RUU	63.52	95.70
RUR	181.37	117.03
RUL	126.52	135.68
RRU	146.38	147.09
RRR	89.41	205.08
RRL	84.83	197.88
RLU	68.36	27.42
RLR	71.30	83.95
RLL	46.63	72.22
LUU	57.99	7.15
LUR	73.75	45.06
LUL	101.05	33.73
LRU	119.63	174.17
LRR	77.64	116.96
LRL	87.91	91.52
LLU	40.38	19.50
LLR	40.53	81.07
LLL	**−47.67**	**−48.33**

Table 9. Energy differences between Phase IV (URL) and configurations derived from Phase I and IV of L-serine optimized using PBE TS functional at 8.8 GPa.

Label	ΔE Configuration Derived from Phase I—Phase IV (URL) [kJ/mol]	ΔE Configuration Derived from Phase IV—Phase IV (URL) [kJ/mol]
UUU	42.97	130.69
UUR	102.81	117.65
UUL	1.24	28.61
URU	5.66	92.86
URR	135.18	71.32
URL	0.00	12.14
ULU	156.33	42.25
ULR	217.53	218.73
ULL	91.97	69.47
RUU	77.04	191.69
RUR	126.76	201.43
RUL	174.96	108.89
RRU	94.57	126.20
RRR	52.39	88.01
RRL	69.08	72.90
RLU	179.66	136.13
RLR	149.19	226.55
RLL	74.29	74.16
LUU	54.90	92.82
LUR	113.96	96.00
LUL	127.73	128.93
LRU	156.40	127.72
LRR	134.90	102.62
LRL	11.93	11.86
LLU	157.74	198.32
LLR	108.96	100.81
LLL	86.13	58.89

At ambient conditions, the experimentally observed Phase I configuration (UUU) does not correspond to the lowest-energy structure. Several alternative configurations, most notably LLL and UUL, exhibit significantly lower lattice energies, with LLL representing the global minimum among the analyzed structures. This indicates that, within a static DFT framework, multiple configurations are energetically more favorable than the experimentally observed one. The magnitude of the energy differences, reaching several tens of kJ/mol, highlights the presence of a complex energy landscape with numerous local minima associated with distinct hydrogen-bonding motifs.

A markedly different behavior is observed under compression at 8.8 GPa. In this case, the configuration corresponding to Phase IV (URL) becomes the most stable structure. Only a limited number of configurations, such as UUL and URU, remain close in energy, while the majority are significantly destabilized.

These results demonstrate that increasing pressure not only alters the relative energetic ordering of the configurations but also effectively reduces the number of energetically accessible minima. While multiple configurations are competitive at ambient conditions, compression favors a narrower subset of structures. In particular, the stabilization of the URL configuration, accompanied by the destabilization of alternative arrangements, is consistent with the experimentally observed pressure-induced transition toward Phase IV.

Overall, the results demonstrate that periodic DFT calculations provide a consistent description of both the structural compression and the relative energetic stability of L-

serine polymorphs under pressure. Although the isosymmetric phase transition is not directly reproduced within static geometry optimization, the calculated energy trends clearly support the experimentally observed pressure-induced stabilization of Phase IV. These findings provide important insight into the thermodynamic driving forces governing the transition and highlight the limitations of static approaches in capturing cooperative structural transformations.

3.2. Thermodynamic Parameters Calculations

Despite the significant computational cost of phonon dispersion and phonon density of states calculations, they provide essential insight into the thermodynamic stability of polymorphic forms under pressure. The differences between thermodynamic quantities for Phase I and Phase IV (Δ, Phase I–Phase IV), including Gibbs free energy (ΔG), enthalpy (ΔH), and the entropic contribution (TΔS), calculated using the PBE-TS functional at 8.8 GPa as a function of temperature, are shown in Figure 4.

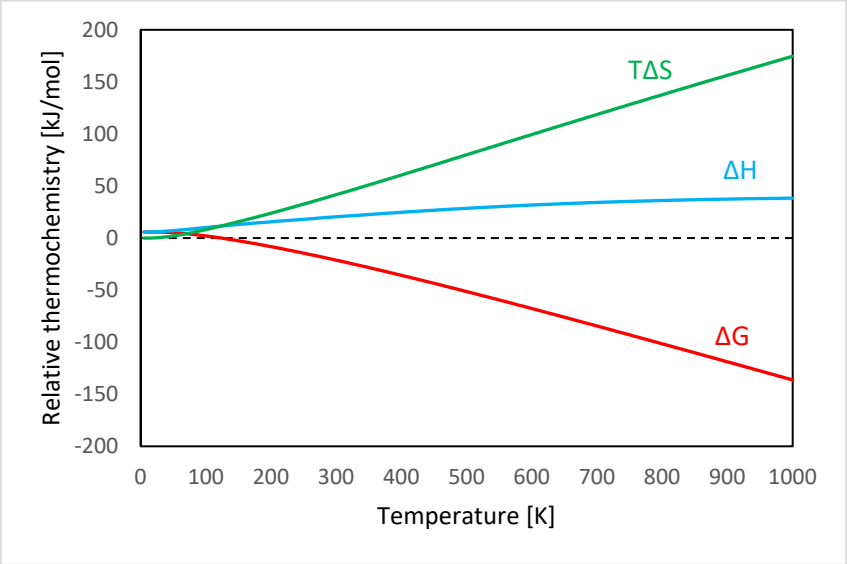

Figure 4. Differences (Phase I–Phase IV) between the thermodynamic parameters of the Gibbs free energy (ΔG), enthalpy (ΔH), and temperature times entropy (TΔS) of the structures modeled using PBE TS functional at 8.8 GPa, with respect to the temperature. The zero reference corresponds to the equal values of thermodynamic properties of Phase I and IV.

The calculated ΔG values reveal a temperature-dependent stability crossover between the two phases. Below approximately 125 K, ΔG remains positive, indicating that Phase IV is thermodynamically more stable in the low-temperature regime. Above this temperature, ΔG becomes negative, demonstrating that Phase I is stabilized at higher temperatures. The magnitude of the free energy differences is small, on the order of a few kJ/mol, which is typical for molecular crystal polymorphs and highlights the delicate balance between competing structures. This behavior indicates that even subtle entropic contributions can determine the relative stability of the phases.

The configurations selected for phonon calculations were chosen based on the results of the initial geometry optimizations of structures derived from experimentally determined Phases I and IV. The adopted notation reflects both the orientation of hydroxyl groups within the crystal lattice and the phase of origin. The three-letter code denotes the orientation of the hydroxyl group in each of the three reference molecules, as described above, while the suffix (I or IV) indicates whether the configuration was derived from Phase I or Phase IV. The experimentally observed structure is denoted as exp-I and corresponds to the UUU configuration.

Notably, the exp-I structure does not correspond to the lowest-energy configuration at 1 atm. Several alternative arrangements are energetically more favorable within the static DFT framework. This discrepancy between experimental stability and lattice energy indicates that static energetic considerations alone are insufficient to describe the relative stability of the system.

To address this, phonon calculations were performed for selected low-energy configurations identified at the optimization stage. This approach enables explicit evaluation of vibrational contributions to phase stability. Based on the computed phonon properties, Gibbs free energy differences (ΔG) between the configurations were evaluated as a function of temperature (Figure 5). For each temperature, the lowest ΔG value was taken as a reference (Min = 0), allowing direct comparison of relative thermodynamic stability.

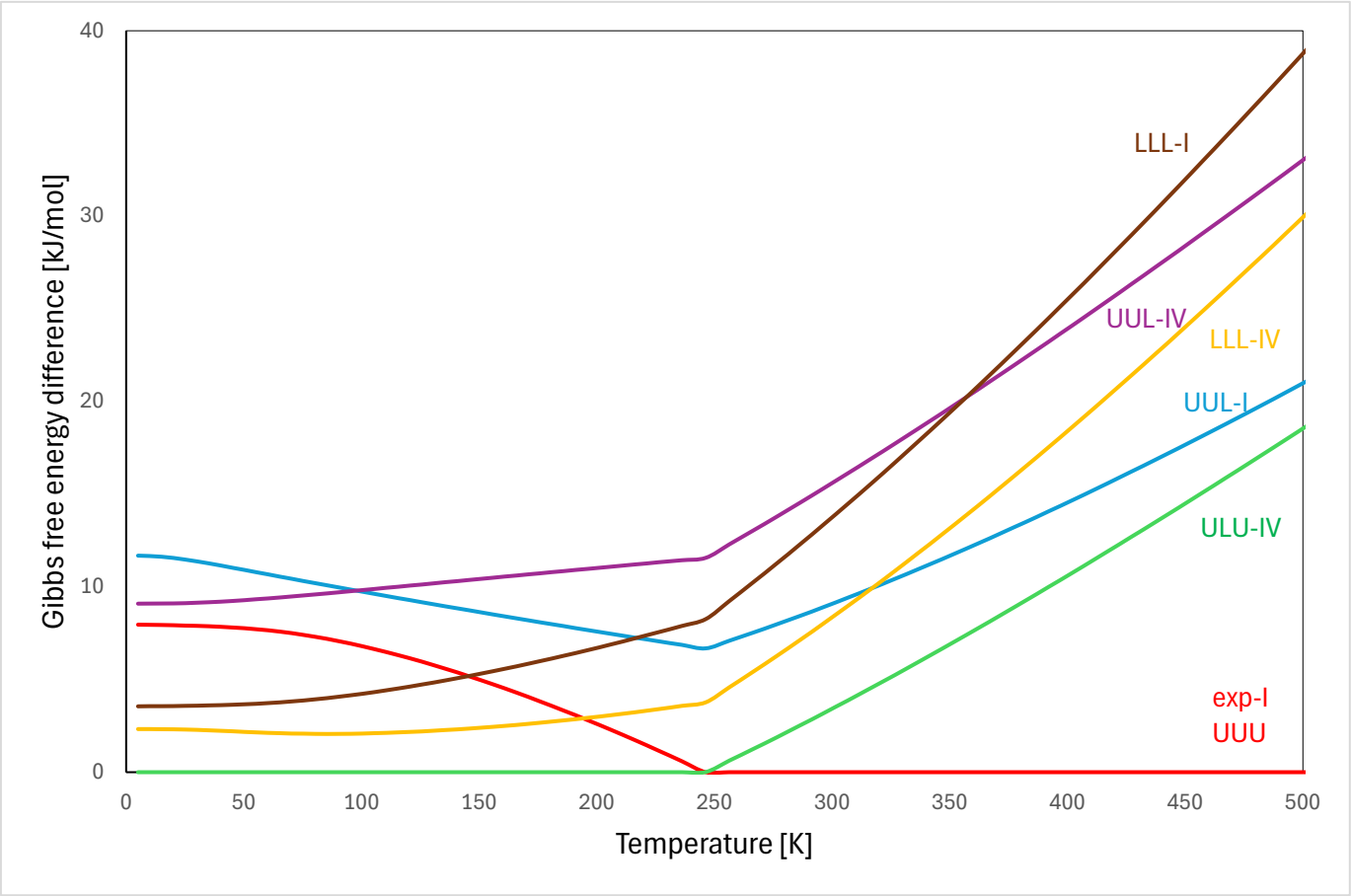

Figure 5. Differences (Phase I–Min) between the thermodynamic parameter of the Gibbs free energy (ΔG) of the structures modeled using PBE TS functional at 1 atm, with respect to the temperature. The zero reference corresponds to the lattice free energy of the most thermodynamically stable phase.

At low temperatures, the configuration labeled GLG-IV is consistently the most stable, exhibiting the lowest ΔG values over a broad temperature range. Other configurations are significantly higher in energy, indicating that, within the harmonic approximation, GLG-IV provides the most favorable balance between lattice energy and vibrational contributions.

With increasing temperature, a gradual decrease in ΔG for exp-I relative to the reference configuration is observed, reflecting the growing importance of vibrational entropy. This trend becomes particularly pronounced above approximately 200 K.

A crossover in thermodynamic stability occurs at around 245 K, above which exp-I becomes the most stable configuration. This behavior is consistent with experimental observations, where Phase I is stable under ambient conditions.

This result clearly indicates that the stability of exp-I at elevated temperatures is not governed by enthalpy alone but is significantly influenced by vibrational entropy. The phase behavior can therefore be described as entropy-driven, with lattice dynamics favoring the experimentally observed structure at higher temperatures.

In contrast, most alternative configurations (excluding GLG-IV) show a monotonic increase in ΔG with temperature, leading to their progressive destabilization. As a result, they are unlikely to represent thermodynamically competitive phases under experimentally relevant conditions.

Overall, these findings demonstrate that the observed phase behavior cannot be explained by static lattice energies alone. Instead, it arises from a cooperative thermodynamic response in which subtle differences in hydrogen-bonding patterns and lattice dynamics are amplified by temperature-dependent vibrational contributions. This supports a mechanism in which the IPT in L-serine is governed by a delicate balance between intermolecular interactions and collective phonon modes, with vibrational entropy playing a decisive role in stabilizing the experimentally observed phase.

A comparison of thermodynamic contributions at 298 K (Table 10) provides further insight into the origin of phase stability. Decomposition of the Gibbs free energy into enthalpic and entropic components shows that the stabilization of exp-I does not arise from enthalpy. In fact, exp-I does not exhibit the most favorable enthalpy (H), as several alternative configurations possess lower H values. Instead, its stability is primarily driven by a larger vibrational entropy contribution (TΔS), which compensates for the less favorable enthalpy. The relatively small differences in thermodynamic quantities indicate that multiple configurations are energetically similar and may compete within a narrow thermodynamic window. This confirms that the stability of Phase I under ambient conditions arises from a delicate balance between enthalpic and entropic contributions. In particular, vibrational entropy stabilizes Phase I at elevated temperatures, consistent with the entropy-driven nature of the isosymmetric phase transition in L-serine.

Table 10. Energy of experimentally obtained Phase I (UUU) and configurations derived from Phase I and IV of L-serine optimized using PBE TS functional at 298 K. Values [kJ/mol] are presented in reference to exp-I.

Label	H	TS	G
exp-I (UUU)	0.00	0.00	0.00
UUL-I	−5.37	−14.28	8.91
UUL-IV	−7.78	−23.10	15.32
LLL-I	−18.47	−31.84	13.37
LLL-IV	−18.78	−26.81	8.03
ULU-IV	−16.51	−19.70	3.19

4. Conclusions

The results of this study demonstrate that periodic DFT calculations provide a consistent and reliable description of the pressure-dependent structural and energetic behavior of L-serine, successfully reproducing the experimentally observed stabilization of Phase IV under elevated pressure. The calculated lattice energy trends reveal a gradual inversion of stability between Phase I and Phase IV, in agreement with experimental observations of the pressure-induced isosymmetric phase transition. At the same time, the absence of spontaneous hydroxyl group reorientation during geometry optimization indicates that the transition cannot be captured within a purely static framework, pointing to the presence of an energy barrier and the cooperative nature of the structural rearrangement.

Analysis of alternative hydroxyl group configurations reveals a complex energy landscape at ambient conditions, characterized by multiple local minima associated with distinct hydrogen-bonding motifs. Under compression, this landscape becomes significantly simplified, with a reduced number of energetically accessible configurations and clear stabilization of the arrangement corresponding to Phase IV. This behavior reflects the increasing importance of molecular packing efficiency and hydrogen-bond reorganization under pressure.

Inclusion of vibrational contributions through phonon calculations resolves the apparent discrepancy between experimental observations and static lattice energy results. The experimentally observed Phase I structure, although not corresponding to the lowest lattice energy, is stabilized at ambient conditions primarily by vibrational entropy. This demonstrates that the phase behavior of L-serine cannot be explained solely in terms of enthalpy, but instead arises from a delicate balance between energetic and entropic contributions.

In addition, the present study highlights the importance of carefully selecting functional–dispersion combinations when modeling molecular crystals under pressure, as different approaches may lead to significant variations in predicted structural and energetic properties. Importantly, the results demonstrate that lattice energy alone is insufficient to describe polymorphic stability, and that inclusion of vibrational contributions to Gibbs free energy is essential for capturing experimentally observed phase behavior. More generally, incorporation of temperature-dependent thermodynamic effects under pressure provides a more complete and physically meaningful description of high-pressure phase transitions, offering deeper insight into their mechanisms and stability relationships.

Overall, the pressure-induced isosymmetric phase transition in L-serine is governed by a cooperative interplay between hydrogen-bond rearrangements, lattice compression, and vibrational dynamics. These findings highlight the necessity of combining static DFT calculations with phonon-based thermodynamic analysis to achieve a comprehensive understanding of polymorphic stability in molecular crystals, particularly in systems where entropy plays a decisive role. Such entropy-driven effects have been reported in a range of molecular crystal systems, including amino acids such as glycine and pharmaceutical compounds such as paracetamol, where small energy differences between polymorphs are significantly influenced by vibrational contributions.

Supplementary Materials: The following supporting information can be downloaded at https://www.mdpi.com/article/10.3390/cryst16040266/s1, Table S1: Energy differences between Phase I and Phase IV of L-serine optimized using PBE TS functional under different pressures; Table S2: Geometrically optimized, using PBE TS functional, unit cell dimensions of generated configurations derived from L-serine Phase I and IV at 1 atm; Table S3: Geometrically optimized, using PBE TS functional, unit cell dimensions of generated configurations derived from L-serine Phase I and IV at 8.8 GPa.

Author Contributions: Conceptualisation, Ł.S., M.F.-R. and A.M.M.; methodology, Ł.S.; software, Ł.S.; validation, Ł.S.; formal analysis, Ł.S. and A.M.M.; investigation, Ł.S. and A.M.M.; resources, Ł.S.; data curation, Ł.S. and A.M.M.; writing—original draft preparation, Ł.S. and A.M.M.; writing—review and editing, Ł.S., M.F.-R. and A.M.M.; visualization, Ł.S. and A.M.M.; supervision, Ł.S. and M.F.-R.; project administration, Ł.S.; funding acquisition, Ł.S. All authors have read and agreed to the published version of the manuscript.

Funding: This research received no external funding.

Data Availability Statement: The raw data supporting the conclusions of this article will be made available by the authors on request.

Acknowledgments: During the preparation of this manuscript, the authors used QuillBot (https://quillbot.com/ accessed on 10 April 2026) for language editing and paraphrasing purposes. The authors have reviewed and edited the output and take full responsibility for the content of this publication.

Conflicts of Interest: The authors declare no conflicts of interest.

References

1. Boldyreva, E.V. High-Pressure Diffraction Studies of Molecular Organic Solids. A Personal View. *Acta Crystallogr. A Found. Crystallogr.* **2008**, *64*, 218–231. [CrossRef] [PubMed]
2. Hemley, R.J. Effects of High Pressure on Molecules. *Annu. Rev. Phys. Chem.* **2000**, *51*, 763–800. [CrossRef] [PubMed]
3. Katrusiak, A. High-Pressure Crystallography. *Acta Crystallogr. A Found. Crystallogr.* **2008**, *64*, 135–148. [CrossRef]
4. Carpenter, M.A.; Salje, E.K.H. Elastic Anomalies in Minerals Due to Structural Phase Transitions. *EJM* **1998**, *10*, 693–812. [CrossRef]
5. Christy, A.G. Isosymmetric Structural Phase Transitions: Phenomenology and Examples. *Acta Crystallogr. B Struct. Sci.* **1995**, *51*, 753–757. [CrossRef]
6. Clarke, S.M.; Steele, B.A.; Kroonblawd, M.P.; Zhang, D.; Kuo, I.-F.W.; Stavrou, E. An Isosymmetric High-Pressure Phase Transition in α-Glycylglycine: A Combined Experimental and Theoretical Study. *J. Phys. Chem. B* **2020**, *124*, 1–10. [CrossRef]
7. Novelli, G.; Maynard-Casely, H.E.; McIntyre, G.J.; Warren, M.R.; Parsons, S. Effect of High Pressure on the Crystal Structures of Polymorphs of L-Histidine. *Cryst. Growth Des.* **2020**, *20*, 7788–7804. [CrossRef]
8. Oswald, I.D.H.; Lennie, A.R.; Pulham, C.R.; Shankland, K. High-Pressure Structural Studies of the Pharmaceutical, Chlorothiazide. *CrystEngComm* **2010**, *12*, 2533. [CrossRef]
9. Bull, C.L.; Funnell, N.P.; Ridley, C.J.; Pulham, C.R.; Coster, P.L.; Tellam, J.P.; Marshall, W.G. Pressure-Induced Isosymmetric Phase Transition in Biurea. *CrystEngComm* **2019**, *21*, 5872–5881. [CrossRef]
10. Li, Q.; Li, S.; Wang, K.; Li, X.; Liu, J.; Liu, B.; Zou, G.; Zou, B. Pressure-Induced Isosymmetric Phase Transition in Sulfamic Acid: A Combined Raman and x-Ray Diffraction Study. *J. Chem. Phys.* **2013**, *138*, 214505. [CrossRef]
11. Nourai, N.E.H.; Sebih, F.; Hadji, D.; Allal, F.Z.; Dib, S.; Kambouche, N.; Rolland, V.; Bellahouel-Benzine, S. Nonlinear Optical and Antimicrobial Activity of N-Acyl Glycine Derivatives. *J. Mol. Liq.* **2024**, *398*, 124260. [CrossRef]
12. Wang, Y.; Liu, S.; Li, L.; Li, H.; Yin, Y.; Rencus-Lazar, S.; Guerin, S.; Ouyang, W.; Thompson, D.; Yang, R.; et al. Manipulating the Piezoelectric Response of Amino Acid-Based Assemblies by Supramolecular Engineering. *J. Am. Chem. Soc.* **2023**, *145*, 15533–15541. [CrossRef]
13. Pensini, E.; Meszaros, P.; Kashlan, N.; Marangoni, A.G.; Laredo, T.; Gregori, S.; Mirzaee Ghazani, S.; van der Zalm, J.; Chen, A. Ferroelectric Hydrogels from Amino Acids and Oleic Acid. *iScience* **2024**, *27*, 110601. [CrossRef]
14. Pasternak, M. Articaine—The queen of infiltrative anaesthesia? A peculiar amino-amide local anaesthetic and its use in the dental practice from a pharmacological perspective. *Prospect. Pharm. Sci.* **2025**, *24*, 31–38. [CrossRef]
15. Boldyreva, E.V.; Sowa, H.; Seryotkin, Y.; Drebushchak, T.N.; Ahsbahs, H.; Chernyshev, V.; Dmitriev, V. Pressure-Induced Phase Transitions in Crystalline l-Serine Studied by Single-Crystal and High-Resolution Powder X-Ray Diffraction. *Chem. Phys. Lett.* **2006**, *429*, 474–478. [CrossRef]
16. Fisch, M.; Lanza, A.; Boldyreva, E.; Macchi, P.; Casati, N. Kinetic Control of High-Pressure Solid-State Phase Transitions: A Case Study on l-Serine. *J. Phys. Chem. C* **2015**, *119*, 18611–18617. [CrossRef]
17. Boldyreva, E.V.; Kolesnik, E.N.; Drebushchak, T.N.; Ahsbahs, H.; Beukes, J.A.; Weber, H.-P. A Comparative Study of the Anisotropy of Lattice Strain Induced in the Crystals of L-Serine by Cooling down to 100 K or by Increasing Pressure up to 4.4 GPa. *Z. Krist.-Cryst. Mater.* **2005**, *220*, 58–65. [CrossRef]
18. Zakharov, B.A.; Kolesov, B.A.; Boldyreva, E.V. Effect of pressure on crystalline L- and DL-serine: Revisited by a combined single-crystal X-ray diffraction at a laboratory source and polarized Raman spectroscopy study. *Acta Crystallogr. Sect. B Struct. Sci.* **2012**, *68*, 275–286. [CrossRef]
19. Szeleszczuk, Ł.; Pisklak, D.M.; Zielińska-Pisklak, M. Can we predict the structure and stability of molecular crystals under increased pressure? First-principles study of glycine phase transitions. *J. Comput. Chem.* **2018**, *39*, 1300–1306. [CrossRef]
20. Drebushchak, T.N.; Sowa, H.; Seryotkin, Y.V.; Boldyreva, E.V.; Ahsbahs, H. L-Serine III at 8.0 GPa. *Acta Crystallogr. Sect. E Struct. Rep.* **2006**, *62*, o4052. [CrossRef]
21. Moggach, S.A.; Marshall, W.G.; Parsons, S. High-Pressure Neutron Diffraction Study of L-Serine-I and L-Serine-II, and the Structure of L-Serine-III at 8.1 GPa. *Acta Crystallogr. B Struct. Sci.* **2006**, *62*, 815–825. [CrossRef]
22. Moggach, S.A.; Allan, D.R.; Morrison, C.A.; Parsons, S.; Sawyer, L. Effect of Pressure on the Crystal Structure of L-Serine-I and the Crystal Structure of L-Serine-II at 5.4 GPa. *Acta Crystallogr. B Struct. Sci.* **2005**, *61*, 58–68. [CrossRef]
23. Rychkov, D.A.; Stare, J.; Boldyreva, E.V. Pressure-Driven Phase Transition Mechanisms Revealed by Quantum Chemistry: L-Serine Polymorphs. *Phys. Chem. Chem. Phys.* **2017**, *19*, 6671–6676. [CrossRef]

24. Reilly, A.M.; Tkatchenko, A. Role of Dispersion Interactions in the Polymorphism and Entropic Stabilization of the Aspirin Crystal. *Phys. Rev. Lett.* **2014**, *113*, 055701. [CrossRef]
25. Qiu, L.; Li, X.-Y.; Miao, B.-W.; Yu, H.; Liu, W.; Sun, Y.; Tang, R.-L. Overcoming the Bandgap–Birefringence Trade-Off: Proton-Transfer Engineering of High-Performance Ultraviolet-Transparent Organic Crystal. *Angew. Chem. Int. Ed.* **2026**, *138*, e24424. [CrossRef]
26. Yang, D.-X.; Tang, R.-L.; Lv, Y.-L.; Miao, B.-W.; Liu, W.; Guo, S.-P. A Novel Metal-Free Crystal Demonstrating Superior Birefringence Attributed to the Synergistic Interaction of Dual π-Conjugated Units. *Sci. China Mater.* **2025**, *68*, 3600–3606. [CrossRef]
27. Neumann, M.A.; Perrin, M.-A. Energy Ranking of Molecular Crystals Using Density Functional Theory Calculations and an Empirical van Der Waals Correction. *J. Phys. Chem. B* **2005**, *109*, 15531–15541. [CrossRef] [PubMed]
28. Fedorov, A.Y.; Rychkov, D.A. Comparison of different computational approaches for unveiling the high-pressure behavior of organic crystals at a molecular level. Case study of tolazamide polymorphs. *J. Struct. Chem.* **2020**, *61*, 1356–1366. [CrossRef]
29. Rychkov, D.A. A Short Review of Current Computational Concepts for High-Pressure Phase Transition Studies in Molecular Crystals. *Crystals* **2020**, *10*, 81. [CrossRef]
30. Dubok, A.S.; Rychkov, D.A. What Is More Important When Calculating the Thermodynamic Properties of Organic Crystals, Density Functional, Supercell, or Energy Second-Order Derivative Method Choice? *Crystals* **2025**, *15*, 274. [CrossRef]
31. Clark, S.J.; Segall, M.D.; Pickard, C.J.; Hasnip, P.J.; Probert, M.I.J.; Refson, K.; Payne, M.C. First Principles Methods Using CASTEP. *Z. Krist.-Cryst. Mater.* **2005**, *220*, 567–570. [CrossRef]
32. Perdew, J.P.; Burke, K.; Ernzerhof, M. Generalized Gradient Approximation Made Simple. *Phys. Rev. Lett.* **1996**, *77*, 3865–3868. [CrossRef]
33. Tkatchenko, A.; Scheffler, M. Accurate Molecular Van Der Waals Interactions from Ground-State Electron Density and Free-Atom Reference Data. *Phys. Rev. Lett.* **2009**, *102*, 073005. [CrossRef]
34. Grimme, S. Semiempirical GGA-type Density Functional Constructed with a Long-range Dispersion Correction. *J. Comput. Chem.* **2006**, *27*, 1787–1799. [CrossRef]
35. Ambrosetti, A.; Reilly, A.M.; DiStasio, R.A.; Tkatchenko, A. Long-Range Correlation Energy Calculated from Coupled Atomic Response Functions. *J. Chem. Phys.* **2014**, *140*, 18A508. [CrossRef]
36. Hammer, B.; Hansen, L.B.; Nørskov, J.K. Improved Adsorption Energetics within Density-Functional Theory Using Revised Perdew-Burke-Ernzerhof Functionals. *Phys. Rev. B* **1999**, *59*, 7413–7421. [CrossRef]
37. Perdew, J.P.; Wang, Y. Accurate and simple analytic representation of the electron-gas correlation energy. *Phys. Rev. B* **1992**, *45*, 13244–13249. [CrossRef]
38. Perdew, J.P.; Chevary, J.A.; Vosko, S.H.; Jackson, K.A.; Pederson, M.R.; Singh, D.J.; Fiolhais, C. Atoms, Molecules, Solids, and Surfaces: Applications of the Generalized Gradient Approximation for Exchange and Correlation. *Phys. Rev. B* **1992**, *46*, 6671–6687. [CrossRef] [PubMed]
39. Ortmann, F.; Bechstedt, F.; Schmidt, W.G. Semiempirical van der Waals correction to the density functional description of solids and molecular structures. *Phys. Rev. B* **2006**, *73*, 205101. [CrossRef]
40. Wu, Z.; Cohen, R.E. More Accurate Generalized Gradient Approximation for Solids. *Phys. Rev. B* **2006**, *73*, 235116. [CrossRef]
41. Perdew, J.P.; Ruzsinszky, A.; Csonka, G.I.; Vydrov, O.A.; Scuseria, G.E.; Constantin, L.A.; Zhou, X.; Burke, K. Restoring the Density-Gradient Expansion for Exchange in Solids and Surfaces. *Phys. Rev. Lett.* **2008**, *100*, 136406. [CrossRef] [PubMed]
42. Becke, A.D. Density-Functional Exchange-Energy Approximation with Correct Asymptotic Behavior. *Phys. Rev. A* **1988**, *38*, 3098–3100. [CrossRef] [PubMed]
43. Lee, C.; Yang, W.; Parr, R.G. Development of the Colle-Salvetti Correlation-Energy Formula into a Functional of the Electron Density. *Phys. Rev. B* **1988**, *37*, 785–789. [CrossRef] [PubMed]
44. Bartók, A.P.; Yates, J.R. Regularized SCAN Functional. *J. Chem. Phys.* **2019**, *150*, 161101. [CrossRef]
45. Baroni, S.; De Gironcoli, S.; Dal Corso, A.; Giannozzi, P. Phonons and Related Crystal Properties from Density-Functional Perturbation Theory. *Rev. Mod. Phys.* **2001**, *73*, 515–562. [CrossRef]
46. Guo, Y.Q.; Zhang, S.H.; Beyerlein, I.J.; Legut, D.; Shang, S.L.; Liu, Z.K.; Zhang, R.F. Synergetic Effects of Solute and Strain in Biocompatible Zn-Based and Mg-Based Alloys. *Acta Mater.* **2019**, *181*, 423–438. [CrossRef]
47. Zhang, W.; Tang, G.; Sahoo, M.P.K.; Liang, Y.; Zhang, Y. Unified Picture for the Pressure-Controlled Band Gap in Inorganic Halide Perovskites: Role of Strain–Phonon and Phonon–Phonon Couplings. *Phys. Rev. B* **2022**, *105*, 075150. [CrossRef]
48. Smirnova, V.Y.; Iurchenkova, A.A.; Rychkov, D.A. Computational Investigation of the Stability of Di-*p*-Tolyl Disulfide "Hidden" and "Conventional" Polymorphs at High Pressures. *Crystals* **2022**, *12*, 1157. [CrossRef]

Disclaimer/Publisher's Note: The statements, opinions and data contained in all publications are solely those of the individual author(s) and contributor(s) and not of MDPI and/or the editor(s). MDPI and/or the editor(s) disclaim responsibility for any injury to people or property resulting from any ideas, methods, instructions or products referred to in the content.

crystals

MDPI

Supplementary Materials

Entropy-Driven Isosymmetric Phase Transition in L-Serine Under Pressure: A Periodic DFT Study

Anna Maria Mazurek [1], Monika Franczak-Rogowska [2] and Łukasz Szeleszczuk [1,*]

[1] Department of Organic and Physical Chemistry, Medical University of Warsaw, 1 Banacha Str., 02-097 Warsaw, Poland; anna.mazurek1@wum.edu.pl
[2] Department of Drug Chemistry, Pharmaceutical and Biomedical Analysis, Medical University of Warsaw, 1 Banacha Str., 02-097 Warsaw, Poland; monika.franczak-rogowska@wum.edu.pl
* Correspondence: lukasz.szeleszczuk@wum.edu.pl; Tel.: +48-501-255-121

Table S1. Energy differences between Phase I and Phase IV of L-serine optimized using PBE TS functional under different pressures.

Pressure [GPa]	ΔE Phase I—Phase IV [kJ/mol]
0	-138.36
0.4	-134.54
0.8	-127.53
1.2	-119.11
1.6	-110.24
2.0	-101.18
2.4	-91.38
2.8	-82.35
3.2	-73.33
3.6	-64.64
4.0	-56.21
4.4	-48.03
4.8	-40.03
5.2	-32.17
5.6	-24.68
6.0	-17.17
6.4	-9.76
6.8	-2.33
7.2	4.40
7.6	11.45
8.0	18.10
8.4	24.39
8.8	30.61

Table S2. Geometrically optimized, using PBE TS functional, unit cell dimensions of generated configurations derived from L-serine Phase I and IV at 1 atm.

	Phase I				**Phase IV**			
Label	**a [Å]**	**b [Å]**	**c [Å]**	**V [Å^3]**	**a [Å]**	**b [Å]**	**c [Å]**	**V [Å^3]**
UUU	16.904	8.493	9.463	1358.6	16.783	8.661	9.455	1374.4
UUR	16.700	8.574	9.768	1398.7	16.404	8.957	9.306	1367.3
UUL	16.624	8.666	9.576	1379.6	16.638	8.937	9.139	1358.9
URU	17.126	8.167	9.902	1384.9	16.560	8.833	9.123	1334.4
URR	16.435	8.676	9.953	1419.3	16.397	9.089	8,881	1323.5
URL	16.860	8.418	9.803	1391.3	16.305	9.113	9.193	1365.9
ULU	16.484	8.773	9.689	1401.2	16.799	8.664	9.373	1364.3
ULR	17.045	8.663	9.219	1361.1	16.460	8.365	10.230	1408.6
ULL	16.573	8.618	9.731	1389.8	16.552	9.193	9.134	1389.9
RUU	17.121	8.285	9.620	1364.6	16.412	9.103	9.182	1371.8
RUR	17.268	7.822	10.139	1369.4	16.370	8.407	10.090	1388.6
RUL	16.867	8.759	9.190	1357.8	16.408	8.339	10.103	1382.3
RRU	16.485	8.651	9.908	1413.0	16.666	8.552	9.754	1390.2
RRR	16.392	8.197	10.307	1384.9	16.545	8.751	9.215	1334.2
RRL	16.474	8.202	10.277	1388.6	16.673	8.760	9.038	1320.0
RLU	16.407	8.818	9.652	1396.5	16.516	8.864	9.435	1381.3
RLR	16.425	8.316	10.150	1386.5	16.569	8.221	10.269	1398.8
RLL	16.558	8.418	10.020	1396.7	16.709	8.509	9.709	1380.4
LUU	17.115	8.420	9.601	1383.6	16.483	9.204	9.124	1384.1
LUR	17.218	8.265	9.667	1375.6	16.635	8.900	9.363	1386.3
LUL	16.547	8.808	9.681	1411.0	16,573	8.986	9.292	1383.8
LRU	16.754	8.572	9.753	1400.8	16.624	8.791	9.098	1329.6
LRR	16.500	8.361	10.103	1393.8	16.673	8.667	9.599	1387.2
LRL	16.794	8.532	9.704	1390.4	16.473	9.068	8.777	1311.1
LLU	16.588	8.583	9.736	1386.2	16.702	8.904	9.212	1370.0
LLR	16.492	8.144	10.210	1371.3	16.754	8.562	9.696	1390.9
LLL	16.525	7.948	10.258	1347.2	16.517	7.937	10.249	1343.5

Table S3. Geometrically optimized, using PBE TS functional, unit cell dimensions of generated configurations derived from L-serine Phase I and IV at 8.8 GPa.

	Phase I				**Phase IV**			
Label	**a [Å]**	**b [Å]**	**c [Å]**	**V [Å^3]**	**a [Å]**	**b [Å]**	**c [Å]**	**V [Å^3]**
UUU	16.264	8.073	8.364	1098.1	15.828	8.342	8.292	1098.1
UUR	16.278	7.778	8.622	1091.5	15.980	8.276	8.203	1091.5
UUL	16.023	8.260	8.208	1086.3	16.011	8.355	8.101	1086.3
URU	16.138	8,101	8.267	1080.7	15.796	8.248	8.236	1080.7
URR	16.204	8.207	8.199	1090.4	15.910	8.389	8.129	1090.4
URL	16.239	8.136	8.172	1079.7	15.940	8.298	8.084	1079.7
ULU	15.848	8.440	8.246	1103.0	15.910	8.163	8.328	1103.0
ULR	16.151	8.154	8.444	1112.0	15.940	8.380	8.173	1112.0
ULL	16.075	8.377	8.102	1091.0	16.082	8.281	8.021	1091.0
RUU	16.569	7.667	8.636	1097.0	15.414	8.113	8.624	1097.0
RUR	16.413	7.932	8.314	1082.4	15.626	7.243	9.477	1082.4
RUL	16.250	8.334	8.062	1091.9	15.733	8.707	7.824	1091.9
RRU	17.010	7.202	8.777	1075.3	15.086	8.482	8.256	1075.3
RRR	17.421	6.915	8.904	1072.7	15.891	8.161	8.337	1072.7
RRL	16.105	8.168	8.183	1076.4	16.018	8.195	8.155	1076.4
RLU	16.504	8.011	8.311	1098.8	16.163	8.344	8.186	1098.8
RLR	16.503	7.997	8.252	1089.1	15.895	8.264	8.277	1089.1
RLL	16.365	8.265	8.009	1083.3	16.369	8.260	8.006	1083.3
LUU	15.867	8.310	8.260	1089.1	15.993	8.380	8,222	1089.1
LUR	16.403	8.016	8.308	1092.5	16.004	8.313	8.180	1092.5
LUL	16.137	8.398	8.175	1107.9	16.102	8.391	8.096	1107.9
LRU	16.361	8.030	8.192	1076.3	15.908	8.291	8.214	1076.3
LRR	16.468	8.134	8.157	1092.5	15.978	8.688	7.635	1092.5
LRL	15.942	8.235	8.027	1053.8	15.947	8.229	8.027	1053.8
LLU	16.091	8.324	8.224	1101.5	16.000	8.513	7.855	1101.5
LLR	16.158	8.370	8.038	1087.0	16.104	8.349	8.078	1087.0
LLL	16.045	8.444	8.135	1102.1	16.231	8.367	8.008	1102.1

Publication co-author statement

As a co-author of the publication entitled:

"Entropy-Driven Isosymmetric Phase Transition in L-Serine under Pressure: A Periodic DFT Study", *published in Crystals (2026, Volume 16, Issue 4, Article 266),*
https://doi.org/10.3390/cryst16040266
Authors: Anna Maria Mazurek, Monika Franczak-Rogowska and Łukasz Szeleszczuk

I agree to include this publication into a collection of thematically related publications forming a doctoral dissertation prepared by mgr farm. Anna Maria Mazurek.

Additionally, I declare my condribution to the publication as follows: conceptualisation, Ł.S., M.F.-R. and A.M.M.; methodology, Ł.S.; software, Ł.S.; validation, Ł.S.; formal analysis, Ł.S. and A.M.M.; investigation, Ł.S. and A.M.M.; resources, Ł.S.; data curation, Ł.S. and A.M.M.; writing - original draft preparation, Ł.S. and A.M.M.; writing - review and editing, Ł.S., M.F.-R. and A.M.M.; visualisation, Ł.S. and A.M.M.; supervision, Ł.S. and M.F.-R.; project administration, Ł.S.; funding acquisition, Ł.S.

Oświadczenie współautora publikacji

Jako współautor publikacji pt.:

"Entropy-Driven Isosymmetric Phase Transition in L-Serine under Pressure: A Periodic DFT Study", *opublikowanej w czasopiśmie Crystals (2026, tom 16, numer 4, artykuł 266),*
https://doi.org/10.3390/cryst16040266
Autorzy: Anna Maria Mazurek, Monika Franczak-Rogowska and Łukasz Szeleszczuk

Wyrażam zgodę na włączenie tej publikacji do zbioru powiązanych tematycznie artykułów naukowych, stanowiących część pracy doktorskiej przygotowanej przez mgr farm. Annę Marię Mazurek.

Jednocześnie potwierdzam, że następujący zakres stanowi mój wkład w publikację: koncepcja, Ł.S., M.F.-R. oraz A.M.M.; metodologia, Ł.S.; oprogramowanie, Ł.S.; walidacja, Ł.S.; analiza formalna, Ł.S. oraz A.M.M.; badania, Ł.S. oraz A.M.M.; zasoby, Ł.S.; opracowanie danych, Ł.S. oraz A.M.M.; pisanie – przygotowanie pierwotnej wersji manuskryptu, Ł.S. oraz A.M.M.; pisanie - redakcja i korekta manuskryptu, Ł.S., M.F.-R. oraz A.M.M.; wizualizacja, Ł.S. oraz A.M.M.; nadzór, Ł.S. oraz M.F.-R.; zarządzanie projektem, Ł.S.; pozyskiwanie finansowania, Ł.S.

28.04.2026
Date / Data

Anna Mazurek
Legible signature / Czytelny podpis

Publication co-author statement

As a co-author of the publication entitled:

"Entropy-Driven Isosymmetric Phase Transition in L-Serine under Pressure: A Periodic DFT Study", *published in Crystals (2026, Volume 16, Issue 4, Article 266),* https://doi.org/10.3390/cryst16040266
Authors: Anna Maria Mazurek, Monika Franczak-Rogowska and Łukasz Szeleszczuk

I agree to include this publication into a collection of thematically related publications forming a doctoral dissertation prepared by mgr farm. Anna Maria Mazurek.

Additionally, I declare my condribution to the publication as follows: conceptualisation, Ł.S., M.F.-R. and A.M.M.; methodology, Ł.S.; software, Ł.S.; validation, Ł.S.; formal analysis, Ł.S. and A.M.M.; investigation, Ł.S. and A.M.M.; resources, Ł.S.; data curation, Ł.S. and A.M.M.; writing - original draft preparation, Ł.S. and A.M.M.; writing - review and editing, Ł.S., M.F.-R. and A.M.M.; visualisation, Ł.S. and A.M.M.; supervision, Ł.S. and M.F.-R.; project administration, Ł.S.; funding acquisition, Ł.S.

Oświadczenie współautora publikacji

Jako współautor publikacji pt.:

"Entropy-Driven Isosymmetric Phase Transition in L-Serine under Pressure: A Periodic DFT Study", *opublikowanej w czasopiśmie Crystals (2026, tom 16, numer 4, artykuł 266),* https://doi.org/10.3390/cryst16040266
Autorzy: Anna Maria Mazurek, Monika Franczak-Rogowska and Łukasz Szeleszczuk

Wyrażam zgodę na włączenie tej publikacji do zbioru powiązanych tematycznie artykułów naukowych, stanowiących część pracy doktorskiej przygotowanej przez mgr farm. Annę Marię Mazurek.

Jednocześnie potwierdzam, że następujący zakres stanowi mój wkład w publikację: koncepcja, Ł.S., M.F.-R. oraz A.M.M.; metodologia, Ł.S.; oprogramowanie, Ł.S.; walidacja, Ł.S.; analiza formalna, Ł.S. oraz A.M.M.; badania, Ł.S. oraz A.M.M.; zasoby, Ł.S.; opracowanie danych, Ł.S. oraz A.M.M.; pisanie – przygotowanie pierwotnej wersji manuskryptu, Ł.S. oraz A.M.M.; pisanie - redakcja i korekta manuskryptu, Ł.S., M.F.-R. oraz A.M.M.; wizualizacja, Ł.S. oraz A.M.M.; nadzór, Ł.S. oraz M.F.-R.; zarządzanie projektem, Ł.S.; pozyskiwanie finansowania, Ł.S.

28.04.2026
Date / Data

Szeleszczuk
Legible signature / Czytelny podpis

Publication co-author statement

As a co-author of the publication entitled:

"Entropy-Driven Isosymmetric Phase Transition in L-Serine under Pressure: A Periodic DFT Study", *published in Crystals (2026, Volume 16, Issue 4, Article 266),* https://doi.org/10.3390/cryst16040266
Authors: Anna Maria Mazurek, Monika Franczak-Rogowska and Łukasz Szeleszczuk

I agree to include this publication into a collection of thematically related publications forming a doctoral dissertation prepared by mgr farm. Anna Maria Mazurek.

Additionally, I declare my condribution to the publication as follows: conceptualisation, Ł.S., M.F.-R. and A.M.M.; methodology, Ł.S.; software, Ł.S.; validation, Ł.S.; formal analysis, Ł.S. and A.M.M.; investigation, Ł.S. and A.M.M.; resources, Ł.S.; data curation, Ł.S. and A.M.M.; writing - original draft preparation, Ł.S. and A.M.M.; writing - review and editing, Ł.S., M.F.-R. and A.M.M.; visualisation, Ł.S. and A.M.M.; supervision, Ł.S. and M.F.-R.; project administration, Ł.S.; funding acquisition, Ł.S.

Oświadczenie współautora publikacji

Jako współautor publikacji pt.:

"Entropy-Driven Isosymmetric Phase Transition in L-Serine under Pressure: A Periodic DFT Study", *opublikowanej w czasopiśmie Crystals (2026, tom 16, numer 4, artykuł 266),* https://doi.org/10.3390/cryst16040266
Autorzy: Anna Maria Mazurek, Monika Franczak-Rogowska and Łukasz Szeleszczuk

Wyrażam zgodę na włączenie tej publikacji do zbioru powiązanych tematycznie artykułów naukowych, stanowiących część pracy doktorskiej przygotowanej przez mgr farm. Annę Marię Mazurek.

Jednocześnie potwierdzam, że następujący zakres stanowi mój wkład w publikację: koncepcja, Ł.S., M.F.-R. oraz A.M.M.; metodologia, Ł.S.; oprogramowanie, Ł.S.; walidacja, Ł.S.; analiza formalna, Ł.S. oraz A.M.M.; badania, Ł.S. oraz A.M.M.; zasoby, Ł.S.; opracowanie danych, Ł.S. oraz A.M.M.; pisanie – przygotowanie pierwotnej wersji manuskryptu, Ł.S. oraz A.M.M.; pisanie - redakcja i korekta manuskryptu, Ł.S., M.F.-R. oraz A.M.M.; wizualizacja, Ł.S. oraz A.M.M.; nadzór, Ł.S. oraz M.F.-R.; zarządzanie projektem, Ł.S.; pozyskiwanie finansowania, Ł.S.

28.04.2026
Date / Data

Franczak-Rogowska
Legible signature / Czytelny podpis